NIST Internal Report
NIST IR 8466

Applied and Computational Mathematics Division

Summary of Activities for Fiscal Year 2022

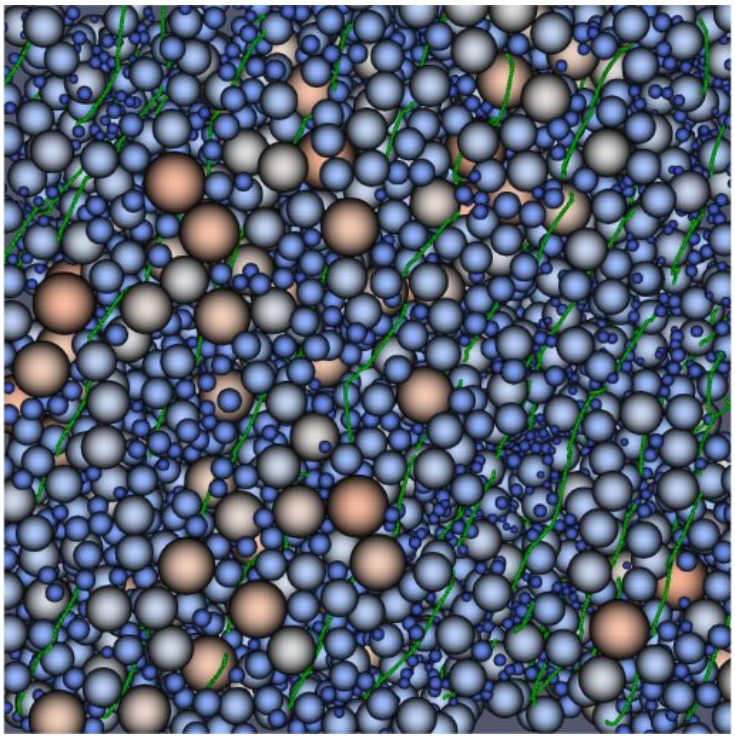

This publication is available free of charge from:
https://doi.org/10.6028/NIST.IR.8466

NIST NATIONAL INSTITUTE OF STANDARDS AND TECHNOLOGY
U.S. DEPARTMENT OF COMMERCE

NIST Internal Report
NIST IR 8466

Applied and Computational Mathematics Division

Summary of Activities for Fiscal Year 2022

Ronald F. Boisvert, Editor
Applied and Computational Mathematics Division
Information Technology Laboratory

This publication is available free of charge from:
https://doi.org/10.6028/NIST.IR.8466

May 2023

U.S. Department of Commerce
Gina M. Raimondo, Secretary

National Institute of Standards and Technology
Laurie E. Locascio, NIST Director and Under Secretary of Commerce for Standards and Technology

Certain commercial equipment, instruments, software, or materials, commercial or non-commercial, are identified in this document in order to specify the experimental procedure adequately. Such identification does not imply recommendation or endorsement of any product or service by NIST, nor does it imply that the materials or equipment identified are necessarily the best available for the purpose.

Publication History
Approved by the NIST Editorial Review Board on 2023-05-16

How to Cite this NIST Technical Series Publication
Ronald F. Boisvert (2023) Applied and Computational Mathematics Division: Summary of Activities for Fiscal Year 2022. (National Institute of Standards and Technology, Gaithersburg, MD), NIST Internal Report (IR) NIST IR 8466. https://doi.org/10.6028/NIST.IR.8466

NIST Author ORCID iD
Ronald F. Boisvert: 0000-0002-4445-1044

Contact Information
Ronald F. Boisvert, 100 Bureau Drive, Mail Stop 8910, NIST, Gaithersburg, MD 20899-8910, phone 301-975-3812, email boisvert@nist.gov, or see the Division's Web site at https://www.nist.gov/itl/math/.

Abstract

This report summarizes recent technical work of the Applied and Computational Mathematics Division of the Information Technology Laboratory at the National Institute of Standards and Technology (NIST). Part I (Overview) provides a high-level overview of the Division's activities, including highlights of technical accomplishments during the previous year. Part II (Features) provides further details on projects of particular note this year. This is followed in Part III (Project Summaries) by brief synopses of all technical projects active during the past year. Part IV (Activity Data) provides listings of publications, technical talks, and other professional activities in which Division staff members have participated. The reporting period covered by this document is October 2021 through December 2022.

Keywords

applied mathematics; computational science and engineering; high-performance computing; materials modeling and simulation; mathematical knowledge management; mathematical modeling; mathematics of biotechnology; mathematics of metrology; scientific visualization; quantum information science.

Cover Visualization

Visualization of a simulation of a high-performance concrete. The sand is modeled as spheres of varying size. In this image, the spheres are colored based on their radius and the suspended semi-stiff fibers are shown in green. See page 66.

Acknowledgements

Thanks to Neal Gammons for assisting in the compilation of Part III of this document, and to Lochi Orr who compiled Part IV. Thanks also to Brian Cloteaux and Kerrianne Buchanan who read the manuscript and offered corrections and suggestions for improvement. The "word cloud," which is found at the start of each Part of this document was created using Wordle (https://www.wordle.net/), and the text of this document as input.

Table of Contents

PART I: OVERVIEW **1**

Introduction **3**

Highlights **5**

Recent Technical Highlights *5*
Technology Transfer and Community Engagement *7*

Staff News **7**

Arrivals *8*
Departures *9*
Recognition *10*

PART II: FEATURES **15**

Reducing Bias and Quantifying Uncertainty in Fluorescence Produced by PCR **17**

Combining Machine Learning with Physics: Enhanced Dark Soliton Detection in Bose-Einstein Condensates **22**

PART III: PROJECT SUMMARIES **25**

Mathematics of Metrology **27**

TOMCAT: X-ray Imaging of Nanoscale Integrated Circuits for Tomographic Reconstruction *27*
True Becquerel: A New Paradigm for 21st Century Radioactivity Measurements *29*
Machine Learning Models to Predict the Mass and Infrared Spectra of Chemical Compounds *29*
Accelerating Scale-up of Carbon-Capture Materials *31*
Linear and Nonlinear Exploration of Rotating Self-Gravitating Inviscid Incompressible Fluid Ellipsoids *32*
A Science Gateway for Atomic, Molecular and Optical Science *34*
Separable Shape Tensors *35*
Computational Tools for Image and Shape Analysis *36*
Numerical Solutions of the Time Dependent Schrödinger Equation *39*
ITVOLT: An Iterative Solver for the Time-Dependent Schrödinger Equation *41*
Computing Ill-Posed Time-Reversed Dissipative Evolution Equations, Using Stabilized Explicit Schemes Run Backward in Time *42*

Mathematics of Biotechnology **46**

Data Analysis for Quantitative Polymerase Chain Reaction Measurements *46*
Advanced Data Analysis for Diagnostics, Biometrology, and COVID-19 ..... *47*
Metrology for Cytometry *48*
Standardization of SARS-CoV-2 Serology Measurements *49*
Mathematical Models for Cryobiology *50*
Modeling for Biological Field Effect Transistor Experiments *51*
Binding, Brightness, or Noise? Extracting Temperature-dependent Properties of SYTO-13 Dye Bound to DNA *53*
Artificial Intelligence for Low-Field Magnetic Resonance Imaging *54*

Modeling Photoreceptor Dynamics ... 57

Materials Modeling ... **59**

OOF: Finite Element Analysis of Material Microstructures ... 59
Micromagnetic Modeling ... 60
Mathematics of Uncertainty in Engineering Reliability ... 61

High Performance Computing and Visualization ... **64**

High Precision Calculations of Fundamental Properties of Few- Electron Atomic Systems ... 64
Simulation of Dense Suspensions: Cementitious Materials ... 66
Visualization of Greenhouse Gas Emissions ... 68
Immersive Visualization for the Design of Wearable Wireless Monitoring System ... 69
Transition to Open Source Visualization Software ... 69
Transportable VR System ... 70
Standards in Visualization ... 71
WebXR Graphics ... 72
Uncertainty in Machine Learning for Quantum Physical Systems ... 73
Towards Robust Autotuning of Noisy Quantum Dot Devices ... 75
Towards Robust Bootstrapping of Quantum Dot Devices ... 77
Tuning Arrays with Rays: Physics-Informed Tuning of Quantum Dot Charge States ... 78
Principled State Identification for Quantum Dot Data ... 80
Combining Machine Learning with Physics: Enhanced Dark Soliton Detection in Bose-Einstein Condensates ... 81

Quantum Information ... **84**

Quantum Information Science ... 84
Quantum Characterization Theory and Applications ... 85
Quantum Algorithms and the Power of Forgetting ... 87
Quantum Depth in the Random Oracle Model ... 89
Local Hamiltonians with No Low-Energy Stabilizer States ... 90
Error-Correction Zoo ... 91
Modern Quantum Tools for Bosonic Systems ... 92
Provable Accurate Machine Learning Algorithms for the Quantum Many-body Problem ... 93
Provably Accurate Quantum Simulation of Gauge Theories and Bosonic Systems ... 93
Standards for Characterizing Quantum Phases ... 94
Tests of Quantumness and Quantum Computational Advantage ... 94
Post-Quantum Cryptography ... 95
NIST Quantum Network Testbed Efforts ... 96
Quantum Network and Component Metrology ... 97
Integrated Quantum Photonics Based on Thin-film Lithium Niobate ... 99
Entangled Photon Pairs Based on Backward-Wave Spontaneous Parametric Downconversion ... 100
Silicon-Carbide-based Integrated Quantum Device Efforts ... 101
Joint Center for Quantum Information and Computer Science ... 102

Foundations of Measurement Science for Information Systems ... **103**

Algorithms for Identifying Important Network Nodes for Communication and Spread ... 103

Towards Risk Evaluation and Mitigation in Networked Systems *104*
Measurements of Cyber Risks in Complex Systems and Optimal Cybersecurity Investments *105*
Distributed Learning with Heterogeneous Datasets and Acceleration via Coordinating Server Learning *107*
Combinatorial Testing for Software Based Systems *108*
Impact of Using Soft Exposure Thresholds in Automatic Contact Tracing *112*
Maximizing Harvested Energy in Coulomb Force Parametric Generators *113*

Mathematical Knowledge Management **116**
Digital Library of Mathematical Functions *116*
NIST Digital Repository of Mathematical Formulae *118*
Scientific Document Corpora for Natural and Mathematical Language Research *120*
Visualization of Complex Functions Data *121*
DLMF Standard Reference Tables on Demand *122*
Fundamental Solutions and Formulas for Special Functions and Orthogonal Polynomials *123*

Outreach and Diversity **126**
Student Internships in ACMD *126*
A Modular Analysis of NIST Institutional Networks *126*
Network Analysis to Investigate Physics Programmatic Survey Results *127*

PART IV: ACTIVITY DATA **131**

Publications **133**
Appeared *133*
Refereed Journals 133
Book Chapters 136
In Conference Proceedings 136
Technical Reports 138
Other Publications 138
Blog Posts 138
Accepted *139*
In Review *139*
Inventions *141*
Invention Disclosures and Patents in Review 141

Presentations **141**
Invited Talks *141*
Conference Presentations 145
Poster Presentations 149
NIST News Releases *151*

Web Services **151**

Software Released **151**

Data Released **152**

Conferences, Minisymposia, Lecture Series, Courses **152**
ACMD Seminar Series *152*
Courses and Shortcourses *153*

Conference Organization *153*
Leadership 153
Committee Membership 154
Session Organization 154

Other Professional Activities **154**

Internal *154*
External *155*
Editorial 155
Boards and Committees 155
Adjunct Academic Appointments 156
Thesis Direction 156
Community Outreach 157

Awards and Recognition **158**

External 158
Internal 158

Funding Received **158**

External 158
Internal 158

Grants Funded **159**

External Contacts **159**

Industrial Labs 159
Government/Non-profit Organizations 160
Universities 160

PART V: APPENDIX **163**

Staff **165**

Glossary of Acronyms **168**

Part I

Overview

Introduction

Founded in 1901, the National Institute of Standards and Technology (NIST) is a non-regulatory federal agency within the U.S. Department of Commerce. Its mission is to promote U.S. innovation and industrial competitiveness by advancing measurement science, standards, and technology in ways that enhance economic security and improve our quality of life. The technical disciplines represented in the NIST Laboratories include physics, electrical engineering, nanotechnology, materials science, chemistry, biotechnology, manufacturing and construction engineering, fire research, information technology, mathematics, and statistics. The NIST Labs operate in two locations: Gaithersburg, MD, (headquarters—234 hectare/578-acre campus) and Boulder, CO (84 hectare/208-acre campus). NIST employs about 3 400 scientists, engineers, technicians, and support personnel, and also hosts about 3 500 associates from academia, industry, and other government agencies, who collaborate with NIST staff and access its facilities.

The Information Technology Laboratory (ITL) is one of six major organizational units that make up the NIST Labs. ITL's singular purpose is to cultivate trust in information technology and metrology. This is done through the development of measurements, tests, and guidance to support innovation in and deployment of information technology by industry and government, as well as through the application of advanced mathematics, statistics, and computer science to help ensure the quality of measurement science.

The Applied and Computational Mathematics Division (ACMD) is one of six technical Divisions in ITL. At its core, ACMD's purpose is to nurture trust in metrology and scientific computing. To do so, ACMD provides leadership within NIST in the use of applied and computational mathematics to solve technical problems arising in measurement science and related applications. In that role staff members

- perform research in applied mathematics and computational science and engineering, including analytical and numerical methods, high-performance computing, and visualization,
- perform applied research in computer science and engineering for future computing and communications technologies,
- engage in peer-to-peer collaborations to apply mathematical and computational techniques and tools to NIST problems,
- develop and disseminate mathematical reference data, software, and related tools, and
- work with internal and external groups to develop standards, tests, reference implementations, and other measurement technologies for current and future scientific computing systems.

Division staff is organized into four groups:

- Mathematical Analysis and Modeling Group (*Timothy Burns, Leader*). Performs research and maintains expertise in applied mathematics, mathematical modeling, and numerical analysis for application to measurement science.
- Mathematical Software Group (*Bonita Saunders, Leader*). Performs research and maintains expertise in the methodology and application of mathematical algorithms and software in support of computational science within NIST as well as in industry and academia.
- High Performance Computing and Visualization Group (*Judith Terrill, Leader*). Performs research and maintains expertise in the methodologies and tools of high-performance scientific computing and visualization for use in measurement science.
- Computing and Communications Theory Group (*Ronald Boisvert, Acting Leader; Oliver Slattery, Project Leader*). Performs research and maintains expertise in the fundamental mathematics, physics, computer science, and measurement science necessary to enable the development and analysis of current and future computing and communications systems.

The technical work of the Division is organized into seven thematic areas; these are described in the sidebar. Project descriptions in Part III of this document are organized according to these broad themes.

Division Thematic Areas

Broad Areas

Mathematics of Metrology. Mathematics plays an important role in measurement science. Mathematical models are needed to understand how to design effective measurement systems and to analyze the results they produce. Mathematical techniques are used to develop and analyze idealized models of physical phenomena to be measured, and mathematical algorithms are necessary to find optimal system parameters. Mathematical and statistical techniques are needed to transform measured data into useful information. We develop fundamental mathematical methods and tools necessary for NIST to remain a world-class metrology institute, and to apply these to measurement science problems.

High Performance Computing and Visualization. Computational capability continues to advance rapidly, enabling modeling and simulation to be done with greatly increased fidelity. Doing so often requires computing resources well beyond what is available on the desktop. Developing software that makes effective use of such high-performance computing platforms remains very challenging, requiring expertise that application scientists rarely have. We maintain such expertise for application to NIST problems. Such computations, as well as modern experiments, typically produce large volumes of data, which cannot be readily comprehended. We are developing the infrastructure necessary for advanced interactive, quantitative visualization and analysis of scientific data, including the use of 3D immersive environments, and applying the resulting tools to NIST problems.

Current Focus Areas

Mathematics of Biotechnology. As proof-of-concept academic work in engineering biology meets the market realities of bringing lab science to product initiation, there are needs to compare biological products, measure whether desired outcomes are realized, and optimize biological systems for desired behaviors. NIST is working to deliver tools and standards to measure such biological technologies, outputs, and processes from healthcare to manufacturing and beyond. We support this effort with the development and deployment of innovative mathematical modeling and data analysis techniques and tools.

Materials Modeling. Mathematical modeling, computational simulation, and data analytics are key enablers of emerging manufacturing technologies. The Materials Genome Initiative (MGI), an interagency program with the goal of significantly reducing the time from discovery to commercial deployment of new materials using modeling, simulation, and informatics, is a case in point. To support the NIST role in the MGI, we develop and assess modeling and simulation techniques and tools, with emphasis on uncertainty quantification, and collaborate with other NIST Laboratories in their efforts to develop the measurement science infrastructure needed by the materials science and engineering community.

Quantum Information Science. An emerging discipline at the intersection of physics and computer science, quantum information science is likely to revolutionize 21st century science and technology in the same way that lasers, electronics, and computers did in the 20th century. By encoding information into quantum states of matter, one can, in theory, enable phenomenal increases in information storage and processing capability. At the same time, such computers would threaten the public-key infrastructure that secures all of electronic commerce. Although many of the necessary physical manipulations of quantum states have been demonstrated experimentally, scaling these up to enable fully capable quantum computers and networks remains a grand challenge. We engage in (a) theoretical studies to understand the power of quantum computing, (b) collaborative efforts with the multi-laboratory experimental quantum science program at NIST to characterize and benchmark specific physical realizations of quantum information processing, and (c) demonstration and assessment of technologies for quantum networking.

Foundations of Measurement Science for Information Systems. ITL assumes primary responsibility within NIST for the development of measurement science infrastructure and related standards for IT and its applications. ACMD develops the mathematical foundations for such work. This can be very challenging. For example, many large-scale information-centric systems can be characterized as an interconnection of many independently operating components (e.g., software systems, communication networks, the power grid, transportation systems, financial systems). Exactly how the structure of such large-scale interconnected systems and the local dynamics of its components leads to system-level behavior is only weakly understood. This inability to predict the systemic risk inherent in system design leaves us open to unrealized potential to improve systems or to avoid potentially devastating failures. A looming new example of importance to NIST is the Internet of Things. We are developing models to aid in the development of applications from individualized health IT devices to large-scale sensor networks.

Mathematical Knowledge Management. We work with researchers in academia and industry to develop technologies, tools, and standards for representation, exchange, and use of mathematical data. Of particular concern are semantic-based representations which can provide the basis for interoperability of mathematical information processing systems. We apply these representations to the development and dissemination of reference data for applied mathematics. The centerpiece of this effort is the Digital Library of Mathematical Functions, a freely available interactive and richly linked online resource, providing essential information on the properties of the special functions of applied mathematics, the foundation of mathematical modeling in all of science and engineering.

Highlights

In this section we identify some of the major accomplishments of the Division during the past year. We also provide news related to ACMD staff.

Recent Technical Highlights

ACMD has made significant technical progress on many fronts during the past year. Here we highlight a few notable technical accomplishments.

- July 1, 2022 marked the 75th anniversary of the establishment of the first mathematical unit on the NIST (NBS, at the time) org chart. This was known as the National Applied Mathematics Laboratory. (By 1954 the organization's name had been changed to the Applied Mathematics Division.) To commemorate this anniversary ACMD and the NIST Statistical Engineering hosted a celebratory online symposium[1] on June 28-30, 2022, which attracted 256 attendees. Twenty talks focusing on NIST history were presented. Featured external speakers included David Alan Grier (a science historian from George Washington University), Karen Kafadar (University of Virginia), Douglas Shier (Duke University), and Youssef Saad (University of Minnesota). Videos of all of the presentations are available on the conference website. In addition to the symposium, an online timeline of major events in the history of mathematics and statistics at NIST was released[2] as well as a repository historical records from the Statistical Engineering Division[3]
- X-ray tomography is capable of imaging the interior of 3D objects non-invasively, with applications in biomedical imaging, materials science, electronic inspection, and other fields. The reconstruction process can be a challenging, ill-conditioned inverse problem. Recently, deep learning has been adopted for tomographic reconstruction. Bradley Alpert of ACMD, working with colleagues in NIST PML, Sandia National Laboratories, and the Massachusetts Institute of Technology, has developed a physics-assisted generative adversarial network for this task. The new method can reduce the photon requirement with limited projection angles to achieve a given error rate, which may further enable low-photon nanoscale imaging. This is being applied to imaging of nanoscale integrated circuits. See page 27.
- Sea-ice formation and defect development in metal alloys share an important feature: a so-called mushy layer. Such phenomena are the result of complex fluid mechanical activity, thermal and chemical transport, phase transformations, nonlinear dynamics, and pattern formation. Directly observing real-world mushy layers is a challenge, and hence mathematical modeling has been a key to develop understanding of such phenomena. ACMD faculty appointee Daniel Anderson and colleagues this year published an excellent summary in *Physics Today* of the historical development and current status of research in this area. See page 50.
- Quantitative PCR (qPCR) is routinely employed in healthcare diagnostics, forensics, and biotechnology research. It can determine the concentration of a specific sequence of nucleic acids present in a sample. However, quantification is limited by systematic and subjective bias, as well as the lack of a quantitative expression for uncertainty. Robert DeJaco and Anthony Kearsley of ACMD, working with colleagues in NIST MML, have developed an improved mathematical model which can reduce several sources of bias and quantify the uncertainty in fluorescence. It also provides new insight into PCR dynamics, sources of error, and limits of detection. See page 17.
- Simon Su, William Sherman, and Judith Terrill of ACMD have developed a transportable virtual reality (VR) system that approximates immersive VR for use at conferences and similar venues. This

[1] https://www.nist.gov/news-events/events/2022/06/75th-anniversary-mathematics-and-statistics-nist
[2] https://www.nist.gov/mathematics-statistics/mathematics-and-statistics-nist-timeline
[3] https://www.nist.gov/itl/sed/historical-information

project has grown out of an effort to enable researchers and developers to have local (i.e., in their office) access to immersive interfaces using consumer tracking technology. The system was on display at the 2022 Supercomputing conference. See page 70.

- Generic computational tasks can be mapped to finding the ground state of a Hamiltonian. This is the basis for adiabatic quantum computing. Here one initializes a system in an easy-to-prepare ground state, after which a time-dependent evolution is performed to transform the system into one whose ground state encodes the solution to the desired problem. However, adiabaticity, i.e., slow evolution, is not a requirement, it is simply a (demanding) condition that guarantees success. This does not exclude the existence of non-adiabatic schedules that take the system to the desired target state more quickly. In a paper to appear in *Physical Review Letters*, Yi-Kai Liu and Lucas Brady of ACMD and colleagues describe general conditions that constrain how fast annealing can be successfully performed, including beyond the adiabatic regime. See page 94.
- Classical and quantum error correction lies at the intersection of computer science, engineering, physics, and mathematics. Classical coding theory has been around for more than 70 years, yielding an enormous literature collection. Quantum error correction is more recent but arguably more diverse, encompassing subfields from solid-state physics to complexity theory. Collecting and accurately synthesizing knowledge in this field is as formidable as it is useful. Victor Albert of ACMD and colleagues have created and actively maintain the Error Correction Zoo to categorize and organize known classical and quantum error-correction schemes. See page 91.
- ACMD's Quantum Network and Component Metrology Project focusses on the characterization of quantum network links, components, and protocols. Measurement protocols and tools are developed in our lab and deployed in our NIST Gaithersburg quantum network testbed as well as in the regional DC-QNet[4]. Last year's highlights include a demonstration to synchronize quantum network nodes to below 200 ps over 128 km distance, distribute entanglement over more than 130 km distance, and measure wavelength-dependent loss in optical fibers with some surprising results. See page 96.
- Quantum technologies are poised to revolutionize communication, time keeping, navigation, as well as fundamental science. However, at present such technologies often require expert knowledge and constant human intervention to initialize, optimize, and operate, limiting their wide-scale adoption. Justyna Zwolak and Lisa Ritter of ACMD are working with NIST PML colleagues to develop machine learning (ML) systems for autonomous closed-loop initialization, optimization, and operation of a quantum system: laser-cooled atoms. Such work serves as a baseline for how to apply ML tools to challenging problems in laboratory apparatus and field-deployable sensors, where performance guarantees and uncertainty quantification are essential. See page 22.
- Automatic viral exposure notification apps primarily operate based on the hard distance/time thresholds outlined by health organizations (e.g., 2 m/15 min by the CDC or 1 m/15 min by the WHO) to determine exposure. However, the possibility of virus transmission through inhalation for longer distances or shorter times still remain. Kamran Sayrafian, Brian Cloteaux, and Vladimir Marbukh of ACMD have developed simulations to analyze the performance of automatic exposure notification by comparing the exposure results when soft or hard thresholds are used. Their work provides insight as to how soft threshold parameters can be optimized for factors such as the surrounding environment (e.g., indoor vs. outdoor), an individual's health, the severity of the outbreak in the community, etc. See page 112.
- Barry Schneider of ACMD continues to provide leadership in the development of a culture of open science within the atomic, molecular, and optical physics community. This is being done through support of the Science Gateway for Atomic Molecular and Optical Science, which is providing access to advanced computational tools and related educational materials. See page 34.

[4] https://www.nist.gov/news-events/news/2022/06/dc-area-us-government-agencies-announce-washington-metropolitan-quantum

Technology Transfer and Community Engagement

The volume of technical output of ACMD remains high. During the last 15 months, Division staff members were (co-)authors of 59 articles appearing in peer-reviewed journals, 39 papers in conference proceedings, and 9 published in other venues. Fifteen additional papers were accepted for publication, while 42 others are undergoing review. Division staff gave 82 invited technical talks and presented 64 others in conferences and workshops. Staff members were co-inventors on six patents undergoing review.

ACMD continues to maintain an active website with a variety of information and services, most notably the Digital Library of Mathematical Functions, though legacy services that are no longer actively developed, like the Guide to Available Mathematical Software, the Matrix Market, and the SciMark Java benchmark still see significant use. During calendar year (CY) 2021, the division web server satisfied more than 6.9 million requests for pages during more than 647 000 user visits. Another indication of the successful transfer of our technology is references to our software in refereed journal articles. For example, our software system for nano-magnetic modeling (OOMMF) was cited in 252 such papers published in CY 2022 alone.

Members of the Division are also active in professional circles. Staff members hold a total of 14 editorial positions in peer-reviewed journals. For example, Barry Schneider is an Associate Editor-in-Chief for IEEE's *Computing in Science and Engineering.* Staff members are also active in conference organization, serving on 23 organizing/steering/program committees.

Service within professional societies is also prevalent among our staff. For example, Bonita Saunders is a member of the Board of Trustees of the Society for Industrial and Applied Mathematics (SIAM). Staff members are also active in a variety of working groups. Ronald Boisvert and Andrew Dienstfrey serve as members of the International Federation for Information Processing (IFIP) Working Group 2.5 on Numerical Software, Donald Porter is a member of the Tcl Core Team, Bruce Miller is a member of W3C's Math Working Group, and Sandy Ressler is a member of the W3C Advisory Committee. Barry Schneider represents NIST on the High-End Computing (HEC) Interagency Working Group of the Federal Networking and Information Technology Research and Development (NITRD) Program. Further details can be found in Part IV of this report.

Staff News

The summer of 2022 marked the first return to campus in two years for many Division staff members, though an increase in telework flexibilities allowed staff members to phase in their return slowly. We are currently experiencing a more truly hybrid working environment than before the pandemic. While this provides staff with greater opportunities to balance work life with homelife, it continues to pose challenges for the types of seamless interactions needed for state-of-the-art research. We are compensating for this in a number of ways. All of our Division seminars are now hybrid affairs to allow participation by both local and remote staff. The Division Chief holds weekly open online office hours in which staff can drop in to ask questions and discuss concerns. In addition a monthly online Division "tea" provides an opportunity for informal staff interaction wherever they might be.

Once again, this year ACMD experienced an unusually large number of staffing changes. We welcomed two new permanent staff members and four new NRC Postdoctoral Associates, while bidding farewell to four NRC postdoc and one temporary Federal staff member. We continue to host a large number of guest researchers, 38 at last count, 22 of whom work on the NIST campus with the rest being off-site collaborators. We provided internship opportunities to 23 students, including 14 graduate students, six undergraduate students, and three high school students. See Table 3 on page 129 for a list of our interns.

Further details on our staff changes and awards are provided below.

Arrivals

In November 2021 **Zachary Grey** made the transition from NRC Postdoctoral Associate to a full-time permanent ACMD staff member in Boulder. Zach received a Ph.D. in Computational and Applied Mathematics from the Colorado School of Mines in November 2019. His research interests focus on the use of differential geometry to solve real-world problems, including those requiring dimension reduction and uncertainty quantification. At NIST he has worked with CTL staff on optimizing unlicensed band spectrum sharing with subspace-based pareto tracing. He also established a collaboration with the National Renewable Energy Laboratory on optimizing the shape of wind turbine blades.

Simon Su joined ACMD as a permanent staff member on November 8, 2021. He comes to us from the Army Research Laboratory where he served as an expert in large-scale scientific data analytics and visualization, including immersive virtual reality. He will continue work on such topics in ACMD's High Performance Computing and Visualization Group. Simon holds a Ph.D. in Computer Science from the University of Houston (2001). He also has experience working at a variety of academic labs, such as the Desert Research Institute, the University of Louisiana, and Princeton University, as well as in industrial labs, such as Ball Aerospace, and Lockheed Martin.

Figure 1. *Two new permanent staff members joined ACMD in late 2021: Zachary Grey (top) and Simon Su.* (Photos provided by the subjects.)

Camilo Montoya joined ACMD as an NRC Postdoctoral Associate on June 21, 2022. Camilo holds a PhD in mathematics from Florida International University, where he explored the geometric relation between the Laplace-Beltrami spectra and eigenfunctions on compact Riemannian symmetric spaces and the Borel-Weil theory using ideas from symplectic geometry and geometric quantization. At NIST Camilo is working with Howard Cohl to study fundamental solutions for linear elliptic partial differential equations on Riemannian manifolds which are symmetric spaces, which can be thought of as special functions.

Deborah McGlynn joined ACMD as an NRC Postdoctoral Associate on September 26, 2022. She received a PhD in Civil and Environmental Engineering from Virginia Tech. In her thesis she studied the chemical impacts of biogenic volatile organic compounds (BVOCs). Such compounds, which are emitted by natural ecosystems, are highly reactive and can have a significant effect on atmospheric composition, including ozone formation. At NIST she is working with Tony Kearsley and colleagues on the development of machine learning methods for classification and uncertainty quantification of microplastics in the NIST Mass Spec Database.

On December 5, 2022, **William Earwood** began a two-year NRC Postdoctoral Associateship in ACMD. He received a PhD in Chemistry from the University of Mississippi, where he developed new theoretical methods and resulting computer software for calculating term energies and dipole polarizabilities of lithiumlike ions. At NIST, William will work with Barry Schneider on numerical methods for the time-dependent Schrodinger equation needed to study atomic and molecular systems exposed to short pulse, intense electromagnetic radiation. The methods and software will be used to calculate polyatomic excitation and ionization cross-sections, but these new methods are quite general and have applications to other areas of chemistry and physics.

Stephen Sorokanich joined ACMD as an NRC Postdoctoral Associate on December 19, 2022. Stephen received a Ph.D. in Applied Mathematics and Mathematical Physics from the University of Maryland College Park in May of 2022. For his thesis he carried out a mathematical analysis of several models for the dilute interacting Bose gas and the phenomenon of Bose-Einstein condensation (BEC). In that work he developed the spectral theory for a family of approximate Hamiltonians via their transformation by a non-

Figure 2. *New NIST/NRC postdoctoral associates this year included (l to r) Deborah McGlynn, William Earwood, Camilo Montoya, and Stephen Sorokanich***.** (Photos provided by the subjects.)

Hermitian pair excitation operator. At NIST he will work with Howard Cohl to study the nonlinear evolution of rotating self-gravitating incompressible inviscid bodies, an application of ellipsoidal harmonics.

A number of new guest researchers with projected tenures of six months or more have come on board this past year.

- Kaitlyn Hood, Assistant Professor of Mathematics at Purdue University, is working with Paul Patrone, Tony Kearsley, and colleagues on theoretical and computational models of fluid-mediated particle-particle interactions in optofluidic flow meters. The work is associated with the NIST-in-a-Drop Innovations in Measurement Science project led by ACMD.
- Joel Bowman, retired Professor of Chemistry at Emory University who has relocated to the Washington area, is working with Barry Schneider, Tony Kearsley, and colleagues on the application of AI and deep learning to problems in chemical physics.

A sharp increase in quantum information funding to support NIST research in quantum networking, including the development of DC-QNet, a multi-agency quantum networking testbed, has led to the engagement of a host of new guest researchers working on our quantum communications experimental program. These include the following postdoctoral researchers:

- Sesha Challa (Pavan Kumar), Pusan National University, India
- Hristina Georgieva, Physikalisch-Technische Bundesanstalt (PTB), Germany
- Nijil Lal Cheriya Koyyottummal, University of Napoli Federico II, Italy
- Navin Lingaraju, University of Maryland
- Samprity Saha, Virginia Commonwealth University
- Yicheng Shi, University of Singapore

Departures

Lucas Brady, a former NRC Postdoctoral Associate at NIST with a joint postdoctoral appointment at the NIST Joint Center for Quantum Information and Computer Science (QuICS) at the University of Maryland, left NIST in February 2022 to take a position at the Quantum Artificial Intelligence Laboratory (QuAIL) at NASA's Ames Research Center in Mountain View, CA. At NIST Lucas studied quantum optimization algorithms, which led to the award-winning discovery of optimal protocols for quantum annealing and quantum approximate optimization algorithms (QAOA).

Matthew (Jake) Roberts, an NRC Postdoctoral Associate who worked with Tony Kearsley, left ACMD in May 2022 to take a position at the Institute for Defense Analysis in Alexandra, VA. At NIST Jake studied mass spectra from DART-MS, a new high resolution device capable of making simultaneous measurements at different energy levels. Jake's new, and quite mathematically sophisticated, techniques for mass spec

data analysis managed to upend the conventional way data mass spectra are compared when trying to identify dangerous compounds like Fentanyl, the illegal synthetic heroin. In addition, he also continued his PhD research on approximating the generalized singular value expansion.

Danielle Brager, an NRC Postdoctoral Associate who worked with Tony Kearsley, left ACMD in August 2022 to take a position with as a data analyst at NASDAQ (yes, the stock market company) in August 2022. At NIST she worked on numerical scaling techniques for the preprocessing of mass spectrometry library data. Such preprocessing is able to maximally separate similarity scores in mass spec library searching, allowing a clearer distinguishing between compounds. In addition, she also continued her PhD thesis research on mathematical models of photoreceptor degeneration in retinitis pigmentosa.

Daniel Flynn, who was on temporary assignment as an administrative assistant in ACMD in Boulder, left NIST in August 2022 to take a position as a program manager for the non-profit Central Visitation Program in Denver. Before his appointment at NIST, Dan worked for the Peace Corps in Tanzania.

Joshua Ziegler, an NRC Postdoctoral Associate working with Justyna Zwolak, departed ACMD in September 2022 to join the research staff at Intel in Portland, OR. While his PhD dissertation at the University of Oregon was a largely experimental effort to identify and engineer optically active defects in certain materials which could serve as qubits for quantum computing, he also managed to develop a proficiency in machine learning techniques and tools. At NIST he applied this to develop techniques for the auto-tuning of quantum dots for computation in the presence of noise.

Recognition

ACMD staff members were recognized with a variety of awards this year, including the following.

Paul Patrone received the Washington Academy of Science (WAS) Award for Excellence in Research in Applied Mathematics, an honor that was conferred at the annual WAS awards banquet held on May 11, 2022. The citation reads "in recognition for contributions to uncertainty quantification of molecular simulations and material science physics of polymers." He was also named a Fellow of the WAS. Two additional ACMD staff members were also named Fellows of the Washington Academy of Science this year:

- **Raghu Kacker**
  For outstanding contributions in enabling the field of combinatorial testing to become a mainstream tool in measurement science and software engineering.
- **Kamran Sayrafian**
  In recognition of outstanding contributions to mathematical and computational modeling of body area networks.

Scott Glancy and **Emanuel Knill** of ACMD, along with four colleagues from NIST's Physical Measurement Laboratory were recipients of the 2022 Department of Commerce Gold Medal. They were honored "for pioneering experimental techniques to generate and precisely measure the quantum entanglement of two macroscopic mechanical resonators." The highest honorary award granted by the Secretary of Commerce, the Gold Medal is awarded for distinguished performance characterized by extraordinary, notable, or prestigious contributions that impact the mission of the Department. The medals were conferred at ceremonies held at DOC headquarters in January 2023. Notably, ACMD postdoc Ezad Shojaee and PREP graduate students Alex Kwiatkowski and Shawn Geller, who helped develop the theory and wrote, analyzed, and tested the data analysis code that enabled this accomplishment were not cited because they are ineligible for DOC awards since they are not Federal employees.

Three ACMD staff members were recipients of the 2021 Department of Commerce Silver Medal, which were conferred in ceremonies held in January 2022. The second highest honorary award granted by the Secretary of Commerce, this recognizes exceptional performance characterized by noteworthy or superlative contributions which have a direct and lasting impact within the Department. These staff members are:

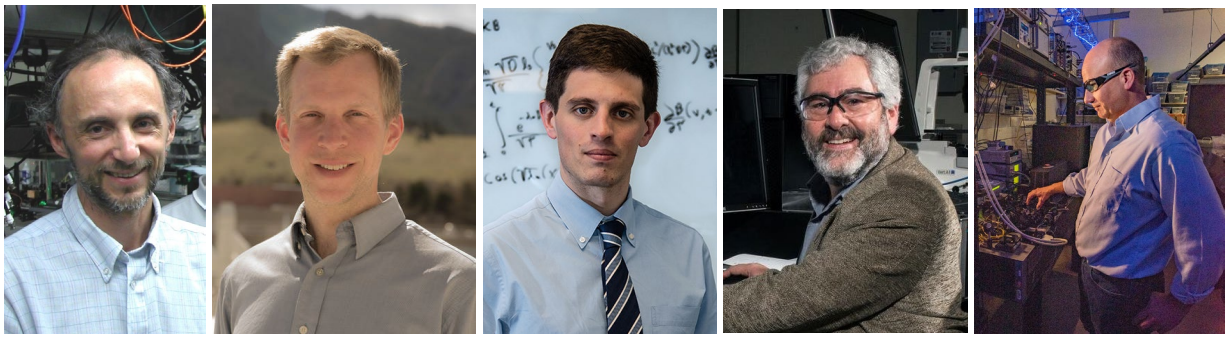

Figure 3. *Department of Commerce Medal winners from ACMD: Left to right: Scott Glancy (Gold), Emanuel Knill (Gold), Ryan Evans (Silver), Anthony Kearsley (Silver), and Thomas Gerrits (Silver).* (Photo credits: NIST)

- **Thomas Gerrits** of ACMD, along with five colleagues in PML and one in CTL were recognized for exceptional scientific achievement culminating in the first demonstration of an array of superconducting nanowire single-photon detectors (SNSPDs) with more than one thousand pixels. The NIST array represents a 15X improvement in size and pixel count and over one hundred million times better noise properties than conventional arrays. Such arrays of SNSPDs are required for the most demanding applications of imaging at ultralow light levels for astronomy, deep space communications, and medical imaging. The group's technology is already being adopted by industry.
- **Ryan Evans** and **Anthony Kearsley** of ACMD and a team of seven research chemists in MML were recognized for advancing the state-of-the-art in methods for determining the higher order protein structure of biotherapeutics. The group led two technically challenging international comparison studies, establishing the reproducibility and limitations of novel precision measurement methods. Additionally, they developed new data acquisition and analysis tools and new hardware that have hastened broad industry adoption and provide a foundation for measurements that ensure quality and accelerate development of life saving biotherapeutics and biosimilars.

Geoffrey McFadden, an ACMD mathematician and NIST Fellow, who retired in 2021, was inducted into the NIST Portrait Gallery of Distinguished Scientists, Engineers and Administrators in ceremonies held on October 28. He was cited for fundamental contributions to the theory of phase transitions, hydrodynamic and morphological stability, and thermo-solutal transport in materials. NIST Portrait Gallery honors NIST alumni for outstanding career contributions to the work of NIST. Portraits and biographies of those selected are displayed in the corridor of the NIST cafeteria at Gaithersburg, and in the Digital Portrait Gallery at NIST Gaithersburg and NIST Boulder sites. At most 10 new alumni are inducted each year.

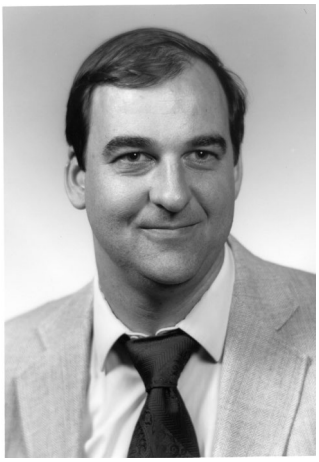

Figure 4. *Geoffrey McFadden was named a Distinguished NIST Alumnus.* (Photo credit: NIST)

In 2022, ACMD captured six of the 11 awards given out in the annual ITL Awards program. The ACMD winners were:

- **Yi-Kai Liu**
  Outstanding Contribution to ITL
  For outstanding service to ITL as Co-Director of the Joint Center for Quantum Information and Computer Science.
- **Paul Patrone and Anthony Kearsley**
  Outstanding Journal Paper
  For the paper "Classification Under Uncertainty: Data Analysis for Diagnostic Antibody Testing" published in *Mathematical Medicine and Biology* on August 13, 2021.
- **Katjana Khrac and Kamran Sayrafian**
  Outstanding Conference Paper

For "A Wearable Wireless Monitoring System for the Detection of Pulmonary Edema" presented at the IEEE Global Communications Conference on Dec. 9, 2021.

- **Chris Schanzle**
  Outstanding Technical Support
  For outstanding Technical Support in converting the High Performance Computing and Visualization Group's CAVE to the Rocky 8 Linux system.
- **Vivian Xiao**
  Outstanding Student
  A student at Poolesville High School mentored by Tony Kearsley, Vivian has made outstanding contributions to NIST research on optimization in chemometrics.
- **Ronald Boisvert**
  Outstanding Mentorship
  For providing consistent and outstanding mentorship and guidance throughout ITL.

Notably, the Outstanding Student and Outstanding Mentorship awards were new awards given out for the first time this year.

ACMD's **Bonita Saunders** was re-elected to a second term on the Society for Industrial and Applied Mathematics (SIAM) Board of Trustees in the fall of 2022. The Board of Trustees is the group responsible for the management of SIAM.

Figure 5. *Danielle Middlebrooks (left) was recognized as an MGB-SIAM Early Career Fellow and Justyna Zwolak (right) was named A QuICS Affiliate Fellow. They are shown here in a lecture hall at the University of Copenhagen, one of the birthplaces of quantum mechanics.* (Photo credit: J. Zwolak)

A contributed talk by ACMD Associate **Prajakta Bedekar** won 2nd place in the competition for best talk at the Workshop in Mathematical and Computational Biology held online on June 9-10, 2022. Her talk was entitled "Time-dependent prevalence estimation and optimal classification for antibody testing." Prajakta, who holds a Ph.D. in mathematics from the University of Houston splits her time between NIST and Johns Hopkins University.

Also, this year ACMD mathematician **Justyna Zwolak** was named an Affiliate Fellow of the NIST/UMD Joint Center for Quantum Information and Computer Science (QuICS). Scientists from NIST with interests appropriate to the QuICS scientific program may be selected as QuICS Affiliate Fellows by a three-quarters majority vote of all active QuICS Fellows. Such an appointment recognizes scientific contributions and job status substantially equivalent to those of a QuICS Fellow. Justyna has collaborated with QuICS members for some time on machine learning techniques for the tuning of quantum dots for computation.

In late 2022 ACMD mathematician Danielle Middlebrooks was selected to receive an MGB-SIAM Early Career (MSEC) Fellowship for the 2023-2025 term. The MGB-SIAM Early Career Fellowship reflects a joint commitment by Mathematically Gifted & Black (MGB) and the Society for Industrial and Applied Mathematics to promote long-term engagement of researchers within SIAM and continued success within the wider applied mathematics and computational sciences community. The fellowship will provide multiple opportunities to network with and contribute to the SIAM community, such as special events, professional development workshops, committee shadowing, cohort-specific activities, as well as formal and informal mentoring by and with other members of the SIAM community.

Finally, ACMD's **Jeffrey Fong** celebrated his 50th anniversary as a NIST staff member this year. Jeffrey started his NIST career as an NRC Postdoctoral Associate in 1966 after receiving a Ph.D. in Applied Mechanics and Mathematics from Stanford University. During his long career, Jeffrey's research has focused on fatigue, the study of how materials and structures age so that we can accurately judge their useful, and safe, lifetimes. He has developed complex mathematical models of the physics of fatigue processes. He has developed techniques for non-destructive monitoring of structures to automatically detect developing flaws. He pioneered the use of computers to carry out fatigue studies. He was a very early user of so-called finite-element modeling, which has revolutionized engineering design. In recent years he has concentrated on understanding the *uncertainty* in mathematical and computational models so that predictions using them can be made more reliably. He has also been a proponent of the use of sound statistical methods in engineering analysis and has taught courses around the world on best practices. While Jeffrey has recently celebrated his 88th birthday, he continues to enthusiastically contribute to the important work of NIST.

Figure 6. *Jeffrey Fong at his 88th birthday celebration.* (Photo credit: R. Boisvert)

Part II

Features

Reducing Bias and Quantifying Uncertainty in Fluorescence Produced by PCR

Quantitative PCR (qPCR) is routinely employed in healthcare diagnostics, forensics, and biotechnology research. It can calculate, or quantify, the concentration of a specific sequence of nucleic acids present in a sample. However, quantification is limited by systematic and subjective bias, as well as the lack of a quantitative expression for uncertainty. We have developed an improved mathematical model which can reduce several sources of bias and quantify the uncertainty in fluorescence. It also provides new insight into PCR dynamics, sources of error, and limits of detection.

Robert DeJaco

Motivation. The Polymerase Chain Reaction (PCR) is a hallmark of molecular biology and applied genetics. It involves a series of heating—cooling cycles during which each DNA strand is replicated. When the progress of the reaction is monitored by a fluorescent probe for each cycle 1 to 45, as depicted in Figure 7, the technique is called quantitative PCR, or qPCR.

To understand why qPCR is called quantitative, it is important to examine the procedure for calculating N_0, the initial number of DNA strands present in the sample, from the measurement of fluorescence.

The quantitative aspect of qPCR arises from the popular equation for PCR kinetics,

$$N_i = N_0(1+p)^i, \tag{1}$$

where N_i is the number of DNA strands present after i cycles, and p is the amplification efficiency. The amplification efficiency usually ranges from 0.85 to 0.99, as not all DNA strands are replicated. After performing a set of control experiments to determine p, N_0 can be quantified, or calculated, from N_i by rearranging Equation (1), or $N_0 = N_i/(1+p)^i$.

However, it is extremely challenging to measure N_i directly. Instead, a fluorescent probe is added to the reaction mixture, and the fluorescence of the solution, F_i, is measured. To calculate N_0 from F_i at a particular cycle i, an additional model is required to relate fluorescence to DNA content. While there are many approaches available, the most common entails

$$F_i = b_1 + b_2 i + dN_i, \tag{2}$$

where b_1, b_2, and d are constants. The term $b_1 + b_2 i$ is often referred to as the background, or baseline, fluorescence. This is the portion of the fluorescence that is not associated with amplification. The term d corresponds to the incremental increase in fluorescence, or the amount that the fluorescence increases for each amplification. Having determined b_1, b_2, d, and p, and measured F_i, quantification involves calculation of N_0 from Equation (1) and (2).

This process is limited by systematic and subjective bias. Equation (2) assumes that the fluorescence increases each time *each strand* is replicated. However, this is not consistent with the underlying biochemistry.

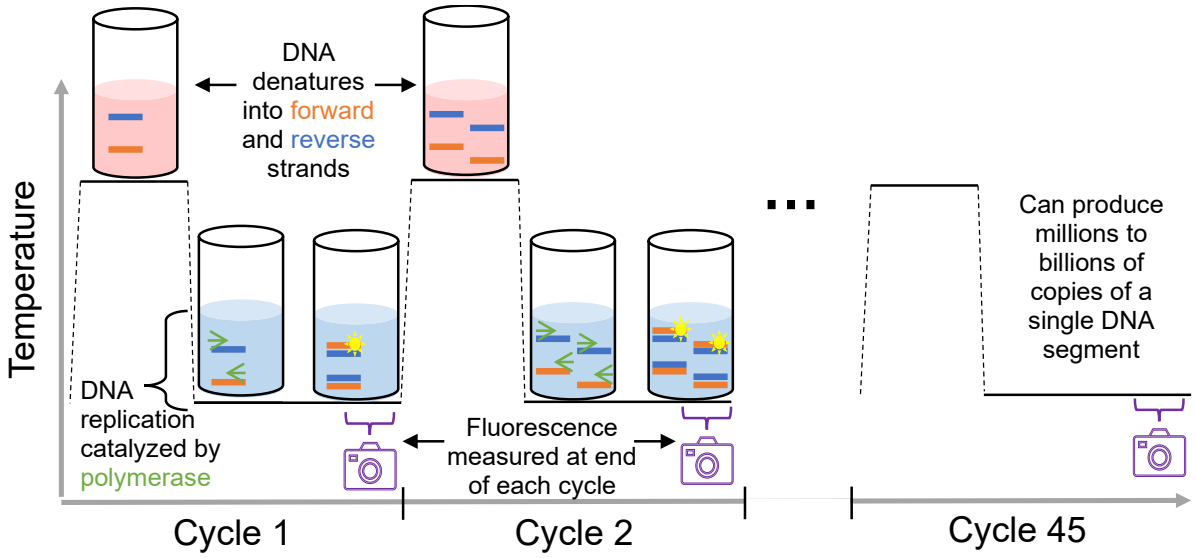

Figure 7. *In the Polymerase Chain Reaction, a sample is subjected to a series of heating—cooling cycles. After each strand is separated at high temperature, DNA replication occurs at low temperature. In real-time PCR, the fluorescence associated with a certain reporter chemistry is measured during each cycle. Often, the fluorescence only increases when one of the strands is replicated.*

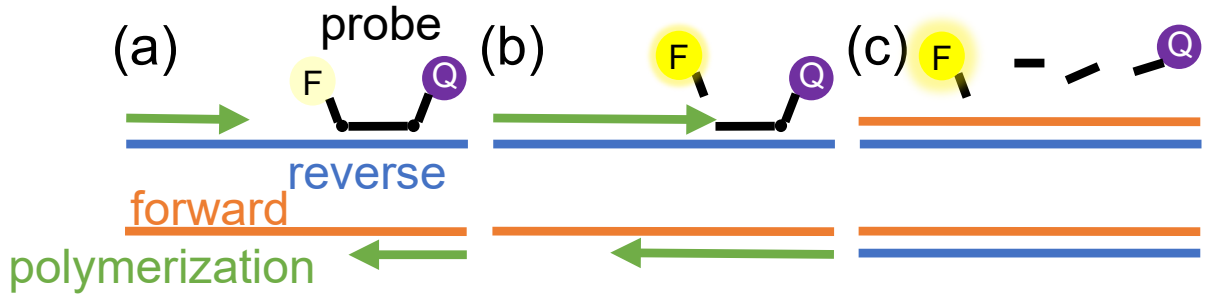

Figure 8. *Illustration of relationship between successful DNA replication and changes in fluorescence associated with a hydrolysis probe. (a) As polymerization begins, the hydrolysis probe binds. The probe is in its inactive state, where fluorescence emitted by the fluorophore ('F') is quenched by the quencher ('Q') in close proximity. (b) As DNA polymerization reaches the location of the probe, the probe is hydrolyzed (activated). (c) After successful production of a forward strand (orange) from a reverse strand (blue), the fluorophore is activated, as it is no longer near the quencher.*

DNA consists of two strands, each consisting of a sequence of nucleotides. As each strand is complementary (i.e., nucleotide A pairs with nucleotide T and nucleotide G pairs with nucleotide C), each strand is different. For most fluorescence reporters [1], the fluorescence only increases when *one* of the complementary strands is replicated (see Figure 8). Equation (2) also assumes that the fluorescence not associated with amplification is a linear function of cycle, or $b_1 + b_2 i$. It is not clear how such terms are related to the underlying physical and chemical phenomena occurring in solution. Furthermore, the terms $b_1, b_2,$ and d are determined subjectively by looking at how the fluorescence changes with cycle and estimating where the linear and exponential regions occur.

qPCR is also limited by a lack of accounting for uncertainty. While Equation (1) does account for the fact that DNA amplification is imperfect (i.e., $p < 1$), it does not account for the uncertainty in the total number of DNA strands due to imperfect amplification. It also does not account for uncertainty in the initial copy number of DNA. Since pipetting errors are always present, the initial copy number is not known exactly. A quantitative expression for uncertainty is necessary to determine a more reliable estimate of the limit of detection, or the lowest concentration of nucleic acids that can be determined with statistical significance.

To reduce bias and quantify uncertainty in the fluorescence produced by PCR, we developed improvements to Equations (1) and (2). Analysis of the new model provides new insight into PCR dynamics and uncertainty. By extracting the baseline *a priori* with a slight modification of control experiments, a more objective description of background fluorescence is obtained. Finally, the approach allows for a more robust estimate of the limit of detection. The more robust estimate of the limit of detection may be particularly useful for application in epidemic diseases, as false positives or false negatives may be instead termed inconclusive.

New Model. To distinguish between complementary strands of DNA, we call one strand the forward strand and the other the reverse strand (see Figure 8, where DNA synthesis (green) occurs in opposite directions).

We model the replication of DNA with the strand-specific, stochastic branching-process

$$X_i = X_{i-1} + \text{Binomial}(Y_{i-1}; p_{\text{rf}}), \tag{3a}$$

$$Y_i = Y_{i-1} + \text{Binomial}(X_{i-1}; p_{\text{fr}}), \tag{3b}$$

where X_i is a discrete random variable representing the number of forward strands present at each cycle $i = 1$ to 45, Y_i is a discrete random variable representing the number of reverse strands, p_{rf} is the efficiency of producing a forward strand from a reverse strand, and p_{fr} is

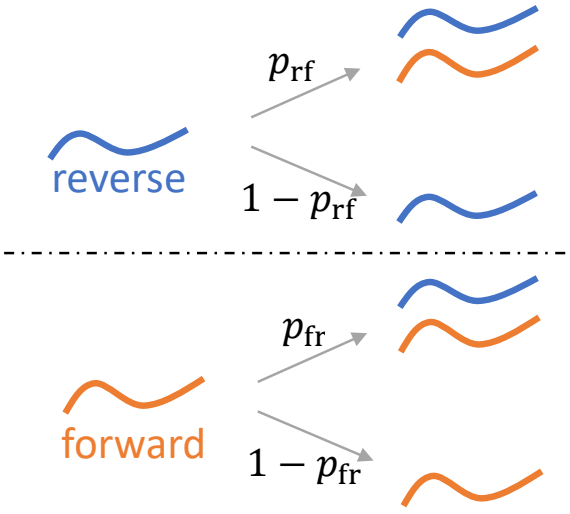

Figure 9. *Illustration of strand-specific model of DNA amplification. (top) After each cycle, the outcome of synthesis of a forward strand (orange) from each reverse strand (blue) present in the previous cycle is modeled as a Bernoulli random variable with success probability $\boldsymbol{p}_{rf}$. (bottom) Similarly, the outcome of synthesis of a reverse strand (blue) from each forward strand (orange) present in the previous cycle is modeled as a Bernoulli random variable with success probability $\boldsymbol{p}_{fr}$.*

the efficiency of producing a reverse strand from a forward strand. The notation Binomial$(n;p)$ denotes a Binomial random variable with n independent trials of success probability p. A schematic of one trial event for each strand is depicted in Figure 9.

Since X_i and Y_i are random variables, we do not know their exact value. However, we were able to compute their expected values $E[X_i]$, $E[Y_i]$ and variances $\mathrm{Var}[X_i]$, $\mathrm{Var}[Y_i]$. We will first discuss the expected values and the revelations they provide for PCR dynamics.

As i becomes large, we derived [4] that

$$E[X_i] = \frac{E[X_0 + RY_0]}{2}(1+\bar{p})^i + O((1-\bar{p})^i)$$
$$E[Y_i] = RE[X_i] + O((1-\bar{p})^i)$$

where $\bar{p} = \sqrt{p_{\mathrm{rf}}p_{\mathrm{fr}}}$ represents the geometric mean of the efficiency of each complementary strand and $R = \sqrt{\frac{p_{\mathrm{rf}}}{p_{\mathrm{fr}}}}$ characterizes the deviation in complementary efficiencies. The term $O((1-\bar{p})^i)$ goes to zero as i becomes large. If we let $N_i = X_i + Y_i$ be a discrete random variable representing the total number of strands at cycle i, we can add these expressions to yield

$$E[N_i] = E[X_0 + RY_0]\left(\frac{1+R}{2R}\right)(1+\bar{p})^i + O((1-\bar{p})^i).$$

The expected values provide new intuition on the dynamics of PCR. By comparing the expression for $E[N_i]$ above with Equation (1), it can be observed that the conventional amplification efficiency in PCR, p, is more generically interpreted as $\bar{p} = \sqrt{p_{\mathrm{rf}}p_{\mathrm{fr}}}$, the geometric mean of the amplification efficiency of each complementary strand. When $R = 1$ (i.e., $p_{\mathrm{rf}} = p_{\mathrm{fr}}$), $E[N_i] = E[N_0](1+p)^i + O((1-p)^i)$. Equation (1) is really the expected value of a discrete random variable. Finally, the expected strand counts do not necessarily tend toward the same values, as

$$\lim_{i\to\infty}\frac{E[X_i]}{E[Y_i]} = R = \sqrt{\frac{p_{\mathrm{rf}}}{p_{\mathrm{fr}}}}.$$

We were also able to calculate the variances $\mathrm{Var}[X_i]$ and $\mathrm{Var}[Y_i]$. As i becomes large,

$$\mathrm{Var}[X_i] = \frac{\nu(1+\bar{p})^{2i}}{4} + O((1+\bar{p})^i),$$
$$\mathrm{Var}[Y_i] = \frac{\nu(1+\bar{p})^{2i}}{4R^2} + O((1+\bar{p})^i),$$

where ν is defined as

$$\nu = \mathrm{Var}[X_0 + RY_0] + E[X_0 + RY_0]\left(\frac{1+R}{2}\right)\left(\frac{1-\bar{p}}{1+\bar{p}}\right) + E[X_0 - RY_0]\left(\frac{1-R}{2}\right)\left(\frac{1+\bar{p}}{3+\bar{p}}\right).$$

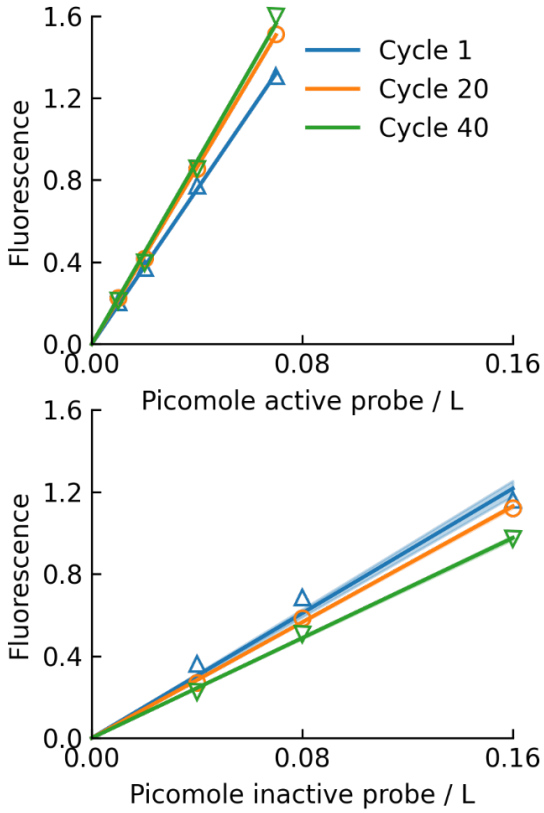

Figure 10. *Fluorescence as a function of concentration of active probe (top) and concentration of inactive probe (bottom) measured (symbols) in well E5 and modeled (lines and shadings). Different colors correspond to different cycles.*

The terms on the right-hand-side of the expression for ν correspond (respectively) to the initial variance, the variance from imperfect amplification, and the variance associated with the change in ratio of expected values from their initial values to R. While the expected values are proportional to $(1+\bar{p})^i$, the variances are proportional to $(1+\bar{p})^{2i}$. In other words, the variance grows at twice the rate as the expected value. However, the coefficient of variation,

$$CV(X_i) = \frac{\sqrt{\mathrm{Var}[X_i]}}{E[X_i]} = \frac{\sqrt{\nu}}{E[X_0 - RY_0]} + O((1+\bar{p})^{-i}),$$

tends toward a constant as $i \to \infty$. Given the initial distribution and values for R and $\bar{p}$, the expression for $CV(X_i)$ is a very practical formula describing the variation in strand count.

To connect DNA content predicted by the expected values and variances to the fluorescence, we use the fluorescence analogue of Beer's Law. In the past, such a model been used to describe the fluorescence associated with aqueous solutions containing DNA and fluorescent dyes [2]. To our knowledge, however, this approach has not been applied to the fluorescence produced by PCR.

In brief, we model the total fluorescence as a sum of the fluorescence arising from two different species:

the inactive and active probe. (For an illustration of the active and inactive probe, see Figure 8.) The fluorescence arising from each species is described as the fluorescence per species times the concentration of each species. The concentrations of each species are altered in response to PCR.

Model Assessment and Application. To assess the validity of the fluorescence model, we performed qPCR experiments with various concentrations of inactive and active probes in the absence of DNA. We used hydrolysis probes associated with the Centers for Disease Control and Prevention 2019-nCoV_N1 assay [3]. The results are shown in Figure 10. Since the experimental data can be described by a line at each cycle, the model is valid. Unlike the conventional approach for modeling fluorescence not associated with DNA amplification, Equation (2), we can assess the validity of our model and use it to describe biophysical phenomena more appropriately.

Having extracted the parameters as depicted in Figure 10, we used the model to relate fluorescence to DNA content. The moments of the fluorescence at cycle i, or F_i, are

$$E[F_i] = b_i + d_i[E[X_i] - E[X_0]],$$
$$\mathrm{Var}[F_i] = d_i^2\left[\mathrm{Var}[X_i] + \mathrm{Var}[X_0] - 2\mathrm{Cov}[X_i, X_0]\right],$$

for $i = 1$ to 45. The background term b_i represents the total fluorescence that the solution would have at cycle i if all probes were present in the inactive state. The incremental increase term represents the change in fluorescence associated with converting one inactive probe to an active probe at cycle i. Note that unlike Equation (2), we do not require b_i to be a linear function of cycle. We also do not require d_i to be constant. As the slopes of the lines in Figure 10 are not independent of cycle, the incremental increase d_i is also not independent of cycle. This is another source of bias that our approach can eliminate.

With b_i and d_i determined from the parameters associated with Figure 10, we used the model to calculate fluorescence curves with uncertainty (assuming each strand initially obeys a Poisson distribution). According to the values for b_i and d_i determined for a typical experiment, $b_i \approx 1$ and $d_i \approx 10^{-6}$. By examining the expression for $E[F_i]$, this demonstrates that $E[X_i - X_0] \approx 10^6$ for the fluorescence to rise above background levels. With such a large sample size, it is natural to invoke the central limit theorem and assume that X_i obeys a normal distribution.

Typical fluorescence curves are depicted in Figure 11. At low cycle numbers, the fluorescence does not increase exponentially with cycle. While DNA is increasing exponentially, the fluorescence is not because the value for b_i (approximately 1) is much larger than the changes in $d_i E[X_i - X_0]$ (recall that $d_i \approx 10^{-6}$). After significant DNA has been amplified, the expected

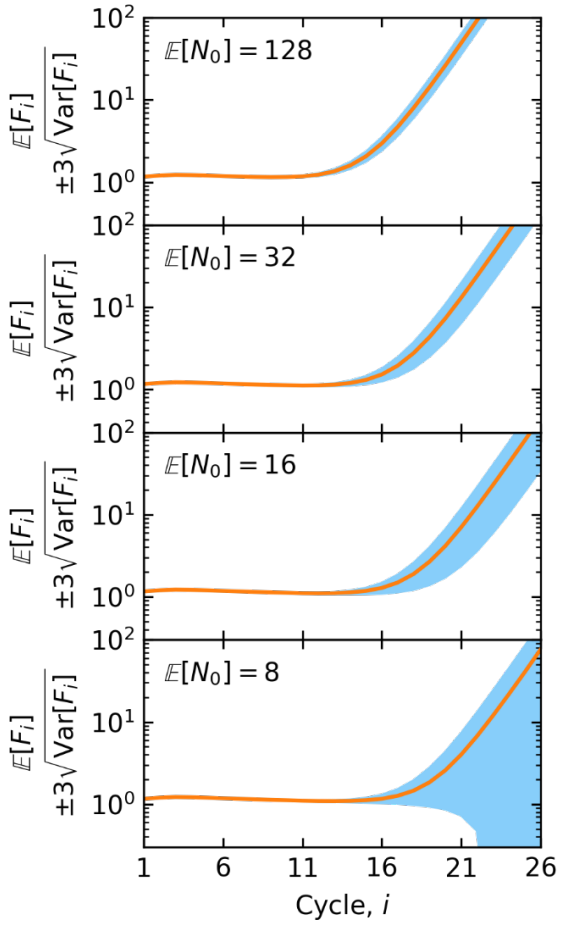

Figure 11. *Fluorescence curves calculated from amplification model with $\bar{\boldsymbol{p}} = \mathbf{0.9}$ and $\boldsymbol{R} = \mathbf{1}$ assuming $\boldsymbol{X_0}$ and $\boldsymbol{Y_0}$ are independent and identically distributed. Each subplot is associated with a different expected total initial copy number, or $\boldsymbol{E[N_0]}$. The orange curve represents $\boldsymbol{E[F_i]}$, while the light blue region depicts 3 standard deviations.*

value for fluorescence (orange line) begins to increase exponentially with cycle. In this regime, the uncertainty in fluorescence (blue shaded region) increases dramatically with cycle. However, the size of the uncertainty region relative to the expected value appears to approach a constant. This is because the coefficient of variation, or $CV(F_i)$, approaches $CV(X_i)$, a constant as $i \to \infty$.

With decreasing $E[N_0]$, several enlightening trends are evident. First, when $E[N_0]$ is smaller, it takes more cycles for exponential growth in $E[F_i]$ to be observed. This is because more replication is needed to release enough fluorescence that is comparable to the background. Second, the error in fluorescence increases. Eventually, the error is so large that the fluorescence does not increase above its initial value in a statistically significant manner (see the bottom row of Figure 11). The smallest value for $E[N_0]$ that admits a fluorescence value that is statistically larger than its background value is referred to as the limit of detection. According to Figure 11, when we expect the initial copy number to be 16

or more, we can detect significant amplification. When we expect the copy number to be 8 or less, however, the initial copy number is below the limit of detection.

It turns out that our observations of the trends in uncertainty can be formalized to develop analytical expressions for the limit of detection [4]. These expressions may be particularly useful for application in epidemic diseases, as false positives or false negatives may be instead termed inconclusive.

In the future, this approach could be extended to reduce bias and quantify uncertainty in DNA content present in a sample. In this case, one might instead call the approach UQ-PCR (Uncertainty Quantification by PCR).

References

[1] J. M. Ruijter, P. Lorenz, J. M. Tuomi, M. Hecker, and M. J. B. van den Hoff. Fluorescent-increase Kinetics of Different Fluorescent Reporters Used for qPCR Depend on Monitoring Chemistry, Targeted Sequence, Type of DNA Input and PCR Efficiency. *Microchimica Acta* **181** (2014), 1689—1696. DOI: 10.1007/s00604-013-1155-8

[2] T. Biver, A. De Biasi, F. Secco, M. Venturini, and S. Yarmoluk. Cyanine Dyes as Intercalating Agents: Kinetic and Thermodynamic Studies on the DNA/Cyan40 and DNA/CCyan2 Systems. *Biophysical Journal* **89** (2005), 374—383. DOI: 10.1529/biophysj.105.059790

[3] National Center for Immunization and Respiratory Diseases (U. S.). Division of Viral Diseases: 2019-Novel Coronavirus (2019-nCoV) Real-time rRT-PCR Panel Primers and Probes. (Jan 24, 2020). URL: https://stacks.cdc.gov/view/cdc/84525

[4] R. F. DeJaco, M. J. Roberts, E. L. Romsos, P. M. Vallone, and A. J. Kearsley. Reducing Bias and Quantifying Uncertainty in Fluorescence Produced by PCR. In review.

Participants

Robert DeJaco, Matthew Roberts, Anthony Kearsley (ACMD); Erica Romsos, Peter Vallone (NIST MML)

Combining Machine Learning with Physics: Enhanced Dark Soliton Detection in Bose-Einstein Condensates

Quantum technologies are poised to revolutionize communication, time keeping, navigation, as well as fundamental science. However, at present such technologies often require expert knowledge and constant human intervention to initialize, optimize, and operate, limiting their wide-scale adoption. Commercialization and deployment of quantum technologies require yet undeveloped tools for autonomous control of physical systems that currently exist only in laboratories. Our efforts focus on overcoming some of these limitations by developing machine learning (ML) systems for autonomous closed-loop initialization, optimization, and operation of a quantum system: laser-cooled atoms. Our work serves as a baseline for future investigation of how to apply ML tools to specific, challenging problems in laboratory apparatus and field-deployable sensors, where performance guarantees and uncertainty quantification are essential.

Justyna Zwolak

Harnessing the power of quantum systems ultimately hinges on measurement: the desired information must first be transferred from a quantum system to a classical measurement system, where the useful quantities in that measurement must then be extracted. The majority of data in quantum-gas experiments comes from direct images. Absorption imaging—by far the most popular technique—provides information about the atoms' spatial distribution, number, and temperature. While the analysis for such data is sophisticated, features are still detected and located using conventional fitting techniques, which are constrained by our limited ability to anticipate patterns in visual data.

ML-based image classification has many applications in science, from particle physics data analysis, dark matter searching, quantum state preparation to material property prediction. In atomic physics, ML has been used to locate topological phase transitions in images of atomic density and to characterize particles in disordered fields. However, while ML techniques have enabled autonomous parameter exploration and optimization in some systems, the use of ML in cold-atom systems remains nascent. In our recent work, we introduced and demonstrated a hybrid framework, shown in Figure 12, that integrates ML techniques with a science-driven analysis to detect, classify, and assess quality of features in experimental data from many-body atomic physics.

Using cold-atom Bose-Einstein condensates (BECs), we focus on solitonic excitations, robust solitary waves that retain their size, shape, and speed as they travel. These properties arise from an interplay between nonlinearity and dispersion that is present in many physical systems. Since their first observation in water channels, solitons have been found in rivers and seas; BECs; optical fibers; astronomical plasmas; and even human blood vesicles. Due to their inherent stability, solitons in optical fibers have found commercial applications in long-distance, high-speed transmission lines.

While the noisy natural environment does not allow for the controlled study of fragile quantum solitons, BECs are an ideal medium where individual or multiple solitons can be created on-demand, with all their properties, such as position and velocity, tuned as necessary [2, 3]. Most measurements in BEC experiments produce raw data in the form of images that, in our context, provide information about the excitations' positions within the BEC. The challenge is to identify the number, type, and the exact location of excitations efficiently and reliably. Prior to this work, such information was obtained starting with traditional fits that were then manually validated and corrected [2], inhibiting the automated

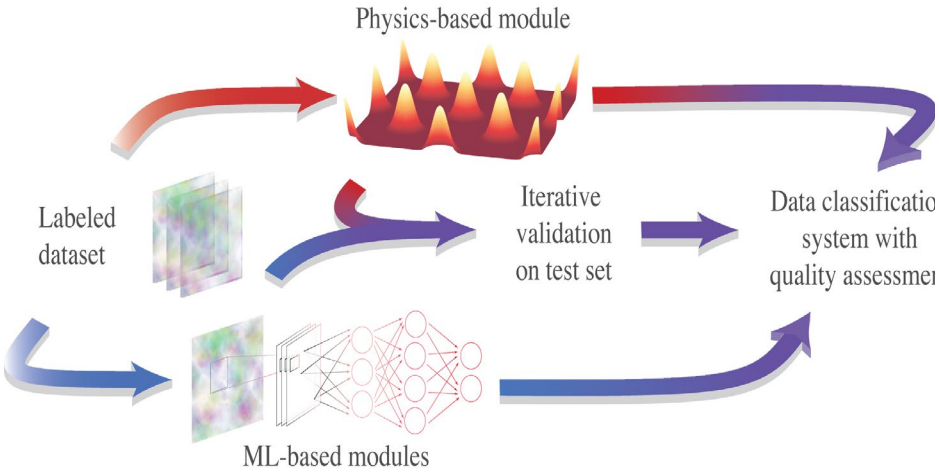

Figure 12. *Framework overview. The colored arrows link the preparation, validation, and application phases of the framework. The red path represents the preparation and implementation of the physics-based-approximation module while the blue path represents the ML modules. Adapted from Ref. [1].*

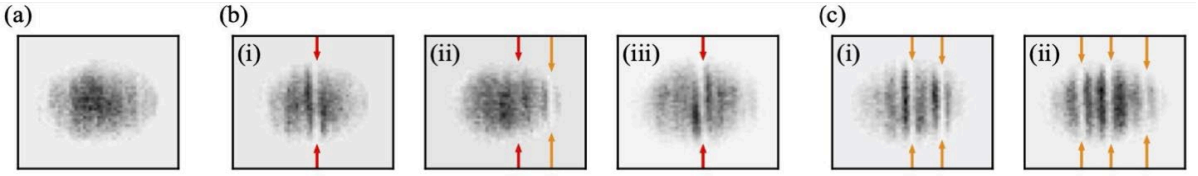

Figure 13. *The pre-processed images from the Dark solitons in BECs dataset. The red arrows mark the location of the deepest depletion in the density fluctuations, while the orange lines mark the solitons' locations found from our object detector. (a) An element of the no-excitation class. (b) Three elements of the single excitation class: (i) a single longitudinal soliton, (ii) an off-center longitudinal soliton, and (iii) a solitonic vortex. (c) Two representative elements of the other excitations class showing multiple solitons. Adapted from Ref. [1].*

analysis of large datasets, which is crucial for solitonic dynamics studies.

Dark solitons appear as local depletions in BEC-density, thus, visual inspection of the data is often sufficient to determine the number and position of solitons in BEC. Experiments involving solitons' dynamics, however, hinge on large datasets and human-driven analysis are both tedious and error-prone. Semi-scripted protocols can process the data, but the final decision about the number and position of the solitons within BECs still has to be validated manually [4].

In our previous work, we developed a solitonic excitation detection and positioning system that takes image data as the input and outputs information about whether a single soliton is present, and, if it is, where it is located [5]. This algorithm comprises a data preprocessor that converts raw data into a ConvNet-compatible format; a ConvNet image classifier that determines if a single soliton is detected; and a traditional least-squares fitting position regressor that locates the soliton within the BEC, when applicable. However, given that the fitting techniques can locate solitons only if the soliton number is known in advance and that the ConvNet classifier requires significant amount of data per expected class for training, the utility of our soliton detection and positioning system left room for improvement.

The revised iteration of the soliton detecting framework includes the ability to detect the precise position of the solitons along with a model that further refined the classification of the images. A final step was also added to determine the quality of the detected solitons. The analysis of the images still begins with the ConvNet classifier developed previously, but then is followed by a ML object detector (OD) which automatically localizes the features of interest (i.e., all solitonic excitations within the BEC). A physics-informed excitation (PIE) classifier then provides a fine-grained classification of individual solitonic excitations into physically motivated categories, such as clear longitudinal solitons, or solitonic vortices. Finally, a quality estimator is applied to the longitudinal solitons class to ascertain if the one-dimensional profile of a given excitation has parameters in the range expected for a well-formed solitonic excitation. This eliminates images of solitons that are faint, or malformed, leaving only well-formed solitons for further analysis. We recently published an article reporting this work [1].

Examples of the categorization of the BEC clouds reported in [1] can be seen in Figure 13. As a practical test case, we concentrate on identifying dark solitons, which are spatially localized excitations that appear as vertically aligned atomic density depletions in BECs, see Figure 13(b,c). Deep depletions are caused by kink solitons (and solitonic vortices viewed from the side), as in Figure 13(b-i), whereas shallow and asymmetric depletions can be caused by solitonic vortices, as in Figure 13(b-iii). Our framework is the first to automatically differentiate between these instances and locate all solitonic excitations in each image. Importantly, neither of the ML modules require data labeled with the physically motivated sub-categories, which significantly lessens the burden of manual labeling. In fact, the OD is trained using only the no excitation and lone excitation data.

As part of this research effort, we established and curated a dataset of over 16,000 experimental images of BECs with and without solitonic excitations [6, 7]. The dataset consists of images manually labeled into the three pre-defined categories (i.e., no excitations, lone excitation, other excitations; 33 % of the data) and unlabeled data. The lone excitation class is in addition tagged with the excitation position, PIE class, and quality score. The remaining 67 % of the data is automatically labeled using our SolDet package [11], an implementation of a physics-informed ML data analysis framework consisting of a convolutional-neural-network -based classifier and object identifier as well a statistically motivated physics-informed classifier and a quality metric. This dataset is available at NIST [6] and at data.gov to provide an opportunity for the data science community to develop more sophisticated analysis tools and to further understand nonlinear many-body physics.

Our current efforts focus on further improving this high-level framework. First, to expand the potential user base of the software, we are shifting the ML framework from TensorFlow to PyTorch. Complimentary to this, generalizing aspects of the PIE classifier are being added. The first iteration of the PIE classifier includes physics-informed cuts that were manually derived from

BEC data coming from a NIST experiment [7]. To ensure the compatibility of SolDet package with data coming from different experimental groups, we are refining these cuts using a more diverse dataset on BEC images. Additionally, it had been noted in [1] that the quality estimator can be unreliable when two or more solitonic excitations appear close together. To address this issue, we are working on an extended version of the quality estimator that will properly handle the multi-excitation cases. With these updates, we hope that SolDet will become a useful tool for data analysis for other groups working on BEC experiments.

The autonomous extraction of information from images is a first step toward demonstration a holistic approach: combining ML, physics-based simulations, and experiment to enable full automation of quantum technologies. Our next steps include autonomous extraction of the relevant magneto-optic trap (MOT) parameters, optimization of the pulses used to load MOTs, and autonomous optimization and operation of cold-atom experiments.

Gases of laser-cooled atoms underpin a host of standards including time and vacuum [8] and can be used for sensitive measurement of inertial forces and magnetic and electric fields. In recent years, miniaturized cold-atom systems to realize field-deployable sensors and standards that promise unmatched precision and accuracy have been developed [9, 10]. Yet, even with these technologies, constant human intervention is required to optimize, control, and explore the large space of tens to possibly a hundred control parameters, leading to limited commercial applications. Realizing fully autonomous, self-calibrating cold-atom based experiments will enable a low cost, high-reliability interface to atomic devices. By combining theoretical, computational, and experimental efforts, this interdisciplinary research will blaze a trail for the broader use of ML to improve complex physics and engineering systems.

References

[1] S. Guo, S. M. Koh, A. R. Fritsch, I. B. Spielman, and J. P. Zwolak. Combining Machine Learning with Physics: A Framework for Tracking and Sorting Multiple Dark Solitons. *Physical Review Research* **4** (2022), 023163.

[2] A. R. Fritsch, Mingwu Lu, G. H. Reid, A. M. Piñeiro, and I. B. Spielman. Creating Solitons with Controllable and Near-zero Velocity in Bose-Einstein Condensates. *Physical Review A* **101** (2020), 053629.

[3] L. M. Aycock, H. M. Hurst, D. K. Efimkin, D. Genkina, H-I Lu, V. M. Galitski, and I. B. Spielman. Soliton Diffusion in Bose–Einstein Condensates. *Proceedings of the National Academy of Sciences* **114** (2017) 2503-2508.

[4] M. Lakshmanan. *Integrable Nonlinear Wave Equations and Possible Connections to Tsunami Dynamics*. In: *Tsunami and Nonlinear Waves* (A. Kundu, ed.), Springer, Berlin, 2007, 31-49.

[5] S. Guo, A. R. Fritsch, C. Greenberg, I. B. Spielman, and J. P. Zwolak. Machine-learning Enhanced Dark Soliton Detection in Bose-Einstein Condensates. *Machine Learning: Science and Technology* **2** (2021), 035020.

[6] National Institute of Standards and Technology. Dark solitons in BECs dataset (2022). Database: data.nist.gov [Internet]. DOI: 10.18434/mds2-2363

[7] A. R. Fritsch, S. Guo, S. M. Koh, I. B. Spielman, and J. P. Zwolak. Dark Solitons in Bose–Einstein Condensates: A Dataset for Many-body Physics Research. *Machine Learning: Science and Technology* **3**, 047001 (2022).

[8] S. Eckel, D. S. Barker, J. A. Fedchak, N. N. Klimov, E. Norrgard, J. Scherschligt, C. Makrides, and E. Tiesinga. Challenges to Miniaturizing Cold Atom Technology for Deployable Vacuum Metrology. *Metrologia* **55** (2018), S182.

[9] W. R. McGehee, W. Zhu, D. S Barker, D. Westly, A. Yulaev, N. Klimov, A. Agrawal, S. Eckel, V. Aksyuk, and J. J. McClelland. Magneto-optical Trapping Using Planar Optics. *New Journal of Physics* **23** (2021), 013021.

[10] D.S. Barker, E.B. Norrgard, N.N. Klimov, J.A. Fedchak, J. Scherschligt, and S. Eckel. Single-Beam Zeeman Slower and Magneto-Optical Trap Using a Nanofabricated Grating. *Physical Review Applied* **11** (2019), 064023.

[11] J. P. Zwolak, S. Guo, S. M. Koh, A. R. Fritsch, and I. B. Spielman. soldet: Solitonic Feature Detection Package. GitHub, May 2022. DOI: 10.18434/mds2-2363

Participants

Justyna P. Zwolak, Lisa Ritter (ACMD); Ian B. Spielman (NIST PML); Sophia M. Koh (Amherst College); Shangjie Guo, Amilson R. Fritsch (University of Maryland).

Part III

Project Summaries

Mathematics of Metrology

Mathematics plays an important role in measurement science. Mathematical models are needed to understand how to design effective measurement systems and to analyze the results they produce. Mathematical techniques are used to develop and analyze idealized models of physical phenomena to be measured, and mathematical algorithms are necessary to find optimal system parameters. Mathematical and statistical techniques are needed to transform measured data into useful information. We develop fundamental mathematical methods and tools necessary for NIST to remain a world-class metrology institute, and to apply these to measurement science problems

TOMCAT: X-ray Imaging of Nanoscale Integrated Circuits for Tomographic Reconstruction

Bradley Alpert
Nathan Nakamura (NIST PML)
Zachary Levine (NIST PML)
Dan Swetz, Joel Ullom, et al. (NIST PML)
Edward Jimenez, Amber Dagel, et al. (Sandia National Laboratory)
George Barbastathis et al. (MIT)

As the leading semiconductor manufacturing techniques progress through 10 nm, 7 nm, and now 5 nm technology nodes, the ability to fabricate these chips has outrun the ability to image them. This limitation makes a variety of diagnostic needs much more difficult to satisfy. The NIST Quantum Sensors Group (PML), in collaboration with researchers at Sandia National Laboratory, is leading a project for IARPA's RAVEN (Rapid Analysis of Various Emerging Nanoelectronics) program to develop a small-laboratory capability to image integrated circuits by x-ray tomography. In distinction from other RAVEN projects, TOMCAT exploits a scanning electron microscope (SEM) rather than a synchrotron beamline and does not destroy the chip under test. This is enabled by the exquisite energy resolution of NIST-developed cryogenic microcalorimeter spectrometers, comprised of transition-edge sensors (TES), which are being extended to larger arrays (now to 3000 detectors), as well as with better individual-detector throughput (up to 1000 counts/s) and energy resolution (< 10 eV FWHM). The detectors measure fluorescent photons produced when SEM electrons strike a target following their differential attenuation by different materials in the chip.

A principal analysis challenge of the project, enabling tomographic structure recovery in this limited exposure angle, limited-photon regime, is the development of physics-assisted machine learning (PAML) customized for the details of photon fluorescence, absorption, and scattering in this instrument configuration. George Barbastathis, who has had considerable success in PAML for optics, is leading this ML work. This year a significant advantage in photon efficiency was demonstrated from ML on simulated x-ray measurements of chip facsimiles generated at random from a simple model of the layered interconnect structure found in semiconductor circuitry.

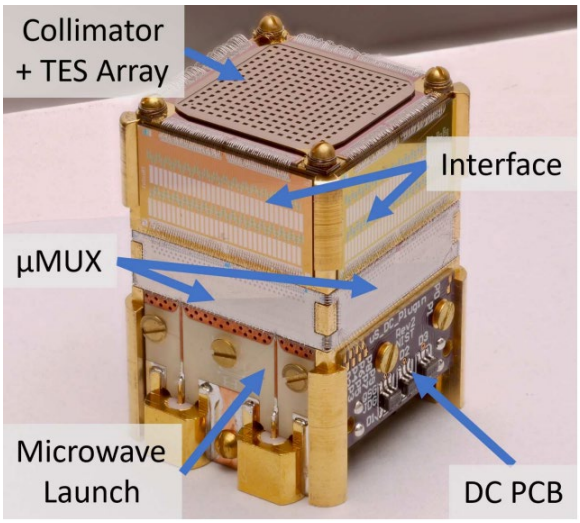

Figure 14. *Photograph of a micro-snout used in the TOMCAT spectrometer. The TES microcalorimeter array is mounted at the top of the micro-snout, and a collimator (aperture) array is used to ensure x-rays are only absorbed in the microcalorimeter absorbers. A set of 4 interface chips and 4 µMUX chips are used to bias and read out the TES microcalorimeter array. A microwave launch board and DC printed circuit board (PCB) are used to route the RF transmission line, flux ramp, and detector bias lines through the micro-snout.*

An integrated circuit (IC) with 160 nm features was imaged from x-ray measurements using customized tomography software that exploited (1) PENELOPE particle transport modeling code to determine x-ray fluorescence spot size from the SEM spot size, (2) corresponding diffuse source in the tomography for the x-ray forward model, (3) analytic modeling of motion blur, (4) region of interest modeling to account for lower photon flux at the edges than the center of the imaged region. Comparisons with the Graphics Design System (GDS) specification file of the IC were made. In addition, nano-patterned varied-material targets were

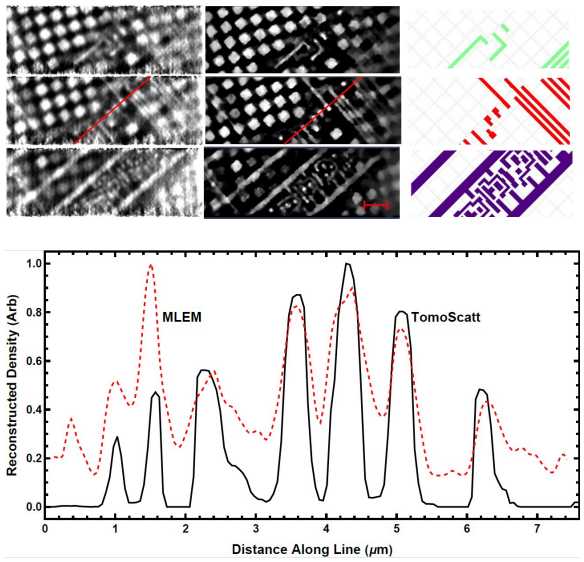

Figure 15. *IC region reconstructions of metal layers M3 (top row), M2 (middle row), and M1 (bottom row) using Sandia code MLEM (left) and summing the energy bands from 4.9 keV to 5.9 keV and 9.2 keV to 9.5 keV with 100 iterations and 1 pixel Gaussian blur, using the NIST code TomoScatt (middle) and the 9.1 keV to 10.1 keV band for the selected slices, compared with the original GDS design (right). According to the GDS, the large L in the top panel is 3.46 μm × 0.71 μm and the facing corner piece is 1.26 μm × 1.16 μm. Those lines have a width of 0.20 μm. The scale bar is 2 μm. The features that dominate the reconstructions but do not appear in the GDS file are CMP fill, which are not a part of the GDS design file as they are added by the foundry. The thin red lines running in the southwest-to-northeast direction across M2 reconstructions (middle row, first and second columns) are used for the separate plot below.*

developed to enable higher spatial resolution for subsequent measurements.

Due to the limited set of IC measurements by SEM source with TES detectors available to date for training a neural network for machine learning, additional samples according to simple IC simulation specifications (dubbed CircuitFaker) were fabricated by additive manufacturing. Full-angle x-ray measurements were taken to obtain ground truth and were sparsely selected for training a neural network. Comparisons of reconstructions between simulated and actual measurements, and among various algorithms, were evaluated with the machine learning enabling a measurement reduction factor of between 2.5 and 8 and a notable improvement in resilience to measurement noise.

[1] J. W. Fowler, B. K. Alpert, G. C. O'Neil, D. S. Swetz, and J. N. Ullom. Energy Calibration of Nonlinear Microcalorimeters with Uncertainty Estimates from Gaussian Process Regression. *Journal of Low Temperature Physics* **LTD19** (2022). DOI: 10.1007/s10909-022-02740-w

[2] Z. Guo, J. Ki Song, G. Barbastathis, M. E. Glinsky, C. T. Vaughan, K. W. Larson, B. K. Alpert, and Z. H. Levine. Physics-assisted Generative Adversarial Network for X-Ray Tomography. *Optics Express* **30**:13 (2022), 23238-23259. DOI: 10.1364/OE.460208

[3] Z. Guo, J. Ki Song, G. Barbastathis, M. E. Glinsky, C. T. Vaughan, K. W. Larson, B. K. Alpert, and Z. H. Levine. Advantage of Machine Learning over Maximum Likelihood in Limited-Angle Low-Photon X-Ray Tomography. In *Machine Learning for Scientific Imaging 2022 Conference*, IS&T Electronic Imaging 2022.

[4] N. Nakamura, P. Szypryt, A. L. Dagel, B. K. Alpert, D. A. Bennett, W. B. Doriese, M. Durkin, J. W. Fowler, D. T. Fox, J. D. Gard, R. N. Goodner, J. Z. Harris, G. C. Hilton, E. S. Jimenez, B. L. Kernen, K. W. Larson, Z. H. Levine, D. McArthur, K. M. Morgan, G. C. O'Neil, N. J. Ortiz, C. G. Pappas, C. D. Reintsema, D. R. Schmidt, P. A. Schulz, K. R. Thompson, J. N. Ullom, L. Vale, C. T. Vaughan, C. Walker, J. C. Weber, J. W. Wheeler, and D. S. Swetz. A Tabletop X-Ray Tomography Instrument for Nanometer-Scale Imaging: Integration of a Scanning Electron Microscope with a Transition-Edge Sensor Spectrometer. In review.

[5] Z. H. Levine, B. K. Alpert, A. L. Dagel, J. W. Fowler, E. S. Jimenez, N. Nakamura, D. S. Swetz, P. Szypryt, K. R. Thompson, and J. N. Ullom. A Tabletop X-Ray Tomography Instrument for Nanometer-Scale Imaging: Reconstructions. In review.

[6] Z. Guo, Z. Liu, G. Barbastathis, Q. Zhang, M. E. Glinsky, B. K. Alpert, and Z. H. Levine. Noise-resilient Deep Tomographic Imaging. In review.

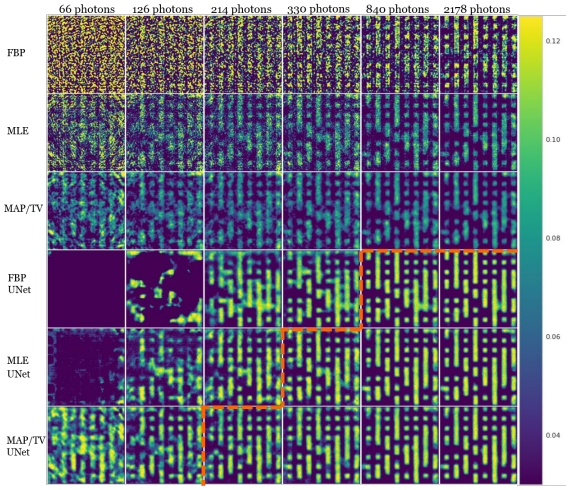

Figure 16. *Additive-manufactured simulated IC has selected 2D reconstructions (in 128 × 128) from different algorithms from x-ray measurements. Each row represents a reconstruction algorithm: filtered back projection, maximum likelihood estimation, maximum a posteriori estimation with total variation penalty, and the same three algorithms followed by reconstruction by a machine-learning-trained UNet. Each column represents an intensity of the photon rays. Reconstruction from the lowest right closely resembles the ground truth of an additive-fabrication-generated sample specified by an integrated-circuit simulator. The dotted orange line is the boundary between acceptable and unacceptable performance as determined by a Mallat Scattering Transform metric.*

True Becquerel: A New Paradigm for 21st Century Radioactivity Measurements

Bradley Alpert
Ryan Fitzgerald (NIST PML)
Denis Bergeron (NIST PML)
Richard Essex (NIST PML)
Svetlana Nour (NIST PML)
Galen O'Neil (NIST PML)
Daniel Schmidt (NIST PML)
Gordon Shaw (NIST PML)
Mike Verkouteren (NIST MML)
Kelsey Morgan, Daniel Swetz, Joel Ullom, et al. (NIST PML)

Expanding applications of radioactivity in medicine, energy, and security demand quantification of complex mixtures at uncertainty levels that are currently unachievable. This project will enable measurement of absolute activity (Bq) of radionuclide mixtures, avoiding chemical separation, by analysis of the decay heat signature of gravimetric samples embedded within microcalorimeter detectors. This capability consolidates multiple measurements into one, reducing cost and uncertainty. Success will create a primary realization of the Bq for direct assay of real-world samples at NIST and beyond, resulting in faster clinical trials of new radiopharmaceuticals and a faster, expanded nuclear forensics "fingerprinting" method for improved decision making.

The project enters its third year of NIST Innovations in Measurement Science funding with establishment of a new transition-edge-sensor (TES) spectrometry laboratory in Gaithersburg and procedures and initial practice with dispensing, weighing, and TES-embedding of mg-quantity radioactive nuclides. This work has involved integration of detectors and low-temperature electronics fabricated in Boulder with commercial room-temperature electronics and a He dilution refrigerator in a new laboratory, in pursuit of the goal of quantitative determination of sample constituents at the level of 0.1 % uncertainty.

The analysis challenges include (1) characterization of detector dynamics, to enable determination of decay energies of events with poor temporal separation, avoiding detector dead time, at an accuracy that reflects the exquisite precision of the TES detector, (2) characterization of the partial energy losses due to transport out of the absorber material of alpha, beta, and gamma rays, and (3) disambiguation of the spectrum into constituents, based on a library of radionuclide decays, with full quantification. Two new tools for detector dynamics characterization are (a) fabricated capability for electronic excitation of the detector with known energy depositions, and (b) algorithms for ODE parameter sensitivity, of much recent attention, to determine an ODE system from its input/output behavior. This machine learning (ML) technique will be combined with more conventional supervised ML for library-based disambiguation of spectra. The uncertainty, and risk, for both techniques is whether the stringent accuracy requirements of the project can be achieved.

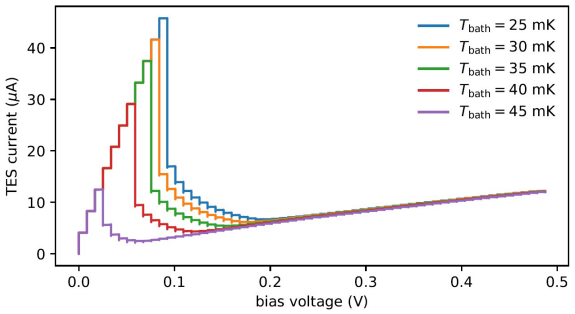

Figure 17. *Characterization of TES detectors includes measurement of current versus voltage through a transition from normal resistance to superconductivity. A new procedure is being developed to enable more complete characterization of TES resistance as a function of current and temperature by decreasing the bias voltage stepwise and measuring temporal dynamics of the current changes, with varied separate heating of the detector. The plot shows the effect of incremental voltage changes—without separate heating—on TES current, where the heat from the current flows to the heat bath at different temperatures. Characterization computations involve also bias and shunt resistances.*

[1] R. P. Fitzgerald, B. K. Alpert, D. T. Becker, D. E. Bergeron, R. M. Essex, K. Morgan, S. Nour, G. O'Neil, D. R. Schmidt, G. E. Shaw, D. Swetz, R. M. Verkouteren, and D. Yan. Toward a New Primary Standardization of Radionuclide Massic Activity Using Microcalorimetry and Quantitative Milligram-Scale Samples. *Journal of Research of the National Institute of Standards and Technology* **126** (2021), 126048. DOI: 10.6028/jres.126.048

Machine Learning Models to Predict the Mass and Infrared Spectra of Chemical Compounds

Chen Qu
Barry I. Schneider
Thomas Allison (NIST MML)
Walid Keyrouz (NIST ITL)
Anthony Kearsley
Joel Bowman
Tyler Martin (NIST MML)
Bradley Sutliff (NIST MML)

Recently, neural network (NN) based machine learning (ML) methodologies have become practical due to the availability of high-speed algorithms implemented on graphics processing units, resulting in an explosion of applications to a wide range of problems.

We have applied machine learning methodologies to solve two problems: (1) predicting the mass spectra of chemical compounds, and (2) predicting the infrared (IR) spectra of hydrocarbons (i.e., molecules only containing carbon and hydrogen atoms).

Mass spectrometry has been widely used in separating and identifying compounds from a mixture, so an accurate predictive model holds the promise of augmenting existing mass spectra libraries, thereby enabling them to better identify unknown compounds. [1, 2] Typically, machine learning-based methods can realize very fast predictions, however they require large amounts of data to ensure high levels of accuracy. Among currently available mass spectral libraries, the NIST/EPA/NIH Mass Spectral Library is one of the largest and most widely used collections of mass spectra, containing more than 300 000 diverse compounds. The size of this data set presents a tantalizing target for the application of machine learning models.

A notable machine learning model that predicts mass spectra was developed by the Google Brain team [3]. Their machine learning tool was trained using the NIST mass spectral library (2017 version) and achieved reasonably good results. We have developed a Graph Neural Network (GNN) model for the prediction of mass spectra, and achieved improved performance compared with the Google model. Our GNN model is similar to the ones we developed in the previous years for Kováts retention indices [4] and boiling points, [5] but is more challenging because the models must predict a *vector* of quantities to yield a histogram, as opposed to a single label or scalar.

Our GNN model is based on the materials graph network (MEGNet) approach developed by Chen et al. [6]. It incorporates a graph network architecture that captures molecular structure in a very natural way. In a GNN, the atoms correspond to vertices in the graph, and chemical bonds correspond to graph edges. The inputs to the MEGNet model are simply the atom, bond, and global features of a molecule. Then these features were successively updated using a "message-passing" network. Finally, a readout layer is used to extract the information from the updated graph to make the final prediction of the mass spectrum. The symmetrized Kullback-Leibler divergence is used as the loss function to measure the difference between the predicted and true spectra. The model also exploits the intrinsic symmetry in the mass spectrum, that is, if a fragment with mass x exists, a fragment with mass M-x is very likely to be present, where M is the molecular mass, by using the bidirectional prediction approach proposed in the Google model [3]. Ultimately this work achieved improved performance compared to the Google model, with significantly smaller error statistics. Figure 18 shows the predictions of the GNN model for four randomly chosen chemical compounds representing different levels of prediction accuracy.

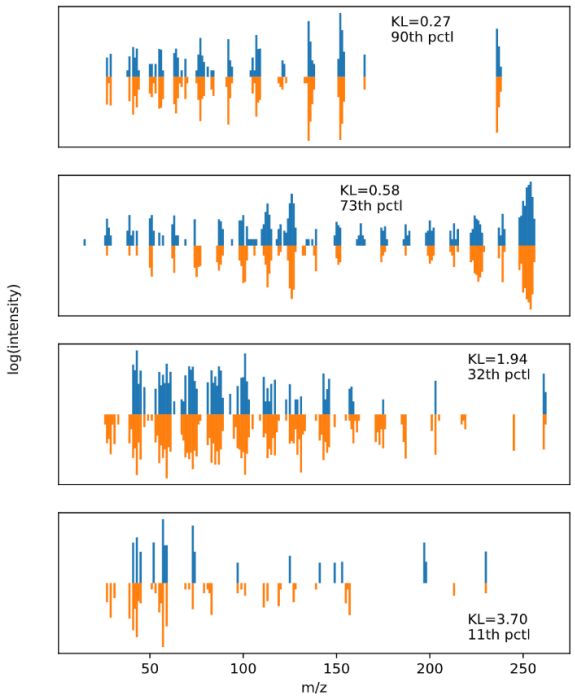

Figure 18. *Selected predictions of the GNN model for four randomly chosen chemical compounds representing different levels of prediction accuracy. Higher percentile rank indicates better agreement between the experimental spectrum (above, blue) and the prediction (below, orange).*

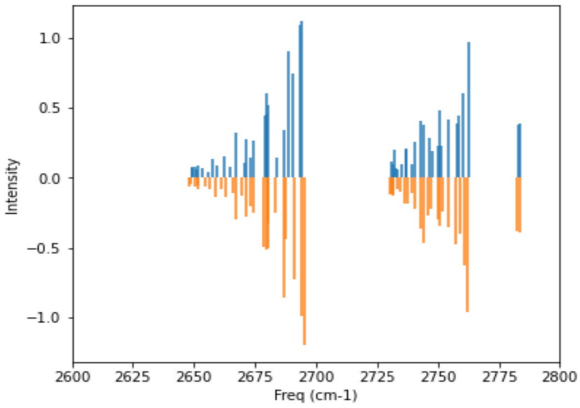

Figure 19. *Comparison between the IR spectrum computed using PM7 (above, blue, used as true spectrum in this work) and the predicted spectrum using the machine learning model (below, orange).*

A similar problem is the prediction of IR spectra of molecules. IR spectroscopy is a common tool to identify polymers, and a model that can accurately and simply predict the IR spectrum when given the molecular structure is extremely valuable to experimentalists such as those in MML.

Specifically, in the experimental IR spectra of polymers, two major bands are observed at ~2850 and ~2920 cm^{-1}, and for some polymers, a third band at a higher frequency is present. We initiated our investigation with smaller hydrocarbons containing tens of

carbon atoms because these calculations are computationally simpler and can also provide information for larger polymers. Based on density functional theory calculations (B3LYP), the two major bands in the IR spectrum are due to the C-H stretches on methylene groups (-CH_2-), while a third band at a higher frequency is due to C-H stretches on methyl groups (-CH_3).

For more quantitative predictions of the IR spectra, molecular dynamics simulations were carried out for hydrocarbons with 10 to 60 carbons, and 1000 conformer configurations were collected for each chain length from the simulation. Then the IR spectrum of each conformer was calculated with the empirical PM7 method [7] and were used to train a densely connected neural network model. The input to this model is the Coulomb matrix computed from the Cartesian coordinates of carbon atoms, and the outputs are the frequencies of all C-H stretches and corresponding IR intensities. The model achieved an accurate prediction of the IR spectra [8], as shown in Figure 19. This model will be extended in the future and used to generate synthetic spectra of polymers on a large scale efficiently, which can facilitate the identification of polymers.

[1] S. E. Stein, Chemical Substructure Identification by Mass Spectral Library Searching. *Journal of the American Society for Mass Spectrometry* **6** (1995), 644–655.

[2] S. Stein, Mass Spectral Reference Libraries: An Ever-Expanding Resource for Chemical Identification. *Analytical Chemistry* **84** (2012), 7274–7282.

[3] J. N. Wei, D. Belanger, R. P. Adams, D. Sculley, Rapid Prediction of Electron–Ionization Mass Spectrometry Using Neural Networks. *ACS Central Science* **5** (2019), 700–708.

[4] C. Qu, B. I. Schneider, A. J. Kearsley, W. Keyrouz, and T. C. Allison. Predicting Kováts Retention Indices Using Graph Neural Networks. *Journal of Chromatography A* **1646** (2021), 462100.

[5] C. Qu, A. J. Kearsley, B. I. Schneider, W. Keyrouz, and T. C. Allison. Graph Convolutional Neural Network Applied to The Prediction of Normal Boiling Point. *Journal of Molecular Graphics and Modelling* **112** (2022), 108149.

[6] C. Chen, W. Ye, Y. Zuo, C. Zheng, and S. P. Ong. Graph Networks as a Universal Machine Learning Framework for Molecules and Crystals. *Chemistry of Materials* **31** (2019), 3564–3572.

[7] J. J. P. Stewart. Optimization of Parameters for Semiempirical Methods VI: More Modifications to the NDDO Approximations and Re-Optimization of Parameters. *Journal of Molecular Modeling*, **19** (2013), 1–32.

[8] C. Qu, B. I. Schneider, A. J. Kearsley, W. Keyrouz, and T. C. Allison. Prediction of Mass Spectra via Molecular Structure Based Machine Learning. In review.

Accelerating Scale-up of Carbon-Capture Materials

Robert DeJaco
Anthony Kearsley
Sean McGivern (NIST MML)
Jeff Manion (NIST MML)
Dan Siderius (NIST MML)
Giang Nguyen (NIST MML)
Amanda Forster (NIST MML)
Pamela Chu (NIST MML)

Capturing carbon dioxide from atmospheric air could reverse its environmental impact. However, as the concentration of CO_2 in air is very small (around 400 parts per million), large process scales are required, and efficient adsorbent materials are necessary.

As carbon capture is a dynamic process involving partial differential equations, it is challenging to determine which materials are more efficient than others without building multiple pilot plants (an extremely costly endeavor). As the process involves many parameters and requires numerical simulations, it is also difficult to scale a carbon capture material from the bench to industrial scale.

A critical step in the evaluation of the performance of carbon capture materials, as well as their scale up, is the break-through curve measurement (see Figure 20). The profile of concentrations exiting, or breaking through, the column as a function of time provides essential information relating material properties to the mechanism of separation, the shape and speed at which solute concentrations move along the adsorption column in response to adsorption into the immobile solid. To further scale up the material, numerical simulations are needed to determine kinetic parameters by fitting to the break-through curve measurement.

In the first portion of our research, we are using perturbation theory in the limit of fast adsorption compared to elution to develop a quantitative relationship between equilibrium properties and the break-through curve. We have found that regular and singular perturbation theory in fast adsorption provide a more generic and quantitative description of the conditions under which several theories of solute movement are valid, as well as how they are related. At the same time, our approach has been able to answer several open questions on the phenomena occurring inside the column. Our results have been submitted to a peer reviewed journal [1]. In the future, we believe that this work could facilitate selection of high-performing materials in a manner that is more consistent with an industrial carbon capture process.

In the second, more recent portion of this project, we are developing numerical simulation, optimization, and uncertainty quantification methods to extract kinetic parameters from break-through curve measurements made by our colleagues in MML. Building on concepts

Figure 20. *Illustration of break-through curve measurement. A column (grey) is packed with solid particles (blue). Mechanical forces on each end are used to ensure that the solid does not move. After flowing a non-adsorbing solvent through the column for a time long enough to reach steady state, the inlet mixture is changed to the mixture of interest and the concentration of fluid exiting, or breaking through, the column is monitored with time. The plot of outlet concentrations versus time is called the break-through curve.*

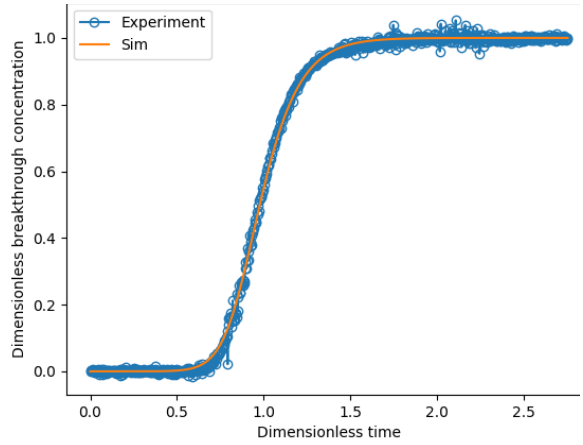

Figure 21. *Dimensionless outlet concentration as a function of dimensionless time for experiment (blue circles) and optimal simulation (orange line). The inlet mixture consists of 1% CO_2 in He at room temperature, and the adsorbent is Zeolite 13X.*

from the first portion of this work, we have implemented a numerical scheme that affords an estimated second-order rate of convergence in space and time. Initial results demonstrate that the simulations can fit experimental measurements with great agreement (see Figure 21). In the future, we expect that quantifying the uncertainty in kinetic parameters, improving accuracy of the numerical scheme, and extending the approach to multicomponent systems will accelerate the transition of new materials from bench to plant.

[1] R. F. DeJaco and A. J. Kearsley. Understanding Fast Adsorption in Break-through-curve Measurements. In review.

Linear and Nonlinear Exploration of Rotating Self-Gravitating Inviscid Incompressible Fluid Ellipsoids

Howard S. Cohl
Stephen Sorokanich
Joel E. Tohline (Louisiana State University)

In the classic book *Ellipsoidal Figures of Equilibrium* [1], Nobel Laureate Subramanian Chandraskhar studied rotating self-gravitating inviscid incompressible fluid ellipsoids. This classic subject has been studied by great mathematicians such as Maclaurin, Jacobi, Meyer, Liouville, Dirichlet, Dedekind, Riemann, Poincaré, Cartan, Roche, Darwin (the fifth child of Charles Darwin), and Jeans. These fluid ellipsoids, being incompressible, have constant density. The steady solution in the case of non-rotation is a sphere. When one introduces rotation, the steady solutions are rotating oblate spheroids. These are referred to as Maclaurin spheroids. It is known that as one increases the angular momentum in the Maclaurin spheroids, the figure becomes unstable to a shape changing instability and the equilibrium configuration becomes a tri-axial ellipsoid. In the case where the angular momentum vector is parallel to the vorticity, these are referred to as Riemann S-type ellipsoids [2].

We have two concurrent research projects related to the evolution and instability of the ellipsoidal equilibrium figures. The first is an advanced numerical exploration and the linear stability of Riemann S-type ellipsoids. The stability analysis proceeds from the linearized Euler equations for the self-gravitating system and maps the stability landscape with respect to the variables of the problem (major axes of the ellipsoid, angular velocity). We hope to resolve this stability diagram with higher order harmonics using the same technique that was pioneered by Chandrasekhar's student Norman Lebovitz in [3]. The second project is an investigation of three-dimensional nonlinear computational fluid dynamics solutions using finite element methods to simulate the nonlinear evolution of these unstable incompressible fluid ellipsoids. This entails simulation of the incompressible Euler equations for rotating self-gravitating masses with particular focus on the evolution of the free-boundary, coupling finite element methods with level-set techniques.

The incompressible Euler equations are a coupled system of nonlinear partial differential equations in two unknowns, $u(x, y, z, t)$ and $p(x, y, z, t)$, the velocity and pressure fields, which describe an idealized incompressible fluid with no viscous effects in a Eulerian frame of reference. The absence of the second-order spatial differential operator describing the kinematic viscosity from the momentum equation (which is present, e.g., in the incompressible Navier-Stokes equations), as well as

the divergence-free incompressibility constraint on the velocity field, renders this system particularly difficult to simulate, due in part to the infinite speed of sound propagation, which is a characteristic property of this system. Numerical solution of the incompressible Euler system using many common methods (e.g., the Finite-Volume method) is rendered impossible, since a vanishing timestep would be required to capture such effects.[5] It is nonetheless desirable to develop a robust tool to simulate the nonlinear development of instabilities for *incompressible* dynamics, since the incompressible, inviscid systems are amenable to quantitative stability analysis [4-7] over more realistic fluid systems. Reproducing the analytical stability results, which exist for this system, will be an important benchmarking tool for our numerical studies.

The above constraints have led us to adopt the finite element method (FEM) as our primary means of simulating the nonlinear evolution of an incompressible, inviscid fluid. A promising aspect of implementing the finite element method for the incompressible Euler equations will be the ability to couple a finite element solver with a level-set method for the evolving boundary of a self-gravitating fluid (and the potential to solve for the dynamics of the surface without considering the dynamics of the volume). Resolving the topological transformation of the surface of a rapidly spinning incompressible ellipsoid is a long-standing open problem (dating at least back to Darwin). A prevailing hypothesis predicts the eventual fission of self-gravitating fluids into two teardrop-shaped objects in orbit around one another when the angular velocity of the parent body is high enough. This is believed to be the primary mechanism behind the formation of binary star systems [8]. Finite Element Methods are particularly well-suited for modeling the time evolution of surfaces and have been used to successfully model incompressible fluid systems.

With respect to the stability analysis of the Riemann ellipsoids, we are refining a numerical method first introduced by Lebovitz et. al. [5-7], and later developed extensively by Cohl [9]. The linear stability analysis of any dynamical system is based on the magnitude of the eigenvalues of the linearized system around a known stable solution. Starting from a linearization of the Euler equations around the known S-type ellipsoids, the resulting eigenvalue problem is truncated in the basis of ellipsoidal harmonics, allowing for the development of a numerical procedure for evaluating the stability of S-type ellipsoids to small perturbations. The form of Eulerian perturbation to the Newtonian gravitational potential, which is diagonal in the basis of ellipsoidal harmonics, allows for this truncation. We are particularly interested in the fine structure of the boundary of the region of stability as the major and semi-major axes of S-type solutions vary.

The ellipsoidal harmonics, like their cousins, the spherical harmonics, are solutions to Laplace's equation in the ellipsoidal coordinate system. The properties of ellipsoidal harmonic functions are critical to the study of problems displaying triaxial symmetry, and their efficient numerical handling is an ongoing subject of research [10,11]. A major component of this project will be the supplementation of the Digital Library of Mathematical Functions [12] with relevant information on the ellipsoidal harmonic functions collected while studying the gravitational equilibrium figures. This project also has a direct application to the study of astronomical and geophysical phenomena [13].

[1] S. Chandrasekhar. *Ellipsoidal Figures of Equilibrium*. Dover Publications, New York, 1969.

[2] B. Riemann. Ein Beitrag zu den Untersuchungen über die Bewegung eines flüssigen gleichartigen Ellipsoids. *Abhandlungen der Königlichen Gesellschaft der Wissenschaften zu Göttingen* **9**, 1860.

[3] N. Lebovitz, and A. Lifschitz. New Global Instabilities of the Riemann Ellipsoids. *The Astrophysical Journal* **458**:2 (1996), 699-713.

[4] S. Chandrasekhar. The Equilibrium and the Stability of the Riemann Ellipsoids I. *Astrophysical Journal* **142** (1965), 890–961.

[5] N. R. Lebovitz. Langrangian Perturbations of Riemann Ellipsoids, *Geophysical & Astrophysical Fluid Dynamics* **47,** no. 1-4 (1989), 225–236.

[6] N. Lebovitz, and A. Lifschitz. The Stability Equations for Rotating, Inviscid Fluids: Galerkin Methods and Orthogonal Bases. *Geophysical & Astrophysical Fluid Dynamics* **46**:4 (1989), 221–243.

[7] N. Lebovitz, and A. Lifschitz. Short-Wavelength Instabilities of Riemann Ellipsoids. Philosophical *Transactions of the Royal Society of London Series A* **354**:1709 (1996), 927–950.

[8] J. E. Tohline. The Origin of Binary Stars. *Annual Reviews in Astronomy and Astrophysics* **40** (2002), 349–385.

[9] H. S. Cohl. Linear Instability Analysis of the Ellipsoidal Figures of Equilibrium. Unpublished.

[10] G. Dassios. Private Communication.

[11] G. Dassios. Ellipsoidal Harmonics: Theory and Applications. *In Encyclopedia of Mathematics and its Applications*, Cambridge University Press, 2012.

[12] F. W. J. Olver, A. B. Olde Daalhuis, D. W. Lozier, B. I. Schneider, R. F. Boisvert, C. W. Clark, B. R. Miller, B. V. Saunders, H. S. Cohl, and M. A. McClain, eds. *NIST Digital Library of Mathematical Functions*. http://dlmf.nist.gov/, Release 1.1.8 of 2022-12-15,

[13] C. Hunter. On Secular Stability, Secular Instability, and Points of Bifurcation of Rotating Gaseous Masses. *Astrophysical Journal* **213** (1977), 497–517.

[5] https://tohline.education/SelfGravitatingFluids

A Science Gateway for Atomic, Molecular and Optical Science

Barry I. Schneider
Klaus Bartschat (Drake University)
Kathryn Hamilton (University of Colorado, Denver)
Igor Bray (Curtin University, Australia)
Armin Scrinzi (Ludwig-Maximilians U., Germany)
Fernando Martiin (U. Autonoma de Madrid, Spain)
Jesus Gonzalez Vasquez (U. Autonoma de Madrid)
Jimena Gorfinkiel (Open University, UK)
Robert Lucchese (Lawrence Berkeley National Lab)
Sudhakar Pamidighantam (Indiana University)
Andrew Brown(University of Belfast, UK)
Nicholas Douguet (Kennesaw State University)

An international effort has been underway since early 2019 to develop and maintain a Science Gateway for Atomic Molecular and Optical Science (AMOSG) [1, 2, 3, 4]. The gateway was renamed from Science Gateway for Atomic and Molecular Physics, to a Science Gateway for Atomic, Molecular, and Optical Science to reflect the broader nature of the ongoing activity. The purposes of the gateway are to:

(i) collect and make available to the community a set of advanced computational tools that are actively being used to study atomic and molecular collisions and the interaction of radiation with atoms and molecules,

(ii) provide educational materials for beginning and advanced users desiring to learn the ideas and concepts of AMOS, both theoretical and computational, and

(iii) make available to the broad community atomic and molecular data needed for many applications.

The availability of collision data is critical to many areas of physics including astrophysics, fusion energy, the study of lighting and microelectronics and is an activity consistent with the mission of NIST.

Codes for modeling and simulation of such phenomena have been developed in specific groups by graduate students and postdocs but are often poorly documented, and unavailable outside the group. This leads to "reinventing the wheel" in too many instances. Maintaining these computational tools, as well as enhancing their capabilities, is one of the major goals of the project and is critical to ensure continued scientific progress in AMOS.

Another important goal is to enable the code developers themselves to compare the calculations of specific well-defined problems using different methodologies. This enables the verification of results of different codes and encourages comparison with experiment, where available. It has already been demonstrated that a few of these codes are often more accurate than experiment and thus provide a predictive capability when experimental results are unavailable.

At the outset, the group acknowledged that in contrast to some other communities, the AMOS community has lagged behind in developing community supported software packages that are robust and widely used outside the group that was responsible for developing the software. Our group was convinced the time had arrived to change existing practices and make these tools available and easily used by future generations of AMOS scientists as well as the developers themselves.

The group wrote a proposal to the NSF Extreme Science and Engineering Discovery Environment (XSEDE) program (now the Advance Cyberinfrastructure Coordination Ecosystem: Services and Support, or ACCESS) to fund some initial development of the gateway. The proposal was successful and, importantly, provided the developers with some hands-on assistance from the Extended Collaborative Support Services arm of XSEDE. This was vital to the success of the effort. In particular, we acknowledge the important contribution of Sudhakar Pamidighantam and his colleagues at Indiana University in making our efforts a success.

There have been some important advances since the first instantiation of the gateway:

a) the original web pages for the gateway have been completely revamped and new material has been added,

b) the original six major codes chosen for initial deployment have been expanded to include eleven codes and many have already been ported to at least three ACCESS supercomputers, and

c) there is a new version of an API available to enable users to perform calculations with at least one of the codes, tRecX, and this is serving as a model for the other applications.

A contract that NIST awarded to Indiana University in 2021 to further develop the needed GUI interfaces has now expired. As a consequence, the need for longer term support for the project is recognized as an essential ingredient to its ultimate success. To that end, the group spent considerable effort during the fall of 2022 in writing an NSF proposal to the Cyberinfrastructure for Sustained Innovation program. Professor Kathryn Hamilton, of the University of Colorado Denver, is the project PI. Co-PI's are Sudhakar Pamidighantam from IU, Klaus Bartschat from Drake University, and Nicholas Douguet from Kennesaw State. Barry Schneider, and Robert Lucchese from Lawrence Berkeley National Laboratory have the role of Senior Investigators. The proposal was submitted to the NSF from the University of Colorado Denver as the lead organization.

The current portal contains a good description of the codes, the people involved, links to documentation, a bibliography, a preliminary data repository, and some

nice graphical material illustrating a few of the calculations that have been done with the codes.

[1] B. I. Schneider, K. Bartschat, O. Zatarinny I. Bray, A. Scrinzi, F. Martin, M. Klinker, J. Tennyson, J. Gorfinkiel, and S. Pamidighanta. A Science Gateway for Atomic and Molecular Physics. arXiv:2001.02286

[2] B. I. Schneider, K. Bartschat, O. Zatsarinny, K. Hamilton, I. Bray, A. Scrinzi, F. Martin, J. G. Vasquez, J. Tennyson, J. Gorfinkiel, R. Lucchese and S. Pamidighantam. Atomic and Molecular Scattering Applications in an Apache Airavata Science Gateway. In *PEARC '20: Practice and Experience in Advanced Research Computing, PEARC20,* July 2020. DOI: 10.1145/3311790.3397342

[3] B. I. Schneider, et al. Atomic and Molecular Scattering Applications in an Apache Airavata Science Gateway. In *PEARC '20: Practice and Experience in Advanced Research Computing*, 2020, 270-277. DOI: 10.1145/3311790.3397342

[4] B. I. Schneider. AMO for All: How Online Portals Are Democratizing the Field of Atomic, Molecular and Optical Physics. NIST Taking Measure Blog, November 2, 2022. URL: https://www.nist.gov/blogs/taking-measure/amo-all-how-online-portals-are-democratizing-field-atomic-molecular-and-optical

Separable Shape Tensors

Zachary J. Grey
Olga Doronina (NREL)
Andrew Glaws (NREL)

Efficient representations and statistics of shapes are important facets of computational tasks in artificial intelligence, design, and manufacturing. The challenge is to define a prudent treatment of data with an intrinsic notion of shape. Example applications include: (i) wind turbine airfoils which must be designed, manufactured, and measured more precisely than ever for next generation offshore wind energy applications, (ii) investigation and statistical hypothesis testing of material microstructures in a manufacturing process, (iii) inference involving contours of measured quantum devices, or (iv) quantifying distributions of persistent structures in general image classification.

The notion of "shape" is typically induced by identifying shape preserving transformations and "dividing out" these transformations to explore what remains in a so-called quotient topology. These topologies can vary from one application to the next but are useful in studying and understanding persistent characteristics and "modes" of shape as data. Moreover, these prudent treatments of shape induce improved metric spaces offering better notions of "distance" between paired shapes in a framework which is inherently non-linear. Thus, with this formalism for defining notions of shape, we can offer improved coordinate systems for domain definition, interpolation, and inferential statistics.

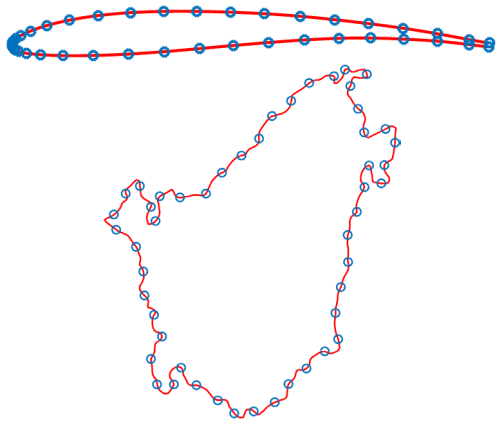

Figure 22. *Top: a discretized airfoil shape with arbitrary ordering of landmarks as blue circles depicted along a red boundary. Bottom: a discretized grain boundary with arbitrary ordering of landmarks depicted along a red boundary.*

In our analysis, a shape can be represented as a boundary defined by a curve, $c\colon [0,1] \to \mathbb{R}^2$. However, in a computational setting, we represent airfoil shapes or grain boundaries as a discrete ordered sequence of *landmarks* $(\mathrm{x}_i) \in \mathbb{R}^2$ for $\mathrm{i} = 1, \dots, n$. That is, we view a shape through an identification with some unknown curve $c(s)$ and compute with reparametrized landmarks $x_i = c(s_i)$ for $0 \le s_1 < s_2 < \cdots < s_n \le 1$. Moving along the curve, this sequence of planar vectors along a shape boundary can be represented as a matrix $\mathrm{X} = [x_1, \dots, x_n]^\top \in \mathrm{R}_*^{\mathrm{n}\times 2}$ constituting a discrete representation of the shape.

We introduce a scaling of landmark data to parametrize new shape deformations over the Grassmann manifold, $\mathcal{G}(\mathrm{n}, 2)$. The nature of this revised representation "divides out" the effect of matrix scaling operations, XM, thus separating affine characteristics of shape---when combined with translations---and offering a novel non-linear (non-Euclidean) domain of discrete shapes.

Computationally, these separable shape tensors become

$$X_0(t, l) = \tilde{X}(t)M(l)$$

where $\tilde{X}(t)$ are representative elements parametrized over coordinates t of a Grassmann submanifold and $M(l)$ are the separated elements of scale variations over subgroups of the general linear group, GL_2—giving rise to product submanifold definitions of discrete-shape spaces. This defines a pair of *independent coordinate vectors* (t, l) describing any shape up to translations. This separability is a desirable characteristic for aerospace/wind-turbine designers who regularly prescribe or fix $M(l) \in GL_2$ but seek undulations $[\tilde{X}](t) \in \mathcal{G}(\mathrm{n}, 2)$ in the shape to explore deformations resulting from blade soiling or manufacturing variations. Moreover, this separability enables a more precise investigation for studying how grain shapes within a material microstructure may be deformed through a manufacturing process or loading condition.

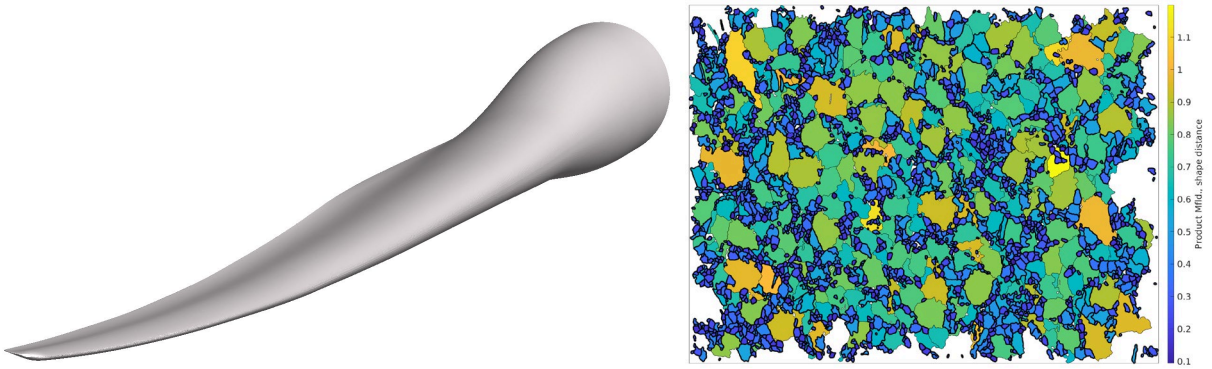

Figure 23. *Left: structured mesh of a wind turbine blade generated by an interpolation of ten defining airfoils over the space of separable shape tensors. Right: a distribution of thousands of grain boundaries colored according to a matrix product submanifold shape distance from a central shape element. Smaller grains are highlighted by a thickened boundary revealing a network of shapes with relatively small distance to a computed origin. This structure was found to be statistically significant with respect to other scans not exhibiting the visual quality.*

In aerodynamic applications, reduced-dimension data-driven domains of transformed separable representations offer improved regularization of deformations and novel methods of interpolation for both 2D and 3D design. In materials science applications, distributions of shapes as grain boundaries measured with electron back-scatter diffraction (EBSD) can be transformed into separable representations for hypothesis testing—indicating which features of shape are statistically significant from one measurement of a set of grains to the next.

These highly scalable non-Euclidean treatments of discrete shapes leverage implementations over matrix manifolds to achieve efficiencies necessary for computations involving tens of thousands of shapes. In one instance, we have successfully explored and deployed data-driven approaches to build wind turbine airfoil shape domains with more than 15000+ shapes represented by refinements of 1000+ landmarks per shape. Alternatively, given scans of material microstructures, we can compute statistical moments of thousands of grain boundaries in a matter of seconds on a common laptop.

These innovations have enabled significantly more tractable inverse designs with machine learning for next generation wind-turbine blades---transforming the classical problem of designing with hundreds of blade design parameters into one involving as few as four parameters. Additionally, these representations are showing promise with two-sample hypothesis testing of segmented grain boundaries subjected to different environmental conditions. This facilitates a novel set of tools for materials scientists to quantify specific structural differences in distributions of grain boundaries from one EBSD scan to another. This interpretation on separable shape tensors was presented at the AI for Design and Manufacturing Conference [1] and recently accepted for publication in the Oxford University Press, Journal of Computational Design and Engineering [2]. A public GitHub code repository for applications relevant to aerodynamic design is also available [3].

[1] O. A. Doronina, Z. J. Grey, and A. Glaws. Grassmannian Shape Representations for Aerodynamic Applications. In *AI for Design and Manufacturing (ADAM) Workshop of the AAAI 2022 Conference* (2022) DOI: 10.48550/arXiv.2201.04649

[2] Z. J. Grey, O. A. Doronina, and A. Glaws. Separable Shape Tensors for Aerodynamic Design. *Journal of Computational Design and Engineering.* To appear. DOI: 10.1093/jcde/qwac140

[3] O. A. Doronina., A. Glaws., R. King, G. Vijayakumar, and Z. J. Grey. G2Aero. Computer Software. USDOE Advanced Research Projects Agency - Energy (ARPA-E). April 20, 2022. DOI: 10.11578/dc.20220422.1

Computational Tools for Image and Shape Analysis

Günay Doğan
Javier Bernal
James Lawrence
Prashant Athavale (Clarkson University)
Emmanuel Atindama (Clarkson University)
Lianchen Lewis (University of Texas at Austin)
Olakunle Abawonse (Northeastern University)

The main goal of this project is to develop efficient and reliable computational tools to detect geometric structures, such as curves, regions, and boundaries, from given direct and indirect measurements, e.g., microscope images or tomographic measurements, as well as to evaluate and compare these geometric structures or shapes in a quantitative manner. This is important in many areas of science and engineering, where the practitioners obtain their data as images and would like to detect and analyze the objects in the data. Examples are

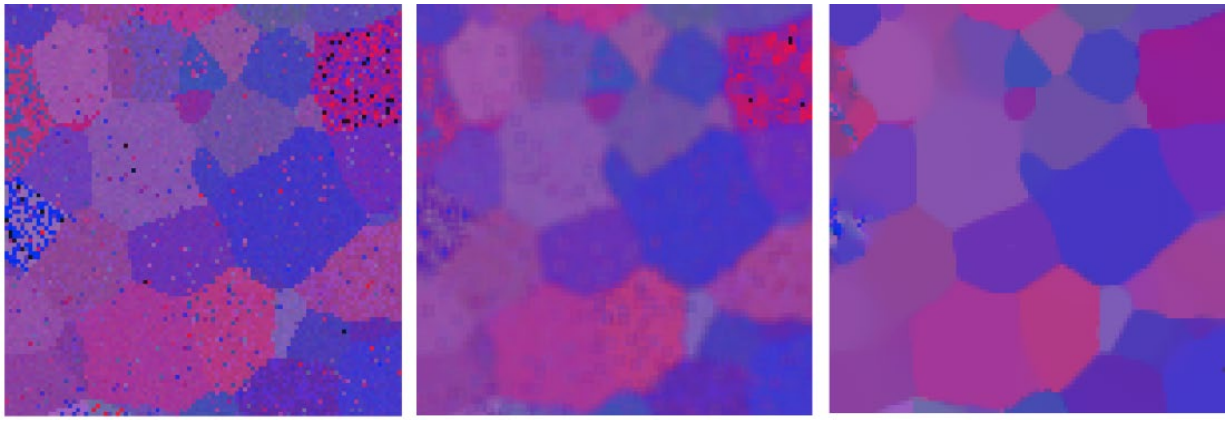

Figure 24. *A noisy electron backscatter diffraction image (left) denoised by Gaussian filtering (middle) and weighted total variation flow (right).*

microscopy images for cell biology or micro-CT (computed tomography) images of microstructures in material science, shoeprint images in crime scenes for footwear forensics. In fiscal year 2022, advances were made in the two fronts of this project: image segmentation and shape analysis. Python implementations of solutions for problems in these areas were implemented, and documentation and examples were provided. In the following, we provide more details on the specific work carried out.

Image Segmentation. Image segmentation is the problem of finding distinct regions and their boundaries in given images. It is a necessary data analysis step for many problems in cell biology, forensics, and material science, as well as other fields in science and engineering. In FY 2022, G. Doğan and his collaborators continued to work on multiple strategies for image segmentation.

Some of the algorithms that Doğan and his collaborators developed in the recent years build on energy minimization principles. In this approach, an artificial segmentation energy is defined to quantify how well a given set of region or boundary representations fit the sought segmentation; the better the fit, the smaller the energy values. A given starting set of regions or boundaries are then evolved iteratively until the minimum of the energy, thus the desired segmentation, is achieved. In FY 2022, Doğan implemented bug fixes and improvements to minimization algorithm for region boundaries. He also concluded his complementary work on region evolution with former graduate intern O. Abawonse (now at Northeastern University). They had implemented an image segmentation algorithm that leverages a convexified version of a piecewise constant segmentation energy. This algorithm is useful for obtaining two-phase segmentations, i.e., background-foreground segmentation of grayscale images. Doğan and Abawonse finished their code and experiments and wrote a paper describing the algorithm and the segmentation experiments [1].

Doğan and graduate summer intern Liangchen Liu from University of Texas at Austin researched the use of deep learning for image segmentation. Deep learning is an artificial intelligence approach that leverages neural networks with many layers to solve various image processing problems. Doğan and Liu reviewed the existing literature on image segmentation with deep learning and tried to determine the feasibility of incorporating variational regularization in deep learning to see if more regular (less noisy) segmentations could be achieved. They implemented a convolutional neural network that included total variation regularization at the final layer. The preliminary results obtained using this neural network were very encouraging. Doğan will further develop this algorithm in FY 2023.

Doğan continued his collaboration with P. Athavale and E. Atindama of Clarkson University on preprocessing and segmentation of orientation images of microstructures. Analysis of such images is instrumental to modeling and understanding physics of real material microstructures. Orientation images, more specifically electron backscatter diffraction (EBSD) images, often come with many misorientation pixels, which have the appearance of noise, and may have regions of missing data. To alleviate these issues, Athavale, Atindama and Doğan have been developing PDE-based denoising and inpainting algorithms to produce high quality reconstructions of the EBSD images. They further improved their algorithms in FY 2022 in terms of efficiency and quality of reconstructions. They developed a new version of their preprocessing algorithm, and significantly reduced the artifacts in the images that are hard to remove by the denoising algorithm. Moreover, they introduced a better spatial weighting function in the denoising PDE. The weighting function controls the amount of smoothing based on the pixel locations and stops smoothing across grain boundaries to avoid blurring of sharp grain boundaries (see Figure 24). They

completed a paper describing their algorithm [2], and implemented the algorithm in Python, to be made publicly available upon publication of the paper.

Shape Analysis. A natural approach to analyze and compare objects in image and data is through their shapes, an aspect that is invariant to rotation, translation, and scaling. Shape-based analysis can facilitate object recognition and can provide a more intrinsic way to perform statistics of geometric data. Previously, Doğan, Bernal, and their collaborators developed an efficient optimization algorithm to compute the elastic shape distances between 2d closed curves [3, 4, 5], building on the square-root velocity framework of Srivastava et al. [7, 8]. This shape distance is the fundamental building block for shape analysis.

In FY 2022, J. Bernal continued his work in the context of shape analysis [8, 9] for the computation of the elastic shape registration of two simple surfaces in 3-dimensional space and therefore of the elastic shape distance between them. Similar work had been carried out by Kurtek, Jermyn et al. in [11, 12]. Bernal's work started with the careful development, as it is done in [11, 12], of the mathematical framework necessary for the elastic shape analysis of 3-dimensional surfaces, which culminated with the definition and justification of the distance between two such surfaces. This distance, and therefore the registration, is the result of minimizing a distance function in terms of rotations of one surface and reparametrizations of the other one. With a simple surface defined as a parametrized surface in 3-d space, that is, the range of a one-to-one function from an elementary region in the plane into 3-d space, Bernal and his collaborators defined a shape function of a parametrized surface in 3-dimensional space, different from the one in [8] but similar to the one in [12] and established some fundamental results about this function. A similar definition and similar results were presented in [6, 7, 8, 9, 10] in the context of the shape function of a parametrized curve in d−dimensional space. Based on this definition of the shape function of a parametrized surface, Bernal et al. defined the elastic shape distance between two parametrized surfaces as well. This was done by alternating computations of rotations of one of the surfaces through the minimization of some double integral in terms of rotations of the surface, and computations of reparametrizations of the other surface through the minimization of the same double integral in terms of homeomorphisms from the elementary region that is part of the definition of the parametrized surfaces, onto itself, the homeomorphisms having Jacobians of positive determinant. That this distance is well defined was demonstrated using arguments similar to those used for justifying the definition of the distance between curves in d−dimensional space found in [8, 9]. Finally, they developed an algorithm that minimizes the distance function in terms of rotations and a special subset of the set of reparametrizations, the optimization over reparametrizations based on Dynamic Programming.

Obviously, this approach does not necessarily produce an optimal solution for the registration and distance problem, but perhaps a solution closer to optimal than the local solution that an algorithm with a gradient approach for optimizing over the entire set of reparametrizations, such as those proposed in [11, 12], may produce. In fact, Bernal and his collaborators propose that when computing the elastic shape registration of two simple surfaces and the elastic shape distance between them with an algorithm based on a gradient approach for optimizing over the entire set of reparametrizations, to use as the input initial solution the optimal rotation and reparametrization computed with our proposed algorithm. This proposed algorithm has been implemented and is currently being evaluated.

Using different shape representations or different versions of the algorithms lead to different shape dissimilarity metrics, and this brings the question of which metric would perform best. In the previous years, Doğan and Fleisig (UC Berkeley) developed a Python program, VEMOS (Visual Explorer for Metrics Of Similarity) that can be used to evaluate and compare multiple competing similarity/dissimilarity metrics, including shape dissimilarity metrics. VEMOS is useful for applications beyond shape distances; it can be used in a versatile manner to evaluate multiple alternative dissimilarity metrics for heterogeneous data sets, including images, shapes, point clouds and other data types. In FY 2022, Doğan continued to develop VEMOS, made bug fixes, and added new features. A report describing capabilities of VEMOS is available in the NIST technical note [13], and the software is available for download at https://github.com/usnistgov/VEMOS.

[1] O. Abawonse and G. Dogan. Image Segmentation using the Split Bregman Algorithm. In preparation.

[2] P. Athavale, E. Atindama, G. Dogan, and P. Lef. Restoration of EBSD Grain Orientation Data. In preparation.

[3] G. Doğan, J. Bernal, and C. R. Hagwood. Fast Algorithms for Shape Analysis of Planar Objects. In *Proceedings of the IEEE Conference on Computer Vision and Pattern Recognition (CVPR'15)*, Boston, MA, June 2015.

[4] G. Doğan, J. Bernal, and C. R. Hagwood. FFT-based Alignment of 2d Closed Curves with Application to Elastic Shape Analysis. In *Proceedings of the 1st International Workshop on Differential Geometry in Computer Vision for Analysis of Shapes, Images and Trajectories (DiffCV'15)*, Swansea, United Kingdom, September 2015.

[5] J. Bernal, G. Doğan, and C. R. Hagwood. Fast Dynamic Programming for Elastic Registration of Curves. In *Proceedings of the 2nd International Workshop on Differential Geometry in Computer Vision and Machine Learning (DiffCVML'16)*, Las Vegas, NV, July 1, 2016.

[6] J. Bernal, J. Lawrence, G. Doğan, and C. R. Hagwood. On Computing Elastic Shape Distances Between Curves

in d-dimensional Space. NIST Technical Note 2164, June 2021, 39 pages. DOI:10.6028/NIST.TN.2164

[7] A. Srivastava, E. Klassen, S. Joshi, and I. Jermyn. Shape Analysis of Elastic Curves in Euclidean Space. *IEEE Transactions on Pattern Analysis and Machine Intelligence* **33**:7 (2011), 1415-1428.

[8] A. Srivastava and E. P. Klassen. *Functional and Shape Data Analysis*. Springer, New York, 2016.

[9] J. Bernal. Shape Analysis, Lebesgue Integration and Absolute Continuity Connections. NISTIR 8217, 2018.

[10] S. H. Joshi, E. Klassen, A. Srivastava, and I. H. Jermyn. A Novel Representation for Riemannian Analysis of Elastic Curves in R^n. In *Proceedings of the IEEE Conference on Computer Vision and Pattern Recognition (CVPR'07)*, Minneapolis, MN, June 2007.

[11] S. Kurtek, E. Klassen, Z. Ding, and A. Srivastava, A Novel Riemannian Framework for Shape Analysis of 3D Objects. In *Proceedings of the IEEE Conference on Computer Vision and Pattern Recognition (CVPR'10)*, San Francisco, CA, June 2010.

[12] I. H. Jermyn, S. Kurtek, E. Klassen, and A. Srivastava. Elastic Shape Matching of Parameterized Surfaces Using Square Root Normal Fields. In *Proceedings of the 12th European Conference on Computer Vision (ECCV'12)*, Volume 5, Springer, Berlin, 2012, 804-817.

[13] E. Fleisig and G. Doğan. VEMOS: GUI for Evaluation of Similarity Metrics of Complex Data Sets. NIST Technical Note 2160, June 2021, 34 pages. DOI: 10.6028/NIST.TN.2160

Numerical Solutions of the Time Dependent Schrödinger Equation

Barry I. Schneider
William Earwood
Heman Gharibnejad (Computational Physics Inc.)
Luca Argenti (University of Central Florida)
Carlos Marante (University of Central Florida)
Siddhartha Chattopadhyay (U. of Central Florida)
Juan Martin Randazzo (Consejo Nacional de Investigaciones Científicas y Técnicas, Argentina)
Jeppe Olsen (Aarhus University, Denmark)
Ryan Schneider (University of California at San Diego)

We have been collaborating with various scientists for a number of years developing numerically robust methods for solving the time-dependent Schrödinger equation (TDSE). Luca Argenti, an Associate Professor from the University of Central Florida, and his research group, Professor Jeppe Olsen from Aarhus University in Denmark, Juan Martin Randazzo from CONICET in Argentina, former postdoc Heman Gharibnejad, now working at Computational Physics Inc, and a new NRC postdoctoral associate, William Earwood, are part of the project. There are three related research threads underway.

1. Developing a hybrid basis set approach using B-spline/finite element discrete variable (FEDVR) and Gaussian type orbitals to treat the interaction of attosecond (10^{-18} sec) radiation with molecular targets.
2. Computing the required hybrid basis function matrix elements via a novel 3D numerical grid based on overlapping atomic grids.
3. Examining the performance of various numerical time propagation techniques for the TDSE and applying them to attosecond science.

The hybrid basis function approach that is being developed is quite general, but the applications to date have concentrated on describing the *single* ionization of electrons exposed to intense, ultra-fast, laser radiation in many-body atomic and molecular systems. These attosecond (10^{-18} sec) pulses provide a new window to study the electronic motion in atoms and molecules on their natural timescale. To put this in context, the motion of electrons responsible for chemical binding and electron transfer processes in nature have a characteristic timescale of about 100 attoseconds. (It takes an electron 152 attoseconds to go around the hydrogen atom.) Many of these processes can only be described using time-dependent quantum mechanics. Where appropriate, this needs to be coupled to Maxwell's equations to describe macroscopic phenomena. Our overall goal is to image quantum phenomena with sub-femtosecond temporal and sub-Angstrom spatial resolution and to provide coherent control of electron dynamics. Eventually, one can contemplate producing "molecular movies" of this motion in much the same way as it is done in molecular dynamics simulations of heavy particle processes.

The basic methodology as applied to atoms and simple diatomic molecules has been described in [1-11]. Reference [4] provides a detailed review of the work. The essential aspects have been

- development of the finite element discrete variable method (FEDVR) and B-spline techniques to spatially discretize the coordinates of the electrons,
- construction of a numerical grid capable of efficiently computing the required one and two electron matrix elements,
- generalizing the hybrid integral library to compute integrals for double and higher ionization, and
- development of a new Volterra integral method (ITVOLT) to replace the short iterative Lanczos method. ITVOLT will be capable of propagating the time dependent wavefunction over much larger time steps than current approaches.

Previous efforts have efficiently parallelized the FEDVR method using MPI, shown that it scales linearly with the size of the FEDVR basis and applied it to selected problems [1-13]. Large scale calculations have

been performed on a number of atoms and molecules using resources provided by the NSF Extreme Science and Engineering Discovery Environment (XSEDE).

In more recent research we have begun to employ a mixed basis of Gaussian functions at short range and FEDVR/B-spline functions at long range to extend our methods to complex polyatomic molecules. This approach has several important advantages over using a single basis over all of space. First, the use of nuclear-centered Gaussians preserves the local atomic symmetry around each nucleus and avoids the poor and often non-convergent behavior of using a single-center basis at all distances. Second, once the electron is far enough away from the nuclear cusps, a single center expansion converges quickly and, importantly, can represent the electrons out to very large distances using an approach that is very amenable to domain decomposition. The major issue is to compute the one and two electron integrals between the two types of basis functions. The formalism we have been developing requires as input, transition density matrices extracted from a high-level quantum chemistry code, in order to compute the additional one and two-electron integrals. Jeppe Olsen from Aarhus University, an extremely talented quantum chemist, has been collaborating with us on the project. The NIST-UCF-Aarhus-CONICET group meets on a weekly basis to discuss the issues and plans. During the past year, the density matrices have been integrated into a new code called ASTRA and the code has been applied very successfully to a number of atoms and molecules. A long paper describing the results is near completion and will be submitted for publication early in 2023. It should be noted that this is a very complex, many-body problem, and even with the most talented of researchers, it is a long-term effort. The group believes the end product will revolutionize our ability to understand attosecond science in polyatomic molecules.

The calculation of the one and two-electron matrix elements over the hybrid basis, must be performed numerically. Given the polycentric nature of the electron distribution and the need to compute these integrals to significantly larger distances than in quantum chemistry calculations, it was necessary to develop an efficient 3D integration scheme. One cannot use methods that fix the coordinate system at a single point in space, as they are at best very slowly convergent and often do not converge at all. To overcome that, a popular approach developed by Axel Becke, based on the partition of unity, defines atomic grids, centered on the atoms where the grid points are appropriately weighted to satisfy the partition of unity. The original method of Becke required substantial modification for our purposes. We require a central grid that can describe the much larger integration region without too much contamination from the points on the nuclear centers at long range. To accomplish that, we define a new partition of unity that constrains the atomic grid points to small atomic spheres. A central grid is then added to take care of the interstitial and longer range parts of configuration space where the atomic grid points are forced to vanish. The new partition of unity does remarkably well in performing very accurate integration for integrands having nuclear cusps as well as oscillating at larger distances. The work has been completed and a paper [14] describing the approach has been published in Computational Physics Communications.

Lastly, we have been engaged in efforts to generalize the short iterative Lanczos (SIL) method used to integrate the TDSE efficiently and accurately for much longer times [15]. A Volterra integral equation formalism [16], with the acronym ITVOLT has been developed which exploits the fact that part of the Hamiltonian is a linear operator and can be treated using an exponential propagator, which is exactly what the SIL provides. The remainder term, involving a time integral over the residual interaction and the unknown wavefunction, is computed by numerical integration over the large time step using the SIL on each of the terms in the integrand. To do the integral requires that we have a previous approximation to the wavefunction. Thus, the entire scheme is iterative starting with the wavefunction from the previous time step. We have been collaborating on this project with a mathematics graduate student, Ryan Schneider, at UCSD. Ryan was initially supported by the Mathematical Sciences Graduate Internship (MSGI) program of the NSF and worked remotely with us for almost three months in 2019. He received a NIST Graduate Student Measurement Science and Engineering Internship (GMSE) in 2021 and has continued to work with us on the problem, spending the summer of 2022 in residence at NIST. The work Ryan has been doing is described in detail in a separate contribution.

For completeness, we also reference a review paper [17] by Schneider and Gharibnejad that was published in *Nature Review Physics* which received the ITL best journal paper award in 2020.

[1] J. Feist, S. Nagele, R. Pazourek, E. Persson, B. I. Schneider, L. A. Collins, and J. Burgdörfer. Nonsequential Two-Photon Double Ionization of Helium. *Physical Review A* **77** (2008), 043420.

[2] X. Guan, K. Bartschat, and B. I. Schneider. Dynamics of Two-photon Ionization of Helium in Short Intense XUV Laser Pulses. *Physical Review A* **77** (2008), 043421.

[3] X. Guan, K. Bartschat, and B. I. Schneider. Two-photon Double Ionization of H_2 in Intense Femtosecond Laser Pulses. *Physical Review A* **82** (2010), 041407.

[4] B. I. Schneider, J. Feist, S. Nagele, R. Pazourek, S. Hu, L. Collins, and J. Burgdörfer. Recent Advances in Computational Methods for the Solution of the Time-Dependent Schrödinger Equation for the Interaction of Short, Intense Radiation with One and Two Electron Systems, in Dynamic Imaging. In *Quantum Dynamic Imaging*, (A. Bandrauk and M. Ivanov eds.), CRM Series in Mathematical Physics, Springer, New York, 2011.

[5] X. Guan, E. Secor, K. Bartschat, and B. I. Schneider. Double-slit Interference Effect in Electron Emission from H_2^+ Exposed to X-Ray Radiation. *Physical Review A* **85** (2012), 043419.

[6] X. Guan, K. Bartschat, B. I. Schneider, L. Koesterke, Resonance Effects in Two-Photon Double Ionization of H_2 by Femtosecond XUV Laser Pulses. *Physical Review A* **88** (2013), 043402.

[7] J. Feist, O. Zatsarinny, S. Nagele, R. Pazourek, J. Burgdörfer, X. Guan, K. Bartschat, and B. I. Schneider. Time Delays for Attosecond Streaking in Photoionization of Neon. *Physical Review A* **89** (2014), 033417.

[8] X. Guan, K. Bartschat, B. I. Schneider, and L. Koesterke. Alignment and Pulse-duration Effects in Two-photon Double Ionization of H_2 by Femtosecond XUV Laser Pulses. *Physical Review A* **90** (2014), 043416.

[9] B. I. Schneider, L. A. Collins, X. Guan, K. Bartschat, and D. Feder. Time-Dependent Computational Methods for Matter Under Extreme Conditions. *Advances in Chemical Physics* **157** (2015), Proceedings of the 240 Conference: Science's Great Challenges, (A. Dinner, ed.), John Wiley.

[10] B. I. Schneider, X. Guan, and K. Bartschat. Time Propagation of Partial Differential Equations Using the Short Iterative Lanczos Method and Finite-Element Discrete Variable Representation. *Advances in Quantum Chemistry* **72** (2016), 95-127.

[11] B. I. Schneider. How Novel Algorithms and Access to High Performance Computing Platforms are Enabling Scientific Progress in Atomic and Molecular Physics. *Journal of Physics: Conference Series* **759** (2016), 012002.

[12] B. I. Schneider. 45 Years of Computational Atomic and Molecular Physics: What Have We (I) Learned. *Journal of Physics: Conference Series* **875** (2017).

[13] B. I. Schneider, L. A. Collins, K. Bartschat, X. Guan, and S. X. Hu. A Few Selected Contributions to Electron and Photon Collisions with H_2 and H_2^+. *Journal of Physics* **50** (2017), 214004.

[14] H. Gharibnejad, N. Douguet, B. I. Schneider, J. Olsen, and L. Argenti, A Multi-Center Quadrature Scheme for the Molecular Continuum, Computer Physics Communications, **263,** 107889 (2021)

[15] H. Gharibnejad, B. I. Schneider, M. Leadingham, and H. J. Schmale. A Comparison of Numerical Approaches to the Solution of the Time-Dependent Schrödinger Equation in One Dimension. *Computer Physics Communications* (2019), 106808, to appear.

[16] R. Schneider, Heman Gharibnejad and Barry I. Schneider, ITVOLT: An Iterative Solver for Volterra Integral Equations with Application to the Time-Dependent Schrödinger Equation. In review.

[17] B. I. Schneider and H. Gharibnejad. Numerical Methods Every Atomic and Molecular Theorist Should Know. *Nature Reviews Physics*, December 2019.

ITVOLT: An Iterative Solver for the Time-Dependent Schrödinger Equation

Barry I. Schneider
Heman Gharibnejad (Computational Physics Inc.)
Ryan Schneider (UC San Diego)

In atomic units, the time-dependent Schrödinger equation (TDSE) takes the form

$$\left[i\frac{\partial}{\partial t} - H(\boldsymbol{r},t) \right]\psi(\boldsymbol{r},t) = 0$$

for a Hamiltonian $H(\boldsymbol{r},t)$ and a corresponding wavefunction $\psi(\boldsymbol{r},t)$, where **r** denotes all of the spatial variables of the system under consideration**.** Solutions to the TDSE are important for a variety of research efforts in physics and quantum chemistry [1-3]. Numerical methods for this problem attempt to balance the need for highly accurate solutions with the computational challenges associated with problems in quantum mechanics.

As an extension of recent work of Gharibnejad et al. [4], we explored propagation techniques for this setting. Motivated by work of Ndong et al. [5], we devised an approach that propagates a solution to the TDSE by solving an equivalent Volterra integral equation.

Our method, referred to as Iterative Volterra Propagator or ITVOLT, solves the TDSE on successive intervals $[\tau_j, \tau_{j+1}]$ by first converting it to the Volterra integral equation

$$\begin{aligned}&\psi(\boldsymbol{r},t)\\ &= e^{-iH_j(\boldsymbol{r})(t-\tau_j)}\psi(\boldsymbol{r},\tau_j)\\ &- i\int_{\tau_j}^{t} e^{-iH_j(\boldsymbol{r})(t-t')}V_j(\boldsymbol{r},t')\psi(\boldsymbol{r},t')dt'\\ &\tau_j \le t \le \tau_{j+1}\end{aligned}$$

Here, $H_j(\boldsymbol{r})$ is the value of H at the midpoint time $\frac{\tau_j+\tau_{j+1}}{2}$ and $V_j(\boldsymbol{r},t)$ is the time dependent part of H minus its value at the same point.

Choosing a set of quadrature points $\{t_p\}_{p=1}^{n}$ in $[\tau_j, \tau_{j+1}]$ and computing a corresponding set of weights $\{w_{p,l}\}$ via Lagrange interpolation, we can replace the Volterra integral equation with a linear system, where at each quadrature point t_p

$$\begin{aligned}&\psi(\boldsymbol{r},t_p)\\ &\approx e^{-iH_j(\boldsymbol{r})(t_p-\tau_j)}\psi(\boldsymbol{r},\tau_j)\\ &- i\sum_{l=1}^{n} w_{p,l}e^{-iH_j(\boldsymbol{r})(t_p-t_l)}V_j(\boldsymbol{r},t_l)\psi(\boldsymbol{r},t_l).\end{aligned}$$

ITVOLT proceeds by solving this linear system iteratively. The numerical details of this approach are

Table 1. *Driven Harmonic Oscillator: Method Comparison. Best-case solution errors for ITVOLT and RK4 when applied to the TDSE for the driven harmonic oscillator. Ground state probability error measures the accuracy of the computed ground state while norm error measures how close the norm of the computed wavefunction is to one.*

ITVOLT			Runge-Kutta (RK4)		
Ground State Probability Error	Norm Error	Run Time	Ground State Probability Error	Norm Error	Run Time
1.07×10^{-14}	1.05×10^{-14}	23.89 s	3.73×10^{-11}	1.27×10^{-12}	199.24 s

flexible, allowing for a variety of choices of quadrature points and iteration techniques. Through all of this, the use of easily accessible Lagrange interpolations promotes efficiency.

Over the summer of 2022, we implemented ITVOLT on several test problems, culminating in the TDSE for a driven harmonic oscillator. As shown in Table 1, we found that ITVOLT is capable of outperforming existing techniques, such as 4th order Runge-Kutta, in both accuracy and efficiency.

These results, as well as a detailed discussion of the methodology, have been submitted for publication [6]. In future work, we plan to test ITVOLT on even more computationally demanding problems, in particular the 3D hydrogen atom.

[1] I. Gainullin. High-performance GPU Parallel Solver for 3D Modeling of Electron Transfer During Ion-Surface Interaction. *Computer Physics Communications* **210** (2017), 72-78.

[2] E. Paquet and H. L. Viktor. Computational Methods for Ab Initio Molecular Dynamics. *Advances in Chemistry* (2018), 9839641.

[3] M. Abu-samha, L. B. Madsen. Multielectron Effect in the Strong-Field Ionization of Aligned Nonpolar Molecules. *Physics Review A* **38** (2022), 013117.

[4] H. Gharibnejad, B. I. Schneider, M. Leadingham, H. J. Schmale. A Comparison of Numerical Approaches to the Solution of the Time-Dependent Schrödinger Equation in One Dimension. *Computer Physics Communications* **252** (2020), 106808.

[5] M. Ndong, H. Tal-Ezer, R. Kosloff, and C. P. Koch. A Chebyshev Propagator with Iterative Time Ordering for Explicitly Time-Dependent Hamiltonians. *The Journal of Chemical Physics* **132** (2010), 064105.

[6] R. Schneider, H. Gharibnejad, B. I. Schneider. ITVOLT: An Iterative Solver for Volterra Integral Equation with Application to the Time-Dependent Schrödinger Equation. Preprint: arXiv:2210.15677.

Computing Ill-Posed Time-Reversed Dissipative Evolution Equations, Using Stabilized Explicit Schemes Run Backward in Time

Alfred S. Carasso

Ill-posed deconvolution problems and related time-reversed dissipative evolution equations, pervade measurement science, and are important in several other technological applications. In numerous scientific measurements, the instrument point spread function is a bell-shaped distribution that may be well-approximated by a Gaussian, or by a heavy-tailed infinitely divisible probability density, often with parameters that are only tentatively known. This is the case in important NIST work on engineered nanostructures, involving scanning electron microscopes (SEM), Helium ion microscopes (HIM), and transmission electron microscopes (TEM). The latter are also frequently used in nanoscale biomedical and plant biology imaging.

Reformulating the integral equation deconvolution problem into an equivalent time-reversed generalized diffusion equation, provides significant advantages. Marching backward in time stepwise, from a positive time T to time $t = 0$, allows the deconvolution to unfold in *slow motion*, provides the ability to *monitor* that process, and the possibility of terminating it prior to time $t = 0$, to prevent serious noise contamination and/or development of ringing artifacts.

Such an approach, involving time-reversed fractional diffusion equations, was previously successfully applied in deblurring of MRI and PET brain scans, nanoscale electron micrographs, and galactic scale Hubble Space Telescope imagery [1-3]. However, most recently, as shown in Figure 25 through Figure 27, logarithmic rather than fractional diffusion has been found to produce superior results in blind deconvolution of electron micrographs. Further exploration of logarithmic diffusion deconvolution of TEM biomedical micrographs is contemplated.

In other contexts, much success has been achieved in environmental forensics, by solving advection diffusion equations backward in time to locate sources of groundwater contamination [4]. In numerical weather

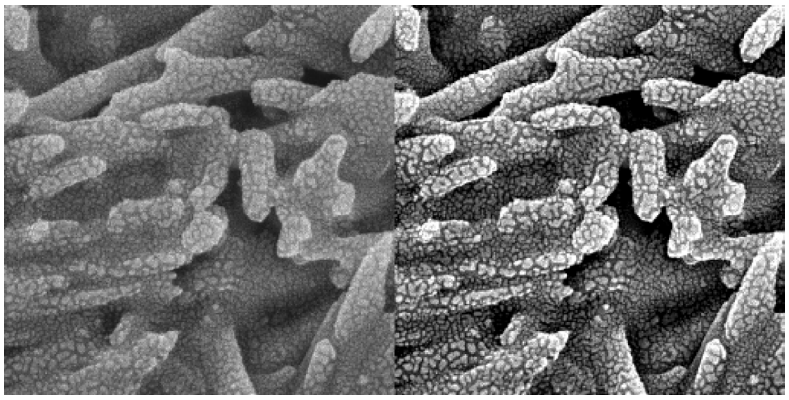

Figure 25. *Blind deconvolution in scanning electron micrograph (SEM) of nanoscale magnetic tape sample. Using time-reversed logarithmic diffusion equations produces significant sharpening, as shown in right hand image.* (Original image courtesy of NIST Microsystems and Nanotechnology Division)

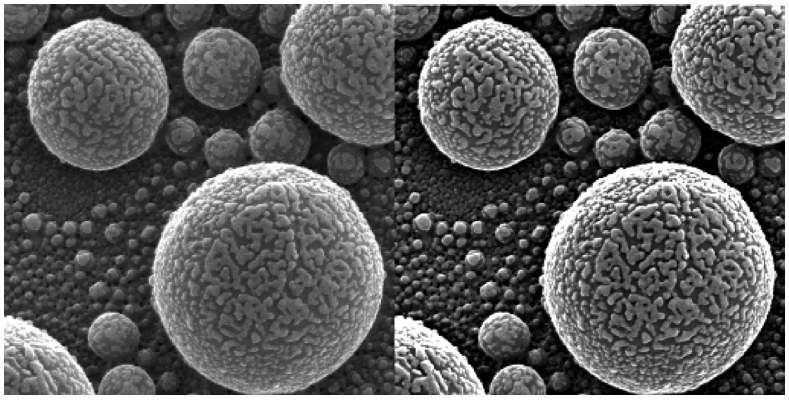

Figure 26. *Blind deconvolution in Helium ion micrograph (HIM) of nanoscale tin balls. Using time-reversed logarithmic diffusion equations produces significant sharpening, as shown in right hand image.* (Original image courtesy of NIST Microsystems and Nanotechnology Division)

prediction and other geophysical computations, data assimilation involving time-reversed dissipative equations plays a major role in initializing prediction models [5-8].

While iterative methods are often used to solve ill-posed evolution equations, such methods are time-consuming and often develop stagnation points. Recently, a powerful non-iterative direct approach has been developed for time-reversed multidimensional nonlinear dissipative equations, based on stabilizing explicit backward marching finite difference schemes. An appropriate easily synthesized compensating smoothing operator is applied at every time step to quench the instability. The stabilized scheme now becomes unconditionally stable, but slightly inconsistent, and eventually leads to a distortion away from the true solution. This is the *stabilization penalty*. However, in many problems of interest, the cumulative error is sufficiently small to allow for useful results. In a series of papers [9-16], such stabilized schemes have been successfully applied to interesting classes of time-reversed nonlinear initial value problems for parabolic equations, viscous wave equations, coupled sound and heat flow, thermoelastic vibrations, 2D viscous Burgers equations, and 2D incompressible Navier-Stokes equations. Such computations had not previously been considered possible.

Data Assimilation In 2d Dissipative Equations. Stabilized backward marching explicit schemes offer significant computational advantages in the growing field of geophysical data assimilation. Current research aims to demonstrate this point by focusing on computational examples involving 8 bit, 256×256 pixel gray-scale images, defined by highly non smooth intensity data. Such data are difficult to synthesize mathematically and pose significant challenges in ill-posed reconstruction. Here, images provide an invaluable exploratory tool in time-reversed dissipative equations.

The 2D viscous Burgers equation is a coupled system of two nonlinear equations in two unknowns, $u(x,y,t), v(x,y,t)$. In [13], the ill-posed problem of backward recovery from inexact data at an appropriately chosen $T > 0$, is studied. Rigorous uncertainty estimates in [17, 18] require a sufficiently small $T > 0$, as well as sufficiently small solution derivatives on $0 \leq t \leq T$, for useful recovery.

A fundamentally different time-reversed problem is discussed in [16]. In a bounded domain $\Omega \subset R^2$, with homogeneous boundary conditions on $\partial\Omega$, and no forcing term, the following data assimilation/inverse design problem associated with that system is considered:

> Find initial values $[u(.,0), v(.,0)]$ that can evolve into a close approximation to a desired target result $[u^*(.,T), v^*(.,T)]$ at some suitable $T > 0$.

In contrast to [13], non-smooth target data are considered that may not correspond to actual solutions at time T, and it may not be possible to find such initial values. Such 2D viscous Burgers problems have not previously been studied. For the 1D Burgers equation, data assimilation is discussed in [5-8], using various iterative methods.

Marching backward in time with a stabilized explicit finite-difference scheme, a large class of examples is presented in [16] where, with realistic values of $T > 0$, and Reynolds numbers as high as 18000, useful initial values can be found that evolve into good

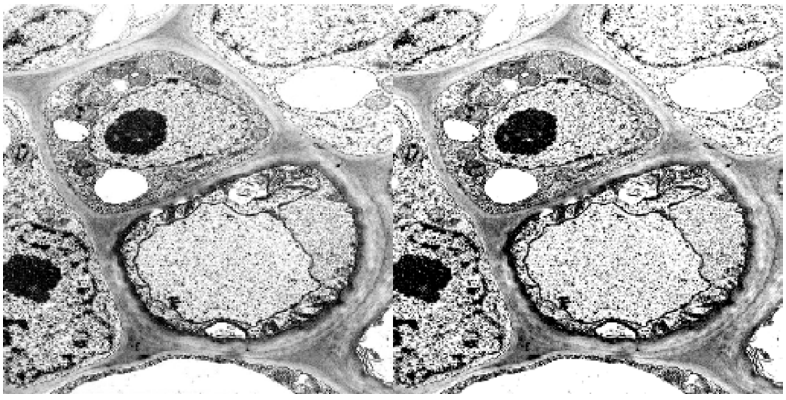

Figure 27. *Blind deconvolution in transmission electron micrograph (TEM) in plant biology study. Using time-reversed logarithmic diffusion equations produces significant sharpening, as shown in right hand image of cotton phloem tissue.* (Original image courtesy of J. Torsch, Cheadle Center for Biodiversity and Ecological Restoration, University of California at Santa Barbara.)

approximations to the desired target data, with modestly small L^1 relative errors. Importantly, there are also unsuccessful examples. Using similar techniques, a class of nonlinear advection diffusion equations is studied in [19]. Here, as shown in Figure 28, modest accuracy is typically the case. There are again unsuccessful examples, and better results are possible with smaller nonlinearities.

Future plans include the study of data assimilation in hyperbolic/parabolic systems, such as thermoelastic vibrations and coupled sound and heat flow. These challenging problems involve three independent sets of initial values, which interact as the evolution progresses.

[1] A. S. Carasso. The APEX Method in Image Sharpening and the Use of Low Exponent Lévy Stable Laws. *SIAM Journal on Applied Mathematics* **63** (2002), 593-618.

[2] A. S. Carasso, D. S. Bright, and A. E. Vladar. APEX Method and Real-Time Blind Deconvolution of Scanning Electron Microscope Imagery. *Optical Engineering* **41** (2002), 2499-2514.

[3] A. S. Carasso. Bochner Subordination, Logarithmic Diffusion Equations, and Blind Deconvolution of Hubble Space Telescope Imagery and Other Scientific Data. *SIAM Journal on Imaging Sciences* **3** (2010), 954-980.

[4] J. Atmadja and A. C. Bagtzoglou. State of the Art Report on Mathematical Methods for Groundwater Pollution Source Identification. *Environmental Forensics* **2** (2001), 205-214.

[5] J. Lundvall, V. Kozlov, and P. Weinerfelt. Iterative Methods for Data Assimilation for Burgers' Equation. *Journal of Inverse and Ill-Posed Problems* **14** (2006), 505-535.

[6] D. Auroux and J. Blum. A Nudging-Based Data Assimilation Method for Oceanographic Problems: The Back and Forth Nudging (BFN) Algorithm. *Nonlinear Processes in Geophysics* **15** (2008), 305-319.

[7] D. Auroux, P. Bansart, and J. Blum. An Evolution of the Back and Forth Nudging for Geophysical Data Assimilation: Application to Burgers Equation and Comparison. *Inverse Problems in Science and Engineering* **21** (2013), 399-419.

[8] H. F. de Campos Velho, V. C. Barbosa, and S. Cocke. Special Issue on Inverse Problems in Geosciences. *Inverse Problems in Science and Engineering* **21** (2013), 355-356.

[9] A. S. Carasso. Stable Explicit Time-Marching in Well-Posed or Ill-Posed Nonlinear Parabolic Equations. *Inverse Problems in Science and Engineering* **24** (2016), 1364-1384.

[10] A. S. Carasso. Stable Explicit Marching Scheme in Ill-Posed Time-Reversed Viscous Wave Equations. *Inverse Problems in Science and Engineering* **24** (2016), 1454-1474.

[11] A. S. Carasso. Stabilized Richardson Leapfrog Scheme in Explicit Stepwise Computation of Forward or Backward Nonlinear Parabolic Equations. *Inverse Problems in Science and Engineering* **25** (2017), 1719-1742.

[12] A. S. Carasso. Stabilized Backward in Time Explicit Marching Schemes in the Numerical Computation of Ill-Posed Time-Reversed Hyperbolic/Parabolic Systems. *Inverse Problems in Science and Engineering* **27** (2019), 134-165.

[13] A. S. Carasso. Stable Explicit Stepwise Marching Scheme in Ill-Posed Time-Reversed 2D Burgers' Equation. *Inverse Problems in Science and Engineering* **27** (2019), 1672-1688.

[14] A. S. Carasso. Computing Ill-Posed Time-Reversed 2D Navier-Stokes Equations, using a Stabilized Explicit Finite Difference Scheme Marching Backward in Time. *Inverse Problems in Science and Engineering* **28** (2020), 988-1010. DOI: 10.1080/17415977.2019.1698564

[15] A. S. Carasso. Stabilized Leapfrog Scheme Run Backward in Time, and the Explicit $O(\Delta t)^2$ Stepwise Computation of Ill-Posed Time-Reversed 2D Navier-Stokes Equations. *Inverse Problems in Science and Engineering* **29** (2021), 3062-3085. DOI: 10.1080/17415977.2021.1972997

[16] A. S. Carasso. Data Assimilation in 2D Viscous Burgers Equation Using a Stabilized Explicit Finite Difference Scheme Run Backward in Time. *Inverse Problems in Science and Engineering* **29** (2021), 3475-3489 DOI: 10.1080/17415977.2021.2009476

[17] R. J. Knops and L. E. Payne. On the Stability of Solutions of the Navier-Stokes Equations Backward in Time. *Archives of Rational Mechanics and Analysis* **29** (1968), 331-335.

[18] D. N. Hào, V. D. Nguyen, and V. T. Nguyen. Stability Estimates for Burgers-Type Equations Backward in Time. *Journal of Inverse and Ill Posed Problems* **23** (2015),41-49.

[19] A. S. Carasso. Data Assimilation in 2D Nonlinear Advection Diffusion Equations, using an Explicit Stabilized Leapfrog Scheme Run Backward in Time. NIST Technical Note 2227}. DOI: 10.6028/NIST.TN.2227

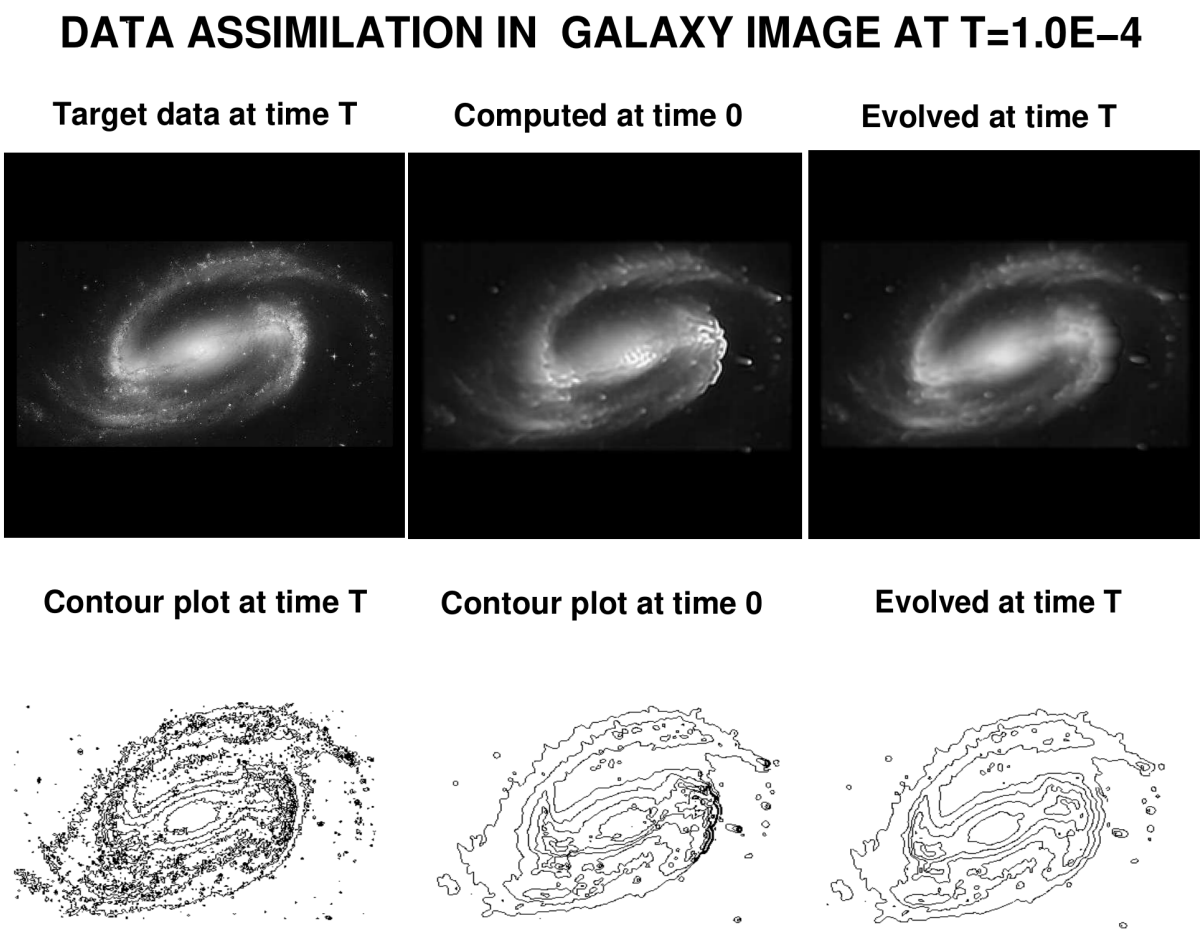

Figure 28. *Barred galaxy NGC1300 data assimilation example in nonlinear advection diffusion equation. Data in rightmost column approximates desired target data in leftmost column with L^1 relative error of 16 %.* (Image courtesy of Hubble Telescope Barred Galaxy Collection)

Mathematics of Biotechnology

As proof-of-concept academic work in engineering biology meets the market realities of bringing lab science to product initiation, there are questions in how to compare biological products, measure whether desired outcomes are realized, and optimize biological systems for desired behaviors. NIST is working to deliver tools and standards to measure such biological technologies, outputs, and processes from healthcare to manufacturing and beyond. We support this effort with the development and deployment of innovative mathematical modeling and data analysis techniques and tools.

Data Analysis for Quantitative Polymerase Chain Reaction Measurements

Paul Patrone
Anthony Kearsley
Peter Vallone (NIST MML)
Erica Romsos (NIST MML)
Patrick Hutchins (USGS)
Adam Sepulveda (USGS)

Quantitative polymerase chain-reaction (qPCR) measurements are a mainstay tool for detection of genetic material, with broad applications to diagnostics, environmental testing, and forensics. Indeed, the COVID-19 pandemic has highlighted the critical role of qPCR in identifying active SARS-CoV-2 infections. Despite its importance, however, there are many open questions regarding uncertainty quantification (UQ) and methods for robust analysis of raw data.

In FY 2020, several of us developed new methods for background subtraction and analysis of qPCR data [1]. The main idea behind our approach was to leverage a previously unknown property that all qPCR amplification curves, including their plateau phases, are identical up to horizontal shifts and multiplicative factors. We showed that it was possible to identify positive samples by transforming a test curve onto a positive control via a constrained optimization formulation; see Figure 29. This led to a manuscript and patent application for the resulting methods.

In FY 2021 and FY 2022, we engaged in collaborative research and technology transfer with external stakeholders. In particular, the US Geological Survey (USGS) uses qPCR measurements to locate invasive species in freshwater systems by testing for environmental DNA (eDNA). However, given the likelihood of "genetic contamination" in such open systems, UQ of the resulting analysis is critical for justifying remediation decisions. This is especially important given that the resulting actions are expensive and have the potential for ecological disruption. To address such questions, we have worked with USGS to identify best practices for

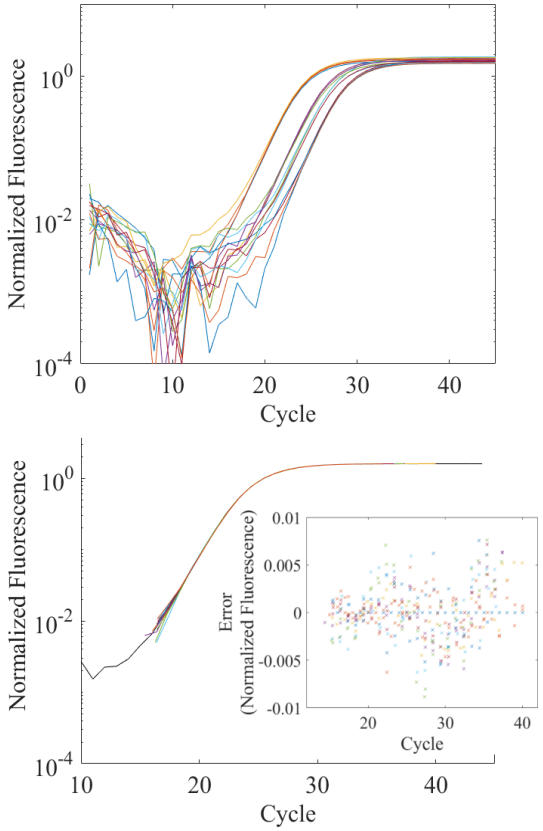

Figure 29. *qPCR amplification curves of the N1 fragment of a SARS-CoV-2 RNA construct. Top: qPCR curves after background subtraction. Bottom: curves after data collapse. The inset shows the error on an absolute scale relative to the master curve. The data collapse is accurate to better than 1 % of the maximum scale of the data.*

data analysis, including determining if certain data analysis routines are statistically consistent with the amount of DNA expected in samples that were tested as part of an interlaboratory study.

In addition to this, work continues in commercializing our qPCR data analysis methods via a CRADA with a private diagnostics lab. On-going research aims to better understand and quantify sources of background in raw data.

[1] P. N. Patrone, E. L. Romsos, M. H. Cleveland, P. M. Vallone, and A. J. Kearsley. Affine Analysis for Quantitative PCR Measurements. Analytical and Bioanalytical Chemistry 412 (2020), 7977–7988.

Advanced Data Analysis for Diagnostics, Biometrology, and COVID-19

Paul Patrone
Anthony Kearsley
Prajakta Bedekar
Rayanne Luke
Christopher Heaney (Johns Hopkins University)
Nora Pisanic (Johns Hopkins University)
Yukari Manabe (Johns Hopkins University)
David Thomas (Johns Hopkins University)

The on-going COVID-19 health crisis has highlighted the critical need for advanced metrology tools that can be used in both clinical and research settings. For example, accurate diagnostic testing is needed to characterize epidemiological patterns, manage healthcare infrastructure, and identify optimal policy decisions. Motivated by such issues, several staff members in ACMD have been collaborating with a range of internal and external stakeholders on projects related to antibody measurements.

Beginning in FY 2021, several of us derived a series of new results showing that diagnostic classification associated with antibody assays can be recast as an optimization problem. From a data analysis standpoint, the underlying measurements return a value r associated with an antibody level, which is used to classify a sample as positive or negative, say for having been infected with SARS-CoV-2. A canonical method assigns r to the positive or negative classes depending on whether the data falls into one of two domains D_p or D_n that partition the measurement space. However, we recently demonstrated that the optimal (i.e., minimum error) domains are given by

$$D_p^* = \{r: qP(r) > (1-q)N(r)\}$$
$$D_n^* = \{r: qP(r) < (1-q)N(r)\}$$

where $P(r)$ and $N(r)$ are models quantifying the conditional probability that a positive or negative sample yields a value r, and q is the disease prevalence [1]. We also proved that unbiased estimates of prevalence can be constructed from a counting exercise that is independent of sample classification but still dependent on these probability models [1]. Thus, we reduced all diagnostics to a problem of correctly modeling probability distributions.

Following up on this, in FY 2022 we began a series of collaborations with the School of Public Health at Johns Hopkins University to improve data analysis associated with saliva-based SARS-CoV-2 antibody tests. A fundamental problem with such assays is the variable nature of the measurement conditions, given that daily activities such as drinking water may dilute samples. As a result, it is sometimes necessary to hold out samples if they are too diluted and/or do not appear to contain a meaningful signal. However, doing so also wastes time and resources if a large amount of the data must be discarded.

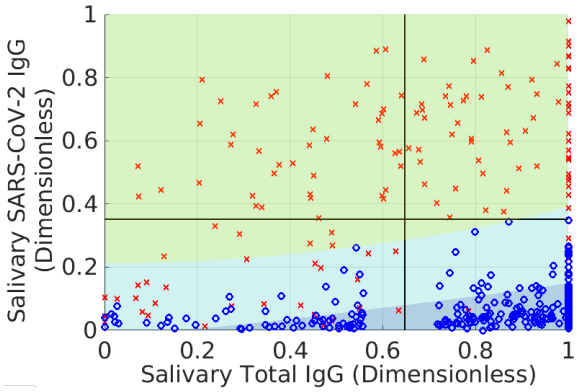

Figure 30. *Illustration of the classification method developed in [2]. Red x and blue o correspond to samples that are known to be positive and negative for SARS-CoV-2. The measurements are associated with two different methods of quantifying antibodies; see [2] for details. The yellow-green domain is the positive classification domain, whereas dark blue is the negative classification domain. The light blue domain is the holdout domain. The original assay defined the upper two quadrants of the plot as the positive domain, the lower right as the negative domain, and the lower left as the holdout domain. The optimal method maintains testing accuracy while reducing the fraction of holdouts by more than 10 %.*

To address this problem, we formulated a constrained optimization problem that minimizes the size of the holdout domain while maintaining a given classification accuracy for the remaining samples [2]. Interestingly, the solution to this problem is given in terms of the bathtub principle. In the context of diagnostic testing, this principle states that we hold out points from the measurement space with the lowest *local classification accuracy* up to a threshold that depends on the target classification accuracy. Figure 30 shows the results of this analysis applied to a SARS-CoV-2 assay developed at Johns Hopkins University.

We have also pursued further extensions of classification theory for diagnostics. More recently, we have (i) showed that bathtub principles can be used to minimize uncertainty in prevalence estimates [3], and (ii) generalized our methods to account for time-varying antibody levels [4], multiple classes [5], and higher dimensional measurements [6]. Work is on-going to transfer this technology to stakeholders.

[1] P. N. Patrone, and A. J. Kearsley. Classification under uncertainty: data analysis for diagnostic antibody testing. *Mathematical Medicine and Biology: A Journal of the IMA* **38**:3 (2021), 396–416. DOI: 10.1093/imammb/dqab007

[2] P. N. Patrone, P. Bedekar, N. Pisanic, Y. C. Manabe, D. L. Thomas, C. D. Heaney, and A. J. Kearsley. Optimal Decision Theory for Diagnostic Testing: Minimizing Indeterminate Classes with Applications to Saliva-based SARS-CoV-2 Antibody Assays. *Mathematical Biosciences* **351** (2022), 108858. DOI: 10.1016/j.mbs.2022.108858

[3] P. N. Patrone, A. J. Kearsley. Minimizing Uncertainty in Prevalence Estimates. In review.

[4] P. Bedekar, A. J. Kearsley, P. N. Patrone, Prevalence estimation and optimal classification methods to account for time dependence in antibody levels. *Journal of Theoretical Biology*, to appear.

[5] R. A. Luke, A. J. Kearsley, and P. N. Patrone. Optimal classification and Generalized Prevalence Estimates for Diagnostic Settings with More than Two Classes. In review.

[6] R. A. Luke, A. J. Kearsley, N. Pisanic, Y. C. Manabe, D. L. Thomas, C. D. Heaney, and P. N. Patrone. Modeling in Higher Dimensions to Improve Diagnostic Testing Accuracy: Theory and Examples for Multiplex Saliva-Based SARS-Cov-2 Antibody Assays. In review.

Metrology for Cytometry

Paul Patrone
Anthony Kearsley
Danielle Middlebrooks
Rayanne Luke
Prajakta Bedekar
Gregory Cooksey (NIST PML)
Matthew DiSalvo (NIST PML)
Jalal Sadeghi (NIST PML)

For more than 30 years, flow cytometry, a technique used to measure characteristics of cells, has been a mainstay for cancer detection, drug development, and biomedical research. It has remained a primarily qualitative metrology platform, however, because measurement uncertainties associated with this technique are so large. While exact economic figures are difficult to estimate, this has clearly had a significant impact on the roughly $200 billion of waste in the healthcare industry and contributed to the broader reproducibility crisis in biomedical research [1]. The challenge of making cytometry an accurate and precise metrological tool arises from the competing requirement that it have high throughput. Typical biological samples can have up to hundreds of millions of cells, which must be analyzed over a few hours.

To achieve this throughput, cytometers direct cells through a microfluidic channel at high-speed, past an optical interrogation region that collects fluorescence light from antibodies attached to surface proteins. The total fluorescence collected from each cell should then, in principle, be proportional to the total number of markers on its surface. But in practice, this idealized picture is complicated by the cumulative effects of the physical phenomena involved: fluid-dynamic forces cause cells to move across streamlines and/or have unpredictable trajectories; optical geometric collection efficiencies depend on position in the interrogation region; and signal

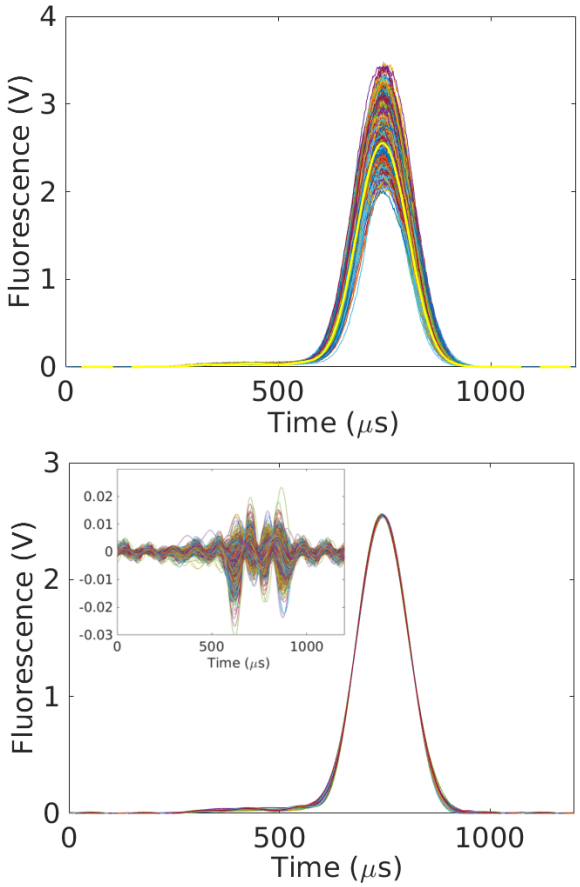

Figure 31. *Top: 1300 cytometry signals corresponding to particles having different velocities and sizes. Bottom: Our theory predicts that the 1300 curves in the top figure can be collapsed onto one another using straightforward linear transformations that depend on the particles' velocities and sizes. The agreement with this theory is on the order of 2% relative to the maximum scale of the measurements. The residuals in the inset can be interpreted as the per-event reproducibility of the measurement process.*

acquisition and processing tools introduce non-linear effects and measurement uncertainties through discrete sampling. These challenges, in addition to the complexity of exactly replicating the necessary measurement infrastructure at the micron scale, have made it virtually impossible to reproduce measurements on a single cell, a necessary first step towards fully assessing and controlling uncertainties in cytometry.

ACMD, PML, and MML staff were awarded a NIST Innovations in Measurement Science (IMS) award to develop a microfluidic-based cytometer, whose design explicitly allows control and study of repeat measurements of cells. Following on work from FY 2020 and FY 2021, we are continuing a series of research projects on uncertainty quantification (UQ) for cytometry. The first of these aims to quantify the per-event uncertainty associated with each method. Recently we derived a key result indicating that all cytometry events (e.g., for a fixed cell-marker type) are identical up to a set of straightforward linear transformations that

depend on physical parameters such as the cell size, speed, and number of biomarkers; see Figure 31. Using optimization, we can determine these unknown parameters by mapping different signals onto one another. Critically, this also yields multiple, model-based but distinct realizations of what a measurement would look like could it be reproduced on the same measurand. Using this, we have been able to estimate for the first time the per-event uncertainty; see Figure 31. This analysis also enables new types of data analysis associated with doublet identification, doublet deconvolution, and more generally, cell counting. This work is summarized in a collection of manuscripts [2, 3, 4], with several more in preparation.

The second UQ project aims to identify the probabilities of measurement outcomes for populations that may have some overlapping signals. The key assumption of this analysis is that the probability densities (PDFs) of measurement values for different populations have partially disjoint supports. Given a "mixed" PDF associated with an unknown combination two or more populations, one can only subtract off the PDF of one population from this mixture until the latter becomes negative. This implies an optimization problem wherein one seeks to maximize the amount of subtracted population subject to a positive-definite constraint. Work is ongoing to apply this algorithm to real cell systems and address issues associated with signal noise.

[1] W. H. Shrank, T. L. Rogstad, and N. Parekh. Waste in the US Health Care System: Estimated Costs and Potential for Savings. *JAMA* **322**:15 (2019), 1501-1509.

[2] P. N. Patrone, M. DiSalvo, A. J. Kearsley, G. B. McFadden, and G. A. Cooksey. Reproducibility in Cytometry: Signals Analysis and its Connection to Uncertainty Quantification. In review.

[3] M. DiSalvo, P. N. Patrone, A. J. Kearsley, and G. Cooksey. Serial Flow Cytometry in an Inertial Focusing Optofluidic Microchip for Direct Assessment of Measurement Variations. *Lab on a Chip* **22**:17 (2022), 3217-3228. DOI: https://doi.org/10.1039/D1LC01169C

[4] J. Sadeghi, P. N. Patrone, A. J. Kearsley, and G. Cooksey. Optofluidic Flow Meter for Sub-nanoliter per Minute Flow Measurements. *Journal of Biomedical Optics* **27**:1 (2022), 017001. DOI: 10.1117/1.JBO.27.1.017001

Standardization of SARS-CoV-2 Serology Measurements

Paul Patrone
Anthony Kearsley
Lili Wang (NIST MML)
Sheng Lin-Gibson (NIST MML)

A key problem associated with antibody measurements for SARS-CoV-2 is the lack of an absolute scale. Typical standards rely on pooled blood samples. Being human derived, however, they have unknown antibody titers, so that subsequent measurements can only be defined on a relative scale. This makes it challenging to understand the degree of protection associated with a given antibody measurement and reduces usefulness of harmonization studies.

To address these problems, NIST has engaged with external stakeholders, including Roche, Abbott, and Regeneron, to develop SARS-CoV-2 monoclonal antibodies (mAbs) as reference materials. Being manufactured proteins, mAbs have well-defined concentrations that are known in absolute terms. However, conformational differences between mAbs and relative to the SARS-CoV-2 antigens suggests that these references may yield significant measurement variation when tested against the variety of commercial assays. Thus, it is necessary to quantify the mAb induced uncertainties to assess their usefulness as reference materials.

To address this problem, we have undertaken an interlab study that combines elements of uncertainty quantification (UQ) with thermodynamics-based modeling to separate distinct sources of measurement variation. Several surprising results have emerged.

- To the best of our knowledge, we have formulated the first mathematical definition of assay harmonization that explicitly incorporates UQ. In particular, we have shown that a both rigorous and useful approach identifies harmonization as the task of finding a mapping operator that takes only measurement values from different assays as inputs and outputs a common consensus value with confidence bounds. In this way, harmonization renders measurements from different assays approximately interchangeable by quantifying the extent they can be brought into agreement.
- Using Gibbs free-energy-based arguments, we have shown that the choice of reference material does not affect confidence bounds associated with consensus values. We have validated using data from the interlab study.
- As a consequence, we have demonstrated, both theoretically and experimentally, that mAbs are equally useful reference materials from a performance standpoint. This conclusion stands in stark

contrast to a long-held belief by the serology community that only human-derived, pooled standards can be used as reference materials.

This work has also yielded several other smaller results, all of which are included in a manuscript in preparation. In particular, we have developed a new method for normalizing antibody measurements to a standard and developed more rigorous notions of correlates of protection, which are currently lacking in the SARS-CoV-2 serology community.

Mathematical Models for Cryobiology

Daniel Anderson
Anthony Kearsley
James Benson (University of Saskatchewan, Canada)
Jessica Masterson (George Mason University)

Cryobiology, the study of biological specimens at cryogenic temperatures, plays an enormous role in a wide range of fields. In the field of medicine, cryobiology is the basis for cryopreservation in assisted reproduction, organ transplantation, biobanking and personalized medicine. Cryo-banking is used in the agriculture industry as well as for initiatives aimed at preserving rare and endangered plant and animal species and in the development of more productive agricultural yields. Applications in forensics arise in the processing and preservation of frozen biological samples that are often important and fragile evidence in criminal investigations. The breadth and depth of these applications reflect the complexity of the biological, chemical, and physical aspects required to describe and model these problems. Mathematical and computational models can be used to probe these complex systems and in conjunction with sophisticated control and optimization schemes, can establish more effective protocols for cryopreservation.

Cryopreservation of a human cell is a form of biomimicry that attempts to do in the laboratory, or in silica, what some frog and amphibian species can do naturally. A cryoprotectant, effectively an antifreeze, aims to play the role that substances like glucose play in the winter preservation of frozen frogs. These cryoprotectants, which are added to the extra-cellular environment, help to remove water from a cell before cooling, thus reducing the likelihood of intracellular ice formation. This, however, comes at a price due to the cell's limited ability to withstand the elevated levels of chemicals, including the naturally occurring salts in the cell, possibly damaging the cell, or causing death by chemical toxicity. Thus, the maintenance of a viable cell during cryopreservation is complicated by two primary factors. Cooling the cell too quickly increases the undercooling and the likelihood of intracellular ice formation and cell damage or death while cooling the cell too slowly can overexpose the cell to high solution concentrations and lead to chemical toxicity. This amounts to a high-stakes goldilocks problem from the cell's perspective.

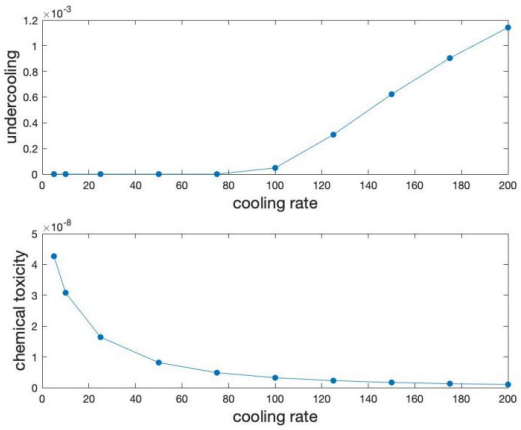

Figure 32. *Computed damage function proxies as a function of cooling rate.*

Mathematical modeling in cryobiology thus requires a detailed understanding of thermal and chemical transport in bulk phases as well as across a semipermeable cell membrane. Additionally, phase transformation of these multicomponent solutions – phenomena that link cryobiology to a wide range of other fields from geophysics to industrial materials processing [6] – must also be included. Cryopreserving a cell requires a delicate balance between two competing damage mechanisms, and thus a delicate optimization problem. We are exploring foundational aspects of biochemical and physical modeling in cryobiology, computational methods for the solution of these models, and applications of these ideas to cryopreservation of cells.

The focus of [1] was to establish the foundations of the chemical thermodynamics necessary to describe transport processes during cryopreservation. This work formulated chemical potentials and related thermodynamics quantities for non-dilute and non-ideal multicomponent solutions of experimental and theoretical interest to cryobiologists. Next, the multiphase, multi-species transport equations were developed along with a consistent characterization of cell membrane dynamics and solid-liquid phase transitions [2]. A critical aspect of our work was to obtain, from first principles, mathematical models that address both spatial and temporal dynamics of chemical species and heat transport. Various aspects of the freezing of a spherical biological cell were addressed in [3] and [4]. Based on a numerical algorithm outlined in [4], we explored in [3] the evolution of the thermal fields in the solid, liquid, and intracellular regions along with the concentration of cryoprotectant and the intra- and extracellular salts. These studies incorporated the effects of confinement and partial solute rejection, which had not previously been examined in cryobiology. These observations led to the

development of objective functions in [4], which provide a measure of both intracellular undercooling and chemical toxicity. These control functions appear more suited to deriving cooling protocols than previously employed toxicity functions [5].

The mathematical models and computational algorithms established in this foundational series of papers [1-4] form the foundation for our current work towards optimal control of these systems. Our current work underway with J. Masterson involves the identification of proxies for cell/tissue damage that can be used in optimal control settings (see Figure 32). The mathematical framework is PDE-constrained optimization in which the bio/chemical/physical model constrains variables such as solid and liquid thermal fields, that help define objective functions such as those measuring tissue undercooling and chemical toxicity. Work is underway to formulate appropriate optimal control equations based on adjoint formulations of the governing equations. Our first objective is to address optimal protocols in the freezing/cooling stage. A second goal is to extend this framework to explore strategies that can optimize protocols for cryo-recovery where warming and/or melting occur. The central role played by phase transformation and transport in multicomponent systems links these cryobiological processes and their mathematical descriptions to related ones that occur under vastly different conditions in geophysics and industrial materials processing [6].

[1] D. M. Anderson, J. D. Benson, and A. J. Kearsley. Foundations of Modeling in Cryobiology I: Concentration, Gibbs Energy, and Chemical Potential Relationships. *Cryobiology* **69** (2014), 349-360. DOI: 10.1016/j.cryobiol.2014.09.004

[2] D. M. Anderson, J. D. Benson, and A. J. Kearsley. Foundations of Modeling in Cryobiology II: Heat and Mass Transport in Bulk and at Cell Membrane and Ice-liquid Interfaces. *Cryobiology* **91** (2019), 3-17. DOI: 10.1016/j.cryobiol.2019.09.014

[3] D. M. Anderson, J. D. Benson, and A. J. Kearsley. Foundations of Modeling in Cryobiology III: Heat and Mass Transport in a Ternary System. *Cryobiology* **92** (2020), 34-46. DOI: 10.1016/j.cryobiol.2019.09.013

[4] D. M. Anderson, J. D. Benson, and A. J. Kearsley. Numerical Solution of Inward Solidification of a Dilute Ternary Solution Towards a Semi-permeable Spherical Cell. *Mathematical Biosciences* **316** (2019), 108240. DOI: 10.1016/j.mbs.2019.108240

[5] J. D. Benson, A. J. Kearsley, and A. Z. Higgins. Mathematical Optimization of Procedures for Cryoprotectant Equilibration using a Toxicity Cost Function. *Cryobiology* **64** (2012), 144-151. DOI: 10.1016/j.cryobiol.2012.01.001

[6] D. M. Anderson, P. Guba, and A. J. Wells. Mushy Layer Convection. *Physics Today* **75** (2022) 34-39. DOI: 10.1063/PT.3.4940

Modeling for Biological Field Effect Transistor Experiments

Ryan M. Evans
Seulki Cho (NIST PML)
Arvind Balijepalli (NIST PML)
Anthony Kearsley

Biological field effect transistors (Bio-FETs) are modern bioelectronics instruments offering novel biomarker measurements. In contrast with traditional measurement techniques that require specialized facilities and expensive equipment, Bio-FETs offer rapid, accurate and low-cost measurements. Since these instruments are hand-held and portable, they promise to yield wider accessibility to critical medical diagnostic tests. During a typical experiment, a chemical reactant bath is injected into a solution-well that contains a buffer fluid. These chemical reactants diffuse through the solution-well and bind with chemical reactants confined to a thin layer known as the biochemical gate on the sensor surface. This produces a time-series signal that can be used to analyze the chemical reaction of interest. See Figure 33 for an experimental Bio-FET signal.

Since estimating parameters associated with these experiments like kinetic coefficients can help us identify biomarkers, accurate mathematical models for these experiments are desired. Previous mathematical models have either not accounted for the time dependent nature of Bio-FET experiments [1–3] or have not included physically relevant transport processes [4–5]. A model recently published by Evans, Kearsley, and Balijepalli is the first dynamic model for Bio-FET experiments that accounts for physically relevant transport effects, and it has been shown that this model compares favorably with experimental data [6].

The nonlinear integrodifferential equation (IDE) presented in [6] takes the form:

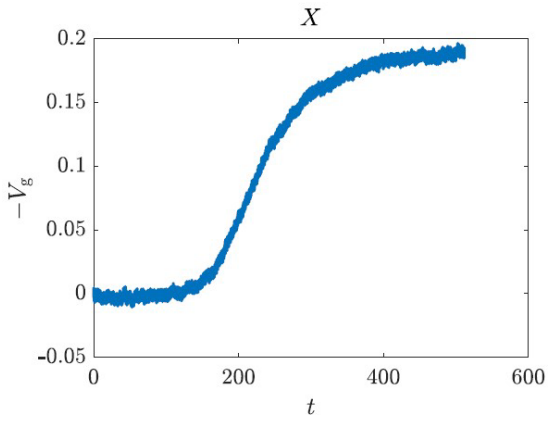

Figure 33. *Experimental Bio-FET signal. The horizontal axis represents time in seconds, and the vertical axis represents voltage that is measured as a result of surface binding.*

$$\frac{\partial B}{\partial t} = (1 - B)C(x, 0, t) - KB,$$

where

$$\begin{aligned} C(x,0,t) = {} & \mathrm{C_i}(x,0,t) \\ & - \frac{\mathrm{Da}\sqrt{D}l_\mathrm{s}}{\sqrt{\pi}} \left\{ \int_{-1/2}^{1/2} \int_0^t \frac{1}{\sqrt{\tau}} \theta_3\left(0, \mathrm{e}^{-\epsilon^2/l_\mathrm{s}^2 \mathrm{D}\tau}\right) \frac{\partial B}{\partial \tau}(\nu, t-\tau)\, \mathrm{d}\tau\, \mathrm{d}\nu \right. \\ & + 2\sum_{n=1}^{\infty} \int_{-1/2}^{1/2} \int_0^t \frac{\mathrm{e}^{-\lambda_\mathrm{n}\mathrm{D}\tau}}{\sqrt{\tau}} \theta_3\left(0, \mathrm{e}^{-\epsilon^2/l_\mathrm{s}^2 \mathrm{D}\tau}\right) \frac{\partial B}{\partial \tau}(\nu, t-\tau) \mathrm{d}\tau \cos\left(\sqrt{\lambda_\mathrm{n}}(\nu + 1/2l_\mathrm{s})\right) d\nu \\ & \left. \cdot \cos\left(\sqrt{\lambda_\mathrm{n}}(x + 1/2l_\mathrm{s})\right) \right\}, \end{aligned}$$

$\theta_3(\cdot,\cdot)$ is a third-order theta function [7, Eq. 20.2.3], $C_\mathrm{i}(x, 0, t)$ satisfies the Neumann Problem on a rectangle with homogeneous boundary conditions and is a compactly supported Gaussian $f(x, y)$ at the initial time $t = 0$, and $B(x, t) = 0$. In [6] Evans and coworkers developed a method of lines (MOL) approximation to this equation that achieves an order of three-halves in time and second in space, the former of which comes from the singularity. After regularizing the singularity by using the definition of $\theta_3(\cdot,\cdot)$ and adding and subtracting

$$\frac{\partial B}{\partial \tau}(\nu, t)$$

from the first integrand, an expansion of the form

$$B(x, t) \approx \sum_{i=1}^{N} \phi_i(x) h_i(t)$$

was developed and substituted into the equation. In the above expansion the $\phi_i(x)$ are locally defined quadratics and the $h_i(t)$ are time-dependent functions that are determined by evaluating each side of the resulting equation at the center of each of the N hat functions, yielding a set of N ordinary differential equations. These equations are solved by with a semi-implicit discretization and the approximation

$$h_i{}'(t_m) \approx \frac{\Delta h^{(m)}{}_i}{\Delta t},$$

which yields a linear system that we can use to solve for $\Delta h_i^{(m)}$ and used to update h_i via the formula

$$h_i^{(m+1)} = h_i^{(m)} + \Delta h_i^{(m)}$$

for each i. We are currently developing a new numerical approximation to this system based on radial basis functions (RBF), which are known to have excellent interpolation properties. In particular, our RBF approximation centers around the expansion:

$$B(x, t) \approx \sum_{j=1}^{M} \sum_{i=1}^{N} w_{ij} \Phi_{ij}(x, t;\, z).$$

The weights w_{ij} are constant; there are many choices for the RBFs $\Phi_{ij}(x, t)$, we chose Gaussians

$$\Phi_{ij} = \mathrm{e}^{-z\left[(x-x_\mathrm{i})^2 + (t-t_\mathrm{j})^2\right]}.$$

The parameter z controls the Gaussians width. Substituting this RBF expansion into our IDE and evaluating at each of the nodes (x_i, t_j) gives a nonlinear system for the weights w_{ij}. A key advantage of this method is that, since the Gaussian is a known separable function of x and t, the singularity can be regularized with a substitution. It is expected that a numerical solution of the nonlinear algebraic can be rapidly achieved with Anderson acceleration [8]. It is expected that our RBF approximation will be even faster and more accurate than the MOL approximation, giving even more rapid and precise simulations of Bio-FETs.

[1] S. Baumgartner, M. Vasicek, A. Bulyha, N. Tassotti, and C. Heitzinger. Analysis of Field-Effect Biosensors Using Self-Consistent 3D Drift-Diffusion and Monte-Carlo Simulations. *Procedia Engineering* **25** (2011), 407-410.

[2] C. Heitzinger, N. J. Mauser, and C. Ringhofer. Multiscale Modeling of Planar and Nanowire Field-Effect Biosensors. *SIAM Journal on Applied Mathematics* **70**:5 (2010), 1634-1654.

[3] D. Landheer, G. Aers, W. R. McKinnon, M. J. Deen, and J. C. Ranuarez. Model for the Field Effect from Layers of Biological Macromolecules on the Gates of Metal-Oxide-Semiconductor Transistors. *Journal of Applied Physics* **98**:4 (2005), 044701.

[4] X. Duan, Y. Li, N. K. Rajan, D. A. Routenberg, Y. Modis, and M. A. Reed. Quantification of The Affinities and Kinetics of Protein Interactions Using Silicon Nanowire Biosensors. *Nature Nanotechnology* **7**:6 (2012), 401-407.

[5] G. Tulzer, S. Baumgartner, E. Brunet, G. C. Mutinati, S. Steinhauer, A. Kck, P. E. Barbano, and C. Heitzinger. Kinetic Parameter Estimation and Fluctuation Analysis of CO at SNO2 Single Nanowires. *Nanotechnology* **24**:31 (2013), 315501.

[6] R. M. Evans, A. Balijepalli, and A. J. Kearsley. Transport Phenomena in Biological Field Effect Transistors. *SIAM Journal on Applied Mathematics* **80**:6 (2020), 2586-2607.

[7] F. W. J. Olver, A. B. Olde Daalhuis, D. W. Lozier, B. I. Schneider, R. F. Boisvert, C. W. Clark, B. R. Miller, B. V. Saunders, H. S. Cohl, and M. A. McClain, eds. *NIST Digital Library of Mathematical Functions*. http://dlmf.nist.gov/, Release 1.1.8 of 2022-12-15.

[8] Alex Toth and C. T. Kelley. Convergence Analysis for Anderson Acceleration. *SIAM Journal on Numerical Analysis* **53**:2 (2015), 805-819.

Binding, Brightness, or Noise? Extracting Temperature-dependent Properties of SYTO-13 Dye Bound to DNA

Robert DeJaco
Anthony Kearsley
Jacob Majikes (NIST PML)
J. Alexander Liddle (NIST PML)

In many areas of biotechnology, such as food safety, health diagnostics, and forensics, practitioners are given a sample and need to determine the concentration or strandedness of a given sequence of DNA. Since sample volumes are often small and high throughput is needed, fluorescence monitoring is used. Specifically, a probe is added to the solution that possesses different fluorescence properties associated with different concentrations and types of DNA. From measurements of the fluorescence, underlying properties of DNA are inferred.

Unfortunately, the inference process is limited by subjective and systematic bias. This is especially true for fluorescent dyes that bind to DNA. Here, the conventional approach is empirical with no clear connection to or discrimination between dye binding, dye brightness, and experimental noise. Accounting for binding and brightness is further hindered by a lack of property data available above room temperature.

To address these challenges, we developed a new mathematical model that discriminates between binding strength and adsorbed molar fluorescence. We also found that, by focusing on the low dye coverage regime, where the fraction of DNA bases occupied by dye is small and the fluorescence is linear in dye concentration, bias due to quenching and deviations from Beer's Law could be eliminated. In close collaboration with PML, we devised a series of experiments that would allow us to extract the binding strength and fluorescence per mole of dye at a variety of different temperatures using numerical optimization. To ascertain the extent of noise, we repeated the same measurement two or three times.

The experimental data, as depicted in Figure 34, exhibited significant noise both within the same 96-well plate and between different plates. From visualizing the data, the sources and extent of noise is not readily apparent. Calculating the linear trends by minimizing the error in fluorescence suggests that the instrument significantly overpredicts the signal on one day and significantly underpredicts on the next. This is obviously not realistic for an instrument that is routinely calibrated; instead, additional sources of error should be

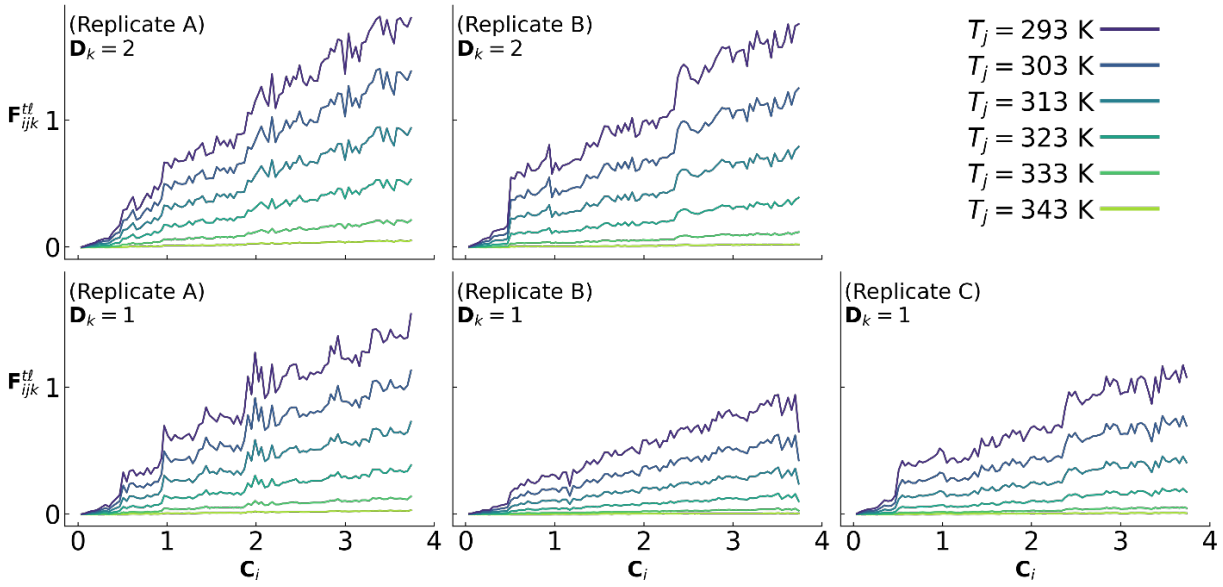

Figure 34. *Dimensionless fluorescence as a function of dimensionless dye concentration at a variety of temperatures (colors, see legend). Each subplot corresponds to measurements from the same 96-well plate. Each row corresponds to a series of replicate measurements.*

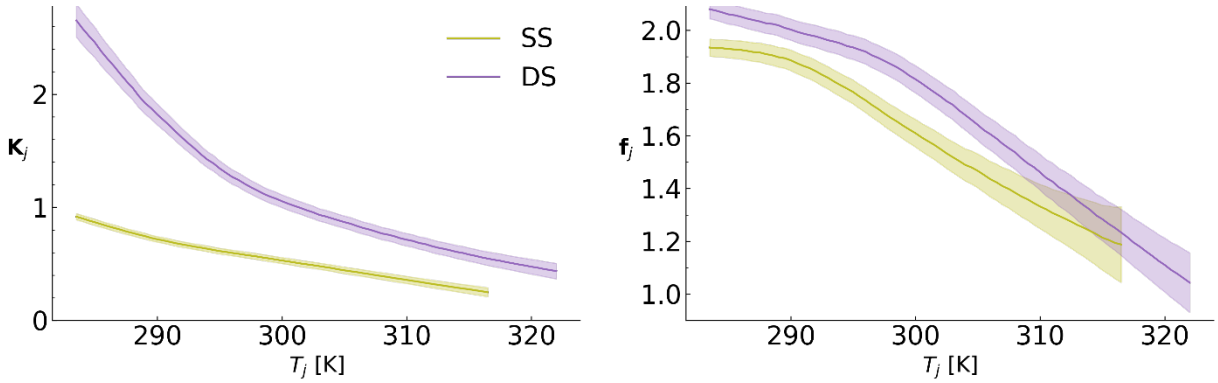

Figure 35. *Left: Dimensionless binding constant $\boldsymbol{K_j}$ as a function of temperature $\boldsymbol{T_j}$. Right: Dimensionless fluorescence per dye adsorbed to DNA $\boldsymbol{K_j}$ as a function of temperature. Properties for single-stranded DNA (SS) are depicted in yellow, while those for double-stranded DNA (DS) are depicted in purple.*

present. We assume that the error arising either from fluorescence or dye concentration yields residuals that possess small errors in fluorescence and errors in dye concentration that are consistent with the pipetting procedure. By quantifying the noise in this manner, the different trends in Figure 34 are attributed to result from different working concentrations that were used on the different days of experimentation. This knowledge of uncertainty could be used to improve reproducibility in the future by focusing on the procedural details of generating working concentrations and dilutions.

Having quantified the noise, we used the numerical optimization and experimental workflow to extract the binding constant and adsorbed molar fluorescence at a wide variety of temperatures. For comparison, we applied the computational procedure to single-stranded DNA (SS) and double-stranded DNA (DS) independently. The properties computed are depicted in Figure 35. As expected, the dye binds more strongly to DS than SS. In comparison to other dyes (not shown) the binding strength of SYTO-13 is small. This explains its relatively weak inhibition of PCR and influence on melting temperature. However, each dye bound to DS does not always fluoresce more than each dye bound to SS (Figure 35, right). At high temperature, there is no statistically significant difference between the fluorescence of dye bound to SS and DS. By discriminating between K_j and f_j at each temperature T_j, we can explain why the fluorescence of dye in a solution containing DS is larger than that containing SS. In the future, this approach of discriminating between binding, brightness, and noise could be extended to improve quantification of DNA concentration by real-time PCR and quantification of DNA melting fraction by sequential temperature cycling. Our results [1] are currently undergoing peer review.

[1] R. F. DeJaco, J. M. Majikes, J. A. Liddle, and A. J. Kearsley. Temperature-dependent Thermodynamic and Photophysical Properties of SYTO-13 Dye Bound to DNA. In review.

Artificial Intelligence for Low-Field Magnetic Resonance Imaging

Andrew Dienstfrey
Zydrunas Gimbutas
Adele Peskin (NIST ITL)
Joe Chalfoun (NIST ITL)
Kathryn Keenan (NIST PML)
Kalina Jordanova (NIST PML)
Stephen Ogier (NIST PML)

Emerging low-field (64 mT) magnetic resonance imaging (MRI) systems offer the promise of low-cost, point-of-care imaging that could be conducted in, for example, developing countries, rural locations, and eventually even in an ambulance. However, present low-field MRI results in images with low spatial resolution and high noise. These poor qualities complicate quantitative analyses that are critical for advanced diagnostics. Recent research suggests that machine learning (ML) methods can potentially restore image quality and furthermore may enable quantitative mapping of tissue parameters [1]. Such claims must be validated via rigorous comparisons to existing measurement standards for high-field (1.5 or 3.0 T) MRI. In FY 2022, we continued our investigation of ML-based analysis in low-field MRI measurement contexts.

Diffusion MRI. For background, scope, and motivations for the NIST Use-Inspired AI Program on Low-Field MRI see [2]. In FY2022 we continued our investigation of low-field MRI measurement of the apparent diffusion coefficient of water (ADC) measured in units $\mu m^2/s$. This parameter is a measure of water mobility which, in turn, can serve as a biomarker for several medical conditions including stroke, traumatic brain injury, and Alzheimer's disease. From a physics perspective, water mobility is insensitive to static magnetic field strengths. Thus, previous quantitative measurements of

ADC conducted at high-fields should be directly applicable to low-field contexts.

The system of equations governing spin-dynamics in the presence of diffusion are known as the Bloch-Torrey equations and are given by

$$\frac{d\mathbf{M}}{dt} = \gamma \mathbf{M} \times \mathbf{B} - \frac{M_x \hat{\mathbf{x}} + M_y \hat{\mathbf{y}}}{T_2} - \frac{(M_z - M_0)\hat{\mathbf{z}}}{T_1} + D\nabla^2 \mathbf{M}$$

$$\mathbf{B} = (B_0 + \mathbf{G}\cdot\mathbf{r})\hat{\mathbf{z}} + \mathbf{B}_{rf}.$$

Here **M**, is proton spin magnetization resulting from an ensemble of water molecules, D is the diffusion coefficient of this ensemble, and **B** is the applied magnetic field, which consists of a static field, a gradient component, and a radiofrequency (RF) field.

The principle underlying diffusion weighting can be described briefly. Assume no RF field and that one may ignore the decay terms associated with the time constants T_1 and T_2.[6] The Bloch-Torrey equations suggest a system in which the precessional frequency of the magnetization is the sum of a static and a positionally-dependent gradient field. Consider a pulse sequence in which one applies a gradient field over a short period of time, waits for some time interval, and then applies the same gradient pulse with the polarization reversed. Recall that the gradient field points in the z-direction and the magnitude depends linearly on position. Thus, the first pulse applied over a short time interval results in an accumulation of precessional phase, the total amount of which depends on position. Assuming that all spin-packets are stationary, then from the reversibility of the precessional dynamics, it follows the reverse gradient pulse completely unwinds this phase. Thus, the signal at the end of this sequence is the same as it was in the beginning. However, if the water molecules move in the time between pulses, then the rephasing is incomplete. In this case, the vector sum of spin-packet magnetic moments partially cancels, resulting in an attenuated signal.

Steksjal was the first to propose and then analyze the solution to the Bloch-Torrey equations under the above excitation [3]. The gradient field strength, the duration of the gradient pulse, and the time between the gradient pulses all combine into a pulse-specific factor commonly denoted by b measured in s/mm^2. Assuming a homogeneous, isotropic material, Steksjal showed that the magnitude of the detected signal follows an exponential law

$$S(b) = S_0 e^{-b\cdot D}.$$

In biomedical contexts, the homogenous and isotropic assumptions may not hold. Variations on this measurement process have been devised which result in an estimation of a full diffusion tensor providing information on anisotropy. However, even in these cases it can prove clinically useful to refer to a single diffusivity (which may be considered as the trace of the diffusion tensor) as the apparent diffusion coefficient (ADC). Replacing D by ADC, the signal model is otherwise the same.

The standard workflow for estimating ADC consists of fixing set of b-values and obtaining the corresponding diffusion-weighted images. For each pixel, this results in a collection of data points $\{(b_1, y_1), (b_2, y_2), \ldots, (b_N, y_N)\}$ where y_i are the image intensities at that location. A non-linear least-squares fit to the exponential signal model determines the ADC for that pixel.

An example of this workflow is shown in Figure 36. On the left we show diffusion-weighted images of the NIST Diffusion Phantom scanned at four b-values: b=0, 500, 900, and 2000 s/mm^2. The NIST Diffusion Phantom is a standard reference object developed with consortium partners from the Radiological Society of North America and the National Cancer Institute. The phantom is used to assess the quality of ADC measurements obtained by MRI scanners. Thirteen vials, which we refer to as regions of interest (ROI), contain one of six polymer solutions (5 duplicates and 1 triplicate) with well-characterized diffusivities ranging from 128 to 1127 μm^2/s at 0º C [4]. For illustration purposes, we show the boundary of Tube 5 as determined by an ML segmentation model developed by us previously [2]. The intensities at a single pixel are shown in the plot on the right, along with the non-linear regression which returns an estimated ADC of 832.0 μm^2/s. This exponential fit is performed pixel-by-pixel resulting in an ADC map. Note that as the polymer solutions are homogeneous and isotropic, the ADC is a true measure of diffusivity, D.

Machine Learning Analysis. In FY 2022, we pursued an alternative workflow based on machine learning. From a dataset acquired under a previous ADC study, we selected 432 scan instances of the Diffusion Phantom. Notably, these diffusion weighted images were acquired by one type of MRI system and the phantom was maintained at 0º C as per standard protocols [4]. This training set was augmented using a combination of techniques. In addition to the geometric transformations commonly used in ML-based image analysis (i.e., translations, rotations, reflections, and Gaussian blur) we also developed a non-linear, image warping algorithm and incorporated it into the augmentation strategy.

We experimented with training several ML models using this dataset and augmentation strategy. We trained

[6] The RF field is controlled by the user. Thus, the first assumption is no restriction. The second assumption amounts to executing the gradient pulses and interpulse delay on a sufficiently short time scale such that these decays are not significant.

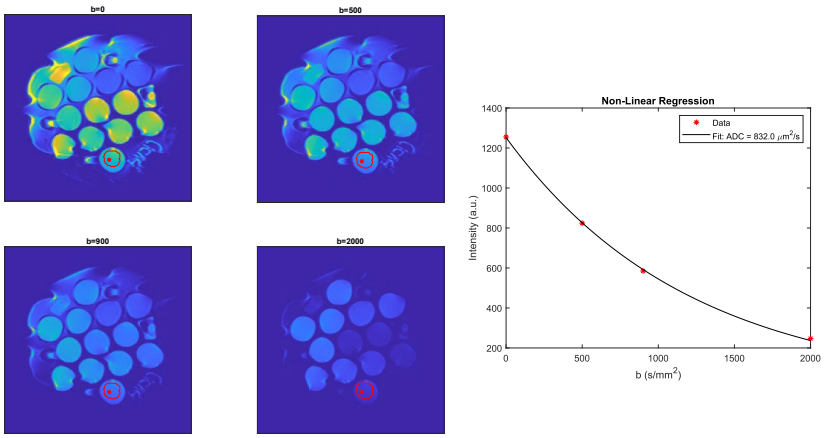

Figure 36. *Example of the standard ADC measurement process. The four images on the left show the NIST Diffusion Phantom scanned on an MRI using a diffusion weighted sequence corresponding to b=0, 500, 900, and 2000 s/mm². The red contour shows the boundary of one of the phantom vials. This segmentation was performed by an ML model trained previously. The boundary was eroded into the interior of the vial to eliminate signal aberrations due to edge effects. Also shown is a pixel (red asterisk) within this region of interest. The signal intensities are plotted on the right along with the non-linear, exponential regression curve. The estimated ADC is 832.0 μm²/s.*

two neural network architectures: a U-Net and an FC-Densenet. The U-net is shown in Figure 37. The dataset labels are rich in that they include both quantitative data in the form of ADC values and qualitative, geometric information arising from the segmentation of the 13 ROI's. For training we experimented with combinations of different loss functions designed to enforce ADC accuracy, ADC stability within an ROI, and segmentation accuracy. All models trained successfully.

Our testing protocol was extensive. As a minimal consideration, we used 20 unseen scan instances of the same type as appeared in training set. To assess the generalization capabilities of the trained networks, we included additional scans acquired on a different MRI system, as well as scans of the diffusion phantom taken at room temperature. MRI scanners have many proprietary characteristics that can result in images that are subtlety different but nevertheless confound ML analysis. Thus, training on one scanner and testing on another is a strong test for generalization. Furthermore, as diffusivity is temperature dependent, room-temperature scans contain ADC values that were not seen as part of the training protocol. Finally, as the NIST Diffusion phantom is a calibration object, it is structured by design consisting of 6 polymer solutions loaded into 13 vials in a fixed orientation. Thus, there is a natural concern that the network may be memorizing the phantom and its ADC inference consists essentially of modulating this fixed underlying structure either up or down based on some primitive assessment of signal value. To test for this, we implemented an algorithm to synthetically swap ROI locations.

The result is a tremendous amount of test set data; performing and reporting a detailed assessment is a problem in its own right. One possibility is to frame the analysis as a measurement comparability problem comparing ADC measurement by ML to the non-linear regression approach. This type of analysis is common in clinical settings investigating the possibility of using two measurement techniques interchangeably [5]. An example of this is shown in Figure 38. Here we show all ADC measurements within the ROI in Figure 37 (N=247). Histograms of the ADC measurements obtained by both non-linear regression and one of our ML models are shown on the left. Both distributions may be assumed to be Gaussian. The 95 % coverage interval for the means of the distributions are (832.7±1.7) μm²/s for non-linear regression, and (875.9±2.2) μm²/s for the ML model. Both estimates are statistically different from the reference value of (843±6) μm²/s [3]. However, this level of discrepancy is clinically acceptable. Concerning the comparability of the measurement techniques, the dispersion of ADC values over the ROI are approximately the same. On the right we plot the difference versus the mean (i.e., a Bland-Altman plot) to assess measurement comparability. Within this ROI there is no discernible trend in difference versus the mean. The bias is shown as a solid line at 43.2 μm²/s, the limits of variation are computed as twice the standard deviation of the difference and are shown as dashed lines in the figure.

Discussion. Machine learning is typically used for qualitative problems. For example, a classifier can be understood as a measurement problem on a nominal scale. Quantitative ML is less studied, and the problem is substantially different. For example, data acquisition is more structured, and the goal, at least in the present case, is to infer quantities of an underlying law. Furthermore, for the ML inference to serve as a measurement it must be accompanied by an assessment of uncertainty [6]. Preliminary analysis of our results suggests a number of surprising conclusions in these regards. For one, there is the question of training data diversity. Careful quantitative experiments require significant commitment to organize, and it is not always the case that one will have a training set that covers all possibilities desired for inference. Our training data consisted of one scanner type and 6 ADC values. The generalization of our models to unseen ADC values and to different scanners is encouraging. Another surprising result concerns using synthetic data (i.e., generated by the model) as a "physics-informed" augmentation strategy to train models with generalizability to *b*-values. Generally speaking, synthetic dataset generation should be used

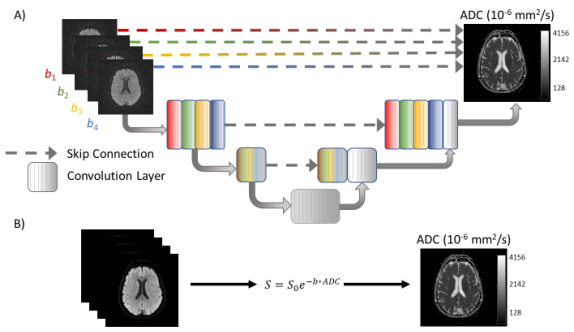

Figure 37. *Schematic of U-Net architecture. (A) The network shown here includes four input images for purposes for inverting for ADC map. The same architecture was used with a single input image for purposes of segmentation training and inference. (B) Traditional ADC analysis fits an exponential model on a pixel-by-pixel basis.*

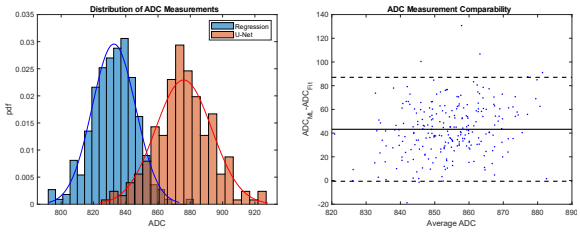

Figure 38. *Comparability of ML measurement of ADC to standard analysis. The left plot shows the distributions of ADC measurements within the ROI identified in Figure 18. The dispersions are the same order of magnitude whereas the ML value shows a bias of 43.2 μm²/s. On the right is a Bland-Altman plot for this same data. There is no discernible trend in difference vs mean. The mean difference is plotted as a solid horizontal line, and the expected limits of variation as the two dashed lines.*

very cautiously as it relates to notions of "inverse crimes" and the overly optimistic results associated with this [7]. While this experiment is too elaborate to describe in this document, here too we observed a more robust result than expected.

A preliminary takeaway from this work is that machine learning of an underlying mathematical structure may have significant differences from traditional contexts. In the upcoming year we will complete our assessment of ML-based diffusion measurement, and we will investigate how such findings might inform these more general considerations.

[1] M. Figini, H. Lin, G. Ogbole, *et. al*. Image Quality Transfer Enhances the Contrast and Resolution of Low-Field MRI in African Paediatric Epilepsy Patients. arXiv (2020). URL: https://arxiv.org/abs/2003.07216

[2] A. Dienstfrey, Z. Gimbutas, A. Peskin, *et. al*. Artificial Intelligence for Low-Field Magnetic Resonance Imaging. In *Applied and Computational Mathematics Division: Summary of Activities for Fiscal Year 2021* (R. Boisvert, ed.), 62-65, 2022. DOI: 10.6028/NIST.IR.8423

[3] E. O. Stekjsal and J. E. Tanner. Spin Diffusion Measurements: Spin Echoes in the Presence of a Time-Dependent Field Gradient. *The Journal of Chemical Physics* **42** (1965), 288. DOI: 10.1063/1.1695690

[4] S. E. Russek. *NIST/NIBIB Medical Imaging Phantom Lending Library*. NIST Public Data Resource, 2021. DOI: 10.18434/mds2-2366

[5] J. M. Bland and D. G. Altman. Applying the Right Statistics: Analyses of Measurement Studies. *Ultrasound in Obstetrics and Gynecology* (2003), 85-93. DOI: 10.1002/uog.122

[6] B. Taylor and C. Kuyatt. *Guidelines for Evaluating and Expressing the Uncertainty of NIST Measurement Results 1994 Edition*. NIST Technical Note 1297 (1994). DOI: 10.6028/NIST.tn.1297

[7] E. Shimron, J. I. Tamir, K. Wang, and M. Lustig. Subtle Data Crimes: Naively Training Machine Learning Algorithms Could Lead to Overly-Optimistic Results. arXiv (2021). URL: https://arxiv.org/abs/2109.08237

Modeling Photoreceptor Dynamics

Danielle C. Brager
Anthony J. Kearsley
Daniel Anderson

Photoreceptors are light-sensing cells in the retina that play an essential role in the vision process. Light enters the eye through the cornea and passes through the pupil before reaching the lens where the light is focused onto the retina. Photoreceptors convert light into electrical signals that are sent to the brain via the optic nerve so that we can see. There are two types of photoreceptors in the human retina - rods and cones. Rods are concentrated in the outer areas of the retina and are responsible for vision at low light levels while cones are concentrated in the macula, an area in the center of the retina, and are responsible for color vision as well as visual acuity. Photoreceptors have an inner segment (IS) and an outer segment (OS). The IS is the photoreceptor's metabolic center and is filled with mitochondria. The OS is filled with stacks of membranes that contain the visual pigment molecules. The photoreceptors undergo continuous renewal and periodic shedding of their OS discs to prevent the toxic effects of accumulated photo-oxidative products. Following a circadian rhythm that is governed by light and temperature modulation, discs formed at the OS base are discarded at the tip and phagocytized by the neighboring retinal pigment epithelium (RPE).

Retinal degenerations include a group of disorders that lead to photoreceptor loss. This photoreceptor cell loss is common to degenerative eye disorders such as retinitis pigmentosa, age-related macular degeneration, and cone-rod dystrophy. Research in this field is focused on developing strategies to delay or prevent the onset of photoreceptor degeneration [2, 3]. However, there is currently no cure for diseases linked to photoreceptor degeneration.

Mathematical modeling plays a crucial and beneficial role in this research effort [1]. There exist

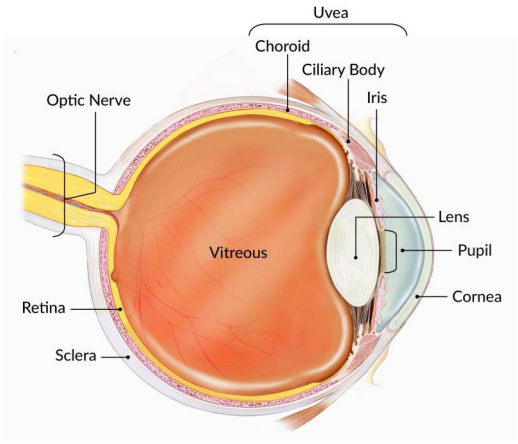

Figure 39. *Components of the eye.* Image source : National Eye Institute (nih.gov).

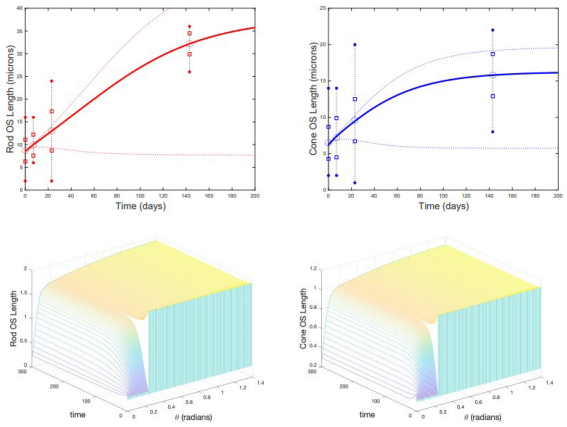

Figure 40. *Averaged Rod OS and Cone OS lengths in the macular region during regrowth along with data from Guerin et al. (upper plots). Rod OS and Cone OS length dynamics as a function of position on the retina for macular region OS regrowth.*

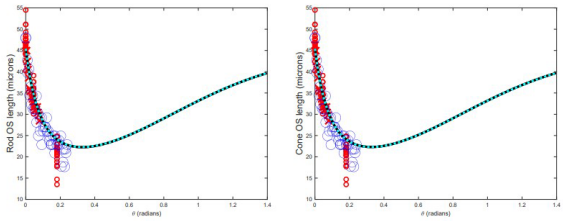

Figure 41. *Rod OS and Cone OS length predictions in comparison with Wilk et al. data of photoreceptor lengths.*

mathematical and computational models of various regions of the retina in retinal development, health, and disease. One of these is the Camacho and Wirkus ordinary differential equation-based model [4], which has been compared with retinal OS regrowth data by Guerin *et al*. [5, 6]. However, to our knowledge, there is no mathematical model of the physiology of photoreceptors in a healthy eye, that incorporates the interplay between the spatial density distribution, OS length, and nutrient source. We have recently developed a novel mathematical model of these processes to be used as a framework for future mathematical modeling in this field. Predictions from our model compare well with the Guerin *et al.* regrowth data and now additionally accounts for the spatial dependence of the retinal detachment data (Figure 40). Our model also compares well with spatial measurements of photoreceptor OS length from Wilk *et al.* [7] (Figure 41). While our efforts have focused on healthy eye conditions, the model we have developed establishes the framework in which future studies of retinal pathologies may be undertaken.

[1] D. C. Brager. *Modeling and Analyzing the Progression of Retinitis Pigmentosa*. Doctoral dissertation, Arizona State University, 2020.

[2] E. T. Camacho, L. A. Melara, M. C. Villalobos, and S. Wirkus. Optimal Control in the Treatment of Retinitis Pigmentosa. *Bulletin of Mathematical Biology* **76**:2 (2014), 292-313.

[3] E. T. Camacho, S. Lenhart, L. A. Melara, M. C. Villalobos, and S. Wirkus. (2020). Optimal Control with MANF Treatment of Photoreceptor Degeneration. *Mathematical Medicine and Biology: A Journal of the IMA* **37**:1 (2020), 1-21.

[4] E. T. Camacho and S. Wirkus. Tracing the Progression of Retinitis Pigmentosa Via Photoreceptor Interactions. *Journal of Theoretical Biology* **317** (2013), 105-118.

[5] C. J. Guerin, D. H. Anderson, R. N. Fariss, and S. K. Fisher. Retinal Reattachment of the Primate Macula. *Investigations in Ophthalmology and Visual Science* **30** (1989), 1708-1725.

[6] C. J. Guerin, G. P. Lewis, S. K. Fisher, and D. H. Anderson. Recovery of Photoreceptor Outer Segment Length and Analysis of Membrane Assembly Rates in Regenerating Primate Photoreceptor Outer Segments. *Investigations in Ophthalmology and Visual Science* **34** (1993), 175-183.

[7] M. A. Wilk, B. M. Wilk, C. S. Lango, R. F. Cooper, and J. Carroll. Evaluating Outer Segment Length as a Surrogate Measure of Peak Foveal Cone Density. *Visual Research* **130** (2017) 57-66.

Materials Modeling

Mathematical modeling, computational simulation, and data analytics are key enablers of emerging manufacturing technologies. The Materials Genome Initiative (MGI), an interagency program with the goal of significantly reducing the time from discovery to commercial deployment of new materials using modeling, simulation, and informatics, is a case in point. To support the NIST role in the MGI, we develop and assesses modeling and simulation techniques and tools, with emphasis on uncertainty quantification, and collaborate with other NIST Laboratories in their efforts to develop the measurement science infrastructure needed by the materials science and engineering community.

OOF: Finite Element Analysis of Material Microstructures

Stephen A. Langer
Günay Doğan
Andrew C.E. Reid (NIST MML)
Prashant Athavale (Clarkson University)
Shahriyar Keshavarz (Theiss Research)

http://www.ctcms.nist.gov/oof/

The OOF Project, a collaboration between ACMD and MML, is developing software tools for analyzing real material microstructure. The microstructure of a material is the (usually) complex ensemble of polycrystalline grains, second phases, cracks, pores, and other features occurring on length scales large compared to atomic sizes. The goal of OOF is to use data from a micrograph of a real or simulated material to compute its macroscopic behavior via finite element analysis.

The OOF user loads images into the program, assigns material properties to the features of the image, generates a finite element mesh that matches the geometry of the features, chooses which physical properties to solve for, and performs virtual experiments to determine the effect of the microstructural geometry on the material. OOF is intended to be a general tool, applicable to a wide variety of microstructures in a wide variety of physical situations. OOF2 and OOF3D are used by educators and researchers in industry, academia, and government labs worldwide.

There are two versions of OOF, OOF2 and OOF3D, each freely available on the OOF website. OOF2 starts with two dimensional images of microstructures and solves associated two-dimensional differential equations, assuming that the material being simulated is either a thin, freely suspended film or a slice from a larger volume that is unvarying in the third dimension (generalizations of plane stress and plane strain, respectively). OOF3D starts with three dimensional images and solves equations in three dimensions. Development this year continued on multiple fronts.

During this past year, A. Reid and S. Keshavarz made progress on the effort to implement crystal plasticity in the OOF software. The plastic computational scheme had been working for some time but was not yet integrated with the OOF mechanism for generating outputs. This work has now been completed, and an example stress-strain curve has been generated for a simple power-law plastic constitutive rule entirely within OOF3D.

There remain some issues with the set-up. It seems to be anomalously sensitive to some constitutive parameters and is currently a relatively low-performance solution. The next task is to identify opportunities for optimization which retain the existing basic functionality and the modular, extensible architecture.

Reid and Keshavarz are also continuing to work with collaborators in the Center for Hierarchical Materials Design to implement a machine-learning-based rapid evaluation scheme for plastic constitutive rules. Current efforts are focused on implementing an early solution into a basic FEM code framework.

G. Doğan has been developing algorithms to help automate segmentation and meshing of microstructure images. Segmentation identifies distinct regions in a microstructure, and a mesh properly aligned with the segmented regions and their boundaries leads to accurate finite element simulations of the microstructure physics. In FY 2021, Doğan implemented texture segmentation algorithms using texture features and machine learning. Textures in images are repeated patterns of pixel values, which can be used to distinguish different regions in images. Doğan's implementation relied on predefined texture features to classify pixel locations into different classes using classification algorithms, such as support vector machines (SVM) and random forests.

Doğan worked with P. Athavale and his students, Peter Lef, Emmanuel Atindama from Clarkson University to implement algorithms for restoration of electron backscattering diffraction (EBSD) images. EBSD is an important imaging modality to analyze and understand microstructure images by measuring the crystal orientations at individual locations and generating a map of the orientations. However, EBSD maps are often noisy and incomplete; orientation measurements are missing in some locations, and some measurements contain errors. Doğan and his collaborators implemented a reconstruction algorithm using a weighted total variation equation,

a nonlinear partial differential equation that applies regularizing diffusion selectively to pixels. Their implementation included critical preprocessing components, specific to EBSD images. In this way, they were able to obtain state-of-the-art restorations of EBSD images. More details about Doğan's work on image segmentation and restoration can be found in this report's section on Computational Tools for Image and Shape Analysis.

OOF2 and OOF3D still rely on some old third-party software that will soon become obsolete. S. Langer has continued to work on the switch to the new versions of the aging software. In particular, the GUI toolkit gtk+2 needs to be upgraded to Gtk3, Python 2.7 to Python 3.x, and a substitute for the graphics library libgnomecanvas needed to be written because no Gtk3-compatible third-party software was available.

Much of the year was spent on updating the OOF2 GUI test suite to work with Gtk3. As expected, this uncovered numerous bugs and inefficiencies in both OOF2 and in the testing machinery. This also took an unexpected amount of time. Because the GUI test files needed to be rebuilt for Gtk3, this was a good time to make user-interface improvements that also broke the GUI test files. For example, users had been confused by the old way of determining when newly created objects (images, meshes, etc.) were automatically displayed in the graphics window. Now the user can choose one of three options, and hopefully find one that feels intuitive.

The replacement for libgnomecanvas, called OOFCanvas, is complete. The basic functionality was in place at the beginning of FY 2021, but the code was too tightly tied to OOF2 to be useful elsewhere. Now it is compiled into a stand-alone library, which will be distributed separately from OOF2. Its API has been simplified and bugs have been fixed.

Langer and Reid have continued to work with A. Creuziger of MML who is using OOF2 to study the effects of texture (crystal orientation distribution) on the properties of rolled steel. In particular, the size of Creuziger's computations were revealing memory-use inefficiencies in OOF2, which now have been fixed.

OOF2 and OOF3D continue to be used heavily outside of NIST. OOF2 was downloaded about 700 times this past year, and OOF3D was downloaded about 200 times. OOF2 can be run on the NSF nanoHUB facility, where it was used 7499 times in FY 2021.

Micromagnetic Modeling

Michael Donahue
Donald Porter
Robert McMichael (NIST PML)
Solomon Woods (NIST PML)
Cindi Dennis (NIST MML)

http://math.nist.gov/oommf/

Advances in magnetic devices such as field sensors, spin torque oscillators, magnetic nonvolatile memory (MRAM), and thermal sensors are dependent on an understanding of magnetization processes in magnetic materials at the nanometer level. Micromagnetics, a mathematical model used to simulate magnetic behavior, is needed to interpret measurements at this scale. ACMD is working with industrial and academic partners, as well as with colleagues in the NIST MML and PML, to improve the state-of-the-art in micromagnetic modeling.

We have developed a public domain computer code for performing computational micromagnetics, the Object-Oriented Micromagnetic Modeling Framework (OOMMF). OOMMF serves as an open, well-documented environment in which algorithms can be evaluated on benchmark problems. OOMMF has a modular structure that allows independent developers to contribute extensions that add to its basic functionality. OOMMF also provides a fully functional micromagnetic modeling system, handling three-dimensional problems, with extensible input and output mechanisms. Between October 1, 2021 and December 31, 2022, the software has been downloaded more than 5600 times by more than 3400 distinct client machines. In addition, 241 known peer-reviewed journal articles were published acknowledging the use of OOMMF. Total OOMMF citations are now more than 3500. OOMMF has become an invaluable tool in the magnetics research community.

Developments in the last year include:

- Released version 2.0b0 of OOMMF with improved dark mode, streaming SIMD extension (SSE) unaligned memory access, and a programming manual.[7]
- Added support for multiple coincident meshes. This enables modeling of antiferromagnetic and ferrimagnetic materials.
- Revised representation of time-varying saturation magnetization to enable mean-field model approaches to simulation of thermal effects.
- Updated OOMMF image formats and custom channels in anticipation of migration to Tcl 9 libraries.

[7] https://math.nist.gov/oommf/software-20.html

OOMMF is part of a larger activity, the Micromagnetic Modeling Activity Group (muMAG), formed to address fundamental issues in micromagnetic modeling through two activities: the development of public domain reference software; and the definition and dissemination of standard problems for testing modeling software. ACMD staff members are involved in development of the standard problem suite as well. This year, muMAG published three contributed solutions to the standard problem suite[8] computed by the new MagTense framework[9], demonstrating the continued importance of these benchmarks for micromagnetic modeling software development.

In addition to the continuing development of OOMMF, the project also does collaborative research using OOMMF. M. Donahue is a team member on the NIST Innovations in Measurement Science nanothermometry project Thermal MagIC[10]. Thermal MagIC work includes examination of uncertainty quantification with Mark-Alexander Henn of University of Maryland and antiferromagnetic modeling with Mingyu Hu (and advisor Mark Hoefer) of University of Colorado. Hu completed her PhD in May 2022. M. Donahue has also provided technical guidance on micromagnetic modeling for the DARPA M3IC (Magnetic, Miniaturized, and Monolithically Integrated Components) project[11], completing this work in March 2022. The DARPA M3IC project aims to integrate magnetic components into the semiconductor materials fabrication process to improve electromagnetic systems for communications, radar, and related applications. During the reporting period the ACMD micromagnetic modeling project produced three conference presentations. [1, 2, 3]

[1] T. Q. Bui, A.J. Biacchi, K. N. Quelhas, M. Henn, E. L. Correa, W. Tew, A. R. Hight Walker, C. Dennis, M. J. Donahue, and S. Woods. "Magnetization Dynamics of Magnetic Nanoparticles for Thermal and Magnetic Particle Imaging." MMM-Intermag 2022, New Orleans LA, January 2022.

[2] M. Hu, M. A. Hoefer, and M.J. Donahue. "Energetics of Spin-flop and Spin-flip Transitions in Homogeneous Antiferromagnets." MMM 2022, Minneapolis MN, November 2022.

[3] T. Q. Bui, A. J. Biacchi, K. N. Quelhas, F. M. Abel, M. Henn, E. De Lima Correa, W. L. Tew, A. R. Hight Walker, C. Dennis, M. J. Donahue, P. N. Haney, and S. I. Woods. "Coupled Néel-Brown Magnetization Dynamics of Magnetic Nanoparticles for Thermal and Magnetic Particle Imaging," MMM 2022, Minneapolis MN, November 2022.

Mathematics of Uncertainty in Engineering Reliability

Jeffrey T. Fong
N. Alan Heckert (NIST ITL)
Pedro V. Marcal (MPACT Corp.)
Marvin Cohn (Intertek)

To ensure the safe operation of an engineering structure or system, be it a chemical processing plant, a nuclear power plant, a jet airliner, or a steel bridge, engineers need to first design, manufacture, assemble and install, test in laboratories and in the field, operate with continuous monitoring and scheduled maintenance for all necessary components and connections that are required to make a system work as a whole without failure. Engineers need to estimate the reliability of all such components and connections and construct a fault tree to evaluate the system reliability of the whole structure or system.

Two basic categories of problems of uncertainty come up that require independent modeling approach: (I) Uncertainty in loads, and (II) Uncertainty in material properties. In this project, we first address Category (I) by decomposing complex history of loads into a series of elemental fatigue (cyclic load at a fixed amplitude and frequency) and creep (constant load for a fixed time). We then address Category (II) by conducting fatigue life cycle tests and creep rupture time tests, with uncracked and cracked specimens for all elemental fatigue and creep cycles identified in the decomposed loas series.

We use a linear least squares fit model for each elemental fatigue or creep test to estimate the Category (II) uncertainty at the laboratory specimen-size scale, and the statistical theory of tolerance intervals, a modeling assumption, and a nonlinear least squares fit to obtain a formula for the minimum life (minL) of the full-size structure or component as a function of failure probability upper bound (Fpub). An inversion of the formula yields a Fpub vs. minL curve for each elemental fatigue or creep load. Using a second modeling assumption that Fpub is a measure of fatigue or creep damage and is an intrinsic property of the material with minL as its age marker, we can construct the Fpub vs. mimL curve for the complex load history by piecing together the series of elemental fatigue and creep loads using their individual Fpub vs. minL curves. This solves the Category (I) uncertainty problem, and we have a general model for structural engineering reliability.

[8] https://www.ctcms.nist.gov/~rdm/mumag.org.html

[9] https://www.magtense.org/

[10] https://www.nist.gov/programs-projects/thermal-magic-si-traceable-method-3d-thermal-magnetic-imaging-and-control

[11] https://www.darpa.mil/program/magnetic-miniaturized-and-monolithically-integrated-components

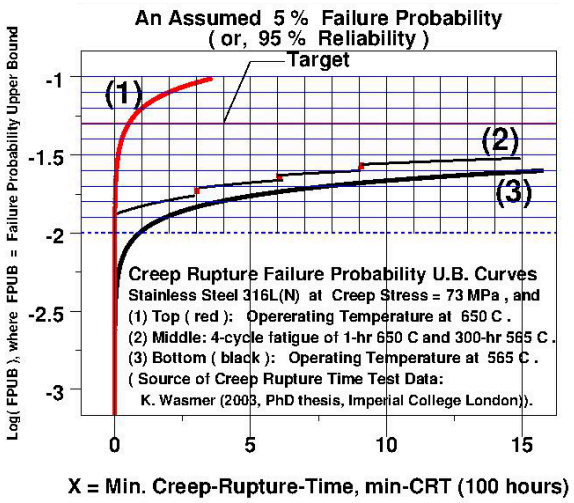

Figure 42. *Three plots of the Creep FPUB (or Creep Damage) curves for stainless steel 316L(N) at applied creep stress of 73 MPa are shown: (1) Top (red) curve for a simple creep history at 650 C. (2) Middle (zigzag) curve for a 4-cycle thermal creep cycling history of one hour in 650 C and 300 hours in 565 C. (3) Bottom (black) curve for a simple creep history at 565 C.*

A Mathematical Model of Structural Reliability with an Application to Creep of SS 316L(N) in Thermal Cycling between 650 C and 565 C at 73 MPa. The American Society of Mechanical Engineers (ASME) Boiler and Pressure Vessel Code (BPVC) Committee has recently developed a new Section XI (Nuclear Components Inspection) Division 2 Code [1] named "Reliability and Integrity Management (RIM)." RIM incorporates a new concept known as "System-Based Code (SBC)" originally due to Asada and his colleagues [2, 3], where an integrated approach from design to service inspection is introduced using three new types of statistical quantities: (1) "system reliability index," or "system co-reliability target" for any system consisting of structures and components, (2) "structural co-reliability," for any structure, and (3) "component co-reliability" for any component, where co-reliability is defined as "1 – reliability" and is equal to failure probability. In a recent paper published in the International Journal of Pressure Vessels and Piping (Vol. 173 (2019), pp. 79-93). Fong, Heckert, Filliben, and Freiman developed a new theory of fatigue and creep rupture life modeling for metal alloys at room and elevated temperatures such that the co-reliability of a smooth component can be estimated from fatigue and creep rupture test data with simple loading histories. In this paper, we extend the theory to include a methodology to estimate the failure probability (or, co-reliability) of a stainless steel 316L(N) component undergoing a complex loading history such as a thermal fatigue cycle. To illustrate an application of this new modeling approach, we present a numerical example using (a) the experimental test data of 7 specimens of S.S. 316L(N) in creep at 565 C as published by Kilian Wasmer in his Ph.D. thesis (Ref. [11]), (b) the experimental test data of 10 specimens of S.S. 316L(N) in creep at 650 C also by Wasmer [11], and (c) a thermal fatigue loading history of 1 hour of creep at 650 C at an operating creep stress of 73 MPa, and 300 hours of creep at 565 C at the same creep stress to simulate a hypothetical powerplant thermal fatigue operation. The resulting creep reliability curves for all three creep histories are shown in Figure 42. This result is significant because it provides a tool for engineers to design and operate plants with components of that material in compliance with the ASME BPVC Sec. XI Div. 2 "Reliability and Integrity Management (RIM)" Code.

[1] ASME, 2019, ASME Boiler and Pressure Vessel Code, Section XI, Division 2 - Requirements for Reliability and Integrity Management (RIM) Program for Nuclear Power Plants, Nov. 11, 2018 Draft for Public Comment. New York, NY: ASME, 2019.

[2] Y. Asada, M. Tashimo, and M. Ueta. System Based Code -Basic Structure. In *Proceedings of the 10th International Conference on Nuclear Engineering* (ICONE-10), Arlington, VA, April 14-18, 2002, ICONE10-22731.

[3] K. Kurisaka, R. Nakai, T. Asayama, and S. Takaya. S., 2011, "Development of System Based Code (1) Reliability Target Derivation of Structures and Components." *Journal of Power and Energy Systems* **5**:1 (2011), 19-32.

[4] J. B. Fussell and W. E. and Vesely. A New Methodology for Obtaining Cut Sets for Fault Trees. American Nuclear Transactions **15** (1972), 262-263.

[5] W. E. Vesely, F. F. Goldberg, N. H. Roberts, and D. F. Haasl. Fault Tree Handbook, NUREG0492. U. S. Nuclear Regulatory Commission, Washington, DC, 1981.

[6] J. T. Fong, Heckert, N. A., Filliben, J. J., and Freiman, S. W., 2019, "A Multi-Scale Failure-Probability-based Fatigue or Creep Rupture Life Model for Metal Alloys," Int. J. of PVP, Vol. 173, pp. 79-93 (2019), https://doi.org/10.1016/j.ijpvp.2019.04.003

[7] J. T. Fong, N. A. Heckert, J. J. Filliben, and S. W. Freiman. A Co-Reliability-Target-based Fatigue Failure Probability Model for Implementing the new ASME Boiler & Pressure Vessel Section XI Division 2 Reliability and Integrity Management Code: A Technical Brief. In *Proceedings of the ASME 2019 Pressure Vessel and Piping Division Conference*, July 14-19, 2019, San Antonio, TX, PVP2019-93508.

[8] J. T. Fong, P. V. Marcal, R. Rainsberger, N. A. Heckert, J. J. Filliben, S. R. Doctor, and N. A. Finney. A MultiScale Failure-Probability-and-NDE-Based Fatigue Life Model for Estimating Component Co-Reliability of Uncracked and Cracked Pipes. In *Proceedings of the ASME 2021 Pressure Vessel and Piping Division Conference*, July 12-16, 2021, Online, PVP2021-62169.

[9] N. E. Dowling. *Mechanical Behavior of Materials*. 2nd edition, Prentice-Hall, 1999.

[10] U.S. Department of Defense. *MIL-HDBK-17-1F (VOL. 1 OF 5) Department of Defense Handbook: Composite Materials Handbook – Polymer Matrix Composites*

Guidelines for Characterization of Structural Materials. Chapter 8. Statistical Methods, 2002.

[11] K. Wasmer. Prediction of Creep Crack Growth in a Range of Steels. Ph.D. Thesis, Imperial College, London, 2003.

[12] P. R. Nelson, M. Coffin, and K.A.F. Copeland. Introductory *Statistics for Engineering Experimentation*. Elsevier, 2006.

[13] W. Q. Meeker, G. J. Hahn, and L. A. Escobar. *Statistical Intervals: A Guide for Practitioners and Researchers*. 2nd edition, Wiley, 2017.

[14] Draper, N. R., and Smith, H., 1966, Applied Regression Analysis, Chap. 1-3, pp. 1-103, and Chap. 10, pp. 263-304. Wiley (1966).

[15] M. G. Natrella. *Experimental Statistics*. National Bur. of Standards. Handbook 91 (Aug. 1, 1963, reprinted with corrections Oct. 1966), Washington, DC, pages 1-14, 1-15, 2-13 to 2-15, Tables A-6 and A-7

[16] J. T. Fong, N. A. Heckert, J. J. Filliben, P. V. Marcal, and R. Rainsberger. Uncertainty of FEM Solutions Using a Nonlinear Least Squares Fit Method and a Design of Experiments Approach. In *Proceedings of the COMSOL Users' Conference*, Oct. 7-9, 2015, Boston, MA.

[17] J. T. Fong, N. A. Heckert, J. J. Filliben, P. V. Marcal, R. Rainsberger, and L. Ma. Uncertainty Quantification of Stresses in a Cracked Pipe Elbow Weldment Using a Logistic Function Fit, a Nonlinear Least Squares Algorithm, and a Super-parametric Method. *Procedia Engineering* **130** (2015), 135-149.

[18] J. J. Filliben, and N. A. Heckert. Dataplot: A Statistical Data Analysis Software System. NIST Gaithersburg, MD, 2002, URL: http://www.itl.nist.gov/div898/software/dataplot.html

[19] N. A. Heckert and J. J. Filliben. NIST Handbook 148: DATAPLOT Reference Manual, Volume I: Commands. NIST, June 2003.

[20] N. A. Heckert and J. J. Filliben. NIST Handbook 148: Dataplot Reference Manual, Volume 2: Let Subcommands and Library Functions. NIST, June 2003.

High Performance Computing and Visualization

Computational capability continues to advance rapidly, enabling modeling and simulation to be done with greatly increased fidelity. Doing so often requires computing resources well beyond what is available on the desktop. Developing software that makes effective use of such high-performance computing platforms remains very challenging, requiring expertise that application scientists rarely have. We maintain such expertise for application to NIST problems. Such computations, as well as modern experiments, typically produce large volumes of data, which cannot be readily comprehended. We are developing the infrastructure necessary for advanced interactive, quantitative visualization and analysis of scientific data, including the use of 3D immersive environments, and applying the resulting tools to NIST problems

High Precision Calculations of Fundamental Properties of Few-Electron Atomic Systems

James Sims
Maria Ruiz (University of Erlangen, Germany)
Bholanath Padhy (Khallikote College, India)

NIST has long been involved in supplying critically evaluated data on atomic and molecular properties such as the atomic properties of the elements contained in the Periodic Table and vibrational and electronic energy level data for neutral and ionic molecules contained in the NIST Chemistry WebBook. Fundamental to this work is the ability to predict, theoretically, a property more precisely than even the best experiments. It is our goal to be able to accomplish this for few-electron atomic systems.

While impressive advances have been made over the years in the study of atomic structure in both experiment and theory, the scarcity of information on atomic energy levels is acute, especially for highly ionized atoms. The availability of high precision results tails off as the state of ionization increases, not to mention higher angular momentum states. In addition, atomic anions have more diffuse electronic distributions, representing more challenging computational targets than the corresponding ground states.

In the past two decades, there has been breathtaking improvements in computer hardware and innovations in mathematical formulations and algorithms, leading to "virtual experiments" becoming a more and more cost effective and reliable way to investigate chemical and physical phenomena. Our contribution in this arena has been undertaking the theoretical development of our hybrid Hylleraas-CI (Hy-CI) wave function method to bring sub-chemical precision to atomic systems with more than two electrons.

Hy-CI has from its inception been an attempt to extend the success of the Hylleraas (Hy) method to systems with more than three electrons, and hence is an attempt to solve not just the three-body problem but the more general N-body problem [1]. Fundamental to the method is the restriction of one r_{ij} per configuration state function (CSF). (For atomic systems with greater than four electrons, all relatively precise calculations nowadays adopt the Hy-CI methodology of one r_{ij} term per CSF). In the case of three electron lithium systems, we have computed four excited states of the lithium atom to two orders of magnitude greater than has ever been done before [2]. At the four-electron level, to get truly precise chemical properties like familiar chemical electron affinities and ionization energies, it is important to get close to the nanohartree level we achieved for the three-electron atom, a significantly more difficult problem for four electrons than for three. By investigating more flexible atomic orbital basis sets and better configuration state function filtering techniques to control expansion lengths, we have been able to successfully tackle the four-electron case.

Progress to date has included computing the non-relativistic ground state energy of not only beryllium, but also many members of its isoelectronic sequence to eight significant digit precision. With the results from our calculations and a least-squares fit of the calculated energies, we have been able to compute the entire beryllium ground state isoelectronic sequence for Z = 4 through Z = 113 [3]. Li^- (with Z=3), nominally the first member of this series, has a decidedly different electronic structure and was not included in those calculations and subsequent discussions, but that omission has been corrected and we have subsequently carried out a large, comparable calculation for the Li^- ground state [4].

The first member of the Be isoelectronic ground state sequence, the negative Li^- ion, is also a four- electron system in which correlation plays a very important part in the binding. However due to the reduced nuclear charge, it is a more diffuse system in which one of its outer two L shell electrons moves at a greater distance from the nucleus than the other; hence its nodal structure is different from that of a coupled L shell with an identical pair of electrons. The ground state of the singlet S state of Li^- is the same type of problem as the first excited state of Be; it is like Be(2s3s), not Be(2s2s). Completing this calculation has provided the necessary insight to enable the calculation of the Be first excited

state of singlet S symmetry, Be(2s3s), to an order of magnitude better than previous calculations. Armed with this result, we have been able to continue this level of precision to the Be(2s4s) excited state and have calculated the higher, more diffuse Be(2s5s) through Be(2s7s) states as well, and in the process have demonstrated that Hy-CI can calculate the higher, more diffuse Rydberg states with more complicated nodal structures to the same level of precision as the less excited states [5].

While our work has demonstrated the efficacy of Hy-CI as a solution to the N-body problem for four or more electrons, this work has also shown the presence of a "double cusp" $r_{12}r_{34}$ term type slow convergence problem at the nanohartree precision level which is ultimately built into Hy-CI for four or more electrons. We have investigated a generalization of the Hy-CI method to an exponentially correlated Hy-CI (E-Hy-CI) method in which the single r_{ij} of an Hy-CI wave function is generalized to a form which pairs an exponential r_{ij} factor with linear r_{ij}, producing a correlation factor which has the right behavior in the vicinity of the r_{ij} cusp, and also as r_{ij} goes to infinity. While this was proposed in 2012 and there have been several papers on E-Hy-CI integrals, there were no computational tests until our calculations. Not only has the E-Hy part (the part that differs from conventional Hy-CI) been tested, but E-Hy-CI calculations have been done for spherically symmetrical and non-symmetrical orbitals as well.

The purpose of this research has been to determine how effective exponential correlation factors can be. By comparing convergence of the E-Hy-CI wave function expansion to that of the Hy-CI wave function without exponential factors, both convergence acceleration and an improvement in the precision for the same basis are demonstrated. This makes the application of the E-Hy-CI method to systems with N > 4, for which this formalism with at most a single exponentially correlated and linear r_{ij} factor leads to solvable integrals, very promising. The ground 1 singlet S state non-relativistic energy of He is computed to be -2.9037 2437 7034 1195 9831 1084 hartrees (Ha) for the best expansion.

We followed the success on the ground state of the He atom with calculations on the ground 1 singlet S and the 2 singlet S through 6 singlet S excited S states of the Li^+ ion with the same technique, with results comparable to the He atom. This demonstrates the utility of the Hy-CI approach for not only ground but also excited states of S symmetry as well [7]. For a review of high precision studies of both Hy-CI and E-Hy-CI studies of atomic and molecular properties, see [8].

Work is presently in progress to compare the convergence of the E-Hy-CI wave function expansion to that of the Hy-CI wave function without exponential factors for states of non-S symmetry, specifically the 1s2p 2 singlet P state of the He atom and members of its isoelectronic sequence. Almost all of the computed P state wave functions are orders of magnitude better than previous calculations and are being used with the previously obtained S state wave functions (and some new ones for Be II, C IV and O VI) to calculate oscillator strengths, including rigorous quantum mechanical upper and lower bounds, for the lowest singlet S to lowest singlet P transition. Results to date are fairly tight rigorous bounds to these computed oscillator strengths, which should give confidence in the validity of the computed non-relativistic results. A paper is being prepared on this work [9].

[1] J. S. Sims and S. A. Hagstrom. Combined Configuration Interaction – Hylleraas Type Wave Function Study of the Ground State of the Beryllium Atom. *Physical Review A* **4**:3 (1971), 908. DOI: 10.1103/PhysRevA.4.908

[2] J. S. Sims and S. A. Hagstrom. Hy-CI Study of the 2^2S Ground State of Neutral Lithium and the First Five Excited ^2S States. *Physical Review A* **80** (2009), 052507. DOI: 10.1103/PhysRevA.80.052507

[3] J. S. Sims and S. A. Hagstrom. Hylleraas-Configuration Interaction Nonrelativistic Energies for the Singlet S Ground States of the Beryllium Isoelectronic Series up Through Z = 113. *Journal of Chemical Physics* **140** (2014), 224312. DOI: 10.1063/1.4881639

[4] J. S. Sims. Hylleraas-Configuration Interaction Study of the Singlet S Ground State of the Negative Li Ion. *Journal of Physics B: Atomic, Molecular and Optical Physics* **50** (2017), 245003. DOI: 10.1088/1361-6455/aa961e

[5] J. S. Sims. Hylleraas-Configuration Interaction (Hy-CI) Non-Relativistic Energies for the 3 Singlet S, 4 Singlet S, 5 Singlet S, 6 Singlet S and 7 Singlet S States of the Beryllium Atom. *Journal of Research of the National Institute of Standards and Technology* **125** (2020), 125006. DOI: 10.6028/jres.125.006

[6] J. S. Sims, B. Padhy and M. B. Ruiz. Exponentially Correlated Hylleraas-Configuration Interaction (E-Hy-CI) Non-Relativistic Energy of the 1 Singlet S Ground State of the Helium Atom. *International Journal of Quantum Chemistry* **121**:4 (2020), e26470. DOI: 10.1002/qua.26470

[7] J. S. Sims, B. Padhy, and M. B. Ruiz. Exponentially Correlated Hylleraas-Configuration Interaction (E-Hy-CI) Studies of Atomic Systems. II. Non-relativistic Energies of the 1 singlet S through 6 singlet S States of the Li^+ Ion. *International Journal of Quantum Chemistry* **122**:1 (2021), e26823. DOI: 10.1002/qua.26823

[8] M. B. Ruiz, J. S. Sims, and B. Padhy. High-precision Hy-CI and E-Hy-CI Studies of Atomic and Molecular Properties. *Advances in Quantum Chemistry* **83** (2021), 171-208.

[9] J. S. Sims, B. Padhy, and M. B. Ruiz. Exponentially Correlated Hylleraas-Configuration Interaction (E-Hy-CI) Studies of Atomic Systems. III. Upper and Lower Bounds to He-Sequence Oscillator Strengths for the Resonance 1 singlet S to 2 singlet P Transition. In preparation.

Simulation of Dense Suspensions: Cementitious Materials

William George
Nicos Martys (NIST EL)
William Sherman
Simon Su
Steven Satterfield
Judith Terrill

A suspension is a collection of solid inclusions embedded in a fluid matrix. Suspensions play an important role in a wide variety of applications including paints, cement-based materials, slurries, and drilling fluids. Understanding the flow properties of a suspension is necessary in many such applications. However, measuring and predicting flow properties of suspensions remains challenging.

Suspensions can be quite complex, as the inclusions may have a wide range of shapes and a broad size distribution. Further complicating matters is that different matrix fluids may have quite disparate flow behavior. While the simplest type of matrix fluid is Newtonian, where the local stress is proportional to the shear rate, the matrix fluid can also be non-Newtonian, exhibiting quite complex behavior including shear thinning (viscosity decreases with shear rate), shear thickening (viscosity increases with shear rate), viscoelasticity (exhibiting both viscous and elastic properties), or even have a time dependent viscosity (thixotropic). We have two on-going studies on the rheology of cementitious materials, which are dense suspensions in non-Newtonian matrix fluids.

The dense suspension simulation code, QDPD, that we have developed is generic in that it can be applied not only to cement, mortar, and concrete, but also to any dense suspension of interest including pharmaceuticals such as suspensions of monoclonal antibodies or industrial suspensions such as paints and drilling fluids. Although some modification to the code may be needed in each case, QDPD is fully parameterized to handle a wide range of dense suspensions from rocks suspended in a mortar to proteins suspended in a fluid.

SRMs for Mortar and Concrete. Rotational rheometers, devices that measure fluid properties such as viscosity, are routinely used for homogeneous materials such as oils, but their use on dense suspensions, such as concrete, is relatively new. Since measurements with rheometers involve flow in a complex geometry, it is important that they are calibrated with a well characterized standard reference material (SRM). We are developing such SRMs in collaboration with NIST EL.

NIST produced an SRM for cement paste (SRM 2492) as the first step in the development of a reference material for concrete rheometers. The second step, the development of an SRM for mortar (SRM 2493), was

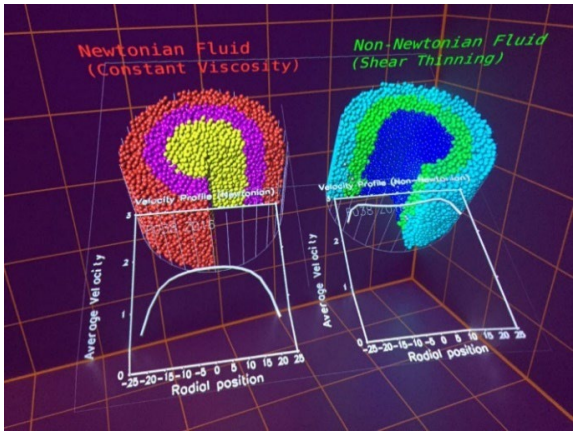

Figure 43. *Side-by-side comparison of identical systems, in the NIST immersive visualization system, with only a single property of the matrix fluid changed, one Newtonian and the other non-Newtonian (shear thinning).*

completed in 2017 and is currently available. The material properties of the mortar SRM, such as viscosity, could not be measured in fundamental units with certainty. Thus, simulation was used to determine the viscosity of the mortar. To obtain the necessary fidelity in the simulations, computations at a high-performance computing facility were necessary. Results of these simulations were compared with physical experiments as validation.

In 2019 we released SRM 2497, a standard reference concrete for rheological measurements [1]. The concrete SRM is comprised of the previously released mortar SRM with the addition of suspended 10 mm diameter hard glass spheres. The certified values for SRM 2497 were determined using the simulation results previously computed for the mortar SRM. As an indication of the impact of this work, the use of the cement paste and mortar SRMs are referenced in the new ASTM standard test method for measuring the rheological properties of cementitious materials [2]. A more detailed description of the development and validation of these SRMs has recently been published [3].

We are currently running a suite of simulations of the concrete SRM using the cement paste as the matrix fluid in which both 1 mm and 10 mm diameter hard spheres are suspended. The results of these simulations should match the results from simulations comprising the mortar SRM as the matrix fluid was with suspended 10 mm hard spheres. Depending on the outcome of these simulations, the concrete SRM certification may need to be updated. These simulations have not yet reached an equilibrium state and so we continue running them.

Flow of Dense Suspensions in Pipes. Understanding the flow of suspensions in pipes is important for a wide variety of applications. For example, in the construction industry, concrete is often placed by pumping it through extensive pipe systems. However, research on predicting the pumpability of concrete has been limited due to

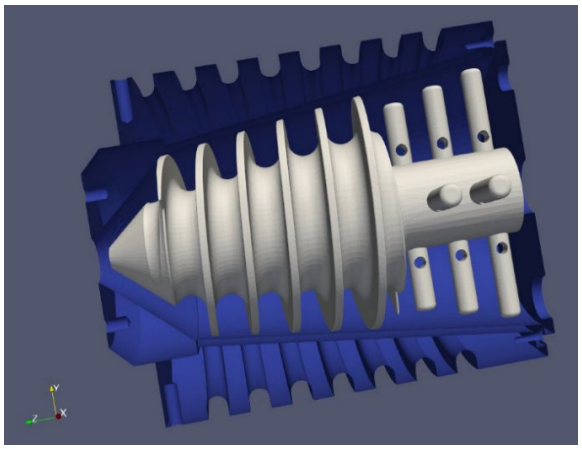

Figure 44. *NIST EL's proposed active mixer for additive manufacturing with cementitious material. The rotor is shown in gray and the housing, which is clipped in half to show the rotor inside, is shown in blue. The additives to be mixed are injected through the openings in the shafts on the right side (input side) of the rotor.*

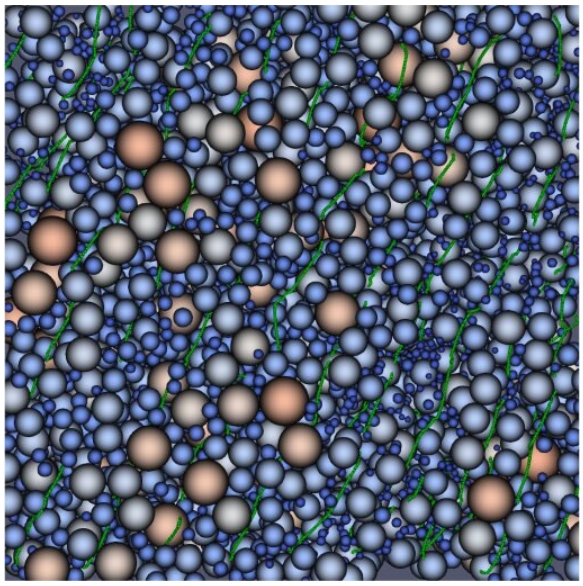

Figure 45. *A snapshot of an early simulation of a high-performance concrete. The sand is modeled as spheres of varying size. In this image, the spheres are colored based on their radius and the suspended semi-stiff fibers are shown in green.*

the heavy equipment and large amounts of material needed. Suspension flow in pipes is also important in the developing field of 3D additive manufacturing.

Predicting the flow of this complex fluid, which is composed of a non-Newtonian matrix fluid with suspended solid inclusions flowing under pressure, is challenging. Flow in these systems is also complicated by variety of phenomena such as slip at the wall and shear induced migration, which has only been studied for the simpler case of a suspensions with a Newtonian matrix fluid. A detailed discussion of this topic is available in a NIST Technical Note [4]. It is also the case, especially in the case of 3D additive manufacturing, that the placement of these materials is time sensitive, especially from the time the material is initially mixed to the time it is pumped and placed [5].

We have been conducting detailed simulations of the flow of suspensions through pipes to enable the development of predictive flow models and to advance measurement science in this field. Through quantitative analysis and visualization of results, we have gained insight into shear-induced migration and slip behavior in these systems. For example, Figure 43 shows a side-by-side comparison of identical systems with only a single property of the matrix fluid changed, one Newtonian and the other non-Newtonian (shear thinning). Over the last year we have been conducting a suite of simulations of shear thinning and shear thickening suspensions flowing in pipes, varying the properties of the matrix fluid and the driving force.

Studying the flow velocity fields as a function of driving force we have discovered a useful scaling relationship. Given that the matrix fluids have a viscosity, μ, that relates to the strain rate $\dot{\gamma}$ such that

$$\mu \sim \dot{\gamma}^n,$$

we have determined that the system velocity in the pipe, v, is related to the driving force, g, as

$$v \sim g^{\frac{1}{1+n}}$$

So, for example, with a shear thinning matrix fluid with $n = -0.5$, we have

$$v \sim g^{\frac{1}{1-0.5}} = g^2$$

and with a matrix fluid which is shear thickening, with $n = 0.5$, we have

$$v \sim g^{\frac{1}{1+0.5}} = g^{\frac{2}{3}}$$

Notice that this scaling relation depends on the power-law behavior of the non-Newtonian matrix fluid. As a consequence, given a few measurements of the flow velocity versus the driving force of the suspension, one can determine the power law behavior of the suspension, and indeed we can then also determine the power law behavior of the matrix fluid.

All of our pipe-flow simulations, except for the shear-thickening mortars, have reached steady state. The shear thickening mortars in pipes has proven to be very slow to approach steady state and so we continue to run those simulations. Our current results, which show agreement with the model predictions to within 15 percent, were published in 2020 in the *Journal of Rheology* [6].

In support of NIST researchers investigating 3D additive manufacturing using cementitious materials, we have begun developing a simulation of the flow through a pipe and then through a reactive mixer device. This device is being designed to mix additives to a cement

paste or mortar at the point of placement, that is, immediately before the material is placed. See Figure 44. The additives to be mixed are injected through the openings in the shafts on the right side (input side) of the rotor. These injected additives will be designed to accelerate the rate of curing of the mortar in order to improve the additive manufacturing process.

In addition to the simulation of an "active mixer" we have developed simulation code to study the rheology of high-performance cement-based materials that consist of cement paste, sand particles of varying size, and suspended semi-stiff fibers. Figure 45 shows such a system. We will use this capability to study the rheology of these systems with varying fiber material properties, such as elastic and flexible versus stiff, as well as varying sand volume fraction and size distribution. The suitability of these formulations for additive manufacturing is of interest to industry.

[1] Nicos S. Martys, William L. George, Ryan P. Murphy, Katheen Weigandt. Certification of SRM 2497: Standard Reference Concrete for Rheological Measurements. NIST Special Publication 260-194, April 2019, 116 pages. DOI: 10.6028/NIST.SP.260-194

[2] ASTM International C1874-19. New Test Method for Standard Test Method for Measuring the Rheological Properties of Cementitious Materials using a Coaxial Rotational Rheometer. ASTM International, West Conshohocken, PA, 2019.

[3] N.S. Martys, W.L. George, S.G. Satterfield, B. Toman, M.A. Peltz, S.Z. Jones, and C.F. Ferraris. Standard Reference Materials for Rheological Measurements of Cement-Based Materials. *ACI Materials Journal* **118**:6 (November 2021). DOI: 10.14359/51733132

[4] M. Choi, C. F. Ferraris, N. S. Martys, V. K. Bui, H. R. Trey Hamilton, and D. Lootens. Research Needs to Advance Concrete Pumping Technology. NIST Technical Note 1866, 2015. DOI: 10.6028/NIST.TN.1866

[5] S. Z. Jones, D. P. Bentz, N. S. Martys, W. L. George, and Thomas. Rheological Control of 3D Printed Cement Paste. In *Digital Concrete 2018: First International Conference on Concrete and Digital Fabrication*, Zurich Switzerland, September 9-12, 2018. DOI: 10.1007/978-3-319-99519-9_7

[6] N. S. Martys, W. L. George, R. P. Murphy, and K. Weigandt. Pipe Flow of Sphere Suspensions Having a Power-Law-Dependent Fluid Matrix. *Journal of Rheology* **64**:2 (March/April 2020). DOI: 10.1122/1.5131021

Visualization of Greenhouse Gas Emissions

William Sherman
Simon Su
Judith Terrill
James Whetstone (NIST SPO)
Israel Lopez Coto (NIST SPO)
Anna Karion (NIST SPO)
Kimberly Mueller (NIST SPO)

The NIST Greenhouse Gas (GHG) Measurements Program develops advanced tools and standards for accurately measuring GHG emissions so industries and governments will have the information they need to manage emissions effectively. ACMD's High Performance Computing and Visualization Group (HPCVG) is collaborating with James Whetstone, Leader of NIST's Greenhouse Gas Measurements Program and his team of climate and weather simulation researchers to produce interactive visualizations of their data.

One of our goals in the High-Performance Computing and Visualization Group is to reduce the turnaround time of immersive visualization development. Leveraging our work in transitioning to open source visualization software (ParaView), we are able to load

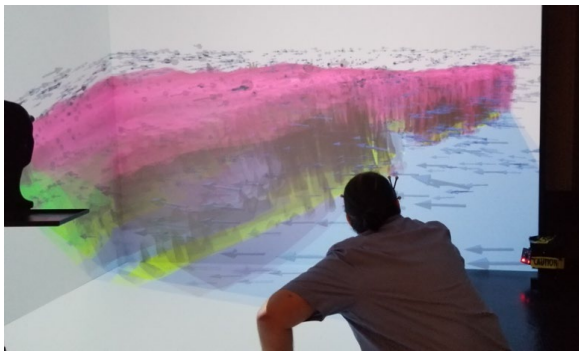

Figure 46. *NIST atmospheric sciences researcher Israel Lopez Coto interacts with data from his greenhouse gas simulation in the NIST CAVE.* (Photo courtesy of Simon Su, NIST.)

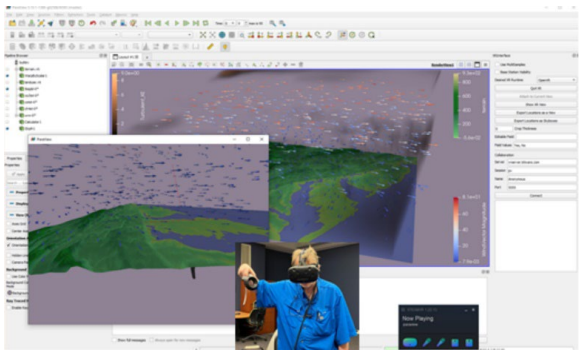

Figure 47. *Desktop view of ParaView displaying to an HMD VR system, with inset of researcher using the HMD.* (Photo courtesy of Simon Su, NIST.)

the data generated by the GHG Measurements Program in both CAVE and Head Mounted Display (HMD) immersive visualization environments without the need to develop custom immersive visualization application.

Using this workflow, we are able to manipulate various ParaView visualization features in response to input from the NIST scientist, who helped direct us toward what aspects of the data are important to see. The ParaView interface allows for rapid adjustments of the visualization parameters, which are immediately reflected in the immersive environment. We worked, in-person, and on-the-fly, with members of the GHG measurements team to produce an interactive visualization.

As detailed below (Transition to Open Source Software), the HPCVG continues to work with Kitware Inc. to enhance ParaView's immersive capabilities to make transitioning between desktop and immersion (CAVE or HMD) as seamless as possible. HPCVG also participated in a Kitware workshop providing information on the creation of new ParaView features by way of their plugin system, which will be used to enhance the capability of reading additional formats directly into ParaView such as those used by the GHG effort.

Immersive Visualization for the Design of Wearable Wireless Monitoring System

Simon Su
William Sherman
Judith Terrill
Kamran Sayrafian
Katjana Ladic (University of Zagreb, Croatia)

The NIST ITL Building the Future Program project, *A Wireless Wearable Technology to Detect Accumulation of Fluid in the Lungs*, strives to detect fluid buildup in the human lungs by developing a methodology to computationally emulate human lungs. A sequence of virtual experiments has been developed to evaluate the performance of different wearable system designs.

Immersive visualization plays a crucial role in the visual analytics of the computationally generated data of the simulation experiments. Leveraging our work in transitioning to open source visualization software (ParaView), we are able to load ParaView desktop visualizations provided by the simulation team to immediately visualize the data in both CAVE and Head Mounted Display (HMD) immersive visualization environments. As described below, our effort to enhance ParaView with immersive capabilities enables us to move from desktop visualization directly to immersive displays without requiring custom development of an immersive visualization application.

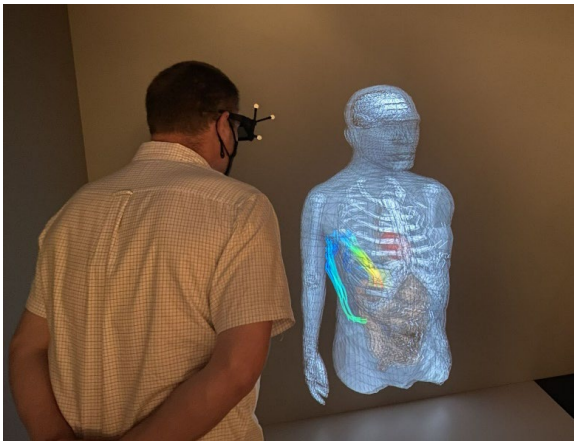

Figure 48. *Immersive visualization showing the streamlines of RF energy data around a virtual human.* (Photo courtesy of Simon, Su, NIST.)

As shown in Figure 48, immersive visualization showing the streamlines of RF energy data around virtual human clearly demonstrated the result of the computational model. Using this workflow, we are also able to concentrate our efforts on optimizing the data to improve user's immersive visualization experience. ParaView's ability to immediately provide feedbacks while the scientist views the data in the CAVE or HMD significantly reduces the time needed to develop useful visual analytics.

Transition to Open Source Visualization Software

William George
Terence Griffin
Sandy Ressler
Steven Satterfield
William Sherman
Simon Su
Judith Terrill
Cory Quammen (Kitware)
Scott Wittenburg (Kitware)

As part of our research on Virtual Measurements and Analysis, the ACMD High Performance Computing and Visualization Group (HPCVG) operates a fully immersive visualization environment (IVE) and has developed high end visualization (HEV) software to run it. We started developing this software for our IVE more than two decades ago. During this time, we have upgraded and rewritten this software as our understanding of scientific visualization in an IVE developed and as outside innovations in hardware appeared. However, there were many limitations to our software. For example, it could only run on one specially configured operating system, and it had not kept up with recent advances in hardware

visualization capabilities. Internally this software uses a scene-graph-based framework. Our IVE is on a critical path for the success of collaborations with several NIST research groups and is used at every stage of these collaborations. These projects are diverse and span applications from nanotechnology to medical to materials, and often contribute to standard reference data and materials. For example, the IVE was essential in the success of NIST's development of standard reference materials (SRMs) for the measurement of the flow of cement paste, mortar, and concrete.

To take advantage of recent advances in visualization hardware, we are moving our IVE to ParaView, a fully open source software environment. The ParaView software system is complex. Internally it uses a pipeline and proxy-based framework. The software consists of a Qt interface, which uses over 2000 VTK C++ classes to produce visualizations. It runs in an IVE as well as on Windows, Mac OS X, Linux, SGI, IBM Blue Gene, Cray and various Unix workstations, clusters, and supercomputers. It supports rendering shaders. It has a new real-time path-tracing back end using NVIDIA RTX technology. ParaView extends the environments that the HPCVG HEV can work in, as well as provides access to real time ray tracing and global illumination made possible with the new GPUs. Access to high-end GPU rendering will continue to grow as ParaView adopts the ANARI rendering standard from the Khronos Group.

This year we completed adding support for OpenXR in ParaView and it is now in the released version. We fixed a longstanding problem with stereo and improved volume rendering. These fixes are also now in the released version. ParaView now functions as well in the CAVE as our HEV software did and we now routinely use it for our applications. We have also nearly completed adding the ability to classify geometric objects into functional groups that can be associated with a particular coordinate system. We also have a prototype of a Python scripting interaction feature for the CAVE that immensely broadens the user's capabilities in the CAVE; this feature will be enhanced and documented in the next year. We also gave multiple talks to highlight the advancements we have made in ParaView [1-6].

In the coming, year we will complete the coordinate system work as well as the Python scripting feature and merge it into the released version of ParaView. We will verify that glTF functions as expected in ParaView. We will define other new capabilities to add to ParaView and work on adding those capabilities, such as more fully integrated live collaboration between users at different sites.

[1] W. Sherman. "Immersive Visualization with the ParaView Open Source Tool." FOSS-XR 2022, Minneapolis, MN, October 6, 2022.

[2] S. Su. "High Performance Computing and Visualization Group at NIST." IEEE ISMAR 2022 Pitch Your Lab, Singapore, Oct 20, 2022.

[3] W. Sherman. "Open-source and Standards-based Immersive Visualization." SIGGRAPH '22, Online, July 28, 2022.

[4] S. Su. Obstacles to adoption of XR, particularly in the federal / DOD space, APL XR Symposium July 27-28, (July 28, 2022).

[5] W. Sherman and S. Su. "Immersive Visualization with ParaView & VTK." Sandia XR 2022 Conference, July 14, 2022.

[6] S. Su, W. Sherman, I. Lopez Coto, K. Sayrafian, and J. Terrill. "Immersive ParaView: An Immersive Scientific Workflow for the Advancement of Measurement Science." IEEE ISMAR 2022 Workshop on Visual Analytics in Immersive Environments (VAinIE), Singapore, October 21, 2022.

Transportable VR System

William Sherman
Simon Su
Judith Terrill

A new project this year is our effort to develop a transportable VR system that approximates CAVE-style VR for use at conferences and similar venues. This project has grown out of the HPCVG effort to enable researchers and developers to have local (i.e., in their office) access to immersive interfaces using consumer tracking technology, which we have previously discussed as part of our effort to transition to open source software suites as our immersive visualization solution.

Now, as more conferences are again meeting in person, we decided that we could best demonstrate our immersive visualization efforts by bringing a medium-sized CAVE-style display to particular venues. This year we setup and demonstrated our hardware and software at the FOSS-XR 22 conference in Minneapolis MN, and at the Supercomputing 22 conference in Dallas TX. The large-screen method of virtual reality is better suited to group demonstrations than the more isolated HMD experiences.

Because our software has been written to be sufficiently flexible to handle screens of different sizes and arrangements and building upon our previous efforts to integrate consumer position tracking technology into our environment, nothing more than collecting the software together and making a proper configuration were required on the software side of the technology.

On the hardware side, the effort was primarily to identify and test which specific products would address the need to provide a somewhat large projection surface with minimal supporting framework, along with providing stereoscopic display. The primary key to the solution is an ultra-short-throw projector from BenQ that can rest on the floor and provide 2.286 m wide projection with stereoscopic display. We used a projection screen from

Figure 49. *The Transportable-VR system on display at the Supercomputing 22 conference in Dallas*. (Photo courtesy of Lochi Orr, NIST.)

Screenworks that folds up into a transportable case. The fully constructed system can be seen in Figure 49.

The system can be brought to major conferences, and setup in approximately two hours, but there is some effort required, and an expert must be on-hand to deploy the system. Transporting the system requires three or four boxes to be shipped to the conference location, containing the screen, the projector, a computer, an ancillary support hardware such as the tracking system and stereoscopic glasses.

Software should be pre-installed on the computer, with a 10 minute calibration step performed once the screen, projector, and position tracking are in place. Thus far we have demonstrated our work with the ParaView visualization tool we are improving in collaboration with Kitware. Other test and demonstration software are also often included.

Standards in Visualization

William Sherman
Sandy Ressler
Simon Su
Judith Terrill

The HPCVG group continues to work with the Khronos Group[12] as participating members of several standards working groups, including OpenXR[13], ANARI[14], 3D Commerce[15], and glTF[16].

OpenXR. The Khronos OpenXR working group continues to advance this burgeoning standard for software interfaces to immersive technologies. This year there is a new chair (Alfredo Muniz), and with the increased activity there is a newly created vice-chair position now held by Ron Bessems. With the reopening of in-person events, Khronos hosted an in-person meeting in Phoenix AZ this year, in which NIST participated. The broader immersive technology (XR) community continues to grow, with more software tools adopting the standard for their product deployments.

This year the HPCVG group made progress on getting OpenXR working on Linux systems using the open source "Monado" tool. We also continue to push Kitware to advance the OpenXR integration into the VTK and ParaView visualization efforts as described in the "Transition to Open Source Visualization" section. The HPCVG group is also looking to expand the OpenXR ecosystem by exploring software that can provide an OpenXR runtime capable of rendering to CAVE-style virtual reality systems.

ANARI. The ANARI (Analytic Rendering Interface for Data Visualization) continues to move toward a 1.0 specification release. The provisional release continues to be tested allowing final refinements to be integrated into the full 1.0 release. This year the ANARI working group has begun the process of developing a conformance test suite to ensure new renderers conform to the standard. ANARI provides a standard rendering API for rendering of scientific (and other) data. In particular, ANARI provides a consistent interface for volumes, point clouds and polygonal mesh data that can be rendered using different methodologies, and tuned to the available graphics rendering hardware. The low-level rendering can be CPU-based or make use of GPU features such as the RTX ray-tracing cores.

This past year the HPCVG group has continued to work on the software end of ANARI, including creating new simple applications that both serve as rendering tests, but also can be the basis of a tutorial to help new users adopt ANARI as a standard. Further, the HPCVG group has begun working on a simple back end that can be used as a guide for new renderer software authors to work within the ANARI ecosystem. In the coming year, the VTK visualization toolkit will be releasing an ANARI rendering option, which can be followed by a ParaView interface.

3DCommerce, glTF and Metaverse. The 3DCommerse and glTF Khronos working groups focus on creating modern file and transmission formats for 3D object models that can easily flow between software

[12] https://www.khronos.org/
[13] https://www.khronos.org/openxr
[14] https://www.khronos.org/anari
[15] https://www.khronos.org/3dcommerce
[16] https://www.khronos.org/gltf

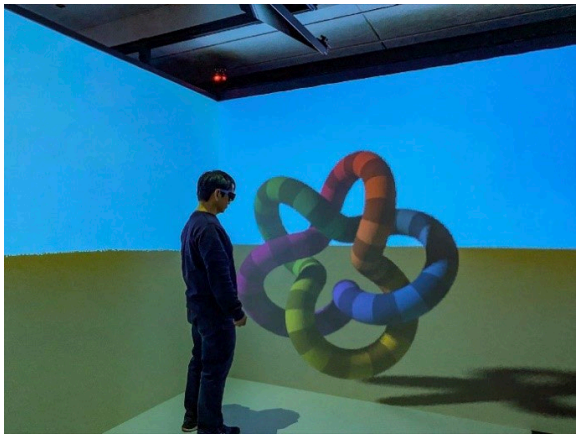

Figure 50. *Image generated with ANARI in the NIST CAVE.* (Photo courtesy of Simon Su, NIST.)

tools and rendering technologies from immersive displays to web browsers. Shared virtual worlds, especially those with immersive interfaces are increasingly being referred to as the "Metaverse" (a term coined by the 1992 Neil Stephenson novel "*Snow Crash*"). Khronos and other organizations have sought to create a non-vendor controlled standard around which future Metaverse technologies can provide a level commerce playing field while also allowing technological advancement. The HPCVG relationship to these efforts is further described in the next section of this report.

WebXR Graphics

Sandy Ressler
Russel Sitka (US Holocaust Memorial Museum)
Jane Klinger (US Holocaust Memorial Museum)
Robert Ehrenreich (US Holocaust Memorial Museum)

WebXR is the Web and eXtended Reality. A widely encompassing term WebXR covers VR (virtual reality), AR (augmented reality), and MR (mixed reality), all distributed via the Web. It is a coalescence of technologies which have much in common with each other. First, a device such as a headset, or soon a pair of glasses display images close to your eyeballs, in stereo. Second, your head is tracked so that as you move the images being displayed are modified, in real-time, to give the illusion that you are in the space of whatever you are being shown. You are "immersed" into a scene of data or a simulated object. In the case of VR, you are cut off from the real world and are purely in a virtual world. In the case of AR, you remain in the real world because you still see the real world, with the graphics as an overlay. A current common method of using AR is via a mobile phone which uses its camera to capture the real world environment and overlays graphics on it. A compelling example is holding your phone up to the world after just emerging from a subway. A set of large arrows appears telling you which direction to go [1].

We remain convinced that "The Web" is the most powerful information dissemination technology of the last couple of decades. Now let's examine standards and museums two domains in which we are active. Standards enable us to perform the integration and museums happen to be an "application" in great need of this integration and both benefit the public good, part of NIST's mission.

3D Object Input and Capture. Viewing a 3D object on a web site first requires the object itself. Historically we have obtained our objects either from CAD systems or by visualizing data. Missing from that set of objects are representations of "real" objects, artifacts that exist in real life. As the cost of hardware for capturing the shape and texture of real objects has plummeted, 3D object capture is becoming democratized. Last year we published a blog article for the Khronos Group on just this topic. See: *Will LiDAR Scanning break the 3D Asset Creation Bottleneck?* [2].

Almost all museums that have objects cannot display the vast majority of those object due to space limitations. 3D object capture is a promising approach to making those objects available via the web when physical exhibition is not possible. We are currently helping staff of the United States Holocaust Memorial Museum (USHMM) explore the use of 3D objects on their web sites. Figure 51 illustrates an actual artifact being used to conduct an internal museum study with the education group. 3D object scanning remains a difficult and time-consuming task. Standards and best practices will eventually help lead towards more public access to priceless artifacts.

3D Standards Participation. We are involved with several efforts run by three different groups. First the 3D Formats Group, part of the Khronos Group responsible for the continued evolution of glTF a 3D graphics format becoming the "jpeg of 3D". Other members of our group participate in the OpenXR Group of Khronos. Second, the Immersive Web Group of the World Wide Web consortium (W3C) working on formal W3C specifications. Finally, we have taken the lead trying to have NIST join a new standards group called the Metaverse Standards Forum [3]. This is a new group with over 2000 industry members which is likely to have a great deal of influence in how standards for the Metaverse evolve. NIST is expected to become a member of this group soon.

The 3D Formats Group is actively involved in a variety of extensions to glTF. Primarily concerned with achieving high quality and high performance, taking advantage of GPU hardware is a signature overarching goal of the group. glTF is becoming more and more popular as a representation of 3D objects. Our participation ensures that it is aligned to our, and the public's needs,

Figure 51. *Actual scanned artifact being used to conduct internal museum test with an education group.* (Image courtesy of the US Holocaust Memorial Museum.)

and keeps us on the leading edge of 3D format developments. The Khronos Group is an industry-led consortium, and the participants are a highly skilled collection of technologists focused on real world practical problems. In particular, we assisted in helping the Khronos Group move glTF into ISO and it now is approved ISO standard [4].

[1] S. Ressler, "Google's 'Live View' the First Useful Augmented Reality Application," November 5, 2019, Medium. URL: https://medium.com/@sressler/googles-live-view-the-first-useful-augmented-reality-application-91525209743f

[2] S. Ressler. "Will LiDAR Scanning break the 3D Asset Creation Bottleneck? September 15, 2021. URL: https://www.khronos.org/blog/will-lidar-break-the-3d-asset-creation-bottleneck

[3] Metaverse Standards Forum. URL: https://metaverse-standards.org/

[4] ISO/IEC 12113:2022 Information technology – Runtime 3D asset delivery format – Khronos glTF™ 2.0. URL: https://www.iso.org/cms/%20render/live/en/sites/isoorg/contents/data/standard/08/39/83990.html

Uncertainty in Machine Learning for Quantum Physical Systems

Joshua Ziegler
Justyna P. Zwolak
Zachary J. Grey
Craig Greenberg (NIST ITL)

Machine learning (ML) models have shown widespread success in achieving human-level performance in a variety of tasks that are traditionally difficult for computers. Yet, these models often fail in quite unexpected ways [1]. To date, much effort has been devoted to developing metrics necessary to assess the expected performance and uncertainty of ML models to mitigate such failures. However, the problem of uncertainty quantification (UQ) in ML remains unsolved [1]. Despite the lack of a rigorous approach to UQ, ML has seen broad applications in physics, from simulations [2], to complex data analysis [3], to experimental control [4, 5]. While some of these implementations include attempts at uncertainty estimation [2,3], these demonstrations are very limited and tuned to the problem at hand. Thus, despite the need for informative metrics to enable trust in automation, applications of ML in experiments still lack sufficient uncertainty measures [1].

There are many sources of broadly defined dataset shift [1] in physics experiments that negatively affect automation algorithms. Changes in noise levels, disturbance of an experimental setup, or the order in which control parameters are adjusted may cause different kinds of data transformations. The necessity to use quantitative (partial) labels further complicates this problem: in some applications, a [50 %, 50 %] classification of an image should represent a transition between two system states, but it might indicate model confusion in state assessment. To automate experiments effectively, metrics must be developed that encompass uncertainty due to these varied nonlinear data transformations and state transitions. Moreover, many experimental applications necessitate a robust ML model that can be used to automate the control of devices with varying designs and potential defects.

In this project, we first reviewed relevant literature for popular and current methods of estimating uncertainty in convolutional neural networks (CNN). In doing so, we leveraged our mixed expertise (i.e., in physics, mathematics, and computer science) to develop a greater shared understanding of the methods than would be possible without this collaboration. To test these methods and identify potential limitations, we implemented two of the most promising approaches (deep ensembles and deep kernel learning)—negotiating various tradeoffs in ease-of-use, effectiveness, and computational burden. We then tested these methods on a dataset of Bose-Einstein condensate images for detection of solitons in the

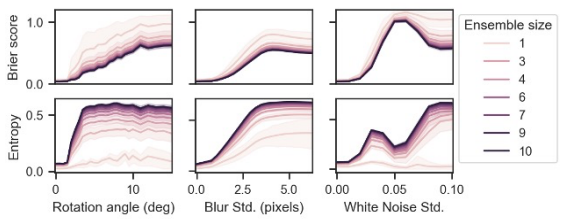

Figure 52. *Deep ensembles evaluated on solitonic excitations data with rotation, blur, or white noise added. Ensembles often capture decreased Brier score via predictive entropy.*

presence of various types of synthetic but physically motivated noise. Through a variety of uncertainty metrics computed with deep ensemble predictions, we observed an anticipated and intuitive response in the model's entropy subject to synthetic physics-informed noise—increased entropy subject to increased levels of observed types of noise, see Figure 52. The deep kernel learning methods, while requiring less computational resources, did not demonstrate an intuitive response to synthetic noise conditioned on our data and implementation.

To interpret the apparent effectiveness of the deep ensemble approach, we applied computational geometry to augment inferences about the model evolution over ensemble averaging by visualizing empirical distributions of a reduced set of significant model features. For the three classes posed in this computational experiment, we projected analogues of "logits" onto the orthogonal complement of the logistic (last) layer null space, Ker([1,1,1]). Consequently, we visualized the final empirical distributions of features pulled back onto this space—which are also paired with corresponding images—to demonstrate and diagnose improved robustness through a decrease in the scattering of labelled features. This approach is comparable to visualizations of the output probabilities over a simplex but now pulled back to a vector space to visualize uncertainties more clearly.

The improved distribution of features from the ensemble of 10 trained models was compared to individual models and demonstrated a desirable concentration of features, i.e., variation of features within distinct low entropy regions is reduced using an ensemble of 10 models as opposed to a single model. These visualizations supplemented increased explainability and trustworthiness for a method, which achieved high levels of accuracy in the classification task coupled with an intuitive behavior subject to increasing levels of synthetic noise applied to the data. Figure 53 depicts this explanation via visualization for the concentrated features of the ensemble model.

The better of the uncertainty methods we have implemented will be directly useful for our experimental collaborators that are currently using CNNs without uncertainty estimation for experimental data analysis. Insights that are gained from a computational geometry perspective of deep ensemble methods are useful for understanding their effectiveness and may be useful for the general machine learning community.

[1] Y. Ovadia, E. Fertig, J. Ren, Z. Nado, D. Sculley, S. Nowozin, J. V. Dillon, B. Lakshminarayanan, and J. Snoek. Can You Trust Your Model's Uncertainty? Evaluating Predictive Uncertainty Under Dataset Shift. *Advances in Neural Information Processing Systems (NeurIPS)* **32** (2019).

[2] G. J. Anderson, J. A. Gaffney, B. K. Spears, P.-T. Bremer, R. Anirudh, and J. J. Thiagarajan. Meaningful Uncertainties from Deep Neural Network Surrogates of Large-Scale Numerical Simulations. arXiv:2010.13749, 2020.

[3] K. T. Butler, M. D. Le, J. Thiyagalingam, and T. G. Perring. Interpretable, Calibrated Neural Networks for Analysis and Understanding of Inelastic Neutron Scattering Data. *Journal of Physics: Condensed Matter* **33** (2021), 194006.

[4] J. P. Zwolak, T. McJunkin, S.S. Kalantre, J.P. Dodson, E.R. MacQuarrie, D.E. Savage, M.G. Lagally, S.N. Coppersmith, M.A. Eriksson, and J.M. Taylor. Autotuning of Double-Dot Devices in Situ with Machine Learning. *Physical Review Applied* **13** (2020), 034075.

[5] S. S. Kalantre, J. P. Zwolak, S. Ragole, X. Wu, N. M. Zimmerman, M. D. Stewart, and J. M. Taylor. Machine Learning Techniques for State Recognition and Auto-Tuning in Quantum Dots. *npj Quantum Information* **5**:1 (2019).

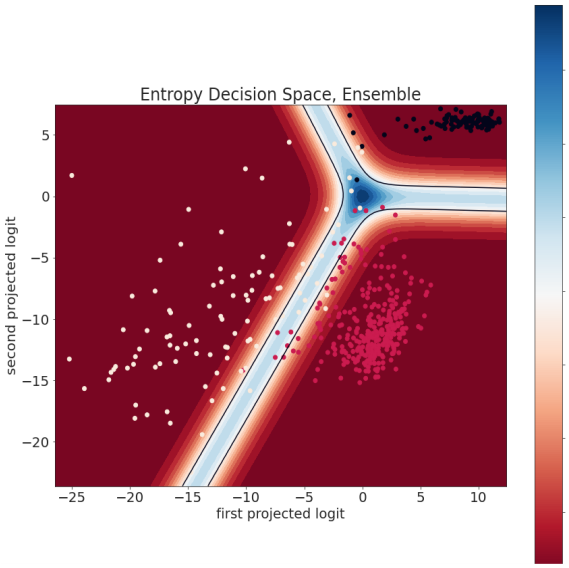

Figure 53. *Entropy decision space orthogonal to the null space of the final classification layer. The scatter of points is colored by labelled class while the filled contours, representing entropy, visualizes three distinct regions defining the three classes separated by level-sets of entropy defining decision manifolds (solid black lines). Uncertain points are those which encroach or fall within the lighter blue/white regions partitioned by the decision manifolds.*

Towards Robust Autotuning of Noisy Quantum Dot Devices

Justyna P. Zwolak
Joshua Ziegler
Jacob M. Taylor (NIST PML)
Thomas McJunkin (NIST PML)
Florian Luthi (Intel Corporation)
Mick Ramsey (Intel Corporation)
Sandesh Kalantre (Stanford University)
E. S. Joseph (University of Wisconsin-Madison)
Mark A. Eriksson (University of Wisconsin-Madison)

Gate-defined quantum dots (QDs), in which electrons in a semiconductor are trapped in electric potential wells, have appealing attributes as a quantum computing platform, such as small device footprint and the possibility of operation at temperatures of a few Kelvin. However, near-term devices possess a range of possible imperfections that need to be accounted for during the tuning and operation of QD devices. These minor inconsistencies inherent to the fabrication process make a deterministic tuning of QD devices impossible. Currently, initialization is performed mostly manually through heuristic calibration, although some recent progress has been made towards automating elements of this process [1].

The best strategies for automating initialization rely on supervised machine learning (ML) methods to autonomously identify the state of the device as parameters are tuned and use an algorithmic optimizer to find the desired state. However, training such ML models requires large amounts of data with labeled device states. There are two paradigms for preparing datasets for training, each having its own advantages and limitations. The first is to use unrealistically noiseless simulated data, which not only necessitates specialized pre-processing of the experimental data, but also makes the trained models less robust when implemented in the experiment [2]. The other paradigm relies on manual labeling of experimental data. This is laborious, less reliable, and not scalable, especially as gate defined QD devices change or grow in qubit numbers and complexity. Thus, approaches demonstrated to date force a choice between scalability and robustness. Furthermore, the ML methods typically do not include an assessment of the quality of the input data, leading to unknown reliability of ML predictions and potential unexpected failures.

An idealized noiseless charge stability diagram shows lines when an electron is added to the device's trapping potential landscape overlayed on a uniform background, as shown in Figure 54A. To overcome these issues, we have expanded the capabilities of our QD simulator [3] to include various types of realistic, physical noise. Depending on the type of added noise, the appearance of simulated data changes as shown in Figure 54B-F. Using a set of 542 manually labeled experimental scans for testing, we found an accuracy improvement of about 46 %, from 48.7(5.5) % when trained on noiseless simulated data to 95.0(9) % when trained on simulated data with all relevant noises added. We also tested how each added noise individually contributes to this performance, as shown in plots B-F in Figure 55(a). Plot G in Figure 55(a) shows the performance for the optimized noise combination. To get best performance sensor jumps, pink (1/f) noise, and white noise were varied together to yield a varied signal-to-noise ratio in our dataset.

We then generated a similar dataset with a broad variation of noise and used the performance of the noise-trained ML state classifiers on it to develop a data quality control (DQC) module. The utility of the DQC module was confirmed by showing a correlation between the accuracy of the state classifiers and the assessed quality. Specifically, for experimental data assessed as "high quality" the state classifier has 96.4(9) % accuracy, for data assessed as "moderate quality" it has 91.9(2.1) % accuracy, and for "low quality" data the state classifier has 69.3(5.6) % accuracy, see Figure 55(b). This validates the ML DQC module as a tool to filter data that might lead to poor performance

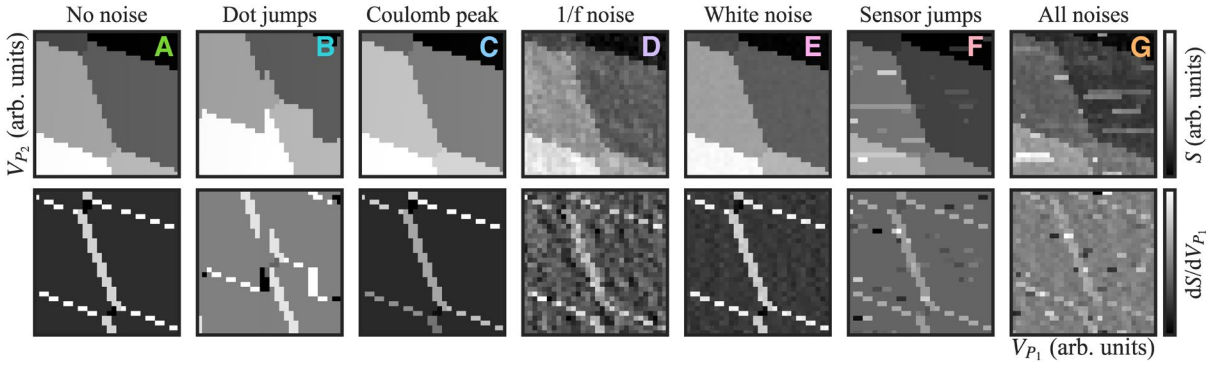

Figure 54. *Various types of noise added to a simulated charge stability diagram for a QD device in a "double QD" state, with electrons trapped in two potential wells. The bright lines in the bottom row indicate a change of electron occupation in the device. All noise magnitudes are the same as for the best accuracy quoted except for Coulomb peak and dot jumps which have increased effect for visibility.*

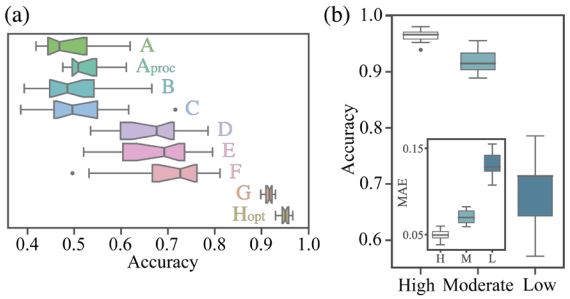

Figure 55. *(a) Box plots depicting the accuracies of state classifier models trained on the data as indicated in Figure 55. A_{proc} models were trained on the same noiseless data as A but preprocessed using thresholding [1]. G_{opt} models were trained on the same data as G, but with a model architecture optimized on the G data [4]. Each box plot depicts the performance of 20 randomly initialized models trained under identical conditions on the relevant dataset. (b) Box plots of model accuracy for each assigned quality class for the experimental data. Inset: box plots of the mean absolute error (MAE) for each quality class.*

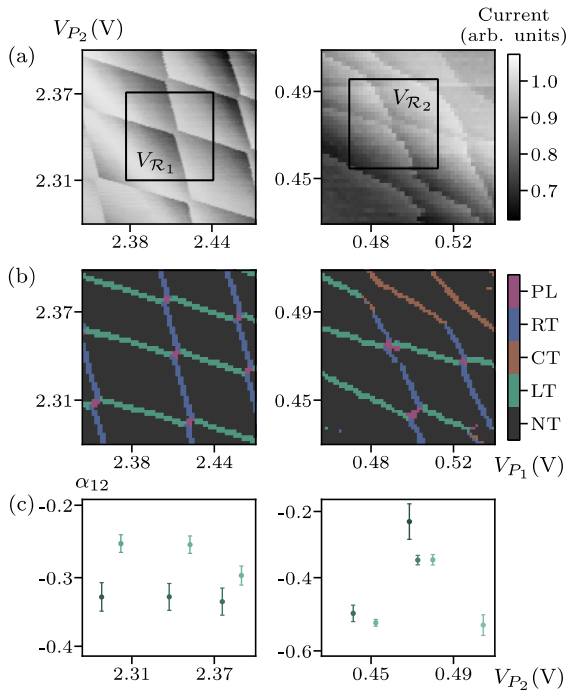

Figure 56. *Spurious dot detections. (a) Two charge stability diagrams: one capturing properly formed QD (left) and one capturing spurious QD (right). The black boxes highlight small 2D scans typical of the auto-tuning approaches [1]. (b) Pixel classification results for charge stability diagrams shown in (a). (c) Plots of fitting results used to determine whether a spurious QD is present.*

of an ML state classifier and, consequently, the autotuner failure. An article reporting this work has recently been published in *Physical Review Applied* [4].

Another difficult to assess tuning failure mode is related to formation of the so-called spurious QDs that may form in small potential wells due to interface defects, surface roughness, or strain within the device. Spurious QD are highly undesirable since they may interfere with the QDs intended for use as qubits and cannot themselves be used as qubits. To avoid device tuning failure, spurious QDs must be identified when present and avoided. Visually, spurious QDs are recognized in large 2D scans as charge transitions with slopes diverging from a monotonic trend. As we show in Ref. [5], spurious dots can be identified automatically as transition lines with anomalous capacitive couplings relative to the transitions around them.

Figure 56(a) shows two charge stability diagrams: one capturing properly formed QD (left panel) and one capturing spurious QD (right panel). The small 2D regions in the plunger-plunger space, highlighted in these scans with the black boxes, are typical for topology setting algorithms. In both cases, they are classified by a state classifier model as double QD state. However, when looked at within a slightly larger voltage range, it is clear that in the latter case, the small scan captures an anti-crossing with a spurious QD, which for practical tuning purposes is a failure.

Our algorithm combines a pixel classifier, used to extract the high-level features from experimental data, as shown in Figure 56(b), with traditional fitting used to extract the slopes of the consecutive charge transitions which are manifestations of the capacitive coupling between the QDs, see Figure 56(c). For properly formed QD, as shown in the left panel in Figure 56(a), the magnitude of the capacitive coupling is expected to increase monotonically while the spacing between consecutive transition lines decreases as a charge is added, as shown in the left panel in Figure 56(c). The different shades of green are used to depict separate groups of transitions, i.e., transitions captured between the blue RT lines. On the contrary, a spurious QD, as shown in the right panel in Figure 56(a), can manifest itself by a non-monotonic behavior of the capacitive coupling between transitions. This is depicted graphically by either the most left or the center point (or group of points) not following the expected decreasing trend in the right panel in Figure 56(c). In practical applications, the automated detection of spurious QD fits nicely within the auto-tuning paradigm.

With these tools, we expand the applicability of ML-based autotuning strategies to non-ideal devices by making the ML models more robust against potential failure modes. This is especially important when considering future, large-scale QD devices. More broadly, we show that making simulated data more physical can greatly improve the efficacy of ML models when deployed in a real lab environment, which may be a useful insight for other experiments combining ML and physics.

[1] J. P. Zwolak and J. M. Taylor. *Colloquium*: Advances in Automation of Quantum Dot Devices Control. arXiv:2112.09362 (2021).

[2] J. P. Zwolak, T. McJunkin, S. S. Kalantre, J. P. Dodson, E. R. MacQuarrie, D. E. Savage, M. G. Lagally, S. N.

Coppersmith, M. A. Eriksson, and J. M. Taylor. Autotuning of Double-Dot Devices in Situ with Machine Learning. *Physical Review Applied* **13** (2020) 034075.

[3] J. P. Zwolak, S. S. Kalantre, X. Wu, S. Ragole, and J. M. Taylor. QFlow Lite Dataset: A Machine-learning Approach to the Charge States in Quantum Dot Experiments. *PLoS ONE* **13** (2018), e0205844.

[4] J. Ziegler, T. McJunkin, E. S. Joseph, S. S. Kalantre, B. Harpt, D. E. Savage, M. G. Lagally, M. A. Eriksson, J. M. Taylor, and J. P. Zwolak. Toward Robust Autotuning of Noisy Quantum Dot Devices. *Physical Review Applied* **17** (2022) 024069.

[5] J. Ziegler, F. Luthi, M. Ramsey, F. Borjans, G. Zheng, J. P. Zwolak. Automated Extraction of Capacitive Coupling for Quantum Dot Systems. arXiv:2301.08654 (2023).

Towards Robust Bootstrapping of Quantum Dot Devices

Danielle J. Middlebrooks
Justyna P. Zwolak
Lara Lausen (University of Copenhagen)
Torbjørn Raasø Rasmussen (U. of Copenhagen)
Anasua Chatterjee (University of Copenhagen)

Quantum computing is a type of computation whose operations can harness the phenomena of quantum mechanics performed on quantum computers. Most models of quantum computation are based on the quantum bit, or *qubit*, which is analogous to the bit in classical computation. One way to build a qubit is by fabricating quantum dots (QDs), or very, very small cages for electrons, formed within a silicon crystal. The tuning and management of QD qubits is a large and complex task. To properly form dots the gate voltages applied to metallic gates used to form and control the QDs must be tuned to just the right values. This tuning is typically done by human operators and require hours of work. The more QDs (and gates) one involves, the harder it is to tune them all simultaneously to get qubits that work together properly.

The tuning process is an essential, yet repetitive, step for initialization of QD-based qubits [1]. This process of tuning an unknown QD device can be divided into a sequence of distinct phases: bootstrapping, coarse tuning, charge state tuning, and fine tuning. Depending on the set up, an additional establishing controllability phase may be carried out after the charge state tuning phase to enable targeted gate control.

The tools used for automated tuning schemes vary from simple fittings to heuristically defined algorithms to traditional computer vision techniques. A host of machine-learning-based techniques have also been utilized. Most of the tuning efforts focused on the more advanced phases of tuning, assuming that the device is already pretuned, with a properly calibrated charge sensor and that the safety regimes for all gates are already known. However, the initial bootstrapping phase of tuning is still nearly always done heuristically, requiring a highly trained researcher to be responsible for the subsequent decisions on how to adjust the relevant parameters.

We are currently developing an automated routine to bridge the gap between the initial device cool-down and a voltage configuration in which other, previously developed automation schemes can take over for a multiple QD device. One important step of the initial bootstrapping phase is to check which gates are functioning properly and which gates are not. To test this, decreasing voltage is applied to each gate and current is measured through the device. By examining the plots of the voltage against the measured current, human experts determine whether the gate is working. We expect the plots to have a sigmoidal shape showing quantum point contact behavior. Figure 57 demonstrates this process of sweeping the gates to use for classification. Instead of relying on human expertise to make these decisions, we automate this process by applying a fitting procedure and extracting relevant features for classification and relevant voltages for subsequent tuning.

The result of this autotuning procedure provides a sufficient starting point for the wide-ranging set of tasks for control of QD qubits. With this approach, we can expand the applicability of automated tuning schemes to non-ideal devices by requiring little predetermined assumptions on the device. This is especially important when considering future, large-scale QD devices.

[1] J. P. Zwolak and J. M. Taylor. *Colloquium*: Advances in Automation of Quantum Dot Devices Control. arXiv:2112.09362 (2021).

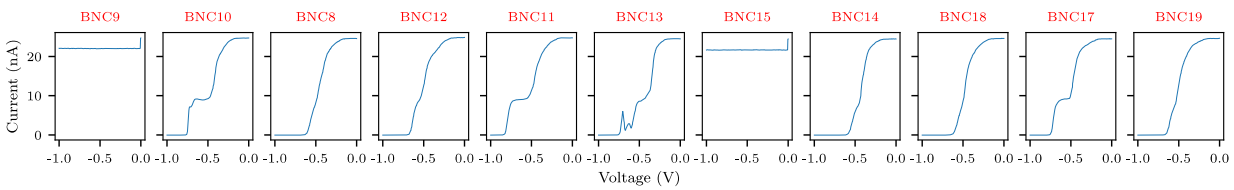

Figure 57. *Gates are stepped from high to low voltage until the signal falls below noise level. The fitting procedure extracts relevant features for classification. Gates BNC9 and BNC15 do not have currents above noise level and are identified as broken. We can extract relevant features from the remaining working gates and use for QD tuning.*

Tuning Arrays with Rays: Physics-Informed Tuning of Quantum Dot Charge States

Justyna P. Zwolak
Joshua Ziegler
Florian Luthi (Intel Corporation)
Mick Ramsey (Intel Corporation)

Gate-defined quantum dots (QDs), formed by trapping electrons using finely calibrated electric gates, are a promising quantum computing platform. Unfortunately, working with single electrons means that the operating regime strongly depends on nanoscale details (e.g., material impurities and fabrication defects) that are difficult to control across devices. For QD devices to scale effectively, this operating regime must be identified using automated methods. There have been several recent demonstrations of automation of QD tuning, yet these approaches have only taken limited advantage of the designed effect of the electric gates on the device state [1].

Recently, we have developed an intuitive, reliable, and data-efficient modular autotuning procedure for automated global state and charge tuning in a framework deemed *physics-informed tuning* (PIT) [2], depicted in Figure 58. In QD devices with the overlapping gates architecture–the type of device we have mostly been focusing on–there are two types of electric gates used to control the flow of electrons. The plunger gates serve to create potential wells that can hold electrons. The barrier gates prevent the flow of electrons between trapping potentials or into the leads. Together, these gates serve to create an electrical potential landscape in which electrons can be trapped and manipulated. Typically, in heuristic tuning procedures, coarse voltage values for barriers and plungers that cutoff electron flow are identified during the so-called "cold-start" stage [1]. These voltages are then used as a starting point for scanning pairs of plungers over a large range of voltages to identify the target regime, that is voltage ranges where single electrons are trapped in each potential well.

In our previous work, we have tackled tuning of pairs of gates using algorithms that seek to maximize a fitness function designed to quantify the difference between the target and the captured state of the device. However, none of the optimization algorithms we considered took into account information about the pre-existing relationship between the states [3, 4] which led to repeated failures for tuning initialized far from the target area in voltage space. The several algorithms for navigating to specific charge states that have been demonstrated recently also show unsatisfactory performance [5-7].

To improve the effectiveness and efficiency of automatically setting the device topology as well as tuning to a desired charge configuration, PIT leverages the intended effect of each gate on the overall QD device state. In principle, changing voltages on a particular plunger gate should lead to a change of the electron occupation only in the corresponding potential well. We show that such targeted control (made possible by the virtue of virtual gates) combined with the knowledge of the expected device topology (i.e., relative position of states in the plunger-plunger space) and a machine learning (ML) model trained to identify the captured state of the QD device, enable meaningful, efficient, and direct navigation to a target region in voltage space over a large range of voltages.

The first module of PIT, shown in Figure 58(a), is an *action-based tuning* algorithm that combines a ML classifier with physics knowledge to navigate to a target

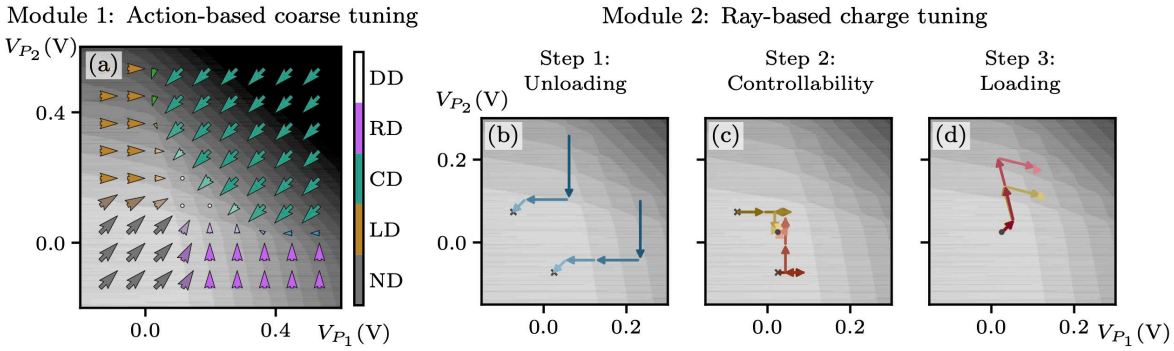

Figure 58. *The flow of the physics-informed tuning (PIT) algorithm visualized using a simulated double-QD device. (a) The action-based coarse tuning module combines ML state predictions with the overall QD state topology to navigate the plunger-plunger gate space. The orientation and size of the arrows overlaying the scan correspond to the suggested gate voltage adjustment direction and magnitude, respectively. The expected outcome for the coarse-tuning module is a gate voltage configuration defining a double-QD state. (b)-(d) The ray-based charge tuning module. The charge tuning process involves three steps: (b) unloading the double QD of all electrons using the physical gates space with the termination point marked with an x; (c) tuning to a region near the first charge transitions for both QDs (marked with a dot) and determining virtual gates; (d) loading the desired number of electrons on each QD using the virtual gate space. Panels (b)-(d) show charge tuning paths for two sample points, with the magnitude of the arrows representing the size of the consecutive steps and the color lightness indicating the progress of the unloading process. Reproduced from Ref. [2].*

global state. When tuning to double-QD (DD) state, the module seems to be quite robust against noise, with an overall performance of 94.6(2.9) % when using ray-based measurements and 98.9(2.1) % when tuning with small two-dimensional (2D) scans. When tested off-line using experimentally acquired large 2D scans, the success rate for the action-based coarse tuning to the DD state using small 2D scans is slightly higher for exp-1 dataset, at 97.1(3.5) %, than for exp-2 dataset, at 92.5(6.5) % (exp-1 consists of seven scans from the QFlow 2.0 dataset [8] and exp-2 includes 16 scans acquired using two double-QD configurations on two different three-QD $Si_x/SiGe_{1-x}$ devices fabricated on an industrial 300 mm process line).

Since local device measurements only contain information about changes in the electron occupation of each potential well, navigation to a specific charge occupation requires a more nuanced approach. We tackle this problem by following the typical procedure of first emptying a QD device of electrons and then loading a desired number back into each potential well. To achieve this most reliably, prior to the reloading stage, we calibrate the capacitive coupling of each gate to the potential wells using virtualization method that combines ML with traditional fitting to derive the orthogonalization matrix [9]. The charge tuning module uses a series of one-dimensional (1D) measurements and a conventional peak finding algorithms to detect transitions in the 1D scans as electrons are loaded off and back on each potential well. It proceeds in three steps to tune to a target charge state by first emptying the QDs of charge, followed by calibrating capacitive couplings and then navigating to the target charge state, see Figure 58(b-d). Tests of this emptying-reloading algorithm on simulated data show a high success rate for navigating from any point within the double QD region (the outcome of the action-based tuning step) to the single-electron regime in moderately noisy simulated scans 95.5(5.4) %, and is only slightly worse for off-line experimental tests, with an average of 89.7(17.4) % (median 97.5 %), see Figure 59.

In all tests, PIT terminates at most two transitions away from the target state. The main factor affecting the charge tuning success rates is either missing a transition or identifying noise as transitions when loading charges. One way to overcome this limitation is to develop a DQC module for the ray-based measurements analogous to the one used for the 2D scans during coarse tuning. Another way to boost the performance is to implement a "repeated measurement with voting" strategy.

PIT combines modern computer vision, machine learning, and data processing techniques with human heuristics to provide an intuitive, efficient, and reliable tool for QD device calibration. Moreover, the significantly reduced one-dimensional data acquisition requirements combined with simplified data analysis techniques make PIT well suited for implementation

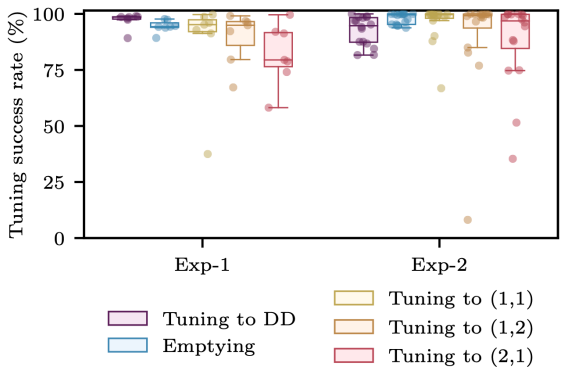

Figure 59. *A box plot showing the off-line performance of the individual components of PIT with three target charge-state configurations. The central lines indicate medians for each test and the central box represents 50 % of the data. The whiskers extend to either the extreme values or 1.5x the interquartile range, whichever is closer to the median. The individual points on top of each box plot show the success rates for each device. Reproduced from Ref. [2].*

with dedicated hardware closely integrated with the QD chip. It is thus a major step toward fully automated and scalable tuning of QD devices, a prerequisite to use QD-based quantum computers.

[1] J. P. Zwolak and J. M. Taylor. *Colloquium*: Advances in Automation of Quantum Dot Devices Control. arXiv:2112.09362 (2021).

[2] J. Ziegler, F. Luthi, M. Ramsey, F. Borjans, G. Zheng, and J. P. Zwolak. Tuning Arrays with Rays: Physics-Informed Tuning of Quantum Dot Charge States. arXiv:2209.038374 (2022).

[3] J. P. Zwolak, T. McJunkin, S. S. Kalantre, J. P. Dodson, E. R. MacQuarrie, D. E. Savage, M. G. Lagally, S. N. Coppersmith, M. A. Eriksson, and J. M. Taylor. Autotuning of Double-Dot Devices in Situ with Machine Learning. *Physical Review Applied* **13** (2020), 034075.

[4] J. P. Zwolak, T. McJunkin, S. S. Kalantre, S. F. Neyens, E. R. MacQuarrie, M. A. Eriksson, and J. M. Taylor. Ray-Based Framework for State Identification in Quantum Dot Devices. *PRX Quantum* **2** (2021) 020335.

[5] [R. Durrer, B. Kratochwil, J.V . Koski, A. J. Landig, C. Reichl, W. Wegscheider, T. Ihn, and E. Greplova. Automated Tuning of Double Quantum Dots into Specific Charge States Using Neural Networks. *Physical Review Applied* **13** (2020), 054019.

[6] S. Czischek, V. Yon, M. Genest, M. Roux, S. Rochette, J. Camirand Lemyre, M. Moras, M. Pioro-Ladrière, D. Drouin, Y. Beilliard, and R. Melko. Miniaturizing Neural Networks for Charge State Autotuning in Quantum Dots. *Machine Learning: Science and Technology* **3** (2021), 015001.

[7] [7] M. Lapointe-Major, O. Germain, J. Camirand Lemyre, D. Lachance-Quirion, S. Rochette, F. Camirand Lemyre, and M. Pioro-Ladrière. Algorithm for Automated Tuning of a Quantum Dot into the Single-Electron Regime. *Physical Review B* **102** (2020) 085301.

[8] [8] J. P. Zwolak, J. Ziegler, S. S. Kalantre, J. M. Taylor. QFlow 2.0: Quantum dot data for machine learning, NIST (2022). DOI: 10.18434/T4/1423788

[9] J. Ziegler, F. Luthi, M. Ramsey, F. Borjans, G. Zheng, and J. P. Zwolak. Automated Extraction of Capacitive Coupling for Quantum Dot Systems. arXiv:2301.08654 (2023).

Principled State Identification for Quantum Dot Data

Justyna P. Zwolak
Brian J. Weber (ShanghaiTech University)

Confining electrons in arrays of semiconductor nanostructures, called quantum dots (QDs), is a promising approach to quantum computing. Due to the ease of control of the relevant parameters, fast measurement of the spin and charge states, relatively long decoherence times, and their potential for scalability, QDs are gaining popularity as building blocks for solid-state quantum devices. However, the relevant parameter space scales exponentially with QD number (dimensionality), making heuristic control unfeasible. In semiconductor quantum computing, devices now have tens of individual electrostatic and dynamical gate voltages that must be carefully set to isolate the system to the single electron regime and to realize good qubit performance.

There has been recent work using machine learning (ML) techniques as part of the automating process. However, training ML models requires large amounts of labeled data indicating the true state of the device for a given voltage range. So far, ML efforts for QD rely on datasets that either come from simulations (and thus may lack some important features representing real-world noise and imperfections) or are labeled manually (and thus are subject to qualitative or erroneous classification). Automatic labeling will streamline creation of large, accurate datasets for purposes of ML training. Moreover, the ML approach currently lacks explainable and interpretable features for reliable diagnostics. Thus, it is desirable to have a simplified and theoretically motivated automated protocol for labelling experimental data.

The configuration space of a QD array supports irregular polytope tiling of the space, with each polytope indicating a distinct quantum state (e.g., a left or right single dot for a double QD device). The polytope shapes provide information about electron behavior within the discrete states they represent. Polytopes with similar characteristics will cluster together, allowing the subdivision of configuration space into distinct *domains* where the system exhibits a consistent behavior.

Our work is aimed at creating automatic procedures for identifying this domain decomposition and, if possible, automatic characterization of individual polytopes within each domain. The project currently focuses on the case of double QD devices, where the polygonal tessellation is readily understandable. In the past, we have successfully implemented the ray-based domain classification (RBC) schema, the theory behind which was developed in an earlier series of papers from our group [1-2].

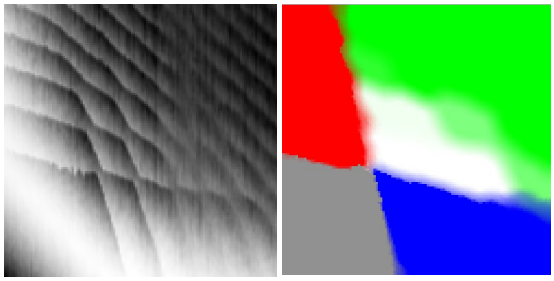

Figure 60. *RBC domain decomposition for a real device. Original charge stability diagram (left) has noise and spurious sensor artifacts. The RBC-based domain decomposition (right) is created by modeling polygonal regions and assigning to each point a probability of belonging to each of the domains.*

Building on this previous success, we are now developing an RBC-based domain decomposition methods for experimentally acquired large two-dimensional charge stability diagrams of double QD devices (see the left panel in Figure 60 for an example of such measurement). In this approach, we create a selection of "observation points" (OPs) using a simple centralization technique. From each OP we create a "fingerprint," which is a list of distances along a set of evenly spaced rays from the OP to the nearest transition boundary along that ray. From each fingerprint we create a polygon model, an idealized representation of the charge region the OP lies within.

From theory, we know these polygons should cluster together by type into well-defined domains—hexagons should represent double-QD states, for example (colored white in the right panel in Figure 60). However, due to inherent noisiness in the measurements, many of these idealized models can be wrong. This means we cannot create a domain decomposition by individually classifying each polygon.

To overcome this, we created a statistical inferencing technique to identify groupings of polygons. The idea is that "incorrect" polygons will be wrong in more-or-less random ways, whereas "correct" polygons will be correct systematically. Our statistical method recognizes groupings of systematically similar polygons and ignores those that don't fit into statistically observed local patterns. These statistically determined groupings allow us to create the desired domain divisions. The exact locations where one domain transitions to another are also statistically determined. This is the reason for the "fuzziness" along domain boundaries in the right panel in Figure 60. Each point receives a probability of being in each of the five domains, represented there as a combination of five colors.

The fingerprinting method, developed in dimension two, is well suited to higher dimensional generalizations, where no serious theoretical barrier exists to using our methods of model-building followed by statistical grouping. Technical hurdles exist in the form of understanding details of high-dimensional geometry, such as ray placement and polytope recognition. Our group has already done work on this by creating ray-placement estimates and rough polytope classifications [3].

Determining the robustness of our methods across various noise regimes and device architectures is an ongoing effort. The main hurdle is availability of datasets. Our team has benefited from sophisticated tools for the simulation of many device architectures and noise regimes [4]. Our data-labeling methods have been tested successfully against these simulations.

However, no substitute exists for real-world data. Although our methods work against those real-world datasets that are available to us [5], we have relatively few such datasets. A major project goal is to collect datasets from many research teams around to world to establish a repository of datasets along with standardized labeling created using our methods hosted at data.nist.gov. Such a standardized repository of labelled data is consistent with the mission of NIST and would be of high value to the scientific community.

Another focus of future work is generalizing our methods to higher dimensions, with an aim of creating autotuning strategies for more than two QD at a time. Although theoretically straightforward, new challenges are expected related to high run-time expense and sparsity of available data. Theoretical understanding of higher-dimensional geometry will be a crucial component of this work.

[1] J. P. Zwolak, S. S. Kalantre, T. McJunkin, B. J. Weber, and J. M. Taylor. Ray-based Classification Framework for High-dimensional Data. In *Third Workshop on Machine Learning and the Physical Sciences (ML4PS @ NeurIPS 2020)*, Vancouver, Canada, December 11, 2020.

[2] J. P. Zwolak, T. McJunkin, S. S. Kalantre, S. F. Neyens, E. R. MacQuarrie, M. A. Eriksson, and J. M. Taylor. Ray-based Framework for State Identification in Quantum Dot Devices. *PRX Quantum* **2**:2 (2021), 020335.

[3] B. J. Weber, S. S. Kalantre, T. McJunkin, J. M. Taylor, and J. P. Zwolak. Theoretical Bounds on Data Requirements for the Ray-Based Classification. *SN Computer Science* **3**:1 (2022), 57.

[4] J. Ziegler, T. McJunkin, E. S. Joseph, S. S. Kalantre, B. Harpt, D. E. Savage, M. G. Lagally, M. A. Eriksson, J. M. Taylor, J. P. Zwolak. Toward Robust Autotuning of Noisy Quantum Dot Devices. *Physical Review Applied* **17** (2022), 024069.

[5] J. P. Zwolak, J. Ziegler, S. S. Kalantre, and J. M. Taylor. QFlow 2.0: Quantum Dot Data for Machine Learning. NIST, 2022. DOI: 10.18434/T4/1423788

Combining Machine Learning with Physics: Enhanced Dark Soliton Detection in Bose-Einstein Condensates

Justyna P. Zwolak
Lisa Ritter
Ian B. Spielman (NIST PML)
Sophia M. Koh (Amherst College)
Shangjie Guo (University of Maryland)
Amilson R. Fritsch (University of Maryland)

[*Note: For a more detailed accounting of this project, see the feature article on page 22.*]

Machine-learning (ML)-based image classification has many applications in science, from particle physics data analysis, dark matter searching, quantum state preparation to material property prediction. In atomic physics, ML has been used to locate topological phase transitions in images of atomic density and to characterize particles in disordered fields. In our work, we introduce and demonstrate a hybrid framework, shown in Figure 62, that integrates ML techniques with a science-driven analysis to detect, classify, and assess quality of features in experimental data from many-body atomic physics.

Using cold-atom Bose-Einstein condensates (BECs), we focus on solitonic excitations, robust solitary waves that retain their size, shape, and speed as they travel. These properties arise from an interplay between nonlinearity and dispersion that is present in many physical systems. Since their first observation in water channels, solitons have been found in rivers and seas; BECs; optical fibers; astronomical plasmas; and even human blood vesicles. Due to their inherent stability, solitons in optical fibers have found commercial applications in long-distance, high-speed transmission lines.

While the natural environment does not allow for the controlled study of quantum solitons, BECs are an ideal medium where individual or multiple solitons can be created on-demand, with all their properties, such as position and velocity, tuned as necessary [1, 2]. Most measurements in BEC experiments produce raw data in the form of images that, in our context, provide information about the excitations' positions within the BEC. The challenge is to identify the number, type, and location of excitations efficiently and reliably. Prior to this work, such information was obtained manually [1], inhibiting the automated analysis of large datasets, which is crucial for solitonic dynamics studies.

We previously developed a solitonic excitation detection and positioning system that takes as input image data and outputs information whether a single soliton is present, and, if so, its location [3]. This algorithm comprises a data preprocessor that converts raw data into a

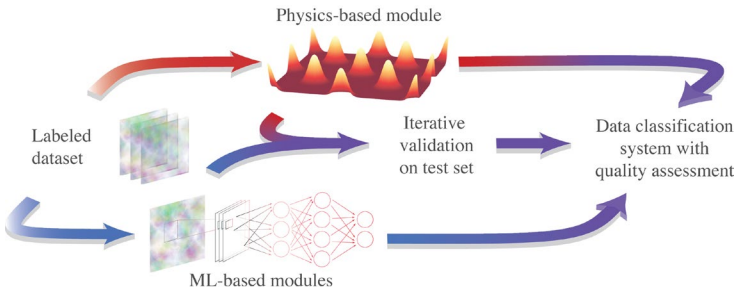

Figure 62. *Overview of the framework. The colored arrows link the preparation, validation, and application phases of the framework. The red path represents the preparation and implementation of the physics-based-approximation module while the blue path represents the ML modules. Adapted from Ref. [4].*

ConvNet-compatible format; a ConvNet image classifier that determines if a single soliton is detected; and a traditional least-squares fitting position regressor that locates the soliton within the BEC, when applicable. However, given that the fitting techniques can locate solitons only if the soliton number is known in advance and the ConvNet classifier require significant amount of data per expected class for training, the utility of our soliton detection and positioning system left room for improvement.

The next iteration of the soliton detecting framework included the ability to detect the precise position of the solitons along with a model that further refined the classification of the images. A final step was also added to determine the quality of the detected solitons. The analysis of the images still begins with the ConvNet classifier developed previously, but then is followed by a ML object detector (OD) which automatically localizes the features of interest (i.e., all solitonic excitations within the BEC). A physics-informed excitation (PIE) classifier then provides a fine-grained classification of individual solitonic excitations into physically motivated categories, such as clear longitudinal solitons, or solitonic vortices. Finally, a quality estimator is applied to the longitudinal solitons class to ascertain if the one-dimensional profile of a given excitation has parameters in the rang expected for a well-formed solitonic excitation. This eliminates images of solitons that are faint, or malformed, leaving only well-formed solitons for further analysis. An article reporting this work has recently been published [4].

Examples of the categorization of the BEC clouds can be seen in Figure 61. As a practical test case, we concentrate on identifying dark solitons, which are spatially localized excitations that appear as vertically aligned atomic density depletions in BECs, see Figure 61(b,c). Deep depletions are caused by kink solitons (and solitonic vortices viewed from the side), as in Figure 61(b-i), whereas shallow and asymmetric depletions can be caused by solitonic vortices, as in Figure 61(b-iii). Our framework is the first to automatically differentiate between these instances and locate all solitonic excitations in each image. Importantly, neither of the ML modules require data labeled with the physically motivated sub-categories, which significantly lessens the burden of manual labeling. In fact, the OD is trained using only the no excitation and lone excitation data.

As part of this research effort, we established and curated a dataset of over 16 000 experimental images of BECs with and without solitonic excitations [5, 6]. The dataset consists of images manually labeled into the three pre-defined categories (i.e., no excitations, lone excitation, other excitations; 33 % of the data) and unlabeled data. The lone excitation class is in addition tagged with the excitation position, PIE class, and quality score. The remaining 67 % of the data is automatically labeled using the SolDet package. This dataset is available via the Midas system at the National Institute of Standards and Technology and at data.gov [5] to provide an opportunity for the data science community to develop more sophisticated analysis tools and to further understand nonlinear many-body physics.

Our current efforts focus on further improving this high-level framework. First, to expand the potential user base of the software, we are shifting the ML framework from TensorFlow to PyTorch. Complimentary to this, generalizing aspects of the PIE classifier are being added. The first iteration of the PIE classifier includes physics-informed cuts that were manually derived from the BEC data coming from an experiment located at NIST. To ensure the compatibility of SolDet package with data coming from different experimental groups, we are refining these cuts using a more diverse dataset

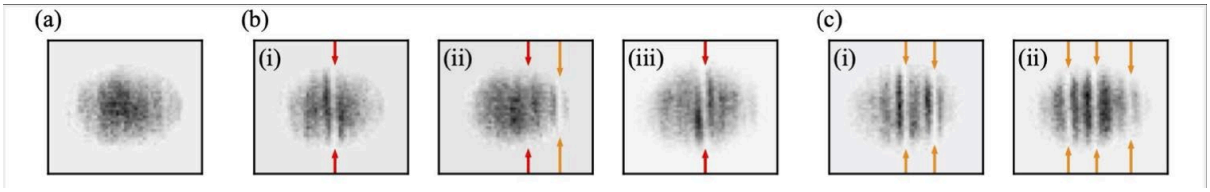

Figure 61. *The pre-processed images from the Dark solitons in BECs dataset. The red arrows mark the location of the deepest depletion in the density fluctuations, while the orange lines mark the solitons' locations found from our OD. (a) An element of the no-excitation class. (b) Three elements of the single excitation class: (i) a single longitudinal soliton, (ii) an off-center longitudinal soliton, and (iii) a solitonic vortex. (c) Two representative elements of the other excitations class. Adapted from Ref. [4].*

on BEC images. Additionally, it had been noted in Ref. [4] that the quality estimator can be unreliable when two or more solitonic excitations appear close together. To address this issue, we are working on an extended version of the quality estimator that will properly handle the multi-excitation cases. With these updates, we hope that SolDet will become a useful tool for data analysis for other groups working on BEC experiments.

[1] A. R. Fritsch, M. Lu, G. H. Reid, A. M. Piñeiro, and I. B. Spielman. Creating Solitons with Controllable and Near-zero Velocity in Bose-Einstein Condensates. *Physical Review A* **101** (2020), 053629.

[2] L. M. Aycock, H. M. Hurst, D. K. Efimkin, D. Genkina, H-I Lu, V. M. Galitski, and I. B. Spielman. Soliton Diffusion in Bose–Einstein Condensates. *Proceedings of the National Academy of Sciences* **114** (2017), 2503-2508.

[3] S. Guo, A. R. Fritsch, C. Greenberg, I. B. Spielman, and J. P. Zwolak. Machine-learning Enhanced Dark Soliton Detection in Bose-Einstein Condensates. *Machine Learning: Science and Technology* **2** (2021), 035020.

[4] S. Guo, S. M. Koh, A. R. Fritsch, I. B. Spielman, and J. P. Zwolak. Combining Machine Learning with Physics: A Framework for Tracking and Sorting Multiple Dark Solitons. *Physical Review Research* **4** (2022), 023163.

[5] National Institute of Standards and Technology. Dark Solitons in BECs Dataset (2022). Database: data.nist.gov. DOI: 10.18434/mds2-2363

[6] A. R. Fritsch, S. Guo, S. M. Koh, I. B. Spielman, and J. P. Zwolak. Dark Solitons in Bose–Einstein Condensates: A Dataset for Many-Body Physics Research. *Machine Learning: Science and Technology* **3** (2022), 047001.

Quantum Information

An emerging discipline at the intersection of physics and computer science, quantum information science is likely to revolutionize 21st century science and technology in the same way that lasers, electronics, and computers did in the 20th century. By encoding information into quantum states of matter, one can, in theory, enable phenomenal increases in information storage and processing capability. At the same time, such computers would threaten the public-key infrastructure that secures all of electronic commerce. Although many of the necessary physical manipulations of quantum states have been demonstrated experimentally, scaling these up to enable fully capable quantum computers remains a grand challenge. We engage in (a) theoretical studies to understand the power of quantum computing, (b) collaborative efforts with the multi-laboratory experimental quantum science program at NIST to characterize and benchmark specific physical realizations of quantum information processing, and (c) demonstration and assessment of technologies for quantum communication

Quantum Information Science

Scott Glancy
Emanuel Knill
Sae Woo Nam (NIST PML)
Konrad Lehnert (NIST PML)
Tasshi Dennis (NIST PML)
Ezad Shojaee (IonQ)
Arik Agavayan (University of Colorado)
Mohammad Alhejji (University of Colorado)
Shawn Geller (University of Colorado)
Alex Kwiatkowski (University of Colorado)
Curtis Rau (University of Colorado)
Akira Kyle (University of Colorado)
Lynden K. Shalm (University of Colorado)
Yanbao Zhang (Oak Ridge National Lab)
James R. van Meter (HRL Laboratories, Palo Alto)
Lucas Kocia (Sandia National Laboratory)

Quantum information processing relies on quantum bits (qubits), quantum gates and quantum networking to gain an advantage for solving certain problems in computation and communication. The ever increasing number of qubits available for testing and the improving quality of the quantum gates has led to a lively exploration of quantum physical phenomena and moderate size quantum algorithms on qubits in laboratories, or quantum registers made available by companies involved in quantum computing research. Clear-cut quantum advantages require fault-tolerant qubits and gates, which have not yet been achieved. Demonstrations of quantum networking are lagging behind and cannot yet be connected to operational quantum registers for computation. Quantum technology is also useful for quantum enhanced measurements, which have promising applications.

ACMD research in quantum information science covers a broad range of topics. Projects summarized in this section include studies on (a) quantum transduction between microwave qubits and optical qubits for quantum networking, (b) quantum-enhanced detection of signals, (c) measuring quadratures of wide-band quantum modes of light, (d) investigations of squeezing caused by changes to the gravitational metric, and (e) statistical methods for confidence intervals of parameters inferred from time-varying experimental data.

Quantum Transduction. To communicate quantum information, it is necessary to transduce quantum information between stationary quantum registers and "flying qubits", usually carried by light. ACMD researchers are participating in projects to transduce quantum information between superconducting qubits at microwave frequencies to photons in telecommunication bands. The projects use either micromechanical or ion or quantum dot intermediaries. Previous investigations delimited the tolerable loss and added noise for transduction with Gaussian processing, which helped to determine the best configurations for micromechanical transduction [1]. Current research is focused on transduction with quantum dots. The available coupling between quantum dots and cavities and the rapid emission process of the quantum dots complicates transduction. However, preliminary investigations show that with a carefully chosen pump pulse sequence, it should be possible to achieve respectable transduction rates.

Quantum Detection of Signals. ACMD collaborators are operating cold cavities coupled to superconducting detectors that may be able to detect the signal of an axion field if it exists. Axion fields are promising dark-matter candidates. If it exists, the axion field acts as a random displacement force on a mode of the detection cavity. As a general rule, dark matter detection experiments aim to exclude regions of parameters space. For axions, this means that the first goal is to reject the presence of the putative signal in specific frequency bands. The goal is to have high-confidence rejection as quickly as possible. ACMD researchers have begun to investigate the fundamental bounds that determine how quickly it is possible to reject the presence of a noise signal, and how these bounds are affected by practical consideration of their

collaborators' apparatus, such as cavity line widths, losses, and added noise.

Quadratures of Wideband Modes. Conventional heterodyne or homodyne quadrature measurements are limited to a relatively narrow band around a given frequency. Some applications require measurements of octave-spanning modes. A motivating application is characterization of Unruh modes to verify vacuum entanglement of the electromagnetic field. One option for detecting photons over such a wide band is to use calorimeters, which measure the total energy deposited rather than the number of photons. ACMD researchers have determined that homodyne measurement strategies can be generalized to take advantage of calorimeters and other types of detectors whose signal is a weighted sum of photon counts in many modes. The local oscillator for such a measurement must be chosen correctly so that the output signal of the scheme approaches the desired quadrature measurement in the limit of high amplitude of the local oscillator. ACMD researchers are determining bounds on how well the output signal approximates a quadrature measurement, as a function of the local oscillator amplitude and a bound on expected number of photons in the relevant modes.

Gravitational Squeezing. Free quantum fields propagating on a curved gravitational background tend to become squeezed. In particular the free vacuum of the fields is not preserved, and energy density can grow. A fundamental if speculative question is how one might control the gravitational background to systematically squeeze the fields. Such squeezing could be a resource for quantum information purposes and would be a test of relativistic quantum theory. ACMD researchers are investigating the growth in energy density when a flat gravitational background is temporarily perturbed by modifying the metric. Such growth could be exponential in the perturbation, and a goal is to determine limits on this exponential growth and what features of the perturbation determine the growth or lack thereof.

Confidence Intervals. ACMD researchers have developed rigorous statistical methods to verify features of entanglement and to determine the amount of quantum randomness available in a device-independent way [2,3]. These applications required methods that do not require that the samples are independent and identical, and that work at all significance levels. ACMD researchers are currently extending these methods to the general problem of determining the running mean of random vectors that are either bounded or have a bounded moment. The methods depend on constructions of "test factors" or "test estimators," and ACMD researchers have shown that for this problem optimal test factors are linear, which greatly simplifies the problem of optimizing the method. They are developing applications of the methods to quantum characterization problems such as fidelity measurements and entanglement verification for qubits or modes.

[1] Alex Kwiatkowski, E. Shojaee, S. Agrawal, A. Kyle, C. Rau, S. Glancy, and E. Knill. Constraints on Gaussian Error Channels and Measurements for Quantum Communication. arXiv preprint arXiv:2206.11842, 2022. DOI: 10.48550/arXiv.2206.11842

[2] E. Knill, Y. Zhang, and P. Bierhorst. Generation of Quantum Randomness by Probability Estimation with Classical Side Information. *Physical Review Research* **2** (2020), 033465. DOI: 10.1103/PhysRevResearch.2.033465

[3] L. K. Shalm, Y. Zhang, J. C. Bienfang, C. Schlager, M. J. Stevens, M. D. Mazurek, C. Abellán, W. Amaya, M. W. Mitchell, M. A. Alhejji, H. Fu, J. Ornstein, R. P. Mirin, S. W. Nam, and E. Knill. Device-independent Randomness Expansion with Entangled Photons. *Nature Physics* **17** (2021), 452-456. DOI: 10.1038/s41567-020-01153-4

Quantum Characterization Theory and Applications

Victor V. Albert
Thomas Gerrits
Scott Glancy
Emanuel Knill
Yi-Kai Liu
Michael J. Gullans (NIST PML)
Dietrich Leibfried (NIST PML)
Daniel Slichter (NIST PML)
Jacob M. Taylor (NIST PML)
Andrew Wilson (NIST PML)
Arik Avagyan (University of Colorado)
Daniel C. Cole (University of Colorado)
Stephen D. Erickson (University of Colorado)
Demitry Farfurnik (University of Maryland)
Srilekha Gandhari (University of Maryland)
Shawn Geller (University of Colorado)
Mohammad Hafezi (University of Maryland)
Pan-Yu Hou (University of Colorado)
Kaixin Huang (University of Maryland)
Hannah Knaack (University of Colorado)
Alex Kwiatkowski (University of Colorado)
Hilma Vasconcelos (Federal University of Ceará)
Jenny J. Wu (University of Colorado)

Many emerging technologies will exploit quantum mechanical effects to enhance metrology, computation, and communication. Developing these technologies requires improved methods to characterize the performance of quantum devices. This characterization requires solving statistical problems such as estimating an underlying quantum state, measurement, or process by using a collection of measurements made on the quantum system. Alternatively, one may also want to estimate figures-of-merit such as fidelity, error rates, and entanglement

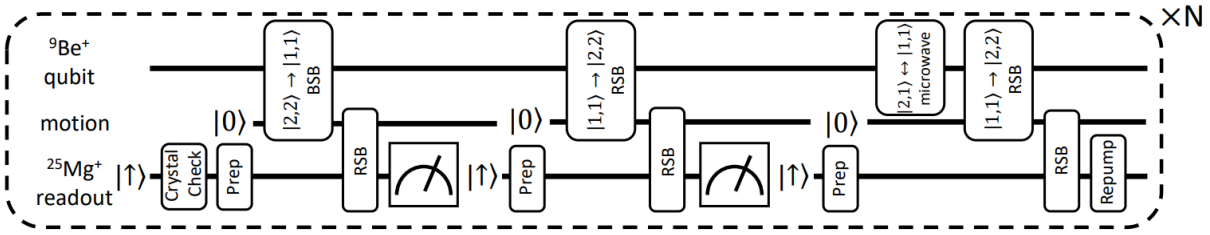

Figure 63. *Quantum circuit for repeated ion measurements. The circuit measures a qubit encoded in the |2,2⟩ and |1,1⟩ levels of a Beryllium (Be) ion. First the Be's |2,2⟩ is coupled to the motion of the 2-ion crystal. Then the motion state is transferred to the Magnesium (Mg) ion and the Mg state is measured. The motion and Mg states are reset. The process is then repeated with the Be's |1,1⟩ state. A final resetting step is performed to remove Be population from other levels. The entire process is repeated N times to increase confidence in the final estimate of the original Be state.*

measures from that data. Accurate quantum characterization allows experimentalists and engineers to answer questions like "What is happening in my quantum experiment?" or "How well will my system perform some quantum information protocol?" and to characterize uncertainty in that answer.

NIST's Ion Storage Group is a world leader in high-fidelity qubits. To keep pace with their recent advances in qubit preparation, logical operation, and measurement fidelities, ACMD researchers are developing more advanced statistical techniques to characterize trapped-ion quantum computers. An ion qubit is measured by counting the number of photons the ion releases when illuminated by a fluorescent laser. A random number of photons will be produced, but the probability distribution depends on the ion's state. Distinguishing the $|0\rangle$ and $|1\rangle$ states requires differentiating between the two, slightly overlapping, probability distributions. Also, the ion might change its state during the measurement. ACMD researchers have developed a hidden Markov model of the fluorescent measurement process, a strategy for manipulating the ion during the measurement based on the incoming photon detections, and a Bayesian system for inferring the hidden Markov model's parameters and the ion's state at the start of the measurement process. These tools enable higher fidelity qubit measurement and a better understanding of measurement error [1]. ACMD researchers also contributed to an experiment demonstrating another technique to improve ion qubit measurements. In this experiment, a single beryllium qubit is measured repeatedly by using quantum logic gates to transfer its state to a magnesium ion, which can be measured without disturbing the state of the beryllium qubit (see Figure 63). ACMD researchers developed a probabilistic model of the repeated measurements and determined that the measurement errors were in the 68 % confidence intervals $[0.6, 2.3]\times10^{-4}$ and $[0, 1.9]\times10^{-5}$ for the two qubit states [2].

Randomized benchmarking is a very popular method to measure the error rates of quantum logic gates. Sequences of random logic gates are applied, and one observes how the probability of obtaining the correct output qubit state decreases with increasing sequence length. ACMD researchers have studied how to choose the sequence lengths so that one can obtain the most precise estimate of the individual gate error rate in a limited wall clock time [3]. They have also studied how randomizing every sequence produces more accurate error rate estimates than repeating the same random sequence. The Ion Storage Group is using these optimization and analysis techniques to estimate the error rates in their ion trap that applies all logic gates with microwave-frequency fields rather than lasers.

Another aspect of quantum device characterization is the measurement of spatial correlations between qubits. These can play an important role in so-called NISQ (noisy intermediate-scale quantum) devices, and in schemes for quantum error correction. To this end, ACMD researchers are continuing to investigate sparse models of correlated dephasing on many qubits. These models can describe physical hardware that contains random defects that cause correlated errors. These models can be learned efficiently using compressed sensing and generalized Ramsey spectroscopy. During the past year, ACMD researchers have proved stronger bounds on the accuracy and sample complexity of these methods [4].

Solid-state qubits often suffer from noise that contains non-Markovian effects, which can be characterized using noise spectroscopy. ACMD researchers are developing random pulse sequences for performing specialized measurements of the noise power spectrum, including parametric fitting, compressed sensing, and real-time monitoring of the total noise strength. ACMD researchers are currently investigating the use of these techniques to learn spectral properties of the nuclear spin bath of a quantum dot system [5].

To characterize nonlinear interactions between photons, such as those being developed for photon logic gates, ACMD researchers have developed a generalization of traditional homodyne detection. Traditional homodyne detection requires a strong reference beam and can only estimate the state in the mode matching the reference beam, but our generalization can use a weak reference beam (as required for some integrated circuit designs) and can learn about correlations between the

signal mode and photons in nearby modes [6]. ACMD and PML researchers are designing an experiment to demonstrate this technique.

ACMD researchers have applied shadow tomography [7] to obtain new rigorous guarantees on well-established tomographic protocols for continuous-variable (CV) systems, such as optical fields or trapped ion motion. Shadow tomography is a novel randomized tomographic framework that is based on approximating a quantum state by succinct "snapshots" or "shadows" that can be easily extracted and stored on a classical computer. The framework comes with rigorously proven guarantees on the minimum number of such shadows required to achieve high accuracy with high probability. While this framework was originally designed for intrinsically multi-qubit systems, we show that certain experimentally relevant CV protocols, such as homodyne and photon-number-resolving tomography, can also be viewed through the lens of this framework. This yields useful guarantees that dictate how many measurement rounds of a protocol are required to reach a desired accuracy of state estimation. The required number of rounds for a multimode CV system scales polynomially with both the number of CV modes and the maximum occupation (e.g., photon) number of each mode. ACMD researchers have benchmarked their bounds against numerical simulation and experimental data from a previous NIST optical homodyne experiment [8]. Details can be found in the preprint [9].

A basic resource state for continuous-variable quantum information processing is a low-temperature squeezed state. Such states are often prepared in optical modes or in the motion of trapped ions. ACMD researchers have developed a method to estimate the amount of squeezing, temperature, and other parameters of a multi-mode squeezed state from measurements of the number of photons or phonons in the state [10,11]. They are using this method to study the squeezing and amplification of ion motion, which was previously characterized assuming that its temperature was 0.

Researchers at JILA have an optical lattice atom trap, which consists of a lattice of cells, each of which may contain some number of Strontium atoms. Single atoms can be loaded into any subset of the cells and allowed to hop from cell to cell as time evolves. If all atoms are indistinguishable, they behave as non-interacting bosons. Such "boson samplers" have computational powers beyond those of classical computers. ACMD researchers are developing tools to measure the atoms' distinguishability and to characterize the dynamics of the atoms in the lattice.

[1] S. Geller, S. Glancy, and E. Knill. Improving Quantum State Detection with Adaptive Sequential Observations. *Quantum Science and Technology* **7** (2022), 034004. DOI: /10.1088/2058-9565/ac6972

[2] S. D. Erickson, J. J. Wu, P.-Y. Hou, D. C. Cole, S. Geller, A. Kwiatkowski, S. Glancy, E. Knill, D. H. Slichter, A. C. Wilson, and D. Leibfried. High-Fidelity Indirect Readout of Trapped-Ion Hyperfine Qubits. *Physical Review Letters* **128** (2022), 160503. DOI: /10.1103/PhysRevLett.128.160503

[3] A. Kiwatkowski, S. Glancy, and E. Knill. Analysis and Experiment Design for Fully Randomized Benchmarking. In preparation.

[4] A. Seif, M. Hafezi, and Y.-K. Liu. Compressed Sensing Measurement of Long-Range Correlated Noise. In preparation. US Patent Application 17/743850, May 13, 2022. Preprint: arXiv:2105.12589

[5] K. Huang, A. Seif, D. Farfurnik, M. Hafezi and Y.-K. Liu. Random Pulse Sequences for Qubit Noise Spectroscopy. Preprint: arXiv:2303.00909

[6] A. Avagyan, E. Knill, S. Glancy, and H. Vasconcelos. State Tomography with Photon Counting after a Beam Splitter. In preparation.

[7] H.-Y. Huang, R. Kueng, and J. Preskill. Predicting Many Properties of a Quantum System from Very Few Measurements. *Nature Physics* **16** (2020), 1050. DOI: 10.1038/s41567-020-0932-7

[8] T. Gerrits, S. Glancy, T. S. Clement, B. Calkins, A. E. Lita, A. J. Miller, A. L. Migdall, S. W. Nam, R. P. Mirin, and E. Knill. Generation of Optical Coherent-state Superpositions by Number-resolved Photon Subtraction from the Squeezed Vacuum. *Physical Review A* **82** (2010), 031802. DOI: 10.1103/PhysRevA.82.031802

[9] S. Gandhari, V. V. Albert, T. Gerrits, J. M. Taylor, and M. J. Gullans. Continuous-Variable Shadow Tomography. Preprint, arXiv:2211.05149

[10] I. Bezerra, H. Vasconcelos, and S. Glancy. Quadrature Squeezing and Temperature Estimation from the Fock Distribution. *Quantum Information Processing* **21** (2022), 365. DOI: 10.1007/s11128-022-03677-5

[11] A. Avagyan, E. Knill, and S. Glancy. Multi-Mode Gaussian State Analysis with Photon Counting. Preprint: arXiv:2209.14453

Quantum Algorithms and the Power of Forgetting

Matthew Coudron
Andrew M. Childs (University of Maryland)
Amin Shiraz Gilani (University of Maryland)

In 2003, Childs et al. [1] proved that there exists a polynomial time quantum algorithm, in particular a quantum walk algorithm, which solves a computational problem known as the Welded Tree Oracle Problem exponentially faster than is possible classically. It was later shown, in [2], that the Welded Tree Oracle Problem was fundamentally different than any previously defined oracle problem, in that it requires polynomially large quantum depth to solve. In fact, this property even separates the Welded Tree Oracle Problem from the quantum factoring algorithm, which can be parallelized

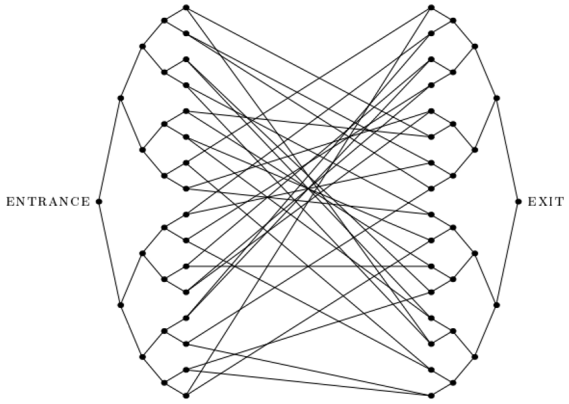

Figure 64. *A welded tree graph for n=4.*

to require just logarithmic quantum depth. This makes the Welded Tree Problem an intriguing object of study when searching for novel quantum properties of algorithms. Our ongoing project, [3], has achieved progress toward resolving a remarkable open question, originally alluded to [1]. To state the open question, we first need to give a more detailed description of the Welded Tree Oracle Problem.

The Welded Tree Oracle Problem is a computational problem concerning a graph consisting of two binary trees of height n, joined together at their leaves by a random cycle. Figure 64 provides an example of such a graph, for n=4.

Each vertex of the graph is assigned a unique, random bit-string label of length $2n$. The root vertex of the left binary tree is called the ENTRANCE, and the root vertex of the right binary tree is called the EXIT. The input to the Welded Tree Oracle Problem is not a complete description of the graph, but rather an "Oracle" black-box function, which, when queried at label of any vertex in the graph, outputs the bit-string labels of its nearest neighbors. In other words, if we think of the Welded Tree graph as a maze, in which each vertex is a room and each edge is a hallway, then the oracle simply tells us which rooms neighbor the room that we are currently in, without revealing any global structure of the graph. The computational goal in the Welded Tree Oracle Problem is, given the oracle function for the graph, and the label of the ENTRANCE vertex, to find the label of the EXIT vertex using as few queries to the oracle as possible. The original result of [1] is that a quantum computer, which can query the oracle in superposition, can solve this problem in polynomially many queries (and with a polynomial time quantum algorithm), whereas an algorithm than only makes classical queries provably requires exponentially many queries to find the EXIT.

Note that the classical hardness result makes some intuitive sense because the Welded Tree Graph has 2^{n+2} vertices total, a number which is exponential in the height, n, of the binary trees, and in the number of bits of the bit string labels. Furthermore, the cycle in the middle is random, so one would expect that a classical algorithm might "get lost" in this maze while searching for the EXIT.

A famous open question, first discussed in [1], is whether or not there exists a polynomial time quantum algorithm which can find a *path* of vertices from ENTRANCE to EXIT in the Welded Tree Oracle Problem. Standard classical intuition would suggest that, since there is an efficient algorithm which can find the EXIT starting from the ENTRANCE, there must also be an algorithm which can find a path from ENTRANCE to EXIT. However, the algorithm which efficiently finds the EXIT starting from the ENTRANCE is a quantum algorithm and not clearly subject to classical intuition. In fact, surprisingly, and for the first time, we have partial evidence that, in the quantum world, this path-finding problem may actually be computationally hard. In particular, we are able to show that perhaps the most natural class of quantum algorithms for ENTRANCE-EXIT path finding, which we call "rooted algorithms," provably cannot find a path from ENTRANCE to EXIT in fewer than exponentially many quantum queries. Informally, "rooted algorithms" are those quantum algorithms for pathfinding which maintain, at every point in the superposition and every step of the algorithm, a memory of at least one path from their current position in the Welded Tree graph, back to the ENTRANCE vertex. Not only is this class the most natural first attempt at a quantum path-finding algorithm, but it is hard to imagine what possible benefit an algorithm could gain from not being rooted, and "forgetting" its way back to the ENTRANCE. It would seem odd to take a such a non-rooted approach given that the entire goal of the algorithm is to output a path from ENTRANCE to EXIT in the end. Our no-go result for rooted algorithms shows that, bizarrely, while a quantum algorithm can find its way from ENTRANCE to EXIT in the Welded Tree Oracle Problem, in order to do so it must necessarily "forget where it started."

At the technical level our result is interesting in that it employs a novel technique we call a "transcript simulation" in order to prove that rooted algorithms cannot have constructive or destructive interference that exceed classical algorithms by more than a polynomial amount. This can then be combined with a new style of classical hardness result, which we also devised, in order to show that rooted quantum algorithms are no more capable of finding the EXIT that classical algorithms. The intuition behind this approach is that the need of rooted algorithms to constantly maintain knowledge of a path from their current position in the graph back to the ENTRANCE actually destroys the constructive and destructive interference that made the original EXIT-finding algorithm of [1] work. The interference is destroyed because storing a path back to the ENTRANCE

forces a separation between different branches of the superposition. Our paper, [3], was published in the proceedings of the 2023 Innovations in Theoretical Computer Science (ITCS) conference and has been accepted for presentation at the 2023 Theory of Quantum Computing, Communications, and Cryptography (TQC) conference. We believe that, with more work, we will eventually be able to prove that there is no polynomial time quantum algorithm of any sort (not just "rooted" algorithms) which can find a path from ENTRANCE to EXIT in the Welded Tree Graph with better than exponentially small probability. Such a result would be a resolution of a long-standing open problem in the field.

[1] A. M. Childs, R. Cleve, E. Deotto, E. Farhi, S. Gutmann, and D. A. Spielman. Exponential Algorithmic Speedup by a Quantum Walk. *In Proceedings of the 35th Annual ACM Symposium on Theory of Computing*, June 9-11, 2003, San Diego, CA, 59–68. DOI: 10.1145/780542.780552

[2] M. Coudron and S. Menda. Computations with Greater Quantum Depth are Strictly More Powerful (Relative to an Oracle). In *Proceedings of the 52nd Annual ACM SIGACT Symposium on Theory of Computing*, 2022. DOI: 10.1145/3357713.3384269

[3] A. M. Childs, M. Coudron, and A. S. Gilani. Quantum Algorithms and the Power of Forgetting. In *14th Innovations in Theoretical Computer Science Conference (ITCS 2023)* (Y. Tauman Kalai, ed.), Leibniz International Proceedings in Informatics (LIPIcs) **251**, Schloss Dagstuhl--Leibniz-Zentrumfür Informatik, 2023, 37:1-37:22. DOI: 10.4230/LIPIcs.ITCS.2023.37

Quantum Depth in the Random Oracle Model

Matthew Coudron
Atul Singh Arora (Caltech)
Andrea Coladangelo (U. of California, Berkeley)
Alexandru Gheorghiu (ETH Zurich)
Uttam Singh (Polish Academy of Sciences)
Hendrik Waldner (Max Planck Institute)

The circuit depth required to perform a quantum or classical computation, which is defined as the minimal number of layers of basic computational gates required to perform the whole computation, has direct relevance to our ability to perform the computation on near term quantum hardware or on a parallel computing architecture, as well as many other applications. Within quantum computing, purely classical operations are considered relatively "cheap" to implement, whereas coherent quantum gate operations are relatively "expensive." Consequently, the model which most aptly captures the power of low-depth quantum circuits in the context of near term quantum computing is that of hybrid quantum circuits formed by the composition of low-depth quantum circuits, interleaved with much higher-depth classical circuits. This notion of interleaving low-depth quantum circuits with high depth classical circuits has no analogous counterpart in the study of circuit depth in classical computer science. It turns out that this novel composition has a number of nuances and subtleties that defy previously known mathematical techniques for studying circuit depth, and yet, are relevant to the most famous quantum computations known to date.

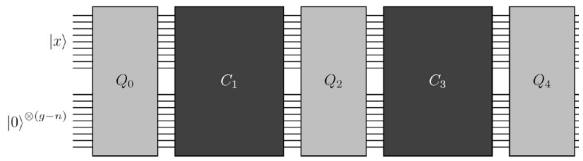

Figure 65. *Q boxes are quantum circuits of depth log(n). C boxes are classical circuits of depth polynomial in n.*

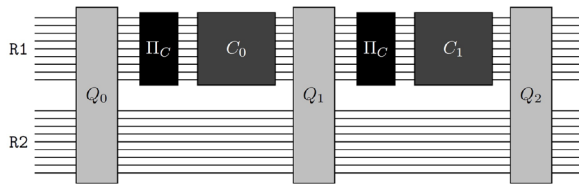

Figure 66. *Q boxes are quantum circuits of depth 1. C boxes are classical circuits of depth polynomial in n. π boxes are measurements in the standard basis.*

The intriguing and subtle nature of these hybrid quantum circuits is best highlighted by two well-known open problems posed in 2005. In the first, [1], Richard Jozsa conjectured that all polynomial size quantum computations, regardless of depth, can be efficiently simulated by hybrid quantum-classical circuits which only employ logarithmic depth quantum circuits, as in Figure 66. In the second, [2], Scott Aaronson's 9th semi-grand challenge in quantum computation asks for a proof of a statement that is technically incomparable to [1], but morally opposite: That there exists a computational problem that can be efficiently solved by polynomial size quantum computations but cannot be efficiently solved by hybrid quantum-classical circuits shown in Figure 65. Despite their intriguing nature, and their fundamental importance to our understanding of quantum computation, these two problems remained open for 17 years. Our work [5] gives the first solution the open problems due to Jozsa and Aaronson [1, 2], resolving Aaronson's conjecture in the affirmative, and Jozsa's conjecture in the negative. Our main result is to construct a computational problem, instantiated using a cryptographic hash function, for which there is a polynomial time quantum algorithm, but for which there provably does not exist an algorithm of the form shown in Figure 65 or Figure 66 that can solve the problem with better than exponentially small probability.

More specifically, our main contribution is to exhibit the first *cryptographically instantiable*

computational problem which provably separates polynomial depth quantum computations from the computations of the forms shown in either Figure 65 or Figure 66. Regular oracle separations between these types of computations were established in 2020 [3, 4], but it is not clear that those oracle separations are cryptographically instantiable. Our strategy was to prove a new oracle separation based on a special type of oracle called a Random Oracle. The significance of a Random Oracle separation, in this context, is that there exists a non-oracular instantiation of the same problem in which the random oracle is replaced by a cryptographic hash function, which is indistinguishable from a random oracle under a widely known cryptographic assumption. This satisfies Aaronson's stipulation that the computational problem must be concretely instantiable (it must be possible to write the problem statement down on paper), rather than a "black box" oracle separation, in order to resolve his 9th semi-grand challenge in quantum computing [2].

The computational problem that we construct is produced by recursively composing a new type of "proof of quantumness," such as the version pioneered by Yamakawa and Zhandry [6]. Concretely, our problem asks: Given a particular type of error correcting code C on $\{0,1\}^{n \cdot m}$ specified by its generator matrix, and a hash function H mapping $\{0,1\}^n \rightarrow \{0,1\}$ which is specified as the composition of d separately provided hash functions, FIND a bit string in $x \in \{0,1\}^{n \cdot m}$ which lies in the error correcting code C, and has the property that all m length n substrings of x are mapped to 0 by the hash function H. The polynomial time quantum algorithm to solve this search problem utilizes the quantum Fourier transform. At the level of techniques, the key contribution that we make is to prove that, because the hash function H is defined as a composition of d separately provided hash functions, no quantum algorithm of depth less than d should make essentially "any progress" towards finding the answer. Since efficient classical query algorithms also cannot make progress toward solving the problem, setting d to be greater than the depth of the quantum circuits in Figure 65 (for example), will then resolve Aaronson's 9th semi-grand challenge in quantum computing [2]. Proving all of this, despite the nuances of the hybrid quantum-classical model, is quite involved. It required importing exponential hiding techniques, and other techniques used [3, 4], as well as developing a new technique which we call "shadow oracles." We also explore a variety of other ways to compose quantum and classical circuits beyond Figure 65 and Figure 66 and show that our techniques yield results about those new classes as well.

[1] R. Jozsa. An Introduction to Measurement Based Quantum Computation. In *Quantum Information Processing* (D. G. Angelakis, et al., eds.), IOS Press, 2006, 137-158.

[2] S. Aaronson. Ten Semi-Grand Challenges for Quantum Computing Theory. 2005. URL: https://www.scottaaronson.com/writings/qchallenge.html

[3] M. Coudron and S. Menda. Computations with Greater Quantum Depth Are Strictly More Powerful (Relative to an Oracle). In *Proceedings of the 52nd Annual ACM SIGACT Symposium on Theory of Computing*, 2020, 889–901. DOI: 10.1145/3357713. 3384269

[4] N.-H. Chia, K.-M. Chung and C.-Y. Lai. On the Need for Large Quantum Depth. In *Proceedings of the 52nd Annual ACM SIGACT Symposium on Theory of Computing*, 2020. 902–915. DOI: 10.1145/3357713.3384291

[5] A. S. Arora, et al. Quantum Depth in the Random Oracle Model. *In Proceedings of the 55th Annual ACM SIGACT Symposium on Theory of Computing*, 2023, to appear.

[6] T. Yamakawa and M. Zhandry. Verifiable Quantum Advantage without Structure. Preprint arXiv:2204.02063 URL: http://arxiv.org/abs/2204.02063

Local Hamiltonians with No Low-Energy Stabilizer States

Matthew Coudron
Nolan J. Coble (University of Maryland)
Jon Nelson (University of Maryland)
Seyed Sajjad Nezhadi (University of Maryland)

The recently-defined No Low-energy Sampleable States (NLSS) conjecture of Gharibian and Le Gall [1] posits the existence of a family of local Hamiltonians where all quantum states of low-enough constant energy do not have succinct representations allowing perfect sampling access. States that can be prepared using only Clifford gates (i.e., stabilizer states) are an example of sampleable states, so the NLSS conjecture implies the existence of local Hamiltonians whose low-energy space contains no stabilizer states. In our work, [3], we take a step towards the NLSS conjecture by constructing families of Hamiltonians that exhibit this requisite "no low-energy stabilizer states" property.

Our construction works via a simple alteration to local Hamiltonians corresponding to CSS codes. Our method can also be applied to the recent No Low-energy Trivial States (NLTS) Hamiltonians of Anshu, Breuckmann, and Nirkhe [2], resulting in a family of local Hamiltonians whose low-energy space contains neither stabilizer states nor trivial states. We hope that our techniques will eventually be helpful for constructing Hamiltonians which simultaneously satisfy NLSS and NLTS.

To understand the motivation behind our work it is important to take a step back and note that each of the conjectures in this particular branch of Hamiltonian complexity, including the NLTS conjecture, the NLSS conjecture, and many others, are all attempts to gain insight into a very widely known open problem in the field

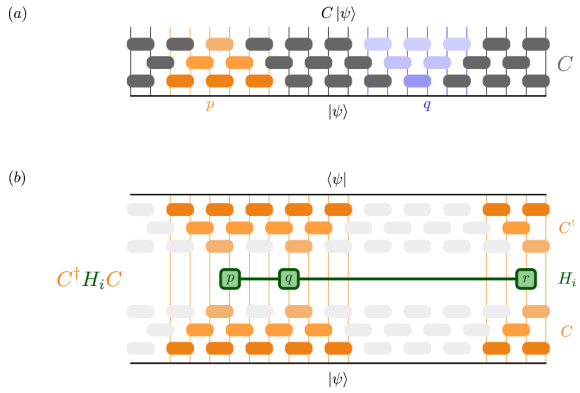

Figure 67. *Conjugation method for modifying local Hamiltonians. See text for discussion.*

called the Quantum Probabilistically Checkable Proof (PCP) conjecture. Classical Probabilistically Checkable Proofs (PCPs) are considered to be one of the crowning achievements of modern theoretical computer science and have numerous emerging applications, from cryptography (SNARKS) to hardness of approximation results. The Quantum PCP conjecture, if resolved, could have analogous applications to quantum computing, and would also have implications for the possibility of experimentally producing entangled quantum states that remain coherent at high temperatures, among other things. The Quantum PCP conjecture itself is a complexity theoretic claim about a computational problem involved in simulating quantum mechanical systems which are governed by a Hamiltonian. Briefly put, the Quantum PCP conjecture postulates that it is QMA-hard (a computational hardness notion involving complexity classes) to approximate the ground state energy of a local Hamiltonian to within a constant. This simple statement, if proven, could have all the widespread implications discussed above, and the proof techniques would likely be valuable in and of themselves. However, a pre-requisite to proving that any problem is QMA-hard is to first prove that it cannot be solved in the smaller complexity class Non-Deterministic Polynomial Time (NP). This pre-requisite is the motivator for the NLTS conjecture, the NLSS conjecture, and for our own work. If the NLTS conjecture had been false, the ground state energy problem for local Hamiltonians would have been contained in NP. If the NLSS conjecture is false then the problem would be contained in a complexity class called MA, which is much smaller than QMA.

Our result is a necessary pre-requisite of the NLSS conjectures, addressing the following important issue: The NLTS conjecture, while now proven, has only been proven with Hamiltonians whose ground state energy problem is clearly contained in MA because the ground states are stabilizer states and therefore efficiently sampleable (the exact reasoning behind all of these connections is non-trivial and is laid out in [1], where the NLSS conjecture was first stated).

At the level of techniques, we contribute a conceptually simple new procedure in which we begin with a regular local Hamiltonian and modify it by conjugating it (multiplying on either side) by low depth quantum circuit as shown in Figure 67. Part (a) of Figure 67 illustrates a generic low-depth quantum circuit C, comprised of a constant number of layers of quantum gates. Part (b) of Figure 67 illustrates what happens when a local Hamiltonian term H_i is conjugated by the low-depth quantum circuit C. A local Hamiltonian which is conjugated by a constant depth quantum circuit remains a local Hamiltonian since its Hamiltonian properties are preserved by the unitarity of the quantum circuit, and its locality is only increased by the spread of the "light cones" within the circuit C which originate from one particular Hamiltonian term (these are the gates colored orange in part (b) of Figure 67). Since C is constant depth, the increase in the locality of the Hamiltonian is merely constant. In [3] we are able to show, through a series of combinatorial arguments that, if we take the local Hamiltonian from known constructions of quantum Low Density Parity Check (LDPC) error correcting codes and conjugate those Hamiltonians by a $\pi/8$ rotation on every qubit (which is a low depth circuit), then no stabilizer state can have low energy relative to the resulting Hamiltonian. Since the resulting Hamiltonian must still be local, by the above argument and Figure 67, the desired result follows. We are hopeful that these techniques will prove useful in further extending known NLTS results to more general settings.

[1] S. Gharibian and F. Le Gall. Dequantizing the Quantum Singular Value Transformation: Hardness and Applications to Quantum Chemistry and the Quantum PCP Conjecture. In *Proceedings of the 54th Annual ACM SIGACT Symposium on Theory of Computing*, June 2022, 19–32. DOI: 10.1145/3519935.351999

[2] A. Anshu, N. Breuckmann, and C. Nirkhe. NLTS Hamiltonians from Good Quantum Codes. June 2022, preprint arXiv:2206.13228. URL: http://arxiv.org/abs/2206.13228

[3] N. J. Coble, M. Coudron, J. Nelson, and S. Sajjad Nezhadi. Local Hamiltonians with No Low-energy Stabilizer States. In: *Proceedings of the TQC 2023*, to appear.

Error-Correction Zoo

Victor V. Albert
Philippe Faist (Freie Universität Berlin)

Classical and quantum error correction lies at the intersection of computer science, engineering, physics, and mathematics. Classical coding theory has been around for over 70 years, yielding an enormous literature collection. Quantum error correction is more recent but arguably more diverse, encompassing subfields from

solid-state physics to complexity theory. Collecting and accurately synthesizing such a hyper-field is as formidable as it is useful.

We have created and actively maintain the Error Correction Zoo [1] to categorize and organize known classical and quantum error-correction schemes. The work involved is taxonomic, i.e., collecting and processing literature as well as developing a classification scheme for the thousands of available classical and quantum error-correcting codes.

Code entries form the primary content of the zoo. An entry can be a specific instance of a well-known code or a large family of codes, depending on community interest. The idea is to have a dedicated up-to-date webpage for each family, collecting original work, related protocols, and real-world implementations. Codes are organized into kingdoms by alphabet (or Hilbert space structure in the quantum case), with "parent" and "cousin" fields listing notable relations and connections. At the time of writing, there are 436 entries.

[5] V. V. Albert and P. Faist. The Error-Correction Zoo. URL: https://errorcorrectionzoo.org

Modern Quantum Tools for Bosonic Systems

Victor V. Albert
Joseph T. Iosue (University of Maryland College Park)
Kunal Sharma (IBM)
Michael J. Gullans (NIST PML)
Eric Culf (University of Ottawa)
Thomas Vidick (Weizmann Institute of Science)
Yijia Xu (University of Maryland College Park)
Yixu Wang (University of Maryland College Park)
En-Juo Kuo (University of Maryland College Park)

Utilization of the features of quantum mechanics promises to eventually increase our understanding of chemical processes, communicate securely, and accurately measure signals. However, most quantum protocols are focused on the abstract qubit (i.e., discrete-variable or DV) systems, and many of them cannot be readily available to continuous-variable (CV) systems — optical fibers, free-space communication, microwave and optical cavities, motional degrees of freedom of atoms and ions, and mechanical resonators—without substantial reformulation.

For example, quantum tomography is a field concerned with characterizing quantum systems, an important task whose completion is necessary for realizing most of the aforementioned long-term goals. However, tomography of quantum many-body systems is plagued with the "exponential wall"—the fact that complete characterization of a state or operation on a many-qubit quantum system requires either a computation time or a memory size that scales exponentially with the number of qubits. An active area of research is thus devoted to developing efficient protocols for such tasks. A recent breakthrough result called shadow tomography has substantially simplified the task of approximating quantum systems [1]. However, it is unclear how to develop similar important tools in CV systems because qubit shadows revolved around the notion of state designs, which have not, up to now, existed in the CV world.

For another example, fiber-based and free-space communication are described by CV systems, so development of secure CV protocols is critical to realizing quantum communication in the real world. However, there is a tradeoff between provable security and ease of use, as some of the simplest CV protocols are not device independent, i.e., such protocols cannot be securely implemented without additional knowledge that the devices involved are also secure.

Members of Victor's group at QuICS, along with collaborators around the world, are spearheading a new research direction to extend state-of-the-art qubit-based tomographic, error-correction, and cryptographic quantum protocols to CV systems in the following ways.

- Theory of appropriately defined CV state designs, and their applications to design-based CV shadow tomography [2]. These results are the first to extend the notion of a design (*a.k.a.* quadrature or summation rule) to infinite-dimensional spaces and are expected to have other applications to state distinction, randomized benchmarking, entanglement detection, fidelity estimation, cryptography, sensing, fundamental physics, and error correction.
- One-sided device-independent cryptographic protocol utilizing squeezed states whose proof of security is based on a CV extension of DV monogamy-of-entanglement games [3]. This work establishes this well-known protocol as the first one-sided device-independent CV protocol, to the authors' knowledge.
- Unified decoding framework for concatenated DV and CV error-correcting codes [4].
- Review of bosonic coding [5] for computer scientists and others outside of physics.

[1] H.-Y. Huang, R. Kueng, and J. Preskill. Predicting Many Properties of a Quantum System from Very Few Measurements. *Nature Physics* **16** (2020), 1050. DOI: 10.1038/s41567-020-0932-7

[2] J. T. Iosue, K. Sharma, M. J. Gullans, and V. V. Albert. Continuous-variable Quantum State Designs: Theory and Applications. Preprint arxiv;2211.05127, 2022.

[3] E. Culf, T. Vidick, and V. V. Albert. Group Coset Monogamy Games and an Application to Device-Independent Continuous-variable QKD. Preprint arXiv:2212.03935, 2022.

[4] Y. Xu, Y. Wang, E.-J. Kuo, and V. V. Albert. Qubit-Oscillator Concatenated Codes: Decoding Formalism and Code Comparison. Preprint arXiv:2209.04573, 2022.

[5] V. V. Albert. Bosonic Coding: Introduction and Use Cases. Preprint arXiv:2211.05714, 2022.

Provable Accurate Machine Learning Algorithms for the Quantum Many-body Problem

Victor V. Albert
Hsin-Yuan Huang (Caltech)
Richard Kueng (Johannes Kepler University Linz)
Giacomo Torlai (Amazon AWS)
John Preskill (Caltech)

Solving quantum many-body problems, such as finding ground states of quantum systems, has far-reaching consequences for physics, materials science, and chemistry. Classical machine learning (ML) has emerged as a powerful approach to solving such problems. However, the advantages of ML over more traditional methods have not been firmly established, reflecting the relative paucity of rigorous theory in ML.

On the other hand, engineered quantum devices are believed to efficiently simulate quantum systems of interest, thereby helping solve many-body problems. Today's noisy intermediate-scale devices do not have the capabilities to simulate a system in perfect error-corrected fashion, but nevertheless should encode useful bits of data about properties of interesting many-body systems. However, since many-body states require exponential (in the number of qubits) memory to be stored exactly, it is unclear how to distill and utilize useful bits from noisy experimental data even at intermediate scale.

Our work [1] combines the best of both the ML and quantum worlds, distilling quantum experimental data and utilizing it with provably efficient ML algorithms. We prove that classical ML algorithms can efficiently reveal properties of quantum many-body states associated with physical systems. In order to circumvent the exponential memory requirement, we devise a way to feed memory-efficient classical snapshots [2] of many-body states — obtained either from experiment or from another classical device — into ML algorithms. We introduce and numerically test ML algorithms for classifying and extrapolating properties of many-body systems and derive information-theoretic bounds on their efficiency.

Viewed from a broader perspective, by illustrating how experimental data can be exploited to make accurate predictions about features of quantum systems that have never been studied directly, our work exemplifies a potentially powerful methodology for advancing the physical sciences. With further theoretical developments, perhaps we can learn how to use experimental data that is already routinely available to accelerate the discovery of new chemical compounds and materials with remarkable properties that could benefit humanity. This work was accepted as a plenary talk at QIP 2022, the most prestigious conference in quantum information science.

[1] H.-Y. Huang, R. Kueng, G. Torlai, V. V. Albert, and J. Preskill. Provably Efficient Machine Learning for Quantum Many-Body Problems. *Science* **377** (2022), eabk3333. DOI: 10.1126/science.abk3333

[2] H.-Y. Huang, R. Kueng, and J. Preskill. Predicting Many Properties of a Quantum System from Very Few Measurements. *Nature Physics* **16** (2020), 1050. DOI: 10.1038/s41567-020-0932-7

Provably Accurate Quantum Simulation of Gauge Theories and Bosonic Systems

Victor V. Albert
Yu Tong (Google & UC Berkeley)
Jarrod R. McClean (Google)
John Preskill (Caltech)
Yuan Su (Google)

Many quantum many-body systems of interest consist of lattices of particles that can occupy states of arbitrarily high energy. Their infinite-dimensional local Hilbert spaces must be truncated in order to perform simulations of real-time dynamics on classical or even quantum computers. To analyze errors resulting from such truncation, we develop [1,] methods for bounding the rate of growth of local quantum numbers such as the occupation number of a mode at a lattice site, or the electric field at a lattice link. We show that, if these models are truncated by imposing an upper limit Λ on each local quantum number (analogue of energy), a truncation error no worse than ϵ can be achieved by choosing Λ to increase polylogarithmically with ϵ^{-1}, an exponential improvement over previous rigorous bounds.

Although formally the local Hilbert spaces are infinite-dimensional in the models we considered, our results show that, at least for some purposes, these models can be accurately approximated by models with finite-dimensional local Hilbert spaces of relatively modest size. Many fundamental results have been derived for quantum spin systems with finite-dimensional spins on each lattice site, and perhaps the tools we have developed can be exploited to extend some of these results to systems with infinite-dimensional local degrees of freedom. This work was accepted as a talk at QIP 2022, the most prestigious conference in quantum information science.

[1] Y. Tong, V. V. Albert, J. R. McClean, J. Preskill, and Y. Su. Provably Accurate Simulation of Gauge Theories and Bosonic Systems. *Quantum* **6** (2022), 816. DOI: 10.22331/q-2022-09-22-816

Standards for Characterizing Quantum Phases

Victor V. Albert

Today's quantum devices are capable of producing exotic quantum many-body states, but their verification is problematic due to several challenges:

1. the exponential memory requirement for perfect storage of a quantum state,
2. a paucity of local observables ("order parameters") whose expectation values characterize the zoo of quantum phases of matter, and
3. a lack of rigorous guarantees on the ability and efficiency of using existing order parameters to characterize said phases.

I have begun a multi-prong effort to resolve these three challenges. The first challenge can be tackled using efficient classical snapshots of a quantum state called *classical shadows* [1]. Armed with such classical descriptions, the goal now is to develop methods to extract from such descriptions the coarse-grained phase properties of their parent quantum states. We have made some progress along this direction with the help of machine learning algorithms [2], but an intuitive understanding of such processes is yet to be fleshed out.

My collaborators and I have made progress on the second issue, concocting an invariant that helps characterize properties of a subset of "topological" many-body states with robust edge excitations [3, 4]. The electronic quantum system exhibiting the quantum Hall effect is an example of such a phase, and its "topologically protected" edge currents have been used to determine values of fundamental physical constants. Robust edge excitations are characterized by a topological invariant called the chiral central charge, and, until our work, it was not known how to extract this quantity from a single copy of a physical many-body wavefunction. This work was accepted as a single-track talk at QIP 2022, the most prestigious conference in quantum information science.

I have also begun a journal club discussion at the University of Maryland College Park on the difficult third issue, bringing together experts from quantum computer science and topological quantum phases of matter.

[1] H.-Y. Huang, R. Kueng, and J. Preskill. Predicting Many Properties of a Quantum System from Very Few Measurements. *Nature Physics* **16** (2020), 1050. DOI: 10.1038/s41567-020-0932-7

[2] H.-Y. Huang, R. Kueng, G. Torlai, V. V. Albert, and J. Preskill. Provably Efficient Machine Learning for Quantum Many-Body Problems. *Science* **377** (2022), eabk3333. DOI: 10.1126/science.abk3333

[3] I. H. Kim, B. Shi, K. Kato, and V. V. Albert. Chiral Central Charge from a Single Bulk Wave Function. *Physical Review Letters* **128** (2022), 176402. DOI: 10.1103/PhysRevLett.128.176402

[4] I. H. Kim, B. Shi, K. Kato, and V. V. Albert. Modular Commutator in Gapped Quantum Many-Body Systems. *Physical Review B* 106 (2022), 075147. DOI: 10.1103/PhysRevB.106.075147

Tests of Quantumness and Quantum Computational Advantage

Yi-Kai Liu
Lucas T. Brady (NASA Ames Research Center)
Jacob Bringewatt (University of Maryland)
Rushil Dandamudi (University of Maryland)
Luis Pedro Garcia-Pintos (University of Maryland)
Dominik Hangleiter (University of Maryland)
Atul Mantri (University of Maryland)
Joel Rajakumar (University of Maryland)
James Watson (University of Maryland)

We, as humans, are macroscopic entities that can only process classical information. For us, the development of quantum computers raises a fundamental question: how can we test a quantum device, using only its classical inputs and outputs? In particular, how can we test whether a quantum device is really behaving "quantumly," in the sense that its behavior could not have been reproduced by a device obeying classical physics? How can we test whether a device is correctly performing a quantum computation that cannot be simulated efficiently on a classical computer?

We are investigating several theoretical approaches to answering these questions. One approach uses quantum speed limits, which upper-bound the speed at which a quantum system can evolve, in terms of mathematical properties of the Hamiltonian and the quantum state of the system [1]. These speed limits can potentially be used to rule out the possibility of a quantum computational advantage when running quantum adiabatic optimization algorithms. Here the speed limits provide a converse to the adiabatic theorem: they say that the algorithm must fail if one runs it too fast. In addition, these speed limits can potentially be used for benchmarking analog quantum simulators, and for detecting the presence of noise and decoherence in these devices. This is because loss of coherence makes it harder for a system to perform a fast unitary time-evolution.

Another approach uses classical algorithms for simulating noisy, low-depth quantum circuits. Such simulations can be used to rule out the possibility of

achieving a quantum computational advantage on some present-day and near-future quantum devices. To this end, we are investigating classical algorithms based on resource theories of coherence, and Monte Carlo sampling from quasiprobability distributions, in order to simulate low-depth quantum circuits with strong dephasing noise [2].

Yet another approach uses interactive protocols and techniques from computationally secure cryptography, such as trapdoor claw-free functions. We are developing improved protocols of this type, using cryptosystems based on the hardness of solving systems of multivariate quadratic equations over finite fields.

Finally, we are developing a new approach to testing quantum simulators, using "trapdoor Hamiltonians." Our goal is to construct Hamiltonians that can be simulated efficiently on a quantum computer, but seem hard to simulate on a classical computer, unless one knows a certain piece of information, called the "trapdoor." (This is loosely analogous to trapdoor one-way functions in cryptography.)

[1] L. P. García-Pintos, L. T. Brady, J. Bringewatt and Y.-K. Liu. Lower Bounds on Quantum Annealing Times. *Physical Review Letters*, to appear. Preprint, arXiv:2210.15687. URL: https://arxiv.org/abs/2210.15687

[2] J. Rajakumar, J. Watson and Y.-K. Liu. In preparation.

Post-Quantum Cryptography

Yi-Kai Liu
Gorjan Alagic (NIST ITL)
Lily Chen (NIST ITL)
David Cooper (NIST ITL)
Quynh Dang (NIST ITL)
Thinh Dang (NIST ITL)
John Kelsey (NIST ITL)
Jacob Lichtinger (NIST ITL)
Carl Miller (NIST ITL)
Dustin Moody (NIST ITL)
Rene Peralta (NIST ITL)
Ray Perlner (NIST ITL)
Angela Robinson (NIST ITL)
Daniel Smith-Tone (NIST ITL)

Since 2016, NIST has been leading an open, competition-like process to develop standards for post-quantum cryptography (PQC). The goal is to standardize new schemes for public-key encryption, key establishment, and digital signatures, in order to replace existing schemes that would be vulnerable to cryptanalysis using quantum computers, such as RSA, Diffie-Hellman, and elliptic curve cryptosystems. While large quantum computers have not yet been built, NIST believes it is prudent to begin preparing for that possibility. These new post-quantum cryptosystems will be crucial for secure web browsing, digital certificates, and secure software updates, and many other applications.

During this process, NIST and the cryptography community have evaluated many proposed post-quantum cryptosystems, based on high-dimensional lattices, error-correcting codes, systems of multivariate polynomial equations, elliptic curve isogenies, hash functions, and other mathematical objects. This evaluation covered many topics, including fundamental research on cryptanalysis, estimates of the security strength of the schemes, measurements of their practical performance in real world use-cases, and potential obstacles to adoption of these schemes, such as concerns about intellectual property.

In July 2022, NIST reached a milestone in this process: after three rounds of evaluation, NIST selected a public-key encryption and key establishment algorithm (CRYSTALS-Kyber), and three digital signature schemes (CRYSTALS-Dilithium, Falcon and SPHINCS+), for standardization [1]. These schemes rely heavily on lattice-based cryptography (except for SPHINCS+, which is a stateless hash-based signature scheme). They are expected to be satisfactory in a wide range of use cases. NIST expects to publish and solicit public comments on the draft standards in 2023.

NIST is also continuing its evaluation process and may select additional cryptosystems for standardization in the future, in order to mitigate the risk of unexpected advances in cryptanalysis, and to support use-cases that require cryptosystems with special properties. For this purpose, NIST has selected four key establishment algorithms (BIKE, Classic McEliece, HQC and SIKE) for a fourth round of evaluation [1]. NIST has also issued a new call for proposals, for additional signature schemes[17].

To engage with the post-quantum cryptography community and other stakeholders, NIST held its Fourth PQC Standardization Conference, on Nov. 29-Dec. 1, 2022, online[18]. NIST is also working with industry on PQC migration issues, through the National Cybersecurity Center of Excellence (NCCoE)[19].

[1] G. Alagic, D. Apon, D. Cooper, Q. Dang, T. Dang, J. M. Kelsey, J. Lichtinger, Y.-K. Liu, C. A. Miller, D. Moody, R. Peralta, R. Perlner, A. Robinson, and D. Smith-Tone. Status Report on the Third Round of the NIST Post-Quantum Cryptography Standardization Process. NISTIR 8413-upd1, September 2022, 102 pages. DOI: 10.6028/NIST.IR.8413-upd1

[17] https://csrc.nist.gov/Projects/pqc-dig-sig/standardization

[18] https://csrc.nist.gov/events/2022/fourth-pqc-standardization-conference

[19] https://www.nccoe.nist.gov/crypto-agility-considerations-migrating-post-quantum-cryptographic-algorithms

NIST Quantum Network Testbed Efforts

Oliver Slattery
Thomas Gerrits
Lijun Ma
Anouar Rahmouni
Yicheng Shi
Nijil Lal
Paulina Kuo
Xiao Tang
Alan Mink
Ya-Shian Li-Baboud (NIST ITL)
Alan Migdall (NIST PML)
Sergey Polyakov (NIST PML)
Josh Bienfang (NIST PML)
Ivan Burenkov (NIST PML)
Neil Zimmerman (NIST PML)
Dhananjay (DJ) Anand (NIST CTL)
Abdella Battou (NIST CTL)
Amar Abane (NIST CTL)
Abderrahim Amlou (NIST CTL)
Lydia Ait Oucheggou (NIST CTL)
Mheni Merzouki (NIST CTL)
Jabir MV (NIST CTL),
Laura Sinclair (NIST, CTL)

The NIST Gaithersburg Quantum Network (NG-QNet), shown in Figure 68, is a suite of testbeds being built on or connected to the NIST Gaithersburg campus to implement and characterize various aspects of quantum networks (QN) while keeping NIST's core metrology mission as fundamental to our approach. The testbeds are being developed collaboratively by NIST's ITL, CTL and PML laboratories and incorporates regional federal government and industry partners.

The NG-QNet includes the Platform for Quantum Network Innovation (PQNI), the Quantum Component Characterization Testbed, the Quantum Network Grand Challenge (QNGC), the Quantum Network Time Synchronization Testbed and the DC regional QN testbed (DC-QNet). The testbeds of the NG-QNet are currently being used to implement a comprehensive research, development and experimental program which includes: develop and test QN capabilities (such as entangled photon sources, interfaces, detectors); implement various foundational QN processes such as polarization and phase stabilization, node-synchronization and link characterization (including for noise, losses, vulnerabilities (such as eavesdroppers) and robustness); develop and test QN control architectures; study classical/quantum co-existence; and (as appropriate in the future) incorporate complex quantum systems such as quantum memories and repeaters. Ultimately, the effort will pursue QN experiments such as entanglement distribution, entanglement swapping and teleportation and will target applications such as distributed quantum computing, quantum communications and quantum sensing. The

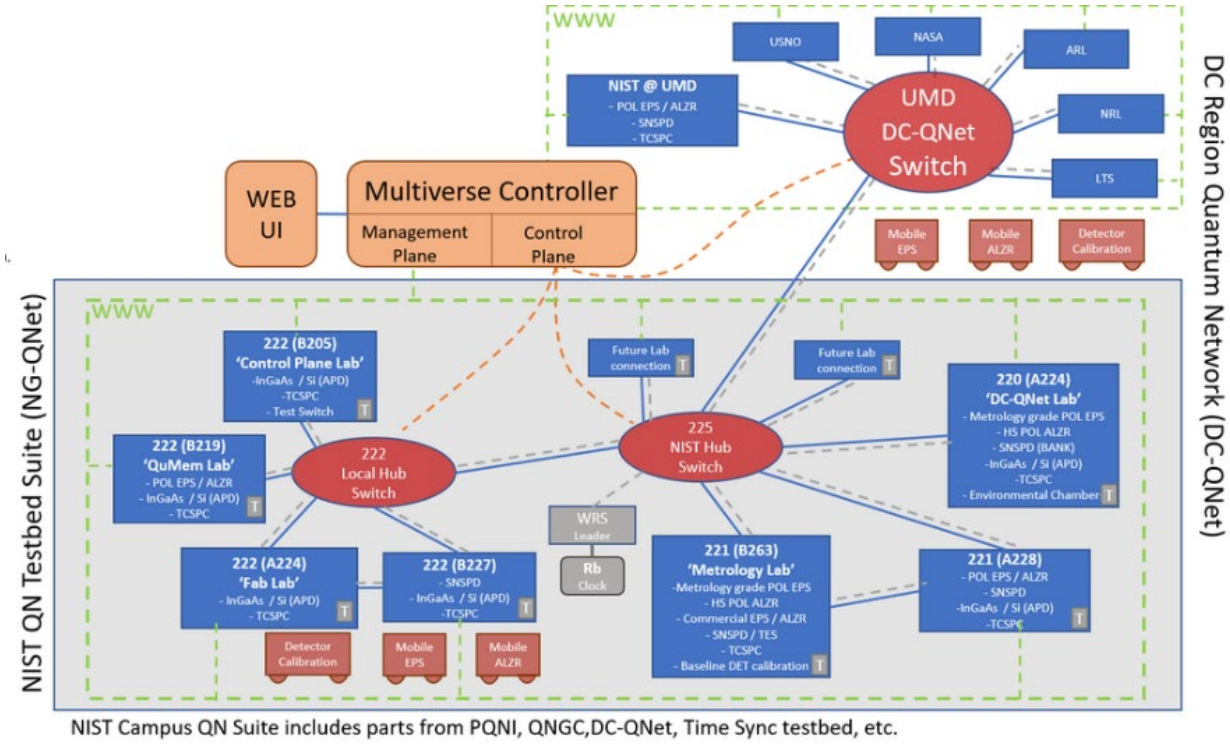

Figure 68. *NG-QNet overview and connection to the DC-QNet.*

Figure 69. *DC-QNet map and DC-QNet member logos.*

NG-QNet will also include a dedicated facility to serve as the NIST node of the DC-QNet.

The DC-QNet, shown in Figure 69, is a consortium of six DC-area federal agencies coming together to build a real-life regional QN testbed to advance cooperation among federal agencies in QN research and development. It will be a non-proprietary environment for test and evaluation of QN concepts, components, protocols, and architectures developed both within and beyond the member agencies. It will enable cross-cutting agency synergy in sensor development, secure communications, distributed computing, and other use case applications. The DC-QNet was codified by an interagency MOU on May 18th, 2022. The six agencies are: Naval Research Laboratory (NRL), Army Research Laboratory (ARL), National Institute of Standards and Technology (NIST), Laboratory for Telecommunication Sciences (LTS), US Naval Observatory (USNO) and National Aeronautics and Space Administration (NASA). The NASA hosted website for the DC-QNet can be viewed at https://esc.gsfc.nasa.gov/partnerships/DC-QNet.

Quantum Network and Component Metrology

Thomas Gerrits
Oliver Slattery
Anouar Rahmouni
Yicheng Shi
Paulina Kuo
Lijun Ma
Xiao Tang
Nijil Lal
Ya-Shian Li-Baboud (NIST ITL)
Dhananjay Anand (NIST CTL)
Abdella Battou (NIST CTL)
Amar Abane (NIST CTL)
Abderrahim Amlou (NIST CTL)
Lydia Ait Oucheggou (NIST CTL)
Mheni Merzouki (NIST CTL)
Jabir Marakkarakath Vadakkepurayil (NIST CTL)
Alan Migdall (NIST PML)
Sergey Polyakov (NIST PML)
Josh Bienfang (NIST PML)
Ivan Burenkov (NIST PML)

Summary. The Quantum Network and Component Metrology Project focusses on the characterization of quantum network links, components, and protocols. Measurement protocols and tools are developed in our lab and deployed in the DC-QNet[20] and our NIST Gaithersburg quantum network testbed (NG-QNet). We collaborate with researchers across different OUs (PML, ITL and CTL) as well as with researchers from other government agencies. Our project also considers measurement challenges for single-photon devices and components, and therefore works closely with companies within the QED-C[21] on component characterization and solving measurement challenges [1]. Last year's highlights are summarized below: A demonstration to synchronize quantum network nodes to below 200 ps over 128 km distance, distribute entanglement over more than 130 km distance, and measure wavelength-dependent loss in optical fibers with some surprising results.

[20] https://www.nist.gov/news-events/news/2022/06/dc-area-us-government-agencies-announce-washington-metropolitan-quantum

[21] Quantum Economic Development Consortium (QED-C): https://quantumconsortium.org/

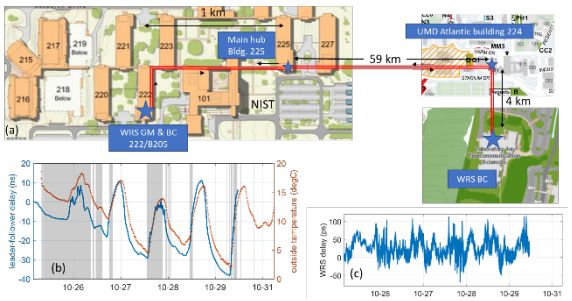

Figure 70. *(a) NIST-LTS link. A 1 km link within NIST connects the lab to the NIST quantum network hub. A 59 km link connects the NIST campus to the University of Maryland campus, where a further 4 km connection is made to LTS. (b) Leader-follower path delay (blue line) vs. time (date in 2022) between the first boundary clock at LTS and the second boundary clock at NIST. The outside ambient temperature (red line) is also shown. The grey shaded areas represent some degree of cloud cover, mist, or fog in the region of deployed fiber. White areas represent clear skies. (c) Total grand master to second boundary clock delay vs. time.*

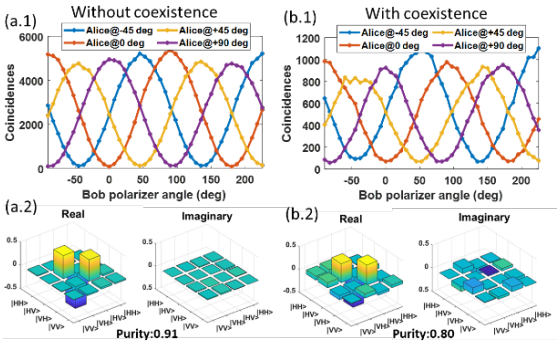

Figure 71. *Experimental results for coexistence. (a.1) [(b.1)] Polarization entanglement fringes as measured without [with] the additional HA-PTP signal in the quantum fiber (2 s integration time). (a.2) [(b.2)] Tomography of polarization entangled state without [with] the additional HA-PTP signal in the quantum fiber.*

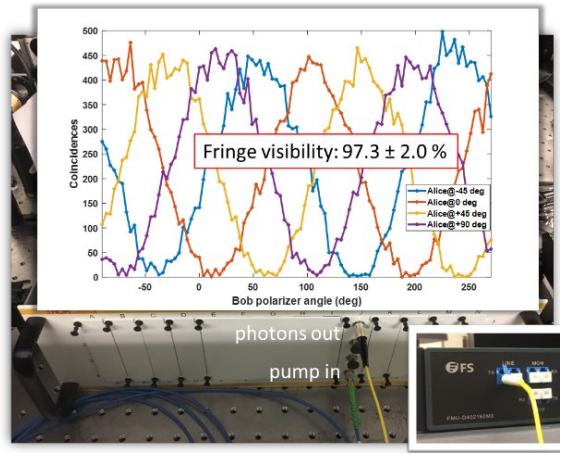

Figure 72. *Experimental results for long-distance entanglement distribution. Polarization entanglement fringes for a 136 km node separation using our mobile polarization entangled photon source and receivers.*

Quantum Network Node Synchronization. High precision synchronization is essential for any quantum network architecture and quantum network metrology. Since optical fibers transport 'flying' qubits at almost the speed of light, precise (picosecond) time stamping through the whole network is a requirement. Compared to classical networks, these synchronization requirements are orders of magnitudes more stringent. Here, we used a two-level White Rabbit Switch (WRS) architecture with one grandmaster (GM) and two boundary clocks (BCs) and show sub-200 ps synchronization between the grandmaster and the final BC, which are separated by 128 km through a link between NIST and the Laboratory for Telecommunication Sciences in College Park, MD. Figure 70(a) shows our experimental setup. A 64 km link is established between the grandmaster WRS and the first boundary clock WRS. The first boundary clock WRS redistributes its high-accuracy precision time protocol (HA-PTP) to a second boundary clock, which is at the same location as the grandmaster (at NIST). This architecture allows the time delay between the 10 MHz grandmaster clock and second boundary clock to be measured using a low-jitter time tagger. Figure 70(b) shows the leader-follower path delay between the first and second boundary clock (blue line) and the ambient outside temperature (orange line). The leader-follower path delay appears to correlate with the ambient outside temperature and its value changes by about 50 ns peak-to-peak, while the ambient outside temperature varies by about 15° C. Figure 70(c) shows the total grandmaster to second boundary clock delay vs. time, *i.e.* representing the synchronization error over the architecture's total link length of 128 km. The peak-to-peak variation is less than 200 ps.

These results show promise for metropolitan-scale quantum network node synchronization. Quantum communication protocols requiring single-photon interference with nanosecond photon coherence times should be achievable. In the upcoming year we will investigate several methods to further improve the synchronization error.

Entanglement Distribution. Entanglement distribution will be a key service in future quantum networks. During entanglement distribution, quantum information is carried by photons traveling over optical fibers from a central source to client nodes separated by long distances. The quality of the entanglement distributed to the nodes is limited by loss, noise, polarization mode dispersion, and cumulative transmission time fluctuations, all of which must be mitigated to offset their detrimental effects.

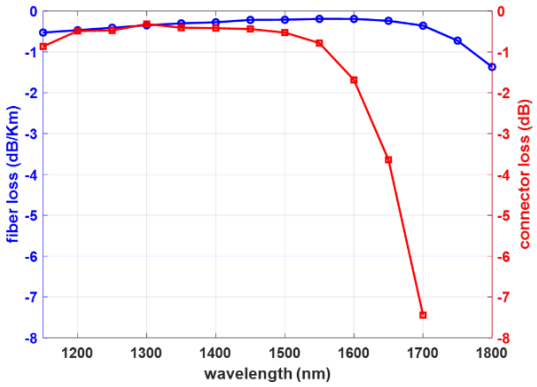

Figure 73. *v-OTDR results. Red line: connector loss, blue line: fiber loss. Results for coexistence.*

We were able to demonstrate the co-existence of the node synchronization protocol with the quantum signal on a single link, which can improve transmission delay measurements and reduce deployment costs. Furthermore, we demonstrated the distribution of polarization entanglement over 136 km distance. Combined with our quantum network node synchronization effort outlined above, we are planning to distribute polarization entangled photons throughout the DC-QNet metropolitan network this upcoming year.

Figure 71(a.1) shows polarization entanglement visibility fringes between two laboratories at NIST (separated by approximately 250 m) without coexistence of the classical synchronization HA-PTP protocol. Figure 71(b.1) shows the entanglement fringes with a coexisting synchronization signal in the same fiber as the quantum signal. Figure 71a.2 (2b.2) shows the tomographic reconstruction of the density matrix and a state purity of 0.91 (0.80) with (without) the coexisting HA-PTP signal in the quantum fiber. These results show that coexistence of a classical HA-PTP for picosecond level synchronization of distant nodes and quantum signals for entanglement distribution in the same optical fiber is possible. The entanglement visibility reduction with classical time synchronization co-existence is due to a combination of additional channel loss and extra noise.

Figure 72 shows polarization entanglement distribution through 136 km of optical fiber. The quantum light was sent through fiber spools located in the same laboratory as the photon source. The fringe visibility was high (97.3 %) and only slightly reduced from the 99.0 % fringe visibility for short (10 m fiber) distance.

The above results show promise for entanglement distribution within the DC-QNet metropolitan distances at rates that are sufficient to investigate various entanglement routing protocols, the effect of noise, polarization stability and loss in the deployed fiber links between two distant sites.

Single-Photon OTDR. A future quantum network will require efficient characterization of the losses to validate the fiber-link's performance. Conventional optical time-domain reflectometry (OTDR) is one of the most used techniques for characterization of fiber-link loss. Photon-counting OTDR (ν-OTDR) using a single-photon detector has been demonstrated at the telecommunication wavelengths at 1310 and 1550 nm. We developed a new approach allowing us to cover a wavelength range from 1000 nm to 1850 nm based on our pulsed supercontinuum laser.

Figure 73 shows a surprising ν-OTDR results. We measured a combination of two fiber spools (25.4 and 12.6 km in length) connected by a standard fiber connector. The blue line in Figure 73 shows the fiber loss as a function of wavelength in dB/km. We observe typical fiber loss values, e.g., 0.4 dB/km@1310 nm and 0.2 dB/km@1550 nm. The red line shows the connector loss, which increases significantly as a function of wavelength and can be as high as 3 dB at a wavelength around 1650 nm. In the coming year, we will perform a more detailed study on fiber connections vs. wavelength. This study should inform the design and connector choices for future quantum networks.

[1] QED-C Single Photon Report: https://quantumconsortium.org/single-photon-report

Integrated Quantum Photonics Based on Thin-film Lithium Niobate

Pavan Sesha Challa Kumar
Paulina Kuo

Performing quantum information processing using integrated optics is an attractive alternative to processing using free-space or bulk optics because integrated optics offers compact size and monolithic construction for high repeatability and phase stability. One integrated-optics platform that is attracting increasing attention is thin-film lithium niobate (TFLN) or lithium niobate on insulator (LNOI). Lithium niobate ($LiNbO_3$) is an interesting material because it offers multiple functions including waveguiding, electro-optic modulation and frequency conversion (the latter for entangled-photon-pair generation). Waveguides made from TFLN offer tight confinement for stronger frequency conversion and modulation that uses lower control voltages. Single-photon sources, photon routing and modulation can be performed on the TFLN same chip, and in some cases, cryogenic single-photon detectors can also be integrated together on the single TFLN chip [1].

We are working to develop the capability to fabricate TFLN waveguides and devices using the NIST nanofabrication facility. Using commercially available TFLN substrates, we are developing patterning and etching recipes using e-beam lithography and inductively coupled plasma (ICP) reactive ion etching (RIE).

Our initial studies confirm the literature findings [2] that post-etch cleaning is very important for achieving low-loss waveguides. We have been investigating waveguide and coupler designs using numerical modeling. We are also developing optical waveguide characterization facilities. In addition, we have performed numerical studies of sensitivity of TFLN waveguide frequency converters to fabrication imperfections [3]. Our goal is to develop a TFLN integrated-optics chip that can perform quantum measurements such as entanglement visibility or Bell-state measurements.

[1] E. Lomonte, M. A. Wolff, F. Beutel, et al. Single-photon Detection and Cryogenic Reconfigurability in Lithium Niobate Nanophotonic Circuits. *Nature Communications* **12** (2021), 6847.

[2] G. Ulliac, V. Calero, A. Ndao, F.I. Baida, and M.-P. Bernal. Argon Plasma Inductively Coupled Plasma Reactive Ion Etching Study for Smooth Sidewall Thin Film Lithium Niobate Waveguide Application. *Optical Materials* **53** (2016), 1.

[3] P. S. Kuo. Noncritical Phasematching Behavior in Thin-Film Lithium Niobate Frequency Converters. *Optics Letters* **47**:1 (2022), 54.

Entangled Photon Pairs Based on Backward-Wave Spontaneous Parametric Downconversion

Paulina Kuo

Entangled photon pairs are a fundamental building block for quantum networking and quantum information. They are used for distributing entanglement and heralded single-photon generation. Spontaneous parametric downconversion (SPDC) is a common method to produce entangled photon pairs, which can be performed using free-space or integrated-optics architectures. We investigated a new way to generate entangled photon pairs using backward-wave (BW) SPDC.

Figure 74. *Illustration of backward-wave SPDC, where the idler propagates in the direction opposite to the pump and signal.*

In conventional SPDC, the pump and downconverted photons (the signal and idler) all propagate in the same direction. In BW SPDC, one of the downconverted photons (the idler) propagates in the direction opposite to the pump and signal (see Figure 74). This process requires very small (less than 1 μm) poling period, which have been achieved in periodically poled $KTiOPO_4$ (PPKTP) [1].

In our experiment [2], we used a PPKTP crystal with 500 nm poling period to obtain SPDC using 800 nm pump, 1400 nm signal and 1870 nm idler. We detected these photons using superconducting nanowire single-photon detectors (SNSPDs) and measured their spectra using a grating monochromator. Measured spectra for BW SPDC are shown in Figure 75. We observed the downconverted signal and idler wavelengths using two different pump wavelengths (800 nm and 805 nm) and found that the idler has very narrow bandwidth and is nearly insensitive to changes in the pump wavelength, an effect that has been previously observed for BW optical parametric oscillation [3]. Such spectral characteristics of the idler wave imply that spectral modulation of the pump beam is transferred to spectral modulation of the signal, which can be used for spectral shaping of the signal photons and enable spectrally shaped, heralded single photons.

We believe that BW SPDC can be used as new source of entangled photon pairs with interesting properties including, (1) having the downconverted photons

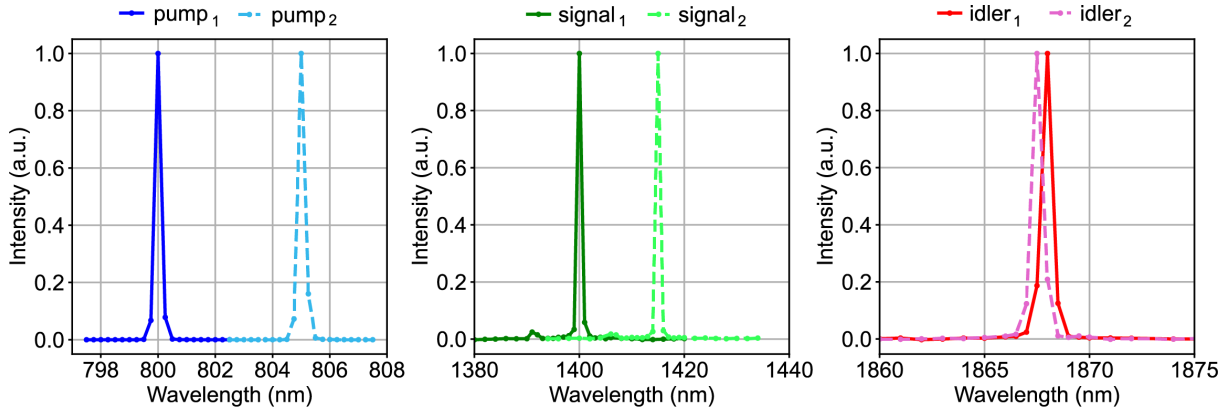

Figure 75. *Normalized BW SPDC spectra for 800-nm and 805-nm pumping. The idler wavelength is nearly insensitive to changing of the pump wavelength.*

emerge in two different directions, (2) offering a nearly separable joint spectral intensity [4] and (3) enabling spectrally shaped, heralded single-photon generation. Further work is in progress to study these properties.

[1] C. Canalias, V. Pasiskevicius, R. Clemens, and F. Laurell. Submicron Periodically Poled Flux-grown $KTiOPO_4$. *Applied Physics Letters* **82**:24 (2003), 4233.

[2] P. S. Kuo. Observation of Backward-Wave Spontaneous Parametric Downconversion in Sub-μm PPKTP. In *Technical Digest Series of Optica, Frontiers in Optics + Laser Science 2022*, Rochester, New York, October 17-20, 2022

[3] A.-L. Viotti, F. Laurell, A. Zukauskas, C. Canalias, and V. Pasiskevicius. Coherent Phase Transfer and Pulse Compression at 1.4 μm in a Backward-wave OPO. *Optics Letters* **44**:12 (2019), 3066.

[4] A. Christ, A. Eckstein, P. J. Mosley, and C. Silberhorn. Pure Single Photon Generation by Type-I PDC with Backward-wave Amplification. *Optics Express* **17**:5 (2009), 3441-3446.

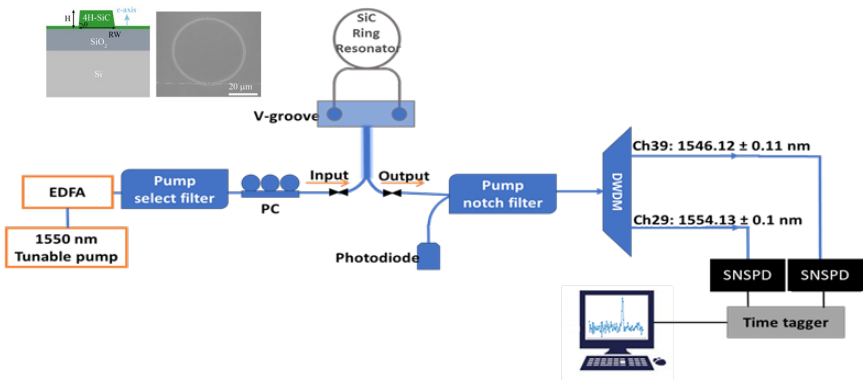

Figure 76. *SiC device and experimental setup.*

Silicon-Carbide-based Integrated Quantum Device Efforts

Lijun Ma
Anouar Rahmouni
Oliver Slattery
Thomas Gerrits
Xiao Tang
Yinxiao Xiang
Qing Li (Carnegie Mellon University)
Lutong Cai (Carnegie Mellon University)
Michael Spencer (Morgan State University)

Silicon carbide (SiC) has emerged as a promising material for integrated quantum devices since it is CMOS compatible with favorable mechanical, electrical, thermal, and photonic properties. To take full advantage of the unique material properties offered by SiC, we have worked with colleagues in Carnegie Mellon University on the development and characterization of prototypes of an entangled photon source based on a SiC micro-ring.

The device is based on a 4H-silicon-carbide-on-insulator platform. A silicon dioxide (SiO2) layer provides isolation from the silicon substrate, and a compact 36-μm-radius SiC micro-ring resonator is employed for the photon pair generation. The optimized nanofabrication has resulted in optical quality factor (Q factor) above 1 million for 36-μm-radius SiC micro-ring resonators.

We have experimentally demonstrated photon pair generation from spontaneous four wave mixing (SFWM) in the telecom wavelength band (1550 nm) on our SiC device (Figure 76). We measured signal/idler photon flux to be on the order of million photons/s with a pump power of 10 mW. In addition, a temporal coincidence rate >12,000 counts/min was measured (Figure 77). To the best of our knowledge, this is the first report of a single photon coincidence measurement from SFWM in any SiC platform. Temporal coincidence is a key signature of the detected photons belonging to a generated 'pair'. This has demonstrated the feasibility of an integrated device of entangled photon-pair generation based on a SiC micro-ring.

During the research, we also studied the limiting factors – such as Raman noise and insertion loss – in the device that lower the coincidence (wanted) to accidental noise (unwanted) ratio. We will further improve device through further noise filtering and better temperature control. If successful, it will be possible to realize chip-scale devices that can be integrated with existing CMOS foundry processes. Furthermore, we anticipate that further engineering development could lead to practical and scalable entangled photon source devices of interest to the emerging quantum industry. With further development and improvement, it is possible for these SiC-

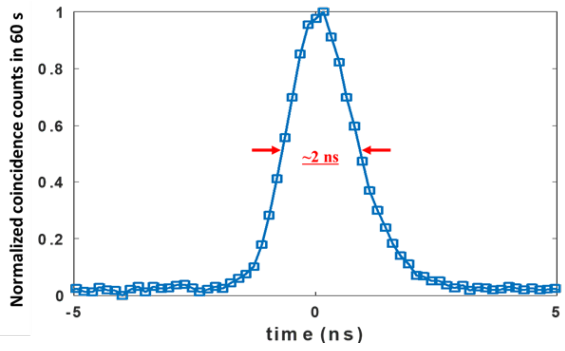

Figure 77. *Coincidence measurement of generated photon pairs from the SiC device*

based entangled photon sources to be deployed into our quantum network testbed effort at NIST, which would provide important proof-of-concept to industry.

Joint Center for Quantum Information and Computer Science

Victor Albert
Matthew Coudron
Yi-Kai Liu
Justyna Zwolak
Carl Miller (NIST ITL)
Gorjan Alagic (NIST ITL)
Andrew Childs (University of Maryland)

http://quics.umd.edu/

Established in October 2014, the Joint Center for Quantum Information and Computer Science (QuICS) is a cooperative venture of NIST and the University of Maryland (UMD) to promote basic research in understanding how quantum systems can be effectively used to store, transport and process information. QuICS brings together researchers from the University of Maryland Institute for Advanced Computer Studies (UMIACS) and the UMD Department of Physics and Computer Science with NIST's Information Technology and Physical Measurement Laboratories, together with postdocs, students, and a host of visiting scientists.

QuICS has quickly established itself as a premier center for research in quantum information science. Twelve Fellows, four Adjunct Fellows, one Affiliate Fellow, 20 postdocs, and 68 graduate students are currently associated with the center. Yi-Kai Liu of ACMD is Co-Director of the Center along with Andrew Childs of the UMD Computer Science Department.

This year a new QuICS Fellow was recruited. Dr. Murphy Yuezhen Niu will join in August 2023 as an Assistant Professor of Computer Science and QuICS Fellow. Niu is currently a senior research scientist in the Google Quantum AI team, where her work focuses on intelligent quantum control optimization and metrology, quantum machine learning, quantum algorithm design and near-term quantum error correction.

The Center continues to be very productive. In CY 2022 some 112 research papers were produced by those associated with the center. One patent was issued, and nine new patent applications were filed. Some 40 seminars by both internal and external speakers were held.

As in past years, QuICS research was featured prominently at QIP 2022, the is the leading annual conference on the theory of quantum information processing, which was held in Pasadena, CA in March 2022. Twelve talks on papers coauthored by current QuICS members were presented at the conference, including two of the three plenary talks and two additional short plenary talks. In addition, four QuICS members served on the program committee for the conference.

March 2022 also saw the publication of a popular science book by QuICS Fellow (and NIST staff member) Nicole Yunger Halpern entitled *Quantum Steampunk: The Physics of Yesterday's Tomorrow* [1]. This book brings Nicole's research at the intersection of quantum information and quantum thermodynamics to a wider audience.

Finally, QuICS Fellow (and ACMD staff members) Victor Albert gave a series of three tutorial talks on quantum error correction and bosonic coding, on August 1, 2, and 4, 2022. These talks attracted a large audience, including many online viewers from NIST and elsewhere.

[1] Nicole Yunger Halpern. *Quantum Steampunk: The Physics of Yesterday's Tomorrow.* Johns Hopkins University Press, 2022.

Foundations of Measurement Science for Information Systems

ITL assumes primary responsibility within NIST for the development of measurement science infrastructure and related standards for IT and its applications. ACMD develops the mathematical foundations for such work. This can be very challenging. For example, many large-scale information-centric systems can be characterized as an interconnection of many independently operating components (e.g., software systems, communication networks, the power grid, transportation systems, financial systems). A looming new example of importance to NIST is the Internet of Things. Exactly how the structure of such large-scale interconnected systems and the local dynamics of its components leads to system-level behavior is only weakly understood. This inability to predict the systemic risk inherent in system design leaves us open to unrealized potential to improve systems or to avoid potentially devastating failures. Characterizing complex systems and their security and reliability properties remains a challenging measurement science problem.

Algorithms for Identifying Important Network Nodes for Communication and Spread

Fern Y. Hunt
Roldan Pozo

The identification of nodes in a network that enable the fastest spread of information is an important, if not fundamental, problem in network control and design. It is applicable to the optimal placement of sensors, the design of secure networks, and the problem of control when network resources are limited. Our approach to this problem has its origins in models of opinion dynamics and the spread of innovation in social networks. The mode of communication between nodes is described by simple models of random or deterministic propagation of information from a node to its neighbors. During the past few years, we have made progress in understanding the structural requirements for sets of nodes for effective spread in networks and have developed scalable algorithms for constructing these sets in real world networks.

We consider a discrete time model of information spread (represented by a variable assigned to each node) in a network with a set of nodes V and a subset $A \subseteq V$ of k nodes representing leaders or stubborn agents that are initially assigned a single value. Propagation occurs by iterated averaging or diffusion defined by a stochastic matrix P. All node values will eventually converge to the single value at a speed determined by the sub-stochastic matrix $P|_{A'}$, the matrix P restricted to the complement of A. An effective spreader in this situation is then a set of nodes for which convergence to this single value is fastest, i.e., the set A for which the Perron-Frobenius eigenvalue of $P|_{A'}$ is largest. Using a classical result of Markov chain theory, the problem can be recast in terms of finding the set A of cardinality k that minimizes the mean first hitting time, i.e., the expected time a random walker reaches the target set A for the first time.

We first proposed a polynomial time algorithm for finding an approximation to the optimal set [1]. It is an extension of the classic greedy algorithm, and it begins with a class of optimal and near optimal starter sets of smaller cardinalities rather than the conventional choice of a best singleton set. An optimal spreader in our setting is defined in terms of a set function F where for a subset $A \subset V$, F (A) is the sum of mean first arrival times to A by random walkers that start at nodes outside of A. Direct comparison of the algorithm results with the actual optimal solution and lower bounds on the performance ratio can be obtained because F is a supermodular set function [2]. However, for large complex networks commonly encountered in applications, another approach is needed.

We then developed a set of fast heuristics that work well on graphs with large hubs, a common feature of complex networks. When the desired set cardinality is k, subsets of hub vertices are rapidly screened to produce candidate sets. Each set consists of k nodes whose first (or higher order) neighborhoods have minimal overlap. After further screening, the offered approximation is selected by ranking the results of a Monte Carlo calculation of the optimal set F for each candidate. This process allows us to find near optimal and optimal spreaders in networks with millions of nodes and dozens of millions of edges in less than a few seconds on a typical laptop. After conducting tests on real world graphs from diverse application areas including molecular biology, traffic control, and social networks, we hypothesize that the method is most effective in terms of speed and quality of offered solutions when it is used on graphs with a large ratio of maximal degree to average degree.

Understanding that the resulting offered set was an approximate solution of a discrete stochastic optimization problem, we established sufficient conditions that imply that it is also an approximate solution of the original problem. The first step was to establish the accuracy of the Monte Carlo calculation of F. The fact that the first hitting time to a set A has a distribution with exponential tails means that a sample average of simulated hitting times produces a consistent estimate of F in the limit of large sample size i.e., number of simulations.

Establishing the degree of optimality of any offered solution is very difficult since supermodularity cannot

be used and the size of the graphs are so large. However, the methods we use make it possible to rapidly sample the distribution of possible F values. We suppose the screening and ranking procedures produce candidate sets with F values that rank in the highest percentile of a distribution of such values over all subsets of fixed cardinality. Independent repetition of the heuristic calculation enables us to produce an estimate of a fixed percentile value along with a confidence interval for that estimate. The latter follows from an application of Chebyshev's inequality. Note that the resulting interval contains both the offered solution value and the optimal value of the original problem. Even in the case of a large number of repetitions, this approach is promising because it takes very little time to perform a single execution. The results of our work are reported in [3].

We have also studied related models of information spread, such as the broadcast model (k-median problem) which seeks the minimal sum of distances, and epidemiological models (Susceptible-Infected-Recovered) that better represent the spread of infectious diseases on network topologies. We have studied and compared the efficacy of several heuristic algorithms used in the literature and have developed a different approach (minimizing overlapping neighborhoods) which aims to produce quality solutions at a fraction of the computational cost, making it appropriate for use on large networks. For example, we are able to process graphs of several million vertices with competitive solutions that run one to two orders of magnitude faster than previous methods. This year we have conducted extensive analysis of over 25 000 experiments of network/algorithm/k-value combinations and have created parallel OpenMP C++ applications for the evaluation of these models. This effort has yielded important insights on establishing best practices for approximating methods on real networks and providing efficient solution techniques to this challenging problem.

[1] F. Hunt. Using First Hitting Times to Maximize the Rate of Convergence to Consensus. Preprint: arXiv:1812.08881, 2018.

[2] F. Hunt. An Algorithm for Identifying Optimal Spreaders in a Random Walk Model of Network Communication. *Journal of Research of the NIST* **121** (2016), 121008. DOI: 10.6028/jres.121.008

[3] F. Hunt and R. Pozo, Fast Methods for Identifying Effective Spreaders in Real Network. Journal of Research of the NIST 125 (2020), 125036. DOI: 10.6028/jres.125.036

Towards Risk Evaluation and Mitigation in Networked Systems

Vladimir Marbukh

The first focus area of this project is evaluation and mitigation of systemic risk due to undesirable contagion in large-scale networked infrastructures. While explosive growth of such infrastructures is driven by economic and convenience benefits of interconnectivity, the same interconnectivity creates systemic risk of undesirable contagion due to cascading overload, computer virus propagation, etc. The goal of system designer/operator is balancing economic benefits and systemic risks associated with increase in the system interconnectivity. The approach proposed in [1-3] to achieving this goal is based on the following key observations (see Figure 78): (a) contagion, being a collective phenomenon, is, in effect, a phase transition, (b) since typically economic and competitive incentives drive system design and operation towards the boundary of this region, the continuous or discontinuous nature of the contagion emergence is of critical importance due to a possibility of occasional breach of this boundary caused by unavoidable exogenous uncertainties, and (c) discontinuous phase transitions are typically associated with existence of metastable, i.e., persistent, regimes with unacceptably high aggregate loss.

Our approach, which lies within the framework of Landau theory of phase transitions, accounts for system proximity to the boundary of the contagion-free region, nature of contagion emergence on this boundary, and time horizon of interest. We are motivated by known facts that Landau theory provides qualitatively, and sometimes even quantitatively accurate yet tractable description of system behavior in a proximity to the point of phase transitions. Currently we are attempting to quantify effect of the system time horizon of interest on the systemic risks. Qualitatively, this effect depends on the relation of the system time horizon and "life expectancy" of the system metastable equilibria.

The second focus area is evaluation/mitigation of adversarial risk in networks. Emerging communication infrastructures, including Fog/Edge computing, are expected to carry users/applications with wide range of Quality of Service (QoS) requirements. For mission-critical applications, in addition to the expected performance, these requirements also include limitations on risk of the performance deterioration below certain level. Since risk mitigation is possible at the cost of either reduced expected performance or expenditure of additional resources, e.g., transmission power in wireless networks, efficient risk mitigation should consider these inherent tradeoffs. In [4, 5] we suggest that diverse user risk tolerance levels can be incorporated into conventional network optimization frameworks by replacing user rate/throughput with the Entropic Rate at

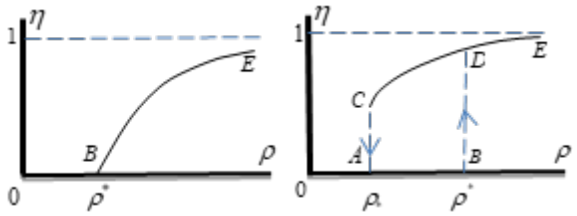

Figure 78. *Portion of system affected by contagion vs. load. Left: Continuous/gradual. Right: Discontinuous/abrupt.*

Risk (ERaR). We consider risk due to scenario-based uncertainty, where different scenarios include a "normal" scenario without jamming as well as feasible jamming scenarios. We demonstrate that ERaR user maximization results in user multi-connectivity to several Base Stations (BSs) when benefits of connectivity diversification outweigh the "inefficiencies" due to connectivity to "distant" BSs. We propose an approximate solution to ERaR maximization for risk averse users, which is based on linear interpolation between the corresponding solutions for risk neutral and extremely risk-averse users. Future research may include considering more realistic and thus more sophisticated game-theoretic models of adversarial uncertainty and developing decentralized solutions for large-scale networks.

The third focus area is risk attribution to individual network components/vulnerabilities, which is the first step in efficient risk mitigation. The challenges are due to highly non-linear contribution of individual vulnerabilities and astronomically large number of mitigation scenarios in real systems. Motivated by (a) uniqueness of Shapley-value based attribution having some desirable properties and (b) successful application of Shapley value-based attribution in various settings, including financial risk attribution, [6] proposes Shapley value-based security risk attribution to individual components/vulnerabilities. The Shapley value is a solution concept in cooperative game theory, which allocates a total surplus generated by the coalition of all players to individual players. We view potential vulnerabilities as players in a cooperative game with characteristic function, i.e., risk due to a coalition of vulnerabilities, equal to the network security risk where the rest of vulnerabilities is eliminated. Future research should address practicality of the proposed risk attribution. Of particular interest is a possibility of overcoming computational challenges for large-scale networks with recently developed approximations of Shapley value.

[1] V. Marbukh. Towards Landau Theory of Systemic Risk in Large-Scale Networked Systems: Work in Progress. In *Book of Abstracts of International School and Conference on Network Science - 7th International Winter Conference* (NetSci'22), Online, February 8-11, 2022

[2] V. Marbukh. Systemic Risk of Undesirable Contagion within System Time Horizon: Work in Progress. In *Proceedings of European Conference on Safety and Reliability* (ESREL'22), Dublin, Ireland, August 28 -September 1, 2022

[3] V. Marbukh. Towards Reliability/Security Risk Metrics for Large-Scale Networked Infrastructures: Work in Progress. In *Proceedings of the Probabilistic Safety Assessment & Management Conference* (PSAM'22), Honolulu, Hawaii, June 26 - July 1, 2022.

[4] V. Marbukh. Towards Robust Fog/Edge Computing Infrastructure with Risk Adjusted Multi-Connectivity. In *Proceeding of the 9th International Conference on Future Internet of Things and Cloud* (FiCloud'22), Rome, Italy and Online, August 22-24, 2022.

[5] V. Marbukh. Towards Risk Adjusted Wireless Access under Jamming: Reliability through Multi-Connectivity. In *Proceedings of the IEEE Consumer Communications & Networking Conference* (CCNC'22), Online, January 8-11, 2022.

[6] V. Marbukh. Towards Shapley Value based Security Risk Attribution in Sensor Networks. In *Proceedings of the IEEE/ACM Information Processing in Sensor Networks* (IPSN'22), Online, May 4-6, 2022.

Measurements of Cyber Risks in Complex Systems and Optimal Cybersecurity Investments

Richard J. La
Van Sy Mai (NIST CTL)
Abdella Battou (NIST CTL)

Modern engineered systems, such as information and communication systems and power systems, are made up of many cooperating subsystems. In order to provide their services, the subsystems must work together and support each other. However, due to this interdependence among subsystems, it is possible for a local failure or infection of a subsystem by malware to spread to other subsystems, potentially compromising the integrity of the overall system. For instance, an outage in one part of a power grid can trigger cascading failures and cause a large-scale blackout (e.g., Northeast blackout of 2003) [5].

Clearly, the structure of underlying interdependence among subsystems, which is modeled using a directed interdependence network, has significant impact on the propagation dynamics of failures or malware infections. This suggests that any sound investments in cybersecurity of complex systems or the control of epidemics should consider the interdependence in the systems and be based on a good understanding of the importance and vulnerability of each subsystem to the overall system.

With this in mind, we have studied the problem of measuring the cyber risks to subsystems, identifying more vulnerable subsystems, and finding optimal cybersecurity investments for hardening vulnerable

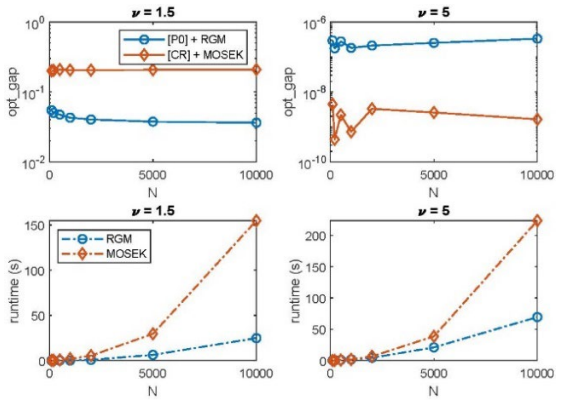

Figure 79. *Comparison of two proposed algorithms – reduced gradient method and convex relaxation-based method (solved using MOSEK) – for two different failure/infection cost parameters.*

subsystems in large systems, which will minimize the long-run average costs of a system operator. Our model accounts for both cybersecurity investments and recovery/repair costs ensuing infections or failures, which we call failure/infection costs.

In the past, we examined a scenario where malicious actors launch external attacks on a subset of subsystems under the assumption that the interdependence network is strongly connected [1, 2]. We formulated the problem of determining the optimal cybersecurity investments that minimize the average costs as an optimization problem. We proposed computationally efficient algorithms for finding good solutions with optimality bounds and sufficient conditions that guarantee the optimality of obtained solutions using a convex relaxation.

Recently, we extended our study to scenarios where the underlying interdependence network is only *weakly* connected [3], but not strongly connected. Relaxing the assumption of strong connectivity of interdependence network leads to several technical difficulties because some key results established for strongly connected networks do not hold any more. For example, the uniqueness of an equilibrium of a differential system that models the dynamics of failure/infection propagation and subsystem states is no longer guaranteed.

By studying perturbed systems and establishing the continuity of *stable* equilibria of the differential system, we were able to establish the uniqueness of a stable equilibrium of the differential system, which determines the vulnerability of each subsystem and its contribution to overall system costs at steady state for fixed cybersecurity investments. Equipped with this finding, we designed computationally efficient algorithms for computing effective cybersecurity investments. Numerical studies demonstrate that the computational requirements for the proposed methods are moderate even for large systems [3]. Furthermore, in almost all studied cases, the optimality gap is shown to be small. Finally, when the failure/infection costs are large, which are more important scenarios, our solution is provably optimal.

We also studied scenarios in which a system operator needs to decide the investments both in resilience of subsystems and in their recovery [4]. The problem of simultaneously determining these investments leads to a more challenging optimization problem. However, under a technical condition, which loosely speaking means that improving the resilience and recovery rates of complex systems is costly, we proposed two algorithms: the first algorithm is based on a reduced gradient method (RGM) and finds a locally optimal solution while avoiding the computation of inverse matrices. The second method is based on a convex relaxation (CR) of the original problem and produces a feasible point from an optimal point of CR. Moreover, we proved that the optimality gap vanishes under a sufficient condition on failure/infection costs.

Figure 79 plots the optimality gap for two scenarios we considered. The parameter ν determines the failure costs, which increase linearly with ν. The top two plots show an upper bound on the optimality gap of solutions obtained by our proposed algorithms, and the bottom two plots illustrate the runtime as a function of the size of the system (N), which is the number of subsystems. The plots suggest that, although the optimality gap is non-negligible when the failure/infection costs are small (top left plot), it vanishes for large failure/infection costs (top right plot) as predicted by our finding.

[1] V.-S. Mai, R.J. La, and A. Battou. Optimal Cybersecurity Investments for SIS Model. In *IEEE Global Communications Conference 2020*, December 2020.

[2] V.-S. Mai, R.J. La, and A. Battou. Optimal Cybersecurity Investments in Large Networks Using SIS Model: Algorithm Design. *IEEE/ACM Transactions on Networking* **29**:6 (2021), 2453-2466.

[3] V.-S. Mai, R.J. La, and A. Battou. Optimal Cybersecurity Investments Using SIS Model: Weakly Connected Networks. In *IEEE Global Communications Conference 2022,* December 2022.

[4] V.-S. Mai, R.J. La, and A. Battou. Investments in Robustness of Complex Systems: Algorithm Design. In *Complex Networks and Their Applications XI. COMPLEX NETWORKS 2022*. Studies in Computational Intelligence **1078**, Springer 2023.

[5] U.S-Canada Power System Outage Task Force. *Final Report on the August 14, 2003 Blackout in the United States and Canada: Causes and Recommendations.* April 2004. URL: https://www.energy.gov/oe/articles/blackout-2003-final-report-august-14-2003-blackout-united-states-and-canada-causes-and

Distributed Learning with Heterogeneous Datasets and Acceleration via Coordinating Server Learning

Richard J. La
Van Sy Mai (NIST CTL)
Tao Zhang (NIST CTL)

With rapid advances in sensing technologies, in many applications, a large amount of data is generated at many spatially distributed devices. For instance, autonomous vehicles equipped with multiple types of sensors, such as cameras and lidar, are expected to locally generate several terabytes of data per day. Clearly, given the volume of data, it is impractical, if not impossible, to transfer all data to a server where centralized learning can be performed. In order to deal with this issue, various forms of distributed learning have been proposed.

Among such distributed learning approaches, federated learning (FL) has recently received much attention, in particular when privacy of data is of importance [1]. In FL, a coordinating server (CS) maintains a global machine learning (ML) model that is communicated to (a subset of) clients at each round, which perform local learning using their own local datasets. Once they finish updating their local ML models, the updated models are forwarded to the CS, which then aggregates the forwarded models to update the global ML model. Since local datasets are only used to update the local ML models at the clients, no data is shared among the clients or with the CS, thereby addressing the issue of data privacy.

It has been demonstrated that FL can perform an ML task efficiently when the clients' datasets are homogeneous with similar distributions. However, when clients' datasets are heterogeneous and their distributions vary considerably, its performance can suffer significantly, leading to slow convergence or oscillations in the trained ML model. In order to address this issue, researchers proposed several different techniques. One such technique requires sharing a small set of samples among all clients.

Although data privacy is important in many applications, in some other applications it may be possible to collect a small dataset that can be used by the CS. For example, when training self-driving vehicles, automobile manufacturers may deploy a small fleet of their own vehicles that will be used to collect a small set of data and train and improve ML models. We consider such cases, where the CS can obtain a small local dataset and use it to perform local learning to improve the overall learning process. We proved that incremental learning by the CS based on even a very small dataset can help alleviate the client data distribution drifts and accelerate the learning when the current global ML is far from a (local) optimum. Moreover, the improvement is shown to depend on the server dataset distribution and its variance, which decreases with the dataset size.

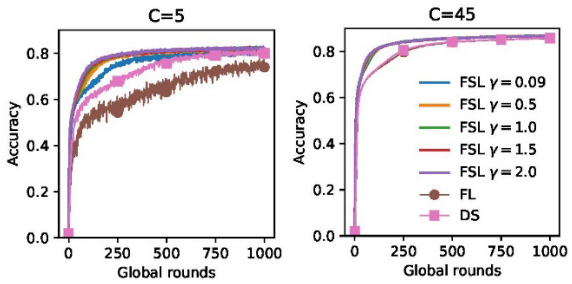

Figure 80. *Plot of test accuracy for EMNIST dataset with varying learning rates. The parameter C is the number of clients with access to samples from a single label. (FL = Federated Learning, DS = FL with data sharing among clients, FSL = FL with server learning)*

Figure 80 plots the test accuracy of a global ML model (convolutional neural network) as a function of training rounds, which is obtained using the EMNIST dataset with 45 labels. The parameter C indicates the number of clients with access to samples from a single label. A smaller value of C implies more heterogeneous datasets at the clients. There are 45 clients. Each client hosts a local dataset consisting of 2400 samples, and the CS has a local dataset with 225 samples. The CS selects 4 clients (out of 45 clients) for updating the ML model during each round.

As expected, when all clients have access to samples from all 45 labels (right plot), the performance of all algorithms is similar because clients' local datasets are homogeneous in this case. On the other hand, when the client datasets are highly heterogeneous (left plot), FL suffers significantly, while data sharing among clients (DS) improves the accuracy significantly over FL. However, our proposed algorithm (FSL) provides a considerable improvement over both DS and FL despite a very small dataset used by the server with only 225 samples. In addition, the performance of the proposed algorithm does not change much with a varying parameter value (γ) of our proposed algorithm, suggesting its robustness to suboptimal choices of the parameter value.

[1] B. McMahan, E. Moore, D. Ramage, S. Hampson, and B.A. y Arcas. Communication-efficient Learning of Deep Networks from Decentralized Data. In *the 20th International Conference on Artificial Intelligence and Statistics*, April 2017.

[2] V.S. Mai, R.J. La, and T. Zhang. Federated Learning with Server Learning: Enhancing Performance for Non-IID Data. Preprint arXiv:2210.02614, 2022.

Combinatorial Testing for Software Based Systems

Raghu N. Kacker
James F. Lawrence (ACMD)
D. Richard Kuhn
M. S. Raunak (NIST ITL)
Yu Lei (University of Texas at Arlington)
Dimitris E. Simos (SBA-Research, Austria)
Eric Wong (University of Texas at Dallas)
Itzel Dominguez-Mendoza (CENAM, Mexico)

https://csrc.nist.gov/projects/automated-combinatorial-testing-for-software

In 1997, the Mars Pathfinder began experiencing system resets at seemingly unpredictable times soon after it landed and began collecting data. Fortunately, engineers were able to deduce and correct the problem, which occurred only when (1) a particular type of data was being collected, and (2) intermediate priority tasks exceeded a certain load, resulting in a blocking condition that eventually triggered a reset. Situations of this type are known as interaction faults. Many real-time failures of software-based systems have been traced to such faults. These are often insidious in that they may remain hidden until the unfortunate combination is encountered during system operation.

Combinatorial testing (CT) is a versatile methodology for detecting interaction faults. CT began as pairwise (2-way) testing in which all pairs of the test values for all pairs of test factors are checked. Thus, pairwise testing can detect faults involving single factors or interactions between two factors. CT is based on an empirical observation, referred to as the interaction rule, that while the behavior of a software system may be affected by many factors, only a few are involved in any given failure. NIST investigations of failures in actual systems have shown that while most faults involved a single factor or interaction between two factors, some faults involved three or more factors [1]. (A fault involving more than six factors has not yet been reported.) Thus, pairwise testing is useful, but it may not be adequate for detecting interaction faults involving more than two test factors.

More than a decade ago, NIST took the initiative to extend pairwise (2-way) CT to higher strength t-way CT for t > 2. NIST has helped make CT practical by developing research tools and techniques for generating combinatorial test suites. CT has now gained significant interest from the international software testing community. Many successful results from the use of CT in aerospace, automotive, and financial service industries, as well as defense, security, and electronic medical systems have since been reported

A suite of test cases for combinatorial *t*-way testing includes (covers) at least once all possible *t*-tuples of the test values for every set (combination) of *t* factors out of the complete set of all *k* factors that are tested ($k > t$). Use of mathematical objects called covering arrays makes it possible to check all *t*-tuples of the test values with a small number of test cases. Table 2 shows a covering array of 13 rows and 10 columns each having two possible value 0 and 1. Columns correspond to the factors and the rows correspond to the test cases. The number of possible sets (combinations) of 3 out of 10 test factors is $(10 \times 9 \times 8)/(3 \times 2 \times 1) = 120$. When each factor has two possible values, each set of 3 factors can have $2^3 = 8$ possible triples of test values ((0, 0, 0), (0, 0, 1), (0, 1, 0), (0, 1, 1), (1, 0, 0), (1, 0, 1), (1, 1, 0), (1, 1, 1)). So, the total number of possible triples of values for all 10 factors is $120 \times 8 = 960$. A test suite based on Table 1 includes ("covers") at least once all 960 distinct triples of the test values of ten factors.

In practice, one wants a minimal covering array, that is an array which covers all possible *t*-tuples of the test values for every set of *t* out of all *k* factors with the least number of rows (test cases). In practice, many factors have dependencies and constraints, and hence not all combinations of the test values may be logically or physically valid. A combinatorial test suite must avoid such forbidden combinations. Generating minimal covering arrays that avoid forbidden combinations is a difficult computational problem [2]. A great deal of research has been done to develop mathematical and computational methods to generate minimal covering arrays of this type. NIST and its collaborators have developed several such algorithms.

NIST-Developed Tools. NIST has developed several research tools to make CT practical. ACTS (for Automated Combinatorial Testing for Software), which was developed in cooperation with the University of Texas at Arlington, includes several algorithms to generate high strength test suites for CT. The ACTS algorithms are optimized to efficiently avoid forbidden combinations of test settings. More than 4545 users have downloaded executable versions of the ACTS algorithms from the NIST webpage for CT. (It is difficult to ascertain the number of users because some users have redistributed to others, and some are students who may have used it only once for a single project.)

A second research tool, CCM (for Combinatorial Coverage Measurement), developed jointly by NIST and a guest researcher from CENAM, the national metrology institute of Mexico, describes the incompleteness of a test suite that may not have been developed from a CT viewpoint. Basic combinatorial coverage measurements describe the incompleteness of a test suite relative to a test suite based on a covering array that includes all possible *t*-tuples of values for every *t*-factor combination for various values of *t*. The combinatorial deficiency of a test suite can be remedied by additional tests. Thus, CCM can help guide the expansion of a test suite to satisfy stated combinatorial

Table 2. *A covering array of 13 rows includes all eight triplets (000, 001, 010, 011, 100, 101, 110, and 111) of the possible values (0 and 1) for every one of the 120 possible sets of 3 out of 10 test factors represented by the columns (for example, see colored entries)*

	Columns									
Rows	**1**	**2**	**3**	**4**	**5**	**6**	**7**	**8**	**9**	**10**
1	0	0	0	0	0	0	0	0	0	0
2	1	1	1	1	1	1	1	1	1	1
3	1	1	1	0	1	0	0	0	0	1
4	1	0	1	1	0	1	0	1	0	0
5	1	0	0	0	1	1	1	0	0	0
6	0	1	1	0	0	1	0	0	1	0
7	0	0	1	0	1	0	1	1	1	0
8	1	1	0	1	0	0	1	0	1	0
9	0	0	0	1	1	1	0	0	1	1
10	0	0	1	1	0	0	1	0	0	1
11	0	1	0	1	1	0	0	1	0	0
12	1	0	0	0	0	0	0	1	1	1
13	0	1	0	0	0	1	1	1	0	1

requirements [3]. The latest version of CCM supports constraints which exclude forbidden combinations of values. A parallel processing version is also available.

Impact of NIST Research. NIST efforts have sparked a surge of research and application of combinatorial testing technology. A 2010 NIST Special Publication on CT was downloaded more than 30 000 times by the end 2014 [4]. In 2013, we published a book with Chapman and Hall/CRC Press on this topic [5]. One of the first large-scale users that we worked with is a group at the U.S. Air Force Base in Eglin, Florida. The behavior of one of their systems depended on the sequential order of certain events. This led to the problem of testing sequences of events, which required development of new mathematical objects called *sequence covering arrays* [6, 7, 8]. Lockheed-Martin, a large U.S. defense contractor, reported (based on eight projects) that use of CT reduced cost of testing by about 20 % with 20 % to 50 % improvement in test coverage [9]. CT methods are now being used in diverse areas such as financial services, automotive, automation, avionics, video coding standards, and for security testing. The NIST webpage for CT cites over forty application papers. For testing a software-based system, no single approach is enough. Plural approaches are generally needed at various stages of software development and installation. CT complements other approaches for testing, verification, and validation of software-based systems. CT is now included in software engineering courses taught in many universities. NIST efforts on technology transfer of CT tools and techniques received the 2009 Excellence in Technology Transfer Award from the Federal Laboratory Consortium-Mid Atlantic Region.

CT has also gained significant interest from the research community. In 2012, NIST took lead in organizing a workshop on CT[22] in conjunction with the 2012 IEEE International Conference on Software Testing, Verification, and Validation (ICST), a premier conference in this field. Since then, an International Workshop on Combinatorial Testing (IWCT) has become an annual event for sharing advancements in CT tools and techniques, as well as results from practical industrial use of CT. The eleventh such IWCT[23] was held (virtually because of the worldwide COVID-19 pandemic) on April 4, 2021, in conjunction with ICST 2022[24]. Four of us (Kacker, Kuhn, Lei, and Simos) were among the co-organizers. The IWCT 2022 received 14 submissions, out of which 10 were research papers and four were on tools relating to combinatorial testing. The Program Committee accepted 8 of the 10 research papers. All four tools-papers were accepted.

Recent Accomplishments.

Combinatorial testing-based approaches to fault localization for explainable artificial intelligence [10]: We briefly reviewed the properties of explainable artificial intelligence (AI) proposed by various researchers. We took a structural approach to the problem of explainable AI, examining the feasibility of these aspects, and extending them where appropriate. Afterwards, we reviewed combinatorial methods for explainable AI which are based on combinatorial testing-based approaches to fault localization. Finally, we view the combinatorial methods for explainable AI through the lens provided by the properties of explainable AI. We pose resulting research questions that need to be answered and point towards possible solutions, which involve a hypothesis about a potential parallel between software testing, human cognition, and brain capacity.

A two-step TLS-based browser fingerprinting approach using combinatorial sequences [11]: The term browser fingerprinting describes the process and the corresponding methods for collecting data about a user's browser and system, often with the goal of uniquely identifying a browser. The term Transport Layer Security (TLS) describes a set of protocols that are designed to secure the communication between two applications. We proposed a two-step TLS-based fingerprinting approach using combinatorial sequences and properties of TLS handshake messages. Our approach combines fingerprinting based on attributes of the initial ClientHello message with the observed behavior of TLS clients when presented with permuted handshake messages to enhance

[22] http://www.research.ibm.com/haifa/Workshops/ct2012/
[23] https://icst2022.vrain.upv.es/home/iwct-2022
[24] https://icst2022.vrain.upv.es/

the granularity of the derived fingerprints without increasing the required number of exchanged messages. We conducted a detailed evaluation against 21 browsers and TLS clients on two operating systems. The presented two-step approach decreases the size of the anonymity sets and increases the entropy of the splitting, allowing for a more precise identification of the TLS client either of the underlying approaches in isolation.

Combinatorial test generation for multiple input models with shared parameters [12]: We addressed the problem of test generation for multiple input models with shared parameters. An approach to generate multiple test sets, one for each input model, that together satisfy *t*-way coverage for all these input models while minimizing the redundancy between these test sets is proposed. An experimental evaluation on five applications shows that redundancy can be significantly reduced.

Combinatorial methods for testing IoT smart home systems [13]: We proposed and evaluated an approach for applying combinatorial testing to Internet of Things (IoT) home automation hub systems. We developed a corresponding test execution framework, which also contains the implementation of the design of two proposed test oracles for this work. We evaluated our approach on a real-world instance of an IoT home automation hub system running the (open source) software HA on the hub. The experiments included *t*-way test sets with interaction strength ranging from one to four and variable-strength covering arrays corresponding to groups of similar primitives present in the IoT home automation hub system. We also executed two random test sets for every combinatorial test set as a means for a comparison. Obtained testing results show that most test sets were able to find (i.e., trigger) all unique structural errors and that increasing the interaction strength of executed *t*-way test sets yielded an increase of both the total number of triggered errors as well as in the number of unique errors revealed by the combinatorial test sets. Timing and resource constraints prohibited a detailed combinatorial fault analysis. A comparison with the random test sets shows that they performed equally well.

A combinatorial testing-based path selection framework for effective IoT testing [14]: Testing IoT systems is challenging. This is not only because of the various aspects of IoT systems, such as software, hardware, and network that need to be tested, but also because of the unexpected issues caused by many heterogeneous devices brought together by IoT systems. When an IoT system has hundreds, or even thousands, of heterogeneous devices, which devices should be tested to detect more faults? How can we systematically test an IoT system and its numerous devices in a cost-effective way? Are there any coverage criteria for testers to evaluate the thoroughness of the testing against IoT systems? We developed and investigated the performance of a combinatorial testing path selection framework for IoT systems. The framework called CT-IoT systematically identifies and recommends testing paths in IoT systems for effective testing. We also propose four coverage criteria that can help testers evaluate the testing thoroughness for IoT systems. We conducted an empirical study of CT-IoT on two real-world IoT systems and evaluated the effectiveness of CT-IoT in terms of coverage achievements. The results show the superiority of CT-IoT over a random approach.

Measurement of the adequacy of a test suite with respect to the modeled test space [15]: The adequacy of a test suite is typically assessed with respect to, for example, requirements coverage or code coverage. This paper presents a metric for the adequacy of a test suite with respect to the modeled test space. A test suite that does not include at least all possible pairs (or triples) of test values is likely inadequate because system failures may involve more than a single parameter.

The path to consensus on artificial intelligence (AI) assurance [16]: To ensure the wide-scale adoption of intelligent algorithms, artificial intelligence (AI) engineers must offer assurances that an algorithm will function as intended. Providing such guarantees involves quantifying capabilities and the associated risks across multiple dimensions, including data quality, algorithm performance, statistical considerations, trustworthiness, and security as well as explainability. 1. Assurance should not be an afterthought; rather, it should be embedded into the lifecycle of development and learning in all AI systems. Recent developments such as surrogate models constitute a positive development toward achieving incremental assurance. 2. Current AI models are almost exclusively statistical, that is, they don't have the ability to grasp or represent context. We deem this contextual aspect critical to the future of AI and its assurance. 3. Consider counterfactual scenarios for AI algorithms: at the end of the day, if AI algorithms cannot explain cause and effect, they may be rendered obsolete by the next big technology. 4. It has been suggested that a system validating a learning algorithm will be as complex as the learning system. Thus, the research and development of AI-assurance approaches needs to receive attention comparable to AI applications research.

Evaluation of t-way testing of DNNs in autonomous driving systems [17]: A Deep Neural Network (DNN) model is used to perform intelligent, safety-critical tasks in Autonomous Driving Systems (ADS). Previously, we proposed a combinatorial testing approach to test DNN models used to predict a car's steering angle. We generate test images by applying a set of combinations on basic image transformations. DeepTest, is a state-of-the-art tool that aims at generating test inputs that maximize neuron coverage. We compared the performance of synthetic images generated using our combinatorial approach to DeepTest. We measured and compared the

neuron coverage achieved using the two approaches. Two pre-trained DNN models from the Udacity (an open-source self-driving car project) driving challenge are used as the subject DNNs. In most cases, the results suggest that the synthetic images generated using the combinatorial approach cover more neurons than the DeepTest approach.

Developing multithreaded techniques and improved constraint handling for the tool CAgen [18]: CAgen is a fast combinatorial test generation tool. It supports an extensive list of features such as constraint handling, higher-index arrays, and import and export of models/test sets in various formats. It is based on the Fast IPO (FIPO) algorithm, which can be considered an improved version of the widely used In-Parameter-Order (IPO) strategy on which the popular ACTS tool is based. To further speed up CAgen, this work first discusses how multithreading can be effectively used to optimally utilize available resources, particularly for large instances. We evaluated three different multithreaded variations of the horizontal extension and used the insights obtained to design the mFIPOG algorithm. In addition, we adopted methods that have previously been utilized to speed up constraint handling of CSP solvers in IPO algorithms into a forbidden tuple approach. To evaluate the performance of the improved tool, we offer results on various benchmarks.

Combinatorial approach to fairness testing of machine learning models [19]: Machine Learning (ML) models can have behaviors which result in unfair or discriminatory outcomes. The bias in the ML model could emanate from various factors such as the training dataset, the choice of the ML algorithm, or the hyperparameters used to train the ML model. In addition to evaluating the model's correctness, it is essential to test ML models for fair and unbiased behavior. In this paper, we present a combinatorial testing-based approach to perform fairness testing of ML models. Our approach is model agnostic and evaluates fairness violations of a pre-trained ML model in a two-step process. First, we create an input parameter model from the training data set and then use the model to generate a *t*-way test set. In the second step, for each test, we modify the value of one or more protected attributes to see if we could find fairness violations. We performed an experimental evaluation of the proposed approach using ML models trained with tabular datasets. The results suggest that the proposed approach can successfully identify fairness violations in pre-trained ML models.

Combination frequency differencing for identifying design weaknesses in physical unclonable functions [20]: Combinatorial coverage measures have been defined and applied to a wide range of problems. These methods have been developed using measures that depend on the inclusion or absence of *t*-tuples of values in inputs and test cases. We have extended these coverage measures to include the frequency of occurrence of combinations, in an approach that we refer to as combination frequency differencing (CFD). This method is particularly suited to artificial intelligence and machine learning (AI/ML) applications, where training data sets used in learning systems are dependent on the prevalence of various attributes of elements of class and non-class sets. We illustrate this method by applying it to analyzing the susceptibility of physical unclonable functions (PUFs) to machine learning attacks. Preliminary results suggest that the method may be useful for identifying bit combinations that have a disproportionately strong influence on PUF response bit values.

We are continuing research involving use of combinatorial methods for explainable artificial intelligence, machine learning models, model debugging, security of smart contracts, cybersecurity, and risk factors identification. The research includes development of supporting tools.

[1] D. R. Kuhn, D. R. Wallace, and A. M. Gallo, Jr. Software Fault Interactions and Implications for Software Testing. *IEEE Transactions on Software Engineering* **30** (2004), 418-421. DOI: 10.1109/TSE.2004.24

[2] L. Kampel and D. E. Simos. A Survey on the State of the Art of Complexity Problems for Covering Arrays. *Theoretical Computer Science* **800** (2019), 107-124. DOI: 10.1016/j.tcs.2019.10.019

[3] D. R. Kuhn, R. N. Kacker and Y. Lei. Combinatorial Coverage as an Aspect of Test Quality. *CrossTalk: The Journal of Defense Software Engineering* (March/April 2015), 19-23.

[4] D. R. Kuhn, R. N. Kacker, and Y. Lei. Practical Combinatorial Testing. NIST Special Publication 800-142, October 2010, National Institute of Standards and Technology, Gaithersburg, Maryland. URL: http://nvlpubs.nist.gov/nistpubs/Legacy/SP/nistspecialpublication800-142.pdf

[5] D. R. Kuhn, R. N. Kacker, and Y. Lei. *Introduction to Combinatorial Testing.* CRC Press, 2013.

[6] D. R. Kuhn, J. M. Higdon, J. F. Lawrence, R. N. Kacker and Y. Lei. Combinatorial Methods for Event Sequence Testing. In *Proceedings of the 5-th IEEE International Conference on Software Testing, Verification and Validation Workshops* (ICSTW), Montreal, Quebec, Canada, April 17-21, 2012, 601-609. DOI: 10.1109/ICST.2012.147

[7] D. R. Kuhn, J. M. Higdon, J. F. Lawrence, R. N. Kacker and Y. Lei. Efficient Methods for Interoperability Testing using Event Sequences. *CrossTalk: The Journal of Defense Software Engineering* (July/August 2012), 15-18. URL: https://apps.dtic.mil/docs/citations/ADA566540

[8] Y. M. Chee, C. J. Colbourn, D. Horsley, and J. Zhou. Sequence Covering Arrays. *SIAM Journal of Discrete Mathematics* **27** (2013), 1844-1861. DOI: 10.1137/120894099

[9] J. Hagar, D. R. Kuhn, R. N. Kacker, and T. Wissink. Introducing Combinatorial Testing in a Large Organization. *IEEE Computer* **48** (2015), 64-72. DOI: 10.1109/MC.2015.114

[10] L. Kampel, D. E. Simos, D. R. Kuhn, and R. N. Kacker. An Exploration of Combinatorial Testing-based Approaches to Fault Localization for Explainable AI. *Annals of Mathematics and Artificial Intelligence* (AMAI) **90** (2021), 951-964. DOI: 10.1007/s10472-021-09772-0

[11] B. Garn, D. E. Simos, S. Zauner, D. R. Kuhn, and R. N. Kacker. A Two-Step TLS-Based Browser Fingerprinting Approach using Combinatorial Sequences. *Computers & Security* **114** (2022), 102575. DOI: 10.1016/j.cose.2021.102575

[12] C. Rao, N. Li, Y. Lei, J. Guo, Y. Zhang, R. N. Kacker, and D. R. Kuhn. Combinatorial Test Generation for Multiple Input Models with Shared Parameters. *IEEE Transactions on Software Engineering* **48** (2022), 2606-2628. DOI: 10.1109/TSE.2021.3065950

[13] B. Garn, D. P. Schreiber, D. E. Simos, D. R. Kuhn. J. Voas, and R. N. Kacker. Combinatorial Methods for Testing IoT Smart Home Systems, *Journal of Software, Testing, Verification and Reliability* **32** (2022), 1805. DOI: 10.1002/stvr.1805

[14] L. Hu, W. E. Wong, D. R. Kuhn, R. N. Kacker, and S. Li. CT-IoT: A Combinatorial Testing-Based Path Selection Framework for Effective IoT Testing. *Empirical Software Engineering* **27** (2022), 32. DOI: 10.1007/s10664-021-10017-1

[15] R. N. Kacker, D. R. Kuhn, Y. Lei, and D. E. Simos. Measurement of the Adequacy of a Test Suite with Respect to the Modeled Test Space. *IEEE Software* **39** (September-October 2022), 62-67. DOI: 10.1109/MS.2021.3108060

[16] L. Freeman, F. Batarseh, D. R. Kuhn, M. S. Raunak, and R. N. Kacker. The Path to Consensus on Artificial Intelligence Assurance. *IEEE Computer* **55** (March 2022), 82-86. DOI: 10.1109/MC.2021.3129027

[17] J. Chandrasekaran, A. R. Patel, Y. Lei, R. N. Kacker, and D. R. Kuhn, Evaluation of t-way Testing of DNNs in Autonomous Driving Systems. In 2021 *IEEE International Conference on Artificial Intelligence Testing*, Oxford, UK, August 23-26, 2021, 17-18. DOI: 10.1109/AITEST52744.2021.00013

[18] M. Wagner, M. Leithner, D. E. Simos, D. R. Kuhn, and R. N. Kacker. Developing Multithreaded Techniques and Improved Constraint Handling for the Tool CAgen. In 2022 *IEEE International Conference on Software Testing, Verification and Validation Workshops* (ICSTW) Valencia, Spain, April 4-13, 2022, 87-93. DOI: 10.1109/ICSTW55395.2022.00029

[19] A. R. Patel, J. Chandrasekaran, Y. Lei, R. N. Kacker, and D. R. Kuhn. A Combinatorial Approach to Fairness Testing of Machine Learning Models. In 2022 *IEEE International Conference on Software Testing, Verification and Validation Workshops* (ICSTW) Valencia, Spain, April 4-13, 2022, 94-101. DOI: 10.1109/ICSTW55395.2022.00030

[20] D. R. Kuhn, M. S. Raunak, C. B. Prado, V. Patil, and R. N. Kacker. Combination Frequency Differencing for Identifying Design Weaknesses in Physical Unclonable Functions. In 2022 *IEEE International Conference on Software Testing, Verification and Validation Workshops* (ICSTW) Valencia, Spain, April 4-13, 2022, 110-117. DOI: 10.1109/ICSTW55395.2022.00032

Impact of Using Soft Exposure Thresholds in Automatic Contact Tracing

Kamran Sayrafian
Brian Cloteaux
Vladimir Marbukh

The automatic exposure notification apps primarily operate based on the hard distance/time thresholds outlined by the health organizations (e.g., 2 m/15 min by the CDC or 1 m/ 15 min by the WHO) to determine exposures as a result of close contacts. However, the possibility of virus transmission through inhalation for distances over two meters might necessitate consideration of a soft distance/time threshold to accommodate all transmission scenarios. In addition, higher transmissibility of the virus variants (such as Omicron) might also require consideration of longer (or shorter) distances/time threshold for exposure determination. Ultimate exposure determination depends on the amount of virus inhaled by the exposed individual; however, there are no simple methodology to ascertain that amount in practice.

Accurate mathematical representation of the spatial distribution of the virus density over distance depends on many factors and scenarios. In this project, using a simplifying approximation of the instantaneous rate of the viral exposure versus distance, we extend the definition of "contact" by proposing a soft distance/time threshold shown in Figure 81. This soft threshold naturally allows the possibility of getting exposed at any distance (within certain limits) around an infected person. By including the CDC exposure guidelines (i.e., 2 m/15 min), the boundary function for exposure zone can be expressed by the following equation:

$$T(D) = \begin{cases} 15(D/2)^{\alpha} & if \quad D \geq d_{min} \\ 15(d_{min}/2)^{\alpha} & if \quad D < d_{min} \end{cases}$$

where α is a parameter that specifies the rate at which viral particles decay with distance. In the simplest scenario, assuming a spherical spatial distribution of viral particles in the space surrounding the source, α may be approximated by 2. However, many environmental characteristics such as obstacles along the exhalation path, indoor vs. outdoor, air flow quality, or even temperature may impact the actual value of α. For example, at indoor environments with low air circulation, the value of α may be much lower than outdoor environments. In addition, α could also be a function of distance itself as droplets may dissipate differently with increasing distance compared to aerosols. The impact of α on the soft threshold (i.e., boundary of the exposure zone) is also shown in Figure 81. As observed, the size of the exposure zone depends on the values of α.

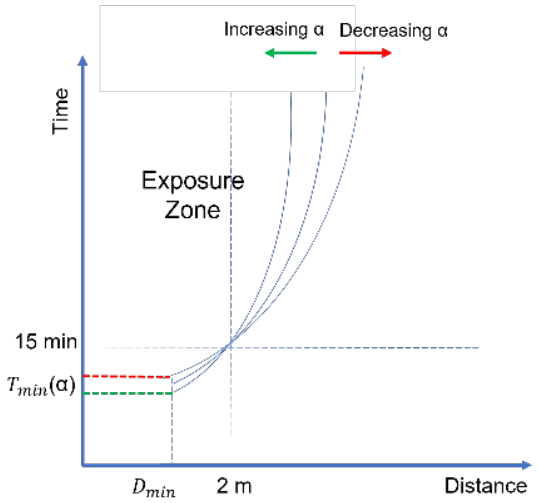

Figure 81. *Exposure zone based on soft thresholds.*

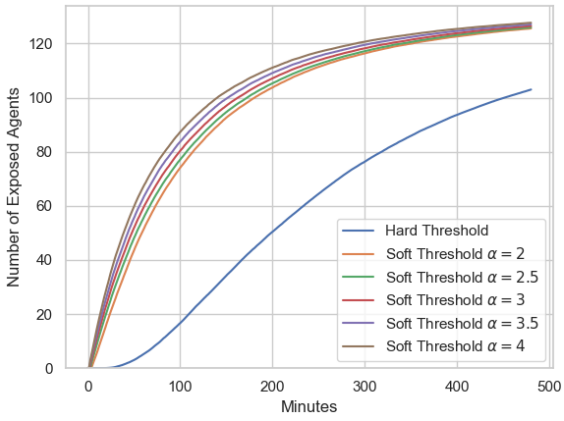

Figure 82. *Impact of* $\boldsymbol{\alpha}$ *on the number of exposed agents when* $\boldsymbol{d_{min} = 1\ m}$

Another parameter to consider when using soft thresholds is d_{min}. It indicates the minimum distance below which the required exposure time for occurrence of a 'contact" does not decrease. A value of $d_{min} < 2$ meters would represent scenarios where less than 15 minutes are sufficient for positive exposure determination. It should be noted that when $d_{min} = 2$ m, increasing value of α would cause the soft threshold exposure zone to asymptotically converge to the exposure zone defined by the hard thresholds (i.e., CDC guidelines).

In this project, we analyze the performance of automatic exposure notification with BLE-based proximity detection by comparing the exposure results when soft or hard thresholds are used. This study is done through an enhanced agent-based simulation platform which was originally presented in [1, 2]. Figure 82 shows the number of exposed agents versus time for the soft exposure threshold with parameter $\alpha = 2, 2.5, 3, 3.5, 4$ as well as the hard thresholds of 2 m/15 min (per CDC guidelines). Here, it is also assumed that $d_{min} = 1\ m$ and the average conversation length between agents is set to 3 min. As observed, the number of exposed agents is noticeably more at any given time during the simulation when a soft threshold is used. In addition, this number grows faster for higher values of α. Although this may be counterintuitive, but the trend versus α depends on many factors such as d_{min}, agents mobility pattern, average conversation length, and population density. For $d_{min} < 2$, as shown in Figure 82, the change in the size of the exposure zone below the 15 min threshold as α changes will impact all agents that fall within the range [d_{min}, 2 m]. When α increases, the size of that zone will increase as well. This will result in higher number of exposed agents, especially when the mobility pattern of the agents leads to more occurrence of agents within that exposure zone.

By tuning the parameters of the proposed soft thresholds, a more accurate determination of possible exposures at any distance would be possible. This flexibility would allow optimization of the soft threshold parameters based on factors such as the surrounding environment (e.g., indoor vs. outdoor), an individual's health, the severity of the outbreak in the community, etc. Further details and results can be found in [3].

[1] K. Sayrafian, B. Cloteaux, V. Marbukh, and C. Emiyah Evaluation of the Bluetooth-based Proximity Estimation for Automatic Exposure Determination. In *IEEE Consumer Communications & Networking Conference (IEEE CCNC)*, Online, Jan. 8-11, 2022.

[2] K. Sayrafian, B. Cloteaux, and V. Marbukh. On the Performance of Automatic Exposure Determination Using Bluetooth-based Proximity Estimation. In *IEEE International Conference on Communications* (ICC 2022), Seoul, South Korea, May 16-20, 2022.

[3] K. Sayrafian, B. Cloteaux, and V. Marbukh. Impact of Using Soft Exposure Thresholds in Automatic Contact Tracing. In *IEEE International Conference on E-health Networking, Application & Services* (IEEE HEALTHCOM 2022), Genoa, Italy, Oct. 17-19, 2022.

Maximizing Harvested Energy in Coulomb Force Parametric Generators

Kamran Sayrafian
Masoud Roudneshin (Concordia University, Canada)
Amir G. Aghdam (Concordia University, Canada)

Energy harvesting (EH) refers to the process of capturing ambient energy from the surrounding environment and converting it into electric energy. A variety of sources such as light, wind, sea waves, heat, and vibrations may be utilized for this conversion. Micro energy-

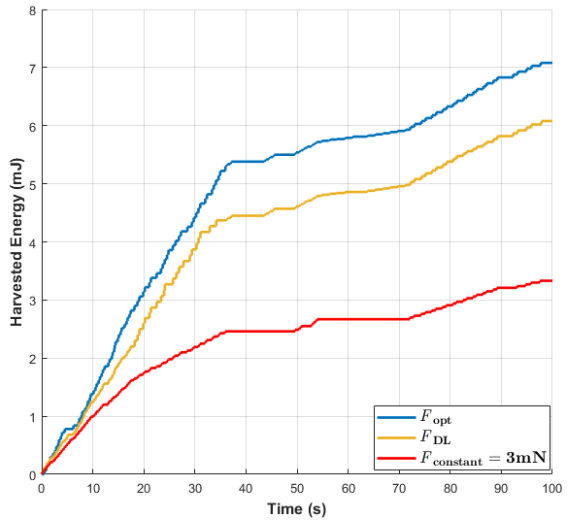

Figure 83. *Harvested energy for the proposed deep learning method compared to the optimal and a sample constant holding force.*

harvesters (MEH), also called micro-generators, typically refer to the class of miniaturized energy harvesting devices that can augment or replace batteries in small low-power electronics. An important application area for micro energy-harvesters includes wearable or implantable medical sensors or actuators [1]. Since frequent recharge or battery replacement may not be practical (or even feasible for medical implants), integrating micro energy-harvesters with such sensors/actuators could provide a viable solution to extend their operational lifetime.

Several fabrication techniques and architectures for kinetic MEH have been presented and discussed in the literature [2]. Among the architectures, the Coulomb force parametric generators (CFPG) can harvest the most amount of energy from nonstationary vibration as shown in [3]. Therefore, this architecture is favorable for harvesting kinetic energy from the human body as a non-vibrating source of movements. CFPG uses an electrostatic force as part of its architecture to generate energy. This electrostatic force is typically kept constant. However, by adaptively changing its value for various human body motions, it is expected to increase the amount of harvested energy for wearable and implant sensors. The adjustment of this electrostatic force within the micro-generator hardware can be done by tuning the electric field between the CFPG's capacitive electrodes.

In this project, we investigate various techniques to adaptively optimize the electrostatic force in a CFPG and evaluate the resulting gain in the output power. The proposed techniques include deep learning (DL), least square methods and an approximate analytical approach. The performance of these techniques is evaluated for sample measured acceleration data representing various human activities. To the best of our knowledge, output power maximization of CFPG through adaptive electrostatic force has not been comprehensively studied before.

Assuming that the electrostatic force can be adjusted at regular time intervals, the objective is to estimate its optimal value at each interval to maximize the average harvested power. The optimal electrostatic force would be a function of the length of this time interval and the input acceleration waveform during the interval. In practice, the estimated optimal electrostatic force can be obtained based on the input acceleration samples during the immediate past time interval. This is possible due to the inherent temporal correlation in the human body motion.

One methodology to estimate the optimal value of the electrostatic force is using Deep Learning (DL). DL is a type of machine learning based on artificial neural networks (ANN) in which multiple layers of processing are used to establish a relationship between sensory stimuli and the output. In other words, DL can be used to uncover the underlying mapping function from the input data to a desired output. A four-layer neural network is proposed to represent the mapping from the input acceleration waveform to the desired electrostatic force. Each node in this architecture, except the nodes on the first hidden layer, applies a nonlinear activation function to the weighted sum of its inputs, and then passes the output to the next layer. Tangent hyperbolic has been chosen as the activation function of our proposed DL approach. The inputs to the ANN are samples of the acceleration waveform in time. The ANN output is the estimated electrostatic force that will be used for the next time interval. Using an adaptation interval of 2 sec and a sampling rate of 10 Hz, Figure 83 demonstrates the amount of the harvested energy with the proposed deep learning method compared to the optimal and a constant electrostatic force=3 mN. As observed, this method performs significantly better than the constant electrostatic force and achieving 85% of the maximum power harvested under the optimal scheme. Further details and results can be found in [4].

Although the proposed ANN results in a significant increase in the harvested power, it also involves a high computational complexity for implementation. This complexity could reduce the overall gain in the output power of the micro-generator. Note that estimating the required computational power for each adaptation method is essential to determine the net gain in the harvested energy. Approximation of the input acceleration waveform with few frequency components and implementation of the deep learning approach in the frequency domain is a possible future research direction. In addition, studying the impact of the length of the adaptation interval and discretization of the holding force on the harvested power is another topic of interest for further research.

[1] D. Budic, D. Simuni, and K. Sayrafian. Kinetic-Based Micro Energy-Harvesting for Wearable Sensors. In *6th IEEE International Conference on Cognitive Infocommunications* (CogInfoCom), 2015.

[2] P. D. Mitcheson, T. Sterken, C. He, E. M. Kiziroglou, E. M. Yeatman, and R. Puers. Electrostatic Microgenerators. *Measurement and Control* **41**:4 (2008), 114–119.

[3] P. D. Mitcheson. Analysis and Optimisation of EnergyHarvesting Micro-Generator Systems. Ph.D. Dissertation, Imperial College London, 2005.

[4] M. Roudneshin, K. Sayrafian, and A. G. Aghdam. Maximizing Harvested Energy in Coulomb Force Parametric Generators. In *IEEE American Control Conference* (IEEE ACC), Atlanta, GA, USA, June 8-10, 2022.

Mathematical Knowledge Management

We work with researchers in academia and industry to develop technologies, tools, and standards for representation, exchange, and use of mathematical data. Of particular concern are semantic-based representations which can provide the basis for interoperability of mathematical information processing systems. We apply these representations to the development and dissemination of reference data for applied mathematics. The centerpiece of this effort is the Digital Library of Mathematical Functions, a freely available interactive and richly linked online resource, providing essential information on the properties of the special functions of applied mathematics, the foundation of mathematical modeling in all of science and engineering.

Digital Library of Mathematical Functions

Barry I. Schneider
Bruce R. Miller
Bonita V. Saunders
Howard S. Cohl
Marjorie A. McClain
Daniel W. Lozier
Ronald F. Boisvert
Charles W. Clark (NIST PML)
Adri B. Olde Daalhuis (University of Edinburgh)
Gergő Nemes (Alfréd Rényi Inst. of Mathematics, Hungary and Tokyo Metropolitan U., Japan)
Wolter Groenvelt (Delft University of Technology)
Tom Koornwinder (University of Amsterdam)
Yuan Xu (University of Oregon)
Bill Reinhardt (University of Washington)

http://dlmf.nist.gov/

Progress in science has often been catalyzed by advances in mathematics. More recently, developments in the physical sciences, such as investigations into string theory, have influenced pure mathematics. This relationship has been extremely beneficial to both fields. Mathematical developments have found numerous applications in practical problem-solving in all fields of science and engineering, while cutting-edge science has been a major driver of mathematical research**.** Often, the mathematical objects at the intersection of mathematics and physical science are mathematical functions. Effective use of these tools requires ready access to their many properties, a need that was capably satisfied for more than 50 years by the *Handbook of Mathematical Functions with Formulas, Graphs, and Mathematical Tables*, which was published by the National Bureau of Standards (NBS) in 1964 [1].

The 21st century successor to the NBS Handbook, the freely accessible online Digital Library of Mathematical Functions (DLMF) together with the accompanying book, the *NIST Handbook of Mathematical Functions* [2], published by Cambridge University Press in 2010, are collectively referred to as the DLMF.

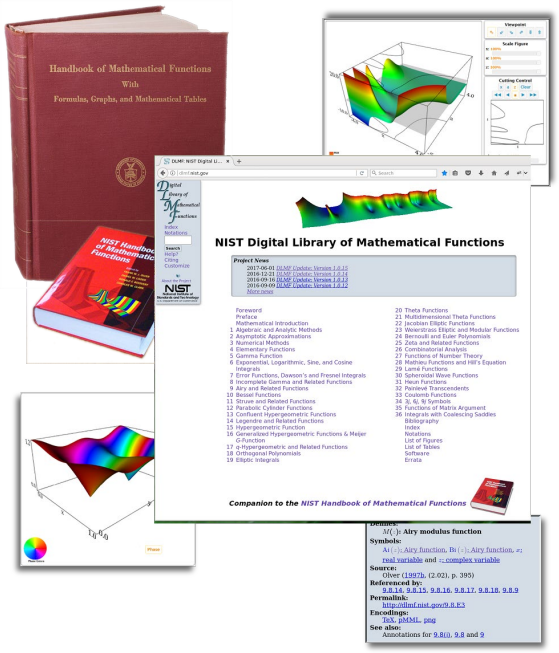

Figure 84. *A visual history of the DLMF from its roots in the 1964 NBS Handbook to the graphical contents of the present DLMF.*

The DLMF continues to serve as the gold standard reference for the properties of the special functions of applied mathematics.

The DLMF has considerably extended the scope of the original handbook as well as improving accessibility to the worldwide community of scientists and mathematicians. To cite a few examples, the new handbook contains more than twice as many formulas as the old one, coverage of more functions, in more detail, and an up-to-date list of references. The website covers everything in the handbook and much more: additional formulas and graphics, math-aware search, interactive zooming and rotation of 3D graphs, internal links to symbol definitions and cross-references, and external links to online references and sources of software.

While the original Handbook still receives an enormous number of citations, citations to the DLMF are steadily growing in relation to the original handbook. Google Scholar now reports more than 8 230 citations to

the DLMF, a roughly 14 % increase from 2021. During calendar 2022, the DLMF website served about 3.1M pages to some 248 000 unique users.

Today's DLMF is the product of many years of effort by more than 50 contributors. Its initial release in 2010, however, was not the end of the project. Corrections to errors, clarifications, bibliographic updates, and addition of new material all need to be made on a continuing basis. And new chapters covering emerging subject areas need to be added to assure the continued vitality of the DLMF deep into the 21st century. Since December of 2021, there were five DLMF releases, 1.1.4 (2022-01-15), 1.1.5 (2022-03-15), 1.1.6 (2022-06-30), 1.1.7 (2022-10-15), and 1.1.8 (2022-12-15), which kept us on our quarterly release schedule. In Release 1.1.0 (2020-12-15) we introduced the capability to create new chapters, sections, subsections, and equations using a decimal numbering scheme using "_" to delimit intermediate numbers for sections, equations, etc. Over the past year, fourteen new equations and one new subsection were introduced into the DLMF.

The updating of various DLMF chapters and the development of new ones continues. These include a new chapter on Several Variable Orthogonal Polynomials (SVOP) and substantial updates to the chapters on Orthogonal Polynomials (OP), Algebraic and Analytic Methods (AL), Painlevé Transcendents (PT), and Zeta and Related Functions (ZE). Four authors and one validator have been carrying out this work. Drafts are now available for two of these chapters and are being internally reviewed. External validation of the chapters is following in much the same manner as the original DLMF. The ZE chapter revision with full validation was completed in release 1.1.4. The OP and AL external validation was completed by Wolter Groenvelt in May 2022, and it is expected that the full revision of the OP and AL chapters, will be released in 2023.

One of the design goals for the DLMF was that each formula would be connected to a proof in the literature. This data, visible as annotations on the website, provides either a proof for the formula, a reference to the proof for the formula or, for definitions, a reference which gives that definition. Unfortunately, this information had not previously been provided in all cases. Our work to systematically verify the completeness and traceability to published proofs for DLMF formulae at the equation level is well underway. This audit has been completed for Chapter 9 (Airy and Related Functions) and Chapter 25 (Zeta and Related Functions, with validation provided by *Gergő Nemes*) and is actively continuing for Chapters 1-5 and 22-30. Furthermore, inherited metadata at the subsection and section levels has been fully deployed.

The DLMF is now fully utilizing GitHub's capabilities for ongoing maintenance, as well as tracking changes and enhancements. Changes to the DLMF are now implemented via GitHub issues and targeted pull requests of GitHub branches, each of which are reviewed by other project members before merging with the master branch in full adoption. All changes are reviewed and discussed by the DLMF team at weekly DLMF meetings of the editorial staff prior to their appearance, which occurs in quarterly DLMF revisions.

There have been notable additional advances during the current reporting period:

- Our mathematics markup now conforms with the MathML Core specification and should be acceptable in most browsers (current Firefox, Safari, and the upcoming Chrome release).
- A significant number of mathematical formulas, errata and new mathematical information have been provided, many of which originated from the DLMF readership, validation staff, and contributors. Furthermore, mathematical constraints and symbols associated with equations and in the text, have been improved, clarified, corrected, or disambiguated.
- Proof sketches in Chapters 9, 25, and elsewhere are now carefully differentiated at the equation level, providing useful metadata for the origination of formulas.
- We have included enhanced coverage of the Lambert *W*-function, which includes a precise description of the multi-valued description with indices for the separate branches. This includes the introduction of the Wright-w function and the tree *T*-function.
- Improved notations and updated citations have been introduced.

[1] M. Abramowitz and I. Stegun, eds. *Handbook of Mathematical Functions with Formulas, Graphs and Mathematical Tables*. Applied Mathematics Series 55, National Bureau of Standards, Washington, DC 1964.

[2] F. Olver, D. Lozier, R. Boisvert and C. Clark, eds. *NIST Handbook of Mathematical Functions*. Cambridge University Press, 2010.

NIST Digital Repository of Mathematical Formulae

Howard S. Cohl
Bonita V. Saunders
Abdou Youssef
Moritz Schubotz
Andre Greiner-Petter (University of Wuppertal)
Miguel Lopez (University of Maryland)
Philipp Scharpf (University of Konstanz)

The NIST Digital Repository of Mathematical Formulae (DRMF) is an online compendium of formulae for orthogonal polynomials and special functions (OPSF) designed to a) facilitate interaction among a community of mathematicians and scientists interested in OPSF; b) be expandable, allowing the input of new formulae from the literature; c) provide information for related linked open data projects; d) represent the context-free full semantic information concerning individual formulas; e) have a user friendly, consistent, and hyperlinkable viewpoint and authoring perspective; f) contain easily searchable mathematics; and g) take advantage of modern MathML tools for easy-to-read, professionally rendered content-driven mathematics.

Our DRMF implementation, previously built using MediaWiki (the wiki software used by Wikipedia), is currently in migration to a different software platform, namely the platform used by the NIST Digital Library of Mathematical Functions (DLMF). See Figure 85 for the current draft of the DRMF home page, and Figure 86 for a sample DRMF formula page. The DRMF has been summarized in a series of papers [1-3]. A key asset in the development of DRMF context free semantic content is the utilization of a set of LaTeX macros and macro call functionality created by Bruce Miller (ACMD) to achieve the encapsulation of semantic information within the NIST Digital Library of Mathematical Functions (DLMF) [4]. These macros give us the capability to tie LaTeX commands in a mostly unambiguous way to mathematical functions defined in an OPSF context. There are currently 540 DLMF LaTeX macros, as well as an additional 156 macros, which have been created specifically for the DRMF. Most, if not all, DLMF macros have at least one DLMF web page associated with them. One goal is to have definition pages for all additional DRMF macros. The use of DLMF and DRMF macros guarantees mathematical and structural consistency throughout the DRMF. We refer to LaTeX source with incorporated DLMF and DRMF macros as semantic LaTeX.

DRMF formula seeding is currently focused on 1) Koekoek, Lesky, and Swarttouw (KLS) chapters 1 (Definitions and Miscellaneous Formulas), 9 (Hypergeometric Orthogonal Polynomials), and 14 (Basic Hypergeometric Orthogonal Polynomials [5]; 2) Koornwinder KLS addendum LaTeX data [5]; 3) Wolfram Computational Knowledge of Continued Fractions Project (eCF) [3]; 4) Continued Fractions for Special Function (CFSF) Maple dataset hosted by the University of Antwerp [3,7]; 5) Bateman Manuscript Project (BMP) books [8]; and 6) Magnus, Oberhettinger, and Soni (MOS) books [3,9]. For these seed projects, we are developing Python and Java software to incorporate DLMF and DRMF macros into the corresponding LaTeX source. Our coding efforts have also focused on extracting formula data from LaTeX source, as well as generating DRMF semantic LaTeX. We have developed Java software for the seeding of the eCF and CFSF projects, which involve conversion from Mathematica and Maple format to DLMF and DRMF macro incorporated semantic LaTeX [3].

In August 2014, the DRMF Project obtained permission and license to use BMP material as seed content for the DRMF from Adam Cochran, Associate General Counsel of Caltech. Caltech has loaned us copies of the BMP. In February 2018, we received permission and license to use the KLS and MOS material as seed content for the DRMF from Springer Nature. We plan on implementing the BMP and MOS datasets using mathematical optical character recognition software to obtain LaTeX source using software developed with MathType.

Current and future DRMF MediaWiki development projects include the production of formula output representations (such as semantic LaTeX, MathML, Mathematica, Maple, and Sage); incorporation of sophisticated DLMF and DRMF macro related formula search; and the development of capabilities for user community

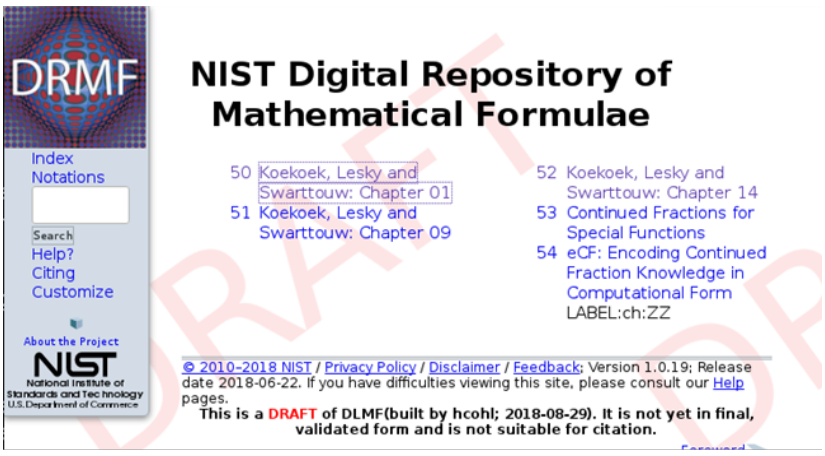

Figure 85. *Draft of the DRMF home page displaying the current table of contents.*

formula input. In this vein, A. Youssef has written a grammar-based mathematical language processor (MLP) that uses JavaCC to parse mathematical LaTeX expressions [10]. Based on the MLP, A. Greiner-Petter has developed a Java tool referred to as LaCASt to convert mathematical LaTeX expressions, which contain DLMF and DRMF macros, to a given computer algebra system source format. This Java tool provides further information of the conversion about possible ambiguities and differences in definitions, domains and branch cuts between the semantic LaTeX source and the CAS source. Furthermore, it is designed to be easily extendable to other computer algebra systems and currently supports Maple and Mathematica input sources. NIST ACMD SURF student Miguel Lopez worked on the project "Conversion of Mathematica source to LaTeX." In [11] which focuses on LaCASt, we present a first comprehensive approach to verify a digital mathematical and two computer algebra systems with one another by converting mathematical expressions from one system to the other. This is accomplished by our development of LaCASt, which translates formulae from the NIST Digital Library of Mathematical Functions to the computer algebra systems Maple and Mathematica. This tool will be actively used in DRMF. In [12], we explore the future of digital mathematics libraries where semantic content is significantly enhanced. In [13], we conceive to generalize citation-based information retrieval methods as applied to mathematical concepts through machine learning-based approaches to the formula concept retrieval and formula concept discovery tasks.

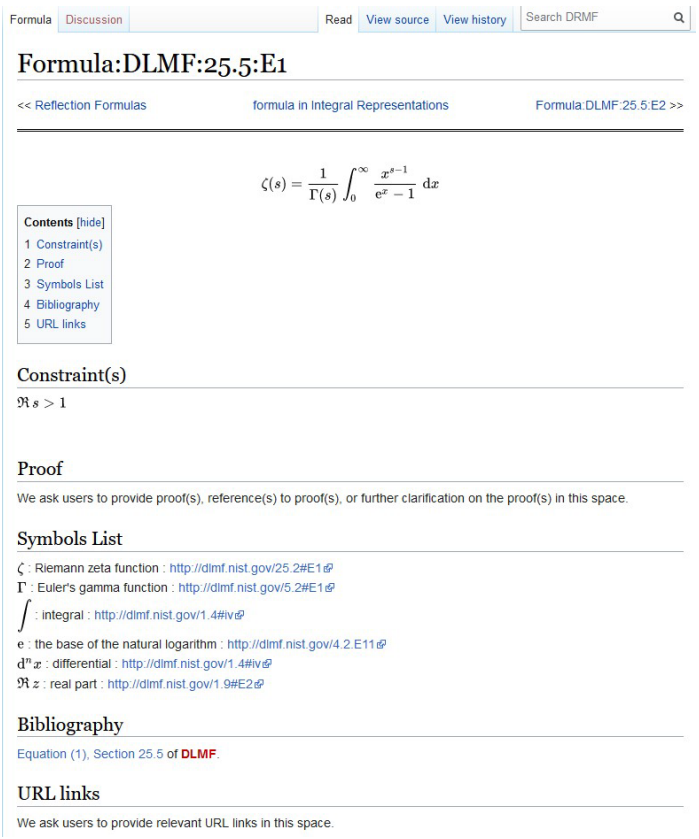

Figure 86. *Sample DRMF page, taken from the KLS Chapter 1 dataset.*

The KLS datasets have been uploaded to our DLMF platform as well as the CFSF and eCF datasets. By working with Andrea Fisher-Scherer, Rights Administrator, Artists Rights Society, New York, NY, we have received permission from Foundation Vasarely to use an image Victor Vasarely's painting as the DRMF logo; see Figure 3.

[1] H. S. Cohl, M. A. McClain, B. V. Saunders, M. Schubotz, and J. C. Williams. Digital Repository of Mathematical Formulae. *Lecture Notes in Artificial Intelligence* **8543** (2014), Proceedings of the Conferences on Intelligent Computer Mathematics 2014, Coimbra, Portugal, July 7-11, 2014, (S. M. Watt, J. H. Davenport, A. P. Sexton, P. Sojka, and J. Urban, eds.), Springer, 419-422.

[2] H. S. Cohl, M. Schubotz, M. A. McClain, B. V. Saunders, Cherry Y. Zou, Azeem S. Mohammed, and Alex A. Danoff. Growing the Digital Repository of Mathematical Formulae with Generic LaTeX Sources. *Lecture Notes in Artificial Intelligence* **9150** (2015), Proceedings of the Conference on Intelligent Computer Mathematics 2015, Washington DC, USA, July 13-17, 2015, (M. Kerber, J. Carette, C. Kaliszyk, F. Rabe, and V. Sorge, eds.), Springer, 280-287.

[3] H. S. Cohl, M. Schubotz, A. Youssef, A. Greiner-Petter, J. Gerhard, B. V. Saunders, M. A. McClain, J. Bang, and K. Chen. Semantic Preserving Bijective Mappings of Mathematical Formulae between Word Processors and Computer Algebra Systems. *Lecture Notes in Computer Science* **10383** (2017), Proceedings of the Conference on Intelligent Computer Mathematics 2017, Edinburgh, Scotland, U.K., July 17-21, 2017, (H. Geuvers, M. England, O. Hasan, F. Rabe, O. Teschke, eds.), Springer, 115-131.

[4] B. Miller. "Drafting DLMF Content Dictionaries." OpenMath Workshop, 9th Conference on Intelligent Computer Mathematics (CICM), Bialystok, Poland, 2016.

[5] R. Koekoek, P. A. Lesky, and R. F. Swarttouw. *Hypergeometric Orthogonal Polynomials and their q-Analogues*. Springer Monographs in Mathematics, Springer-Verlag, Berlin, 2010.

[6] T. H. Koornwinder. Additions to the Formula Lists in Hypergeometric Orthogonal Polynomials and their q-analogues by Koekoek, Lesky and Swarttouw. arXiv:1401.0815, June 2015.

[7] A. Cuyt, V. Petersen, H. Waadeland, W. B. Jones, F. Backeljauw, C. Bonan-Hamada, and S. Becuwe. *Handbook of Continued Fractions for Special Functions*. Springer, New York, 2008.

[8] A. Erdelyi, W. Magnus, F. Oberhettinger, and F. G. Tricomi. *Higher Transcendental Functions*. Vols. I, II, III, Robert E. Krieger Publishing Co., Melbourne, FL, 1981.

[9] H. S. Cohl, A. Greiner-Petter, and M. Schubotz. Automated Symbolic and Numerical Testing of DLMF Formulae using Computer Algebra Systems. *Lecture Notes in Computer Science* **11006** (2018), Proceedings of the Conference on Intelligent Computer Mathematics 2018, Hagenberg, Austria, August 13-17, 2018, (F. Rabe, W. Farmer, G.O. Passmore, A. Youssef, eds.), Springer, 39-52.

[10] A. Youssef. Part-of-Math Tagging and Applications. *Lecture Notes in Computer Science* **10383** (2017), Proceedings of the Conference on Intelligent Computer Mathematics 2017, Edinburgh, Scotland, U.K., July 17-21, 2017, (H. Geuvers, M. England, O. Hasan, F. Rabe, O. Teschke, eds.), Springer, 356-374.

[11] A. Greiner-Petter, H. S. Cohl, A. Youssef, M. Schubotz, A. Trost, R. Dey, A. Aizawa and B. Gip. Comparative Verification of the Digital Library of Mathematical Functions and Computer Algebra Systems. *Lecture Notes in Computer Science* **13243** (2022), Tools and Algorithms for the Construction and Analysis of Systems (TACAS 2022), Held as Part of the European Joint Conferences on Theory and Practice of Software (ETAPS 2022), Springer, (D. Fisman and G. Rosu, eds.), Munich, Germany, April 2-7, 2022, Springer, 87–105.

[12] H. S. Cohl, M. Schubotz. The Digital Shadow of Mathematics and its Ramifications. *Jahrbuch uber die Fortschritte der Mathematik*, to appear.

[13] P. Scharpf, M. Schubotz, H. Cohl, C. Breitinger, and B. Gipp. Discovery and Recognition of Formula Concepts using Machine Learning. *Scientometrics*, to appear.

Scientific Document Corpora for Natural and Mathematical Language Research

Bruce Miller
Deyan Ginev (Chakra Consulting)
Tom Wiesing (University of Erlangen, Germany)

Machine learning is currently a very active research area, both in its theoretical underpinnings and technology, as well as its application to find, understand and reuse information. We would like to see the application of these methods to scientific documents, unique in their style of natural language used, as well as the extensive use of mathematical notation. For this to happen, large collections of scientific documents are needed, first for training and then for mining. To that end, we have been applying our LaTeXML tool to the massive corpus at arXiv.org[25]. To demonstrate the utility of this dataset, we have carried out initial experiments on statement classification using that data set.

As an example of data mining in scientific documents, consider automated classification of paragraphs according to their textual content as not only abstracts, introductions, and conclusions, but as theorems, proofs, definitions, and such. Although the markup normally used in LaTeX documents seldom emphasizes semantics, there are nevertheless a number of macros and environments which reflect the author's intent. We were able to extract some 10M such annotated paragraphs in 50 categories from our conversion of arXiv [1]. Using 80% of the documents as a training set, we discovered that many categories were too similar. For example, theorems, lemmas, and propositions strongly share language patterns. Combining these "confusion nests" yielded 13 clear cut categories into which the paragraphs could be reliably categorized with a 0.91 F1 score. Consequently, the system learns to classify paragraphs that have not been manually annotated.

LaTeXML[26] was originally developed to convert the LaTeX sources of the Digital Library of Mathematical Functions (DLMF)[27] into web format, namely HTML and MathML. Most of the arXiv.org corpus is also in LaTeX format, albeit with significantly less disciplined markup and using a wide variety of uncommon and complex support packages. We have continued to develop LaTeXML, improving robustness and fidelity of TeX simulation. The coverage of LaTeX packages has been increased, while minimizing the loss of latent semantics implied by the markup. This year was a very busy one on arXiv, with the number of documents increasing to 1.97M from 1.8M last year. We have just completed reprocessing the entire current corpus into HTML+MathML with over 75% success rate (documents producing, at worst, warnings).

Additionally, we have been tracking the evolution of web browsers and relevant standards, such as MathML Core which is now natively supported by all major web browsers. This effort has attracted the attention of the arXiv team itself to use our system to make their corpus available in HTML format to improve accessibility as well as availability on both desktop and mobile devices.

[1] D. Ginev and B. R. Miller. Scientific Statement Classification over arXiv.org. arXiv:1908.10993

25 https://arXiv.org/

26 https://dlmf.nist.gov/LaTeXML/

27 https://dlmf.nist.gov/

Visualization of Complex Functions Data

Bonita Saunders
Bruce Miller
Sandy Ressler
Brian Antonishek (NIST EL)
Qiming Wang (NIST retired)

Although the DLMF[28] provides definitions, recurrence relations, differential equations, asymptotic expansions, and other information crucial for understanding complex mathematical functions arising in application areas of the mathematical and physical sciences, interactive visualizations can provide additional clarity as indicated in Figure 87.

Since this work is motivated by the DLMF, ensuring the quality and accessibility of its visualizations is our first priority. When updates of JavaScript and X3DOM[29] graphics libraries associated with the generation of our visualizations introduced anomalies in our color maps, we realized a better understanding of the role of the libraries during the generation process was needed. The first question was whether the new maps were actually more accurate representations, but preliminary examinations of the data files, plots of similar data on other websites, and plots in Jahnke, Emde, and Losch [4] indicated this was not the case. By backing out of several updates we determined the earliest versions of X3DOM producing the altered color maps. Ideally, we want to use the latest update available, but a careful examination of the X3DOM changelog, available through GitHub, might yield a possible "culprit" for the errant maps. Once we know more, we will try contacting X3DOM developers for possible assistance and clarification of the changes made to the library.

Another priority is addressing changes suggested by DLMF users, other members of the DLMF editorial staff, and chapter authors. For example, based on feedback received, modified and new figures related to the Lambert *W*-Function were added to Chapter 4 on Elementary Functions. In particular, notations for the principal and lower branch solutions were changed to coincide with conventions more commonly found in the literature. Another figure was added to show the function's mapping on five branches, or Riemann sheets. Hopefully, this work will eventually lead to the design of interactive 3D visualizations of Riemann surfaces. Additional figures are also under development for the chapter on Orthogonal Polynomials, which is undergoing extensive modifications in content.

We continue to look for opportunities to generalize our work to benefit the larger research community. Our

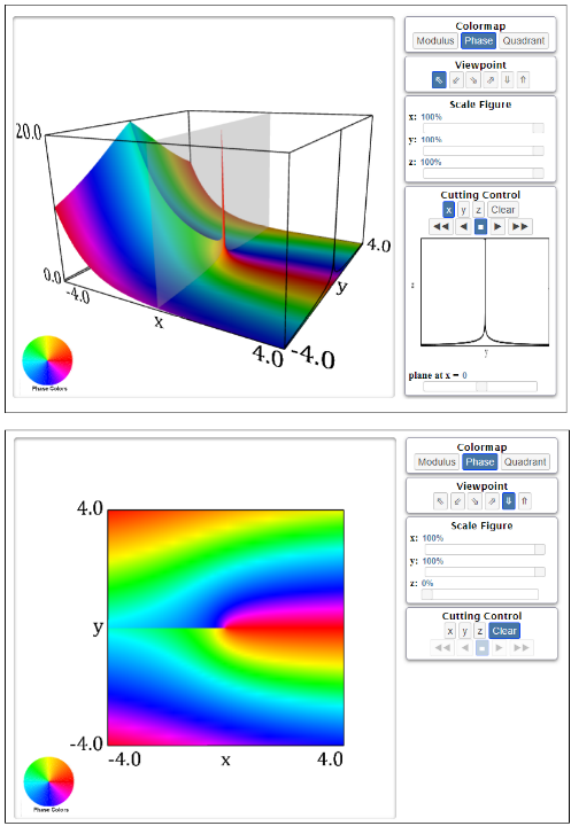

Figure 87. *DLMF visualizations provide several options for exploring mathematical function surfaces. In the top figure, the modulus of the principal value of the exponential integral $E_1(x+iy)$ is shown with a phase color map, cutting plane and pop-up control window indicating convergence to ∞ at the origin. Other options allow users to change the color map, examine different viewpoints and scale the figure in various coordinate directions. In the bottom figure, the function's height is scaled down to create a density plot that reveals the cut along the negative real axis. DLMF Figure 6.3.3:* https://dlmf.nist.gov/6.3.F3

current work on adaptive meshes to improve our underlying computational grids supports our design process, but it may also interest other researchers in the fields of mesh generation, optimization, approximation theory, or any area related to the design of curves and surfaces for mathematical or physical applications. We should also note that some of our recent presentations have also shown that aspects of our work can be appreciated by more general and less specialized audiences [1, 2, 3]. Such talks may not yield immediate collaborators but can still enhance the division's visibility and plant seeds for new connections.

As time permits, we also continue to explore opportunities to increase user visibility. Some DLMF chapters display chapter related thumbnail images on the title page. Creating a gallery of images for all chapters would

[28] https://dlmf.nist.gov/

[29] https://www.x3dom.org/

add visual interest to the DLMF. Each image would link to a short descriptive sidebar that could include links to the chapter's application section or related function visualizations. New and updated DLMF chapters currently under development can provide a test bed for this work.

[1] B. Saunders, "The Handbook of Mathematical Functions and the DLMF." 75th Anniversary of NIST Mathematics and Statistics, NIST, June 28, 2022.

[2] B. Saunders, "Visualizing Complex Functions." George Mason University Mathematics Students Visit, NIST, August 3, 2022.

[3] B. Saunders, "Research in Computational and Applied Mathematics at the National Institute of Standards and Technology: NIST's DLMF and More." Applied Mathematics and Scientific Computing Seminar, Temple University, Philadelphia, PA, November 30, 2022.

[4] E. Jahnke, F. Emde, and F. Losch. *Tables of Higher Functions*. 6th Edition, B. G. Teubner Verlagsgesellschaft mbH, Stuttgart, 1960 (Bilingual).

DLMF Standard Reference Tables on Demand

Bonita Saunders
Bruce Miller
Marjorie McClain (Retired)
Annie Cuyt (University of Antwerp)
Stefan Becuwe (University of Antwerp)
Franky Backeljauw (University of Antwerp)
Sean Brooks (Coppin State University)
Ron Buckmire (Occidental College)
Rachel Vincent-Finley (Southern U. and A&M College)
Christopher Schanzle

http://dlmftables.uantwerpen.be/

Although reliable computing machines, computer algebra systems, and multiple precision computational packages have diminished the need for tables of reference values for computing function values by interpolation, mathematical and physical scientists, numerical analysts, and software developers still need a way to test software for computing mathematical functions. DLMF Standard Reference Tables on Demand (DLMF Tables) is a collaborative project between ACMD and the University of Antwerp Computational Mathematics Research Group (CMA) [1-5] to address this problem. The goal is to develop an online system where users can generate tables of special function values at user-specified precision with an error certification

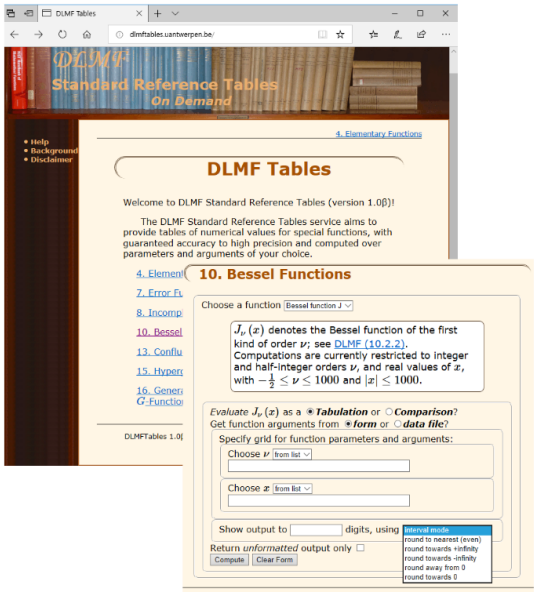

Figure 88. *DLMF Tables generates tables of special function values at user specified precision. Users input real values and parameters where the function is to be evaluated. The user may request output in interval mode, where the output is shown as a table of intervals that bound the true results or may request output in one of several rounding modes. Users may also choose to compare their own table of values to the reference values generated by the system.*

to test their own algorithms or confirm the accuracy of results from a commercial or publicly available package.

The DLMF Tables team has developed a beta site at the University of Antwerp, based on CMA's MpIeee, a multiple precision IEEE 754/854 compliant C++ floating point arithmetic library. Ultimately, the goal is a permanent NIST location accessible from the NIST Digital Library of Mathematical Functions (DLMF). In 2020 three researchers were added to the DLMF Tables team through the inaugural ADJOINT Workshop[30] sponsored by the Mathematical Sciences Research Institute (MSRI) in Berkeley, California [6]. The group members, from various universities, were supported by MSRI through NSF, NSA, and Sloan grants[31] for more than a year. Post-workshop contact has continued with online meetings to discuss and verify applicable results from the literature, including Higham [7] and CMA [1-5]. The ADJOINT group's work led to three invited talks at the 2021 Joint Mathematics Meetings [8] and two more talks at ADJOINT and AWM minisymposia at the 2022 Joint Mathematics Meetings [9, 10]. Also, an update of the group's work was presented at a MSRI reunion during the summer of 2022 [11]. A paper co-authored by the ADJOIINT group with members of the ACMD and U. Antwerp teams is under review [12].

[30] https://www.msri.org/web/msri/scientific/adjoint

[31] S. Brooks, R. Buckmire, and R. Vincent-Finley were supported in this work by National Science Foundation, Grant Nos. DMS-1915954 and DMS-2016406; National Security Agency, Grant No. H98230-20-1-0015; and Sloan Foundation, Grant No. G-2020-12602 as participants in ADJOINT 2020 hosted by the Mathematical Sciences Research Institute in Berkeley, California.

ACMD has primarily been responsible for the front-end interface for DLMF Tables, while CMA designed and maintains the back-end computational engine built around the error analysis and MpIeee library. The work with the ADJOINT group marks a significant step toward merging these capabilities so that CMA's function computation codes can be maintained and eventually, further developed here at NIST.

[1] F. Backeljauw, S. Becuwe, A. Cuyt, J. Van Deun, and D. Lozier. Validated Evaluation of Special Mathematical Functions. *Science of Computer Programming* **10** (2013), 1016.

[2] M. Colman, A. Cuyt, and J. Van Deun, Validated Computation of Certain Hypergeometric Functions. *ACM Transactions on Mathematical Software* **38**:2 (January 2012), 11.

[3] F. Backeljauw. A Library for Radix-independent Multiprecision IEEE-compliant Floating-point Arithmetic. Technical Report 2009-01, Department of Mathematics and Computer Science, Universiteit Antwerpen, 2009.

[4] A. Cuyt, V. B. Petersen, B. Verdonk, H. Waadeland, and W. B. Jones. *Handbook of Continued Fractions for Special Functions*. Springer, New York, 2008.

[5] A. Cuyt, B. Verdonk, and H. Waadeland. Efficient and Reliable Multiprecision Implementation of Elementary and Special Functions. *SIAM Journal of Scientific Computing* **28** (2006), 1437-1462.

[6] B. Saunders, S. Brooks, R. Buckmire, and R. Vincent-Finley. "Validated Numerical Computation of Mathematical Functions." African Diaspora Joint Mathematics Workshop (ADJOINT) 2020, Online, June 26, 2020.

[7] N. Higham. *Accuracy and Stability of Numerical Algorithms.* Second edition. Society for Industrial and Applied Mathematics, Philadelphia, 2002.

[8] B. Saunders, S. Brooks, R. Buckmire, and R. Vincent-Finley. "Validated Computation of Special Functions I: Overview, II: Error Analysis, III: DLMF Tables." ADJOINT Research Showcase, 2021 Joint Mathematics Meetings, Online, January 9, 2021.

[9] B. Saunders, S. Brooks, R. Buckmire, R. Vincent-Finley, "Rounding Error Analysis for Validated Computation of Special Functions." Special Session on the MSRI African Diaspora Joint Mathematics (ADJOINT) Workshop, I, Joint Mathematics Meetings, I, Online, April 6, 2022.

[10] B. Saunders, S. Brooks, R. Buckmire, R. Vincent-Finley, F. Backeljauw, S. Becuwe, B. Miller, M. McClain, A. Cuyt, "Validated Computation of Special Mathematical Functions." AWM Special Session on Celebrating the Mathematical Contributions of the AWM, I, Joint Mathematics Meetings, Online, April 7, 2022.

[11] R. Buckmire, B. Saunders, R. Vincent-Finley, S. Brooks, "Saunders ADJOINT Team Update on Validated Numerical Computations Research." ADJOINT Reunion Workshop, Online, July 1, 2022.

[12] B. Saunders, S. Brooks, R. Vincent-Finley, R. Buckmire, F. Backeljauw, S. Becuwe, B. Miller, M. McClain, A. Cuyt. Validated Computation of Special Mathematical Functions. In review.

Fundamental Solutions and Formulas for Special Functions and Orthogonal Polynomials

Howard S. Cohl
Camilo Montoya
Lisa Ritter
Roberto S. Costas-Santos (U. Loyola Andalucia)
Hans Volkmer (University of Wisconsin-Milwaukee)
Gestur Olafsson (Louisiana State University)
Mourad E. H. Ismail (University of Central Florida)
Tom H. Koornwinder (Korteweg-de Vries Institute for Mathematics)
James Lawrence (George Mason University)
Jessica E. Hirtenstein (University of California Davis)
Philbert R. Hwang (University of Maryland)
Tanay Wakhare (MIT)
Linus Ge (University of Rochester)

The concept of a function expresses the idea that one quantity (the input) completely determines another quantity (the output). Our research concerns special functions and orthogonal polynomials. A special function is a function that has appeared in the mathematical sciences so often that it has been given a name. Green's functions (named after the British mathematician George Green, who first developed the concept in the 1830s) describe the influence of linear natural phenomena such as electromagnetism, gravity, heat, and waves. For example, in electrostatics, a Green's function describes the influence of a point charge, called the source, over all of space. The inputs for fundamental solutions (Green's functions) are all of space (apart from a singular region), and the output is the "force" exerted from the point throughout space. Green's functions are fundamental to the study of inhomogeneous partial differential equations and are powerful in that they provide a mechanism for obtaining their solutions.

We investigate fundamental solutions of linear partial differential equations on highly symmetric Riemannian manifolds (harmonic, rank-one symmetric spaces) such as real, complex, quarternionic, and octonionic, hyperbolic, and projective spaces. Our recent focus has been on applications of fundamental solutions for linear elliptic partial differential operators on spaces of constant curvature. With Olafsson and Camilo Montoya, we investigate fundamental solutions of the Laplace-Beltrami operator on rank one symmetric spaces of compact and noncompact type [1, 2]. Cohl, Ritter, previous SURF student Jessica Hirtenstein, and Jim Lawrence derived Gegenbauer expansions and addition theorems for binomial and logarithmic fundamental solutions of the polyharmonic operator in even-dimensional Euclidean space in Vilenkin polyspherical coordinates for powers of the Laplacian

greater than or equal to the dimension divided by two [3].

With Hans Volkmer, we continue our investigation of a fundamental solution expansions for Laplace's equation in the 17 conformally inequivalent coordinate systems which separate Laplace's equation. Recently, we have been investigating the rotationally invariant cyclidic coordinate systems of this type, namely flat-ring cyclide, bi-cyclide and disk cyclide coordinates. We have completed the investigation for flat-ring [4, 5] and bi-cyclide [6] coordinates.

In the following works, we expand on the properties of terminating and nonterminating generalized and basic hypergeometric functions to study themselves and their respective generalized and basic hypergeometric orthogonal polynomials (hereafter orthogonal polynomials) in the Askey and q-Askey schemes. By utilizing connection relations, we have computed generalizations of generalized and basic hypergeometric orthogonal polynomial generating functions as well as corresponding definite integrals using orthogonality. With Costas-Santos, Hwang and Wakhare, our series-rearrangement technique is extended to generalizations of other generating functions for basic hypergeometric orthogonal polynomials in [7]. Here, we derive generalizations of generating functions for Askey–Wilson, q-ultraspherical/Rogers, q-Laguerre, and little q-Laguerre/Wall polynomials [7]. We are also interested in the fundamental transformation, representation (symmetry) properties of the special functions and orthogonal polynomials which one often encounters in applied mathematics and mathematical physics. With Costas-Santos and Ge, we developed a series of papers which describe transformation and representation theory of symmetric basic hypergeometric orthogonal polynomials, namely the Askey–Wilson polynomials (4 symmetric free parameters (sfp)) and its symmetric subfamilies, the continuous dual q-Hahn polynomials (3 sfp), the Al-Salam–Chihara polynomials (2 sfp), the continuous big q-Hermite polynomials and the continuous q-Hermite polynomials, and their q-inverse analogues [8]. With Costas-Santos, we examine the symmetric transformation and representation properties of the Askey–Wilson polynomials with a focus on the terminating very-well poised ${}_8W_7$ representations. We examine the representation relation to the order of the well-known symmetry group of the terminating ${}_4f_3$ Askey–Wilson representations given by the symmetric group S_6 with respect to their and transformation inversion symmetries [9]. We have also investigated the use of integral representations for nonterminating basic hypergeometric functions and orthogonal polynomials [10, 11].

With Costas-Santos we studied the relation between the Ferrers function of the first kind and Gegenbauer polynomials to derive a collection of new formulas [12]. With Ismail and Ritter, we derive 5-term contiguous relations for the linearization coefficients of generalized and basic hypergeometric orthogonal polynomials such as Laguerre, Gegenbauer, Hermite, Jacobi, continuous q-ultraspherical/Rogers, and continuous q-Jacobi polynomials [13]. We are also continuing this project with Jacobi functions of the first and second kind and their trigonometric limiting functions on the cut *(-1,1)* [14]

Well-known special functions researcher Richard A. Askey passed away on October 9, 2019. Cohl, Ismail, and Wu have edited a memorial article for Dick Askey which was published in *The Notices of the American Mathematical Society* [15]. With 63 colleagues, Cohl and Ismail prepared a *Liber Amicorum for Dick Askey* which was presented to him and his family at an event held on September 4, 2019, at his hometown in Madison, Wisconsin. Cohl and Ismail have submitted an extended version of the Liber Amicorum composed of the remembrances of 83 of his colleagues which will be published online with *Celebratio Mathematica* [16].

Cohl remains editor or co-editor for a special issue on symmetry in special functions and orthogonal polynomials in the journal *Symmetry*; special volume dedicated to the legacy of Dick Askey for *The Ramanujan Journal*, OP-SF NET, SIAM Activity Group on Orthogonal Polynomials and Special Functions; and *The Ramanujan Journal*.

[1] H. S. Cohl, C. Montoya, and G. Olafsson. Fundamental Solutions for the Laplace-Beltrami Operator and its Eigenfunction Expansions in Complex Hyperbolic Geometry. In preparation.

[2] H. S. Cohl, C. Montoya, and G. Olafsson. Fundamental Solutions for the Laplace-Beltrami Operator and its Eigenfunction Expansions in Complex Projective Geometry. In preparation.

[3] H. S. Cohl, J. E. Hirtenstein, J. Lawrence, and L. Ritter. Gegenbauer Expansions and Addition Theorems for a Binomial and Logarithmic Fundamental Solution of the Even-Dimensional Euclidean Polyharmonic Equation. *Journal of Mathematical Analysis and Applications* **517**:2 (2023), 126576.

[4] L. Bi, H. S. Cohl, and H. Volkmer. Expansion for a Fundamental Solution of Laplace's Equation in Flat-ring Cyclide Coordinates. *Symmetry, Integrability and Geometry: Methods and Applications* **18** (2022), 41.

[5] L. Bi, H. S. Cohl, and H. Volkmer. Peanut Harmonic Expansion for a Fundamental Solution of Laplace's Equation in Flat-ring Coordinates. *Analysis Mathematica* **48**:3 (2022), 961-989.

[6] B. Alexander, H. S. Cohl, and H. Volkmer. Internal and External Harmonics in Bi-Cyclide Coordinates. In review.

[7] H. S. Cohl, R. S. Costas-Santos, P. R. Hwang, and T. V. Wakhare. Generalizations of Generating Functions for Basic Hypergeometric Orthogonal Polynomials. *Open Journal of Mathematical Sciences* **6**:1 (2022), 248.

[8] H. S. Cohl, R. S. Costas-Santos, and L. Ge. Basic Hypergeometric Transformations from Symmetric and q-inverse Sub-families of the Askey-Wilson Polynomials in the q-Askey-scheme. In preparation.

[9] H. S. Cohl and R. S. Costas-Santos. Symmetry of terminating basic hypergeometric representations of the Askey–Wilson polynomials. *Journal of Mathematical Analysis and Applications* **517**:1 (2023), 126583.

[10] H. S. Cohl and R. S. Costas-Santos. Utility of Integral Representations for Basic Hypergeometric Functions and Orthogonal Polynomials. *The Ramanujan Journal*, Special Volume Dedicated to Dick Askey, to appear.

[11] H. S. Cohl and R. S. Costas-Santos. Nonterminating Transformations and Summations Associated with Some q-Mellin-Barnes Integrals. In review.

[12] H. S. Cohl and R. S. Costas-Santos. On the Relation Between Gegenbauer Polynomials and the Ferrers Function of the First Kind. *Analysis Mathematica* **48**:3 (2022), 695-716.

[13] H. S. Cohl and L. Ritter. Two-dimensional Contiguous Relations for Linearization Coefficients ff Orthogonal Polynomials in the Askey-scheme. In review.

[14] H. S. Cohl and R. S. Costas-Santos. Multi-Integral Representations for Jacobi Functions. In preparation.

[15] M. E. H. Ismail, H. S. Cohl and H.-H. Wu, Editors. The Legacy of Dick Askey (1933-2019). *Notices of the American Mathematical Society* **69**:1 (2022), 59-75.

[16] H. S. Cohl and M. E. H. Ismail, eds. *Liber Amicorum, a Friendship Book for Dick Askey*. In review.

Outreach and Diversity

ACMD staff engage in a variety of efforts that serve to educate the general public about the work of the division and to encourage students to consider careers in science and engineering. We are also involved in internal efforts to improve diversity and inclusivity, which are important for both recrutiment and retention of a high-performing workforce. Some of these efforts are described here.

Student Internships in ACMD

Ronald Boisvert

ACMD is committed to helping to prepare the next generation of scientific researchers by providing internships of various types to students at each of the graduate, undergraduate, and high school levels. The NIST programs used to enable such internships include the following:

- *Foreign Guest Researcher Program.* Provides stipends to support visits of guest researchers from foreign institutions for periods of a few weeks to several years.
- *Pathways Program.* Provides temporary Federal appointments to students, typically 1 to 2 years. Allows easy conversion to full-time permanent status. (Restricted to US Citizens.)
- *Professional Research Experience Program (PREP)*[32]. A cooperative agreement with nine universities[33] that provides a mechanism for NIST to support internships for students from those institutions on the Gaithersburg campus throughout the year. A similar agreement with four universities[34] exists for the NIST Boulder Labs.
- *Student Volunteer Program.* A mechanism that provides unpaid internships for students.
- *Summer High School Internship (SHIP) Program*[35]. SHIP uses the Student Volunteer Program to organize a competitive summer volunteer program for high school students.
- *Summer Undergraduate Research Fellowship (SURF) Program*[36]. A competitive program providing undergraduates a 10-week research experience at NIST.

Funding for all of these programs comes from the Division hosting the student. The Pathways Program, the PREP Program, and the Foreign Guest Researcher Program can also be used to support postdoctoral researchers.

In total, during the last 15 months, ACMD supported the work of 23 student interns, including 14 graduate students, six undergraduates, and three high school students. See Table 3 for a complete listing.

ACMD staff members are also active in the education of graduate students, serving both as Ph.D. advisers and as members of thesis committees. See page 156.

A Modular Analysis of NIST Institutional Networks

Robert P. Dalka (University of Maryland)
Justyna P. Zwolak

Organizational network analysis (ONA) is a class of methodologies that aim to explore the social ties within and between formal organizations to better understand phenomena such as knowledge and resource transfer, social influences within teams, or the effect of team building on the dynamics of an organization's social network. ONA oftentimes requires personally identifiable information, which in certain organizations can be difficult or impossible to collect. To overcome this limitation, we proposed an alternative method for evaluating interconnectedness within or between organizations. The proposed institutional network analysis uses a projection of anonymous ego-centric data onto organizational units as a proxy to capture the organizational network structure, rather than individual employees [1].

The networks used in this study are built based on the NIST Interactions Survey data [2]. This dataset captures two distinct types of social interactions among NIST employees: their work-related collaborations and advice seeking. The two resulting networks are expected to exhibit somewhat different structures: whereas collaborating on a project necessitates interaction with other employees to fulfill the organization's mission, not everyone seeks advice internally or in a systematic way.

[32] https://www.nist.gov/iaao/academic-affairs-office/nist-professional-research-experience-program-prep

[33] Brown University, Georgetown University, Montgomery College, Towson University, the University of the District of Columbia, the University of Maryland College Park, and a consortium of Johns Hopkins University, Morgan State University, and the State University of New York at Binghamton.

[34] Brown University, the Colorado School of Mines, the University of Colorado Boulder, and the University of Colorado Denver

[35] https://www.nist.gov/careers/student-opportunities/summer-high-school-intern-program

[36] https://www.nist.gov/surf

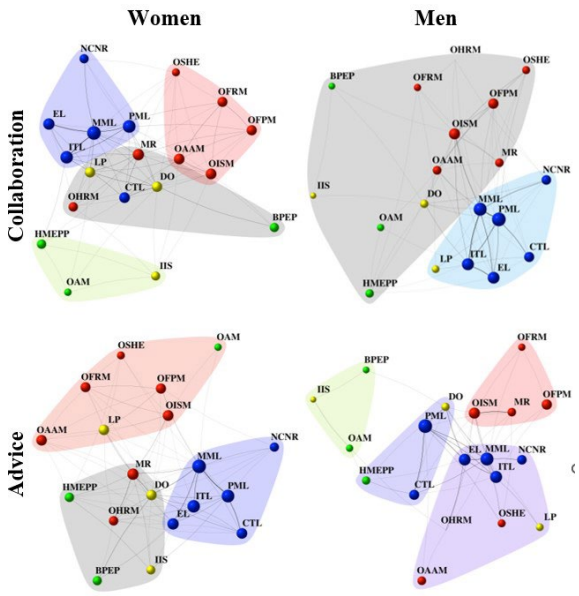

Figure 89. *The communities identified within gendered networks. The gendered networks for both collaboration and advice; women collaboration (top left), men collaboration (top right), women advice (bottom left), and men advice (bottom right). The nodes are sized by the number of responses from each OU. Each OU (node) is labeled and colored by the organizational division to which it belongs, with OUs belonging to Laboratory Programs shown as blue nodes, Management Resources as red nodes, Innovation and Industry Services as green nodes, and OUs serving administrative functions shown as yellow nodes. The shaded regions indicate the identified communities.*

We build and analyze both networks to demonstrate and validate our approach.

Previously, we have employed a modular analysis to determine whether the projected unit-based networks accurately reflect the network structure of the organizational units that comprise NIST. We find that the structure restored in the projected network closely resembles the NIST organizational structure for the collaboration network. The advice network has more variability in the communities identified as well as more intermixing between units. We also find that the community assignment for the advice network is less stable and more susceptible to sampling bias, as opposed to the collaboration network.

The first report based on the NIST Interactions Survey focuses on comparison of work and advice ego-networks between different categories of demographics (e.g., gender, age group, duty station). Unsurprisingly, the study found the organizational unit (OU) affiliation to be the most important factor in shaping the work collaboration networks. Interestingly, in the advice networks, OU affiliation, gender, and age all played a role. While gender-based differences in ego networks were not observed in the work collaboration networks, some distinctions were found in the advice networks. In terms of age-dependencies, it was found that respondents in the 18–39 age range preferred older advice networks. The study in this report did not find any significant differences between minority and non-minority employees for either work collaboration or advice ego-networks.

Our current work focuses on the full inter-OU social networks established based on responses to the two NIST Interaction Survey questions. We study how strong the self-reported connections between OUs are and how they differ between types of networks and respondent demographics. In doing so, we can investigate how the relationships, both work collaboration and advice, map onto the structure of OU-level NIST network [3].

[1] R. P. Dalka and J. P. Zwolak. Restoring the Structure: A Modular Analysis of Ego-Driven Organizational Networks. arXiv preprint, 2201.01290 (2022).

[2] L. Espinal, C. Young, and J. P. Zwolak. Mapping Employee Networks through the NIST Interactions Survey. NISTIR 8375, June 2021. DOI: 10.6028/NIST.IR.8375

[3] R. P. Dalka and J. P. Zwolak. Organizational Network Analysis of NIST Inclusivity Network Data. In preparation.

Network Analysis to Investigate Physics Programmatic Survey Results

Robert P. Dalka (University of Maryland)
Justyna P. Zwolak
Diana Sachmpazidi (University of Maryland)
Charles Henderson (Western Michigan University

In physics education research (PER), the various aspects of student experiences are often assessed via Likert-style surveys. In our previous work, we proposed the *network analysis for Likert-style surveys* (NALS) approach to modeling and evaluating Likert-style survey results [1]. NALS was validated using the results from the Aspects of Student Experience Survey (ASES). ASES is an instrument designed to assess physics graduate student experiences of departmental support structures [2]. Our current work is building on this past project.

NALS involves a series of steps necessary to generate a network from survey responses. These steps involve: (a) creating a bipartite network of respondents and response selections; (b) projecting the network onto response selections using the edge weights to indicate number of respondents selecting both responses; (c) building an item relation matrix for each possible item pair; (d) calculating a similarity value between items and record the ratio of mutual agree to mutual disagree selections as temperature; and (e) determining the backbone of the resulting network through identifying the most significant edges.

In our recently published work [1], we showed that we can not only reliably identify clusters through modular analysis of the resulting network but also that there are important in meaningful differences between the NALS clusters and clusters found through a traditional survey validity method such as the principal component analysis (PCA). In using NALS, we also can identify additional information that is not a result of running PCA. Our analysis found four modular communities within the ASES network: (1) Social and Scholarly Exploration, (2) Mentoring and Research Experience, (3) Professional and Academic Development, and (4) Financial Support. While Mentoring and Research Experience and Financial Support had been previously identified through PCA, Social and Scholarly Exploration and Professional and Academic Development were unique to the NALS approach. Due to our hierarchical community detection techniques, we also were able to investigate the structure of each community. We found that both Social and Scholarly Exploration and Mentoring and Research Experience had sub-communities within them that reveal smaller thematic groupings of items. For example, there are two sub-communities within the Social and Scholarly Exploration cluster: one pertains to interactions with a research group (e.g., journal discussions, presentations, meeting consistency) while the other captures interactions with the mentor (e.g., meeting with a mentor, regular feedback, apprenticeship).

Our current work is focused on applying the NALS approach to the ASES response data to identify differences between respondents based on various demographic information. Each different demographic split will result in distinct set of networks built only from the relevant responses. We intend to compare these networks in a variety of ways. First, we are looking at the different networks through general network characteristics, such as density, degree centralization, closeness centralization, average path length, diameter, and transitivity. Differences in these measures seen when comparing the demographic networks will imply that there are differences in how survey items are related together for those different demographic groups.

Next, we will compare the networks through network-level comparisons, such as node degree cosine centrality and edge existence Jaccard similarity. The network-level analysis focus on comparing specific

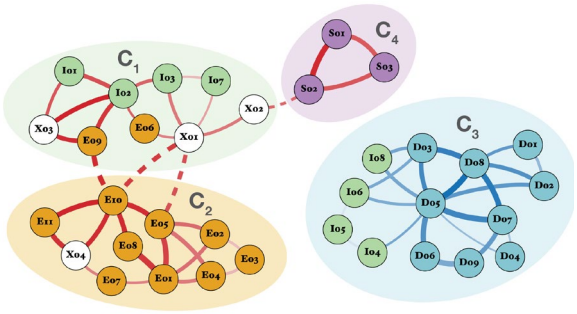

Figure 90. *The modular communities identified in the network of ASES items. The nodes are labeled by the unique question ID and are colored by the earlier identified principal component. Each shaded region corresponds to a community identified in the network. Red (blue) links between nodes indicate similar responses based upon "agree" ("disagree") response selections. Adapted from [1].*

nodes and edges between networks, which will help to identify where the differences may exist within the demographic networks. Finally, we will study the community partition of each network through cluster comparison metrics, such as purity and F-measure. This comparison focuses on the thematic communities that are arise from each demographic network. Differences identified through this analysis will be related to the overall experiences of support structures as reported by different demographic groups. This work will expand and further validate the utility of the NALS approach, demonstrating its usefulness for survey analysis [3].

[1] R.P. Dalka, D. Sachmpazidi, C. Henderson, and J.P. Zwolak. Network Analysis Approach to Likert-style Surveys. *Physical Review Physics Education Research* **18**, (2022), 020113.

[2] D. Sachmpazidi and C. Henderson. Departmental Support Structures for Physics Graduate Students: Development and Psychometric Evaluation of a Self-Report Instrument. *Physical Review Physics Education Research* **17** (2021), 010123.

[3] R. P. Dalka, D. Sachmpazidi, C. Henderson, and J. P. Zwolak. Demographic Comparisons of ASES through NALS. In preparation.

Table 3. *Student interns in ACMD.*

Name	From	Program		Mentor	Topic
Agrawal, Sristy	U. Colorado Boulder	G	FGR	S. Glancy	Resource based quantum information theory
Alhejji, Moham-mad	U. Colorado Boulder	G	PREP	E. Knill	Quantum randomness protocols
Avagyan, Arik	U. Colorado Boulder	G	PREP	E. Knill	Quantum information processing
Campbell, Mitchell	Virginia Tech	U	SURF	S. Ressler	Experiments with Virtual Objects
Centner, Raymond	U. South Florida	G	NSF	H. Cohl	Special values and Poisson kernel for Askey-Wilson polynomials
Eveleth, Jason	Brown U.	U	SURF	A. Kearsley	Optimal Voronoi tessellation
Geller, Shawn	U. Colorado Boulder	G	PREP	E. Knill	Characterization of quantum state prepara-tion and measurement errors
Hu, Mingyu	U. Colorado Boulder	G	PREP	M. Donahue	Modeling of antiferromagnets
Krepets, Mikhail	Montgomery College	U	SURF	M. Mascagni	Database for random number generation computational results
Kwiatkowski, Alexander	U. Colorado Boulder	G	PREP	E. Knill	Quantum networking
Ladic, Katjana	U. Zagreb, Croatia	G	FGR	K. Sayrafian	Ultra Wideband Channel Characterization for Ingestible Microbots
Liu, Liangchen	U. Texas Austin	G	NSF	G. Dogan	Explorations for Better Deep Learning
Lopez, Miguel	U. Maryland	U	SURF	H. Cohl	Conversion of Mathematica Source to LaTeX
Ornstein, Joel	U. Colorado Boulder	G	DGR	S. Glancy	Quantum information journal club
Rezaiyan-Nojani, Armin	T. S. Wootton HS	H	SHIP	K. Sayrafian	Visualization of human body models
Roy, Saunak	T. S. Wootton HS	H	SHIP	H. Cohl	3D N-ary tree art on smooth manifolds
Schneider, Ryan	U. C. San Diego	G	DGR	B. Schneider	Collocation methods to solve the electronic Schrödinger equation
Seshadri, Akshay	U. Colorado Boulder	G	PREP	E. Knill	Quantum measurement statistics
Su, Ruisi	Carnegie Mellon U.	U	FGR	A. Kearsley	Detecting network anomalies
van de Poll, May An	U. Colorado Boulder	G	PREP	E. Knill	Analysis of quantum optical measurements
Varshney, Ayush	Caltech	G	SURF	T. Gerrits	Software interfacing between quantum measurement hardware and quantum net-work management plane
Xiao, Lilian	Poolesville HS	H	SHIP	J. Terrill	Shader glyphs and simulation
Xiao, Vivian	U. Pennsylvania	U	DGR	A. Kearsley	Optimization in chemometrics

Legend

G Graduate Student
U Undergraduate
H High School

PREP Professional Research Experience Program
FGR Foreign Guest Researcher
DGR Domestic Guest Researcher
NSF NSF Mathematical Sciences Graduate Internship Program
SHIP Summer High School Internship Program
SURF Summer Undergraduate Research Fellowship

Part IV

Activity Data

Publications

Note: Names of (co-)authors with a Division affiliation during this reporting period are underlined.

Appeared

Refereed Journals

1. H. Ahmadi, A.Nag, Z. Khar, K. Sayrafian, and S. Rahardja. Networked Twins and Twins of Networks: An Overview on the Relationship Between Digital Twins and 6G, *IEEE Communications Standards* **5**:4 (December 2021), 154-160, Dec. 2021. DOI: 10.1109/MCOMSTD.0001.2000041
2. I. Bezerra, H. Vasconcelos, and S. Glancy. Quadrature Squeezing and Temperature Estimation from the Fock Distribution. *Quantum Information Processing* **21** (2022) 365. DOI:10.1007/s11128-022-03677-5
3. I. Bray, X. Weber, D. Fursa, A. Kadryrov, B. Schneider, S. Pamidighantam, M. Cytowski, and A. Kheifets. Taking the Convergent Close-coupling Method Beyond Helium: The Utility of the Hartree-Fock Theory. *ATOMS* **10**:1 (2022) 22. DOI: 10.3390/atoms10010022
4. A. Carasso. Data Assimilation in 2D Viscous Burgers Equation using a Stabilized Explicit Finite Difference Scheme Run Backward in Time. *Inverse Problems in Science and Engineering* **29**:13 (2022) 3475-3489. DOI: 10.1080/17415977.2021.2009476
5. Z. Chen, J. Wen, A. Kearsley, and A. Pertzborn. Evaluating the Performance of an Inexact Newton Method with a Preconditioner for Dynamic Building System Simulation. *Journal of Building Performance Simulation* **15**:1 (2022) 112-127. DOI: 10.1080/19401493.2021.2007285
6. K. Coakley, J. Splett, and T. Gerrits. Mixture Model Analysis of Transition Edge Sensor Pulse Height Spectra. *Journal of the Optical Society of America B* **39** (2022) 137-144. DOI: 10.1364/JOSAB.440232
7. H. Cohl and R. Costas-Santos. On the Relation Between Gegenbauer Polynomials and the Ferrers Function of the First Kind. *Analysis Mathematica* **48** (2022) 695-716. DOI: 10.1007/s10476-022-0123-0
8. L. Bi, H. Cohl, and H. Volkmer. Expansion for a Fundamental Solution of Laplace's Equation in Flat-Ring Cyclide Coordinates. *Symmetry, Integrability and Geometry: Methods and Applications* **18** (2022) 41. DOI: 10.3842/SIGMA.2022.041
9. L. Bi, H. Cohl, and H. Volkmer. Peanut Harmonic Expansion for a Fundamental Solution of Laplace's Equation in Flat-ring Coordinates. *Analysis Mathematica* **48** (2022) 961-989. DOI: 10.1007/s10476-022-0175-1
10. H. Cohl, R. Costas-Santos, P. Hwang, and T. Wakhare. Generalizations of Generating Functions for Basic Hypergeometric Orthogonal Polynomials. *Open Journal of Mathematical Sciences* **6** (2022) 248-261. DOI: 10.48550/arXiv.1411.1371
11. M. Coudron, J. Stark, and T. Vidick. Trading Locality for Time: Certifiable Randomness from Low-Depth Circuits. *Communications in Mathematical Physics* **382** (2022) 49–86. DOI: 10.1007/s00220-021-03963-w
12. S. Erickson, J. Wu, P.-Y. Hou, D. Cole, S. Geller, A. Kwiatkowski, S. Glancy, E. Knill, D. Slichter, A. Wilson, and D. Leibfried. High-fidelity Indirect Readout of Trapped Ion Hyperfine Qubits. *Physical Review Letters* **128** (2022) 60503. DOI: 10.1103/PhysRevLett.128.160503
13. R. Dalka, D. Sachmpazidi, C. Henderson, and J. Zwolak. Network Analysis Approach to Likert-style Surveys. *Physical Review Physics Education Research* **18**:2 (2022) 020113. DOI: 10.1103/PhysRevPhysEducRes.18.020113
14. M. DiSalvo, P. Patrone, A. Kearsley, and G. Cooksey. Serial Flow Cytometry in an Inertial Focusing Optofluidic Microchip for Direct Assessment of Measurement Variations. *Lab on a Chip* **22**:17 (2022) 3217-3228. DOI: 10.1039/D1LC01169C
15. R. P. Fitzgerald, B. K. Alpert, D. T. Becker, D. E. Bergeron, R. M. Essex, K. Morgan, S. Nour, G. O'Neil, D. R. Schmidt, G. E. Shaw, D. Swetz, R. M. Verkouteren, and D. Yan. Toward a New Primary Standardization of Radionuclide Massic Activity Using Microcalorimetry and Quantitative Milligram-Scale Samples. *Journal of Research of the National Institute of Standards and Technology* **126** (2021), 126048. DOI: 10.6028/jres.126.048
16. J. Fong, N. Heckert, J. Filliben, P. Marcal, and S. Freiman. Estimation of a Minimum Allowable Structural Strength Based on Uncertainty in Material Test Data. *Journal of Research of the National Institute of Standards and Technology* **126** (2021) 126036. DOI:10.6028/jres.126.036
17. J. W. Fowler, B. K. Alpert, G. C. O'Neil, D. S. Swetz, and J. N. Ullom. Energy calibration of nonlinear microcalorimeters with uncertainty estimates from Gaussian process regression. *Journal of Low Temperature Physics* special issue **LTD19** (2022). DOI: 10.1007/s10909-022-02740-w
18. L. Freeman, F. Batarseh, D. R. Kuhn, M. Raunak, and R. Kacker. The Path to Consensus on Artificial

Intelligence Assurance. *IEEE Computer* **55** (2022) 82-86. DOI: 10.1109/MC.2021.3129027

19. B. Garn, D. Schreiber, D. Simos, D. R. Kuhn. J. Voas, and R. Kacker. Combinatorial Methods for Testing IoT Smart Home Systems. *Journal of Software, Testing, Verification and Reliability* **32** (2022) 1805. DOI: 10.1002/stvr.1805

20. S. Geller, D. Cole, S. Glancy, and E. Knill. Improving Quantum State Detection with Adaptive Sequential Observations. *IOP Science* **7** (2022) 034004. DOI: 10.1088/2058-9565/ac6972

21. Z. Grey, S. Mosleh, J. Rezac, Y. Ma, J. Coder, and A. Dienstfrey. Bi-Criteria Radio Spectrum Sharing with Subspace-Based Pareto Tracing. *IEEE Transactions on Communications* **70**:50 (2022) 3512-3525. DOI: 10.1109/TCOMM.2022.3161516

22. S. Guo, S. Koh, A. Fritsch, I. Spielman, and J. Zwolak. Combining Machine Learning with Physics: A Framework for Tracking and Sorting Multiple Dark Solutions. *Physical Review Research* **4**:2 (2022) 023163. DOI: 10.1103/PhysRevResearch.4.023163

23. Z. Guo, J. K. Song, G. Barbastathis, M. E. Glinsky, C. T. Vaughan, K. W. Larson, B. K. Alpert, and Z. H. Levine. Physics-assisted Generative Adversarial Network for X-Ray Tomography. *Optics Express* **30** (13) 23238-23259 (2022). DOI: 10.1364/OE.460208

24. M. Henn, K. Quelhas, T. Bui, and S. Woods. Improving Model-Based MPI Image Reconstructions: Baseline Recovery, Receive Coil Sensitivity, Relaxation and Uncertainty Estimation. *International Journal on Magnetic Particle Imaging* **8**:1 (2022). DOI: 10.18416/ijmpi.2022.2208001

25. M. Henn, K. Quelhas, T. Bui, and S. Woods. Uncertainty Estimation for 2D Magnetic Particle Imaging. In *International Journal on Magnetic Particle Imaging,* **8:1** (2022). DOI: 10.18416/ijmpi.2022.2203082

26. L. Hu, W. Wong, D. R. Kuhn, R. Kacker, and S. Li. CT-IoT: A Combinatorial Testing-based Path Selection Framework for Effective IoT Testing. *Empirical Software Engineering* **27** (2022) 32. DOI: 10.1007/s10664-021-10017-1

27. H.-Y. Huang, R. Kueng, G. Torlai, V. Albert, and J. Preskill. Provably Efficient Machine Learning for Quantum Many-Body Problems. *Science* **377** (2022). DOI: 10.1126/science.abk3333

28. J. Jin, T. Gerrits, and A. Gamouras. Calibration and Comparison of Detection Efficiency for Free-space Single-photon Avalanche Diodes at 850 nm. *Applied Optics* **61:**17 (2022) 5244-5249. DOI: 10.1364/AO.461154

29. C. Joshi, B. Sparkes, A. Farsi, T. Gerrits, V. Verma, S. Ramelow, S. Nam, and A. Gaeta. Picosecond-Resolution Single-Photon Time Lens for Temporal Mode Quantum Processing. *Optica* **9**:4 (2022) 364-373. DOI: 10.1364/OPTICA.439827

30. R. Kacker. Towards Correction of the JCGM International Vocabulary of Metrology. *Measurement: Sensors* **18** (2021) 100063. DOI: 10.1016/j.measen.2021.100063

31. R. Kacker. On Quantity, Value, Unit, and Other Terms in the JCGM International Vocabulary of Metrology. *Measurement Science and Technology* **32** (2021) 125015. DOI: 10.1088/1361-6501/ac28d0/meta

32. R. Kacker, D. R. Kuhn, Y. Lei, and D. Simos. Measurement of the Adequacy of a Test Suite with Respect to the Modeled Test Space. *IEEE Software* **39** (2022) 62-67. DOI: 10.1109/MS.2021.3108060

33. L. Kampel, D. Simos, D. R. Kuhn, and R. Kacker. An Exploration of Combinatorial Testing-based Approaches to Fault Localization for Explainable AI. *Annals of Mathematics and Artificial Intelligence* **90** (2021) 951-964. DOI: 10.1007/s10472-021-09772-0

34. S. Kase, C. Hung, T. Krayzman, J. Hare, B. Rinderspacher, and S. Su. The Future of Collaborative Human-Artificial Intelligence Decision-making for Mission Planning. *Frontiers in Psychology* **13** (2022). DOI: 10.3389/fpsyg.2022.850628

35. I. Kim, B. Shi, K. Kato, and V. Albert. Chiral Central Charge from a Single Bulk Wave Function. *Physical Review Letters* **128** (2022) 176402. DOI:10.1103/PhysRevLett.128.176402

36. I. Kim, B. Shi, K. Kato, and V. Albert. Modular Commutator in Gapped Quantum Many-Body Systems. *Physical Review B* **106** (2022) 075147. DOI: 10.1103/PhysRevB.106.075147

37. P. Kuo. Noncritical Phasematching Behavior in Thin-film Lithium Niobate Frequency Converters. *Optics Letters* **47**:1 (2022) 54. DOI: 10.1364/OL.444846

38. J. Lee, E. Hwang, and R. Kacker. True Value, Error, and Measurement Uncertainty: Two Views. *Accreditation and Quality Assurance* **27** (2022) 235-242. DOI: 10.1007/s00769-022-01508-9

39. L. Madsen, F. Laudenbach, M. Askarani, F. Rortais, T. Vincent, J. Bulmer, F. Miatto, L. Neuhaus, L. Helt, M. Collins, A. Lita, T. Gerrits, S. Nam, V. Vaidya, M. Menotti, I. Dhand, Z. Vernon, N. Quesada, and J. Lavoie. Quantum Computational Advantage with a Programmable Photonic Processor. *Nature* **606** (2022) 75-81. DOI:s41586-022-04725-x

40. N. Martys, W. George, S. Satterfield, B. Toman, M. A. Peltz, S. Jones, and C. Ferraris. Standard Reference Materials for Rheological Measurements of Cement-Based Materials. *ACI Materials Journal* **118**:6 (2021) 325-330. DOI: 10.14359/51733132

41. P. Patrone, P. Bedekar, N. Pisanic, Y. Manabe, D. Thomas, C. Heaney, and A. Kearsley. Optimal Decision Theory for Diagnostic Testing: Minimizing Indeterminate Classes with Applications to Saliva-Based SARS-CoV-2 Antibody Assays. *Mathematical Biosciences* **351** (2022) 108858. DOI: 10.1016/j.mbs.2022.108858

42. P. Patrone and A. Kearsley. Classification Under Uncertainty: Data Analysis for Diagnostic Antibody Testing. *Mathematical Medicine and Biology: A Journal of the IMA* **38**:3 (2021) 396–416. DOI: 10.1093/imammb/dqab007

43. C. Rao, N. Li, Y. Lei, J. Guo, Y. Zhang, R. Kacker, and D. R. Kuhn. Combinatorial Test Generation for Multiple Input Models with Shared Parameters. *IEEE Transactions on Software Engineering* **48** (2022) 2606-2628. DOI: 10.1109/TSE.2021.3065950

44. C. Rau, A. Kyle, A. Kwiatkowski, E. Shojaee, J. Teufel, K. Lehnert, and T. Dennis. Entanglement Thresholds of Doubly Parametric Quantum Transducers. *Physical Review Applied* **17** (2022) 044057. DOI: 10.1103/PhysRevApplied.17.044057

45. M. Roberts, A. Moorthy, E. Sisco, and A. Kearsley. Incorporating Measurement Variability when Comparing Sets of High-resolution Mass Spectra. *Analytica Chimica Acta* **1230** (2022) 340247. DOI: 10.1016/j.aca.2022.340247

46. J. Sadeghi, P. Patrone, A. Kearsley, and G. Cooksey. Optofluidic Flow Meter for Sub-nanoliter per Minute Flow Measurements. *Journal of Biomedical Optics* **27**:1 (2022) 017001. DOI: 10.1117/1.JBO.27.1.017001

47. N. Saito, N. Douguet, H. Sannohe, N. Ishii, T. Kanai, Y. Wu, A. Chew, S. Han, B. Schneider, J. Olsen, L. Argenti, Z. Chang, and J. Itatani. Attosecond Electronic Dynamics of Core-Excited States of N_2O in the Soft X-ray Region. *Physical Review Research* **3** (2021) 043222. DOI:10.1103/PhysRevResearch.3.043222

48. L. Scarlett, M. Zammit, I. Bray, B. Schneider, and D. Fursa. Convergent Close-coupling Calculations of Electron Scattering on HeH^+. *Physical Review A* **106** (2022) 042818. DOI: 10.1103/PhysRevA.106.042818

49. B. Schneider, K. Hamilton, and K. Bartschat. Generalizations of the R-Matrix Method to the Treatment of the Interaction of Short Pulse Electromagnetic Radiation with Atoms. *ATOMS* **10**:3 (2022) 26. DOI: 10.3390/atoms10010026

50. J. Sims, B. Padhy, and M. Ruiz. Exponentially Correlated Hylleraas-Configuration-Interaction Studies of Atomic Systems. II. Non-relativistic Energies of the 1 singlet S through 6 singlet S states of the Li+ ion. *International Journal of Quantum Chemistry* **122** (2022) e26823. DOI: 10.1002/qua.26823

51. C. Qu, A. Kearsley, B. Schneider, W. Keyrouz, and T. Allison. Graph Convolutional Neural Network Applied to the Prediction of Normal Boiling Point. *Journal of Molecular Graphics and Modelling* **1**:112 (2022) 108149. DOI: 10.1016/j.jmgm.2022.108149

52. K. Quelhas, M. Henn, T. Bui, H. Wages, W. Tew, and S. Woods. Flexible Software for Rigorous Simulations of Magnetic Particle Imaging Systems. *International Journal on Magnetic Particle Imaging,* **8** :1 (2022). DOI: 10.18416/ijmpi.2022.2203081

53. M. Stephens, M. White, T. Gerrits, N. Tomlin, and J. Lehman. Quantum Calibrations Traceable through Classical Radiometry. *Measurement: Sensors* **18** (2021) 100267. DOI: 10.1016/j.measen.2021.100267

54. J. Stone, K. Griffin, J. Amstutz, D. DeMarle, W. Sherman, and J. Günther. ANARI: A 3-D Rendering API Standard. *Computing in Science & Engineering* **24**:2 (2022) 7-18. DOI: 10.1109/MCSE.2022.3163151

55. L. Tian, E. Elsheikh, P. Patrone, A. Kearsley, A. Gaigalas, S. Inwood, S. Lin-Gibson, D. Esposito, and L. Wang. Towards Quantitative and Standardized Serological and Neutralization Assays for COVID-19. *International Journal of Molecular Sciences* **22**:5 (2021) 2723. DOI: 10.3390/ijms22052723

56. Y. Tong, V. Albert, J. McClean, J. Preskill, and Y. Su. Provably Accurate Simulation of Gauge Theories and Bosonic Systems. *Quantum* **6** (2022) 816 DOI: 10.22331/q-2022-09-22-816

57. B. Weber, S. Kalantre, T. McJunkin, J. Taylor, and J. Zwolak. Theoretical Bounds on Data Requirements for the Ray-based Classification. *SN Computer Science* **3**:1 (2022) 57. DOI: 10.1007/s42979-021-00921-0

58. C. You, M. Hong, P. Bierhorst, A. Lita, S. Glancy, S. Kolthammer, E. Knill, S. Nam, R. Mirin, O. Magaña-Loaiza, and T. Gerrits. Scalable Multiphoton Quantum Metrology with Neither Pre-nor Post-selected Measurements. *Applied Physics Reviews* **8** (2021) 041406. DOI: 10.1063/5.0063294

59. J. Ziegler, T. McJunkin, E. Joseph, S. Kalantre, B. Harpt, D. Savage, M. Lagally, M. Eriksson, J. Taylor, and J. Zwolak. Toward Robust Autotuning of Noisy Quantum Dot Devices. *Physical Review Applied* **17**:2 (2022) 024069. DOI: 10.1103/PhysRevApplied.17.024069

Book Chapters

1. M. Ruiz, J. Sims, and B. Padhy. High-precision Hy-CI and E-Hy-CI Studies of Atomic and Molecular Properties. *Advances in Quantum Chemistry* (M. Musial, P. E. Hoggan, eds.) **83** (2021) 171-208. DOI: 10.1016/bs.aiq.2021.05.010

In Conference Proceedings

1. J. Chandrasekaran, A. Patel, Y. Lei, R. Kacker, and D. R. Kuhn. Evaluation of t-way Testing of DNNs in Autonomous Driving Systems. In *2021 IEEE International Conference on Artificial Intelligence Testing* (AITest), Oxford, UK, 23-26 August 2021, 17-18. DOI: 10.1109/AITEST52744.2021.00013

2. J. Chandrasekaran, F. Batarseh, L. Freeman, R. Kacker, M. Raunak, and D. R. Kuhn. Enabling AI Adoption through Assurance. In *The International FLAIRS Conference Proceedings* **35** (2022). DOI: 10.32473/flairs.v35i.130726

3. Dontha, Suchetan, S. Jie, S. Tan, S. Smith, S. Choi, and M. Coudron. Approximating Output Probabilities of Shallow Quantum Circuits which are Geometrically Local in any Fixed Dimension. In *17th Conference on the Theory of Quantum Computation, Communication and Cryptography* (TQC 2022), Urbana-Champaign, IL, July 11-15, 2022, 1-17. DOI: 10.48550/arXiv.2202.08349

4. F. Durso, M. Raunak, D. Kuhn, and R. Kacker. Analyzing Failures in AI and Learning Systems (FAILS). In *29th IEEE Software Technology Conference* (2022), Gaithersburg, MD, November 18, 2022. DOI: 10.1109/STC55697.2022.00010

5. J. Fong, P. Marcal, S. Freiman, N. Heckert, and J. Filliben. Fatigue-life Prediction and Design for Uncracked and Cracked Components: Deterministic, A- and B-basis Probabilistic, and Reliability Target Approaches. In *Proceedings of the 2022 ASME Pressure Vessels & Piping Division Conference,* July 17-22, 2022, Las Vegas, NV, PVP2022-84851. DOI: 10.1115/PVP2022-84851

6. T. Gerrits, I. Burenkov, Y. Li-Baboud, A. Rahmouni, D. Anand, Hala, O. Slattery, A. Battou, and S. Polyakov. White Rabbit-assisted Quantum Network Node Synchronization with Quantum Channel Coexistence. In *Proceedings of the 2022 Conference on Lasers and Electro-Optics (CLEO),* San Jose, CA, May 15-20, 2022. DOI: 10.1364/CLEO_QELS.2022.FM1C.2

7. A. Greiner-Petter, H. Cohl, A. Youssef, M. Schubotz, A. Trost, R. Dey, A. Aizawa, and B. Gipp. Comparative Verification of the Digital Library of Mathematical Functions and Computer Algebra Systems. In *Proceedings of Tools and Algorithms for the Construction and Analysis of Systems (TACAS 2022)*, Munich, Germany, April 2-7, 2022, Lecture Notes in Computer Science **13243**, Springer, (D. Fisman and G. Rosu, eds.) DOI: 10.1007/978-3-030-99524-9_5

8. Z. Guo, J. K. Song, G. Barbastathis, M. E. Glinsky, C. T. Vaughan, K. W. Larson, B. K. Alpert, and Z. H. Levine. Advantage of Machine Learning over Maximum Likelihood in Limited-Angle Low-Photon X-Ray Tomography. In *Machine Learning for Scientific Imaging 2022*, IS&T Electronic Imaging 2022. DOI: 10.2352/EI.2022.34.5.MLSI-202

9. C. Hung, J. Hare, B. Rinderspacher, W. Peregrim, S. Kase, S. Su, A. Raglin, and J. Richardson. ARL Battlespace: A Platform for Developing Novel AI for Complex Adversarial Reasoning in MDO. In *Artificial Intelligence and Machine Learning for Multi-Domain Operations Applications IV*, Orlando, Florida, June 6, 2022. DOI: 10.1117/12.2622227

10. K. Krhac, K. Sayrafian, U. Bengi, and S. Dumanli. A Wearable Wireless Monitoring System for the Detection of Pulmonary Edema. In *IEEE Global Communications Conference* (*GLOBECOM*), Madrid, Spain, December 7-11, 2021. DOI: 10.1109/GLOBECOM46510.2021.9685118

11. P. Kuo. Towards Noncritical Phasematching in Thin-film Lithium Niobate Waveguides. In *Proceedings of SPIE 11985, Nonlinear Frequency Generation and Conversion: Materials and Devices XXI*, San Francisco, California, February 21–27, 2022. DOI: 10.1117/12.2614783

12. D. R. Kuhn, M. Raunak, C. Prado, V. Patil, and R. Kacker. Combination Frequency Differencing for Identifying Design Weaknesses in Physical Unclonable Functions. In *2022 IEEE International Conference on Software Testing, Verification and Validation Workshops* (ICSTW) Valencia, Spain, April 4-13, 2022, 110-117. DOI: 10.1109/ICSTW55395.2022.00032

13. L. Ma and L. Ding. Hybrid Quantum Edge Computing Network. In *Proceedings of the 2022 Conference of the Society of Photo-Optical Instrumentation Engineers (SPIE): Optics and Photonics,* October 2022. Proceedings of SPIE **12238** (2022) 122380F-1. DOI: 10.1117/12.2633020

14. V. Mai and R. La. Story of Two Populations in Epidemics: Is Every Infection Counted? In *Complex Networks & Their Applications X. COMPLEX NETWORKS 2021*. Studies in Computational Intelligence **1016** (2021) 229-240. DOI: 10.1007/978-3-030-93413-2_20

15. V. Mai, R. La, T. Zhang, and A. Battou. End-to-End Quality-of-Service Assurance with Autonomous Systems: 5G/6G Case Study. In *Proceedings of the*

2022 IEEE Consumer Communications and networking Conference (CCNC '22), Online, January 8-11, 2022. DOI: 10.1109/CCNC49033.2022.9700514

16. V. Mai, R. La, and A. Battou. Optimal Cybersecurity Investments Using SIS Model: Weakly Connected Networks. In *Proceedings of the 2022 IEEE Global Communications Conference (Globecom'20)*, Hybrid, Rio de Janeiro, Brazil, December 4-8, 2022. DOI: 10.1109/GLOBECOM48099.2022.10001358
17. V. Mai and R. La. Investments in Robustness of Complex Systems: Algorithm Design. In *Complex Networks & Their Applications XI. COMPLEX NETWORKS 2022*, Palermo, Italy, November 8-10, 2022, 407-418. DOI: 10.1007/978-3-031-21131-7_32
18. V. Marbukh. Towards Risk Adjusted Wireless Access under Jamming: Reliability through Multi-Connectivity." In *Proceedings of the IEEE Consumer Communications & Networking Conference* (CCNC'22), Online, January 8-11, 2022. DOI: 10.1109/CCNC49033.2022.9700558
19. V. Marbukh. Towards Robust Fog/Edge Computing Infrastructure with Risk Adjusted Multi-Connectivity. In *Proceeding of the 9th International Conference on Future Internet of Things and Cloud* (FiCloud'22), Hybrid, Rome, Italy, August 22-24, 2022. DOI: 10.1109/FiCloud57274.2022.00029
20. V. Marbukh. Towards Shapley Value based Security Risk Attribution in Sensor Networks. In *Proceedings of the IEEE/ACM Information Processing in Sensor Networks* (IPSN'22), Online, May 4-6, 2022. DOI:10.1109/IPSN54338.2022.00060
21. V. Marbukh. Towards Reliability/Security Risk Metrics for Large-Scale Networked Infrastructures: Work in Progress. In *Probabilistic Safety Assessment & Management Conference* (PSAM'22), Honolulu, Hawaii, June 26 - July 1, 2022, MA26-PSAM16. URL: https://www.iapsam.org/PSAM16/papers/ALL-PSAM16-PAPERS.zip
22. V. Marbukh. Systemic Risk of Undesirable Contagion within System Time Horizon: Work in Progress. In *Proceedings of European Conference on Safety and Reliability* (ESREL'22), Dublin, Ireland, August 28 -September 1, 2022. URL: https://rpsonline.com.sg/rps2prod/esrel22-epro/esrel2022-extended-abstracts-book.pdf
23. A. Patel, J. Chandrasekaran, Y. Lei, R. Kacker, and D. R. Kuhn. A Combinatorial Approach to Fairness Testing of Machine Learning Models. In *2022 IEEE International Conference on Software Testing, Verification and Validation Workshops* (ICSTW) Valencia, Spain, April 4-13, 2022, 94-101. DOI: 10.1109/ICSTW55395.2022.00030
24. A. Rahmouni, T. Gerrits, A. Migdall, O. Slattery, P. Shaw, and J. Rice. "A Self-validated Detector for Characterization of Quantum Network Components." In *proceedings of the 2022 Conference on Lasers and Electro-Optics (CLEO),* May 2022. DOI:9890243
25. A. Rahmouni, T. Gerrits, and O. Slattery. Progress on a Portable Entangled Photon Source and Receiver for Quantum Networking Metrology. In *Proceedings of the 2022 Quantum 2.0 Conference and Exhibition,* June 13-16, 2022, QTh3C.3. DOI: 10.1364/QUANTUM.2022.QTh3C.3
26. A. Rahmouni, L. Ma, X. Tang, T. Gerrits, L. Cai, Q. Li, and O. Slattery. Towards Entangled Photon Pair Generation from a SiC-based Microring Resonator. In *Proceedings of the 2022 Conference of the Society of Photo-Optical Instrumentation Engineers (SPIE): Optics and Photonics,* San Diego, CA, October 2022. DOI: 10.1117/12.2632597
27. A. Rahmouni, S. Saha, O. Slattery, and T. Gerrits. Hyperspectral Photon-counting Optical Time Domain Reflectometry. In *Proceedings of the 2022 Conference of the Society of Photo-Optical Instrumentation Engineers (SPIE): Optics and Photonics,* San Diego, CA, October 2022. DOI: 10.1117/12.2633451
28. A. Rahmouni, T. Gerrits, P. Kuo, R. Dileep, M. Lijun, T. Xiao, and O. Slattery. Portable Polarization-entangled Photon Source & Receiver Toolset for Quantum Network Metrology. In *Proceedings of Quantum Communications and Quantum Imaging XX* **12238** (2022) 122380I. DOI: 10.1117/12.2632997
29. M. Roudneshin, K. Sayrafian, and A. G. Aghdam. Maximizing Harvested Energy in Coulomb Force Parametric Generators. In *IEEE American Control Conference (IEEE ACC)*, Atlanta, GA, USA, June 8-10, 2022. DOI: 10.23919/ACC53348.2022.9867451
30. M. Roudneshin, K. Sayrafian, and A. G. Aghdam. An Asymmetric Adaptive Approach to Enhance Output Power in Kinetic-Based Microgenerators. In *IEEE Sensors 2022 Conference*, Dallas, TX, October 30 - November 2, 2022. DOI: 10.1109/SENSORS52175.2022.9967112
31. M. Särestöniemi, C. Pomalaza-Raez, K. Sayrafian, T. Myllylä, and J. Iinatti. A Preliminary Study of RF Propagation for High Data Rate Brain Telemetry. In *Proceedings of the 16th EAI International Conference on Body Area Networks* (BodyNets 2021), Online, October 25-26, 2021. DOI: 10.1007/978-3-030-95593-9_11
32. K. Sayrafian, B. Cloteaux, V. Marbukh and C. Emiyah. Evaluation of the Bluetooth-based Proximity Estimation for Automatic Exposure Determination.

In *2022 IEEE 19th Annual Consumer Communications & Networking Conference (CCNC)*, 2022, 683-686. DOI: 10.1109/CCNC49033.2022.9700648

33. K. Sayrafian, B. Cloteaux, and V. Marbukh. On the Performance of Automatic Exposure Determination Using Bluetooth-based Proximity Estimation. In *ICC 2022 - IEEE International Conference on Communications*, 2022, 3052-3057. DOI: 10.1109/ICC45855.2022.9838839

34. K. Sayrafian, B. Cloteaux, and V. Marbukh. Impact of Using Soft Thresholds in Automatic Contact Tracing. In *2022 IEEE International Conference on E-health Networking, Application & Services (HEALTHCOM),* 2022. DOI :10.1109/HealthCom54947.2022.9982790

35. O. Slattery, L. Ma, X. Tang, T. Gerrits, A. Rahmouni, and S. Bhushan. The Quantum Communications and Networking Project at the Information Technology Laboratory of NIST. In *Proceedings of the 2021 IEEE Conference on Communications and Network Security: Workshop on Quantum Communication and Quantum Cryptography*, Online, October 2021. DOI: 10.1109/CNS53000.2021.9705051

36. R. Srinivas, S. Burd, H. Knaack, R. Sutherland, A. Kwiatkowski, S. Glancy, E. Knill, D. Wineland, D. Leibfried, A. Wilson, D. Allcock, and D. Slichter. High-fidelity RF/Microwave-based Universal Control of Trapped Ion Qubits. In *IEEE/MTT-S International Microwave Symposium 2022*, Denver, CO, June 19-24, 2022, 80-83. DOI: 10.1109/IMS37962.2022.9865483

37. S. Su, W. Sherman, S. Satterfield, T. Griffin, S. Ressler, W. George, S. Feng, and J. Terrill. Visualization Ecology Applications for Measurement Science: A Visualization Gap Approach. In *VisGap - The Gap between Visualization Research and Visualization Software*, Rome, Italy, June 13, 2022, DOI: 10.2312/visgap.20221057

38. S. Su, W. Sherman, I. Lopez Coto, K. Sayrafian, and J. Terrill. Immersive ParaView: An Immersive Scientific Workflow for the Advancement of Measurement Science. In *Proceedings of 2022 IEEE International Symposium on Mixed and Augmented Reality Adjunct* (ISMAR-Adjunct), Singapore, October 17-21, 2022. DOI: 10.1109/ISMAR-Adjunct57072.2022.00034

39. M. Wagner, M. Leithner, D. Simos, D. R. Kuhn, and R. Kacker. Developing Multithreaded Techniques and Improved Constraint Handling for the Tool CAgen. In *2022 IEEE International Conference on Software Testing, Verification and Validation Workshops* (ICSTW) Valencia, Spain, 4-13 April 2022, 87-93. DOI: 10.1109/ICSTW55395.2022.00029

Technical Reports

1. G. Alagic, D. Apon, D. Cooper, Q. Dang, T. Dang, J. Kelsey, J. Lichtinger, Y.-K. Liu, C. Miller, D. Moody, R. Peralta, R. Perlner, A. Robinson, and D. Smith-Tone. Status Report on the Third Round of the NIST Post-Quantum Cryptography Standardization Process. NISTIR 8413-upd1, September 2022, 102 pages. DOI: 10.6028/NIST.IR.8413

2. A. Arora, A. Coladangelo, M. Coudron, A. Gheorghiu, U. Singh, and H. Waldner. Quantum Depth in the Random Oracle Model. URL: 10.48550/arXiv.2210.06454

3. J. Berg, T. Gerrits, W. Grice, P. Kumar, A. Migdall, A. Miller, and M. Stephens. Single-Photon Measurement Infrastructure for Quantum Applications (SPMIQA): Needs and Priorities. Quantum Economic Development Consortium Report, July 11, 2022. URL: https://quantumconsortium.org/mp-files/qed-c-single-photon-report.pdf/

4. R. F. Boisvert, ed. Applied and Computational Mathematics Division: A Summary of Activities in Fiscal Year 2021. NISTIR 8423, April 2022, 183 pages. DOI: https://doi.org/10.6028/NIST.IR.8423

5. A. Carasso. Data Assimilation in 2D Nonlinear Advection Diffusion Equations, Using an Explicit Stabilized Leapfrog Scheme Run Backward in Time. NIST Technical Note, TN 2227, July 12, 2022. DOI: 10.6028/NIST.TN.2227

Other Publications

1. H. Cohl, M. Ismail, and H.-H. Wu (eds.) The Legacy of Dick Askey (1933-2019). *Notices of the American Mathematica Society* **69** (2022) 59-75. DOI: 10.1090/noti2405

2. R. Kenett and R. Kacker. John Mandel (a brief biography). *Wiley StatsRef: Statistics Reference Online* (2022). DOI: 10.1002/9781118445112.stat08385

3. B. Saunders and W. Hawkins. Reflections on Dr. Genevieve M. Knight: 1939-2021. *MAA Focus: Mathematical Association of America* **41**:6 (2022) 14-20. URL: http://digitaleditions.walsworthprintgroup.com/publication/?i=732159

4. O. Slattery and Y. Kim. Breakthrough in Teleportation Furthers Quantum Network Development. *Nature* **605** (2022) 663-668. DOI :d41586-022-01364-0

Blog Posts

1. J. Fong. My Journey from Designing Dams to Helping Structures Live Their Longest Lives. *Taking Measure Blog*, NIST, August 5, 2022. URL: https://www.nist.gov/blogs/taking-measure/my-journey-designing-dams-helping-structures-live-their-longest-lives

2. A. J. Kearsley. Optimization and Data Analysis for Improved COVID-19 Detection and Measurement. *SIAM News*, February 18, 2022. URL: https://sinews.siam.org/Details-Page/optimization-and-data-analysis-for-improved-covid-19-detection-and-measurement-2
3. B. I. Schneider. AMO for All: How Online Portals Are Democratizing the Field of Atomic, Molecular and Optical Physics. Taking Measure Blog, NIST, November 2, 2022. URL: https://www.nist.gov/blogs/taking-measure/amo-all-how-online-portals-are-democratizing-field-atomic-molecular-and-optical

Accepted

1. V. Albert. Bosonic Coding: Introduction and Use Cases. In *Proceedings of the International School of Physics "E. Fermi."*
2. P. Bedekar, A. Kearsley, and P. Patrone. Prevalence Estimation and Optimal Classification Methods to Account for Time Dependence in Antibody Levels. *Journal of Theoretical Biology.*
3. A. Childs, M. Coudron, and A. Gilani. Quantum Algorithms and the Power of Forgetting. *14th Innovations in Theoretical Computer Science (ITCS).*
4. H. Cohl and R. Costas-Santos. Utility of Integral Representations for Basic Hypergeometric Functions and Orthogonal Polynomials. *The Ramanujan Journal.*
5. H. Cohl and M. Schubotz. The Digital Shadow of Mathematics and its Ramifications. *Jahrbuch über die Fortschritte der Mathematik*.
6. H. Cohl and M. Ismail. Liber Amicorum, a Friendship Book for Dick Askey. *Celebratio Mathematica*.
7. R. DeJaco, J. Majikes, J. Liddle, and A. Kearsley. Binding, Brightness, or Noise? Extracting Temperature-dependent Properties of Dye Bound to DNA. *Biophysical Journal*.
8. S. Freiman and J. Fong. A New Statistical Methodology for Assessing Mechanical Survivability of Brittle Materials. *Journal of Strength, Fracture, and Complexity.*
9. A. Fritsch, S. Guo, S. Koh, I. Spielman, and J. Zwolak. Dark Solitons in Bose-Einstein Condensates: A Dataset for Many-body Physics Research. *Machine Learning: Science and Technology*.
10. Z. Grey, O. Doronina, and A. Glaws. Separable Shape Tensors for Aerodynamic Design. *Journal of Computational Design and Engineering.*
11. N. Lal, I. Burenkov, P. Kuo, Y. Li-Baboud, O. Slattery, T. Gerrits, and S. Polyakov. Towards a Scalable Network Source of Single Photons. *Photonics West*, 2023.
12. C. Lenart, K. Kosko, S. Su, Y. Yang, A. Corsello, and Q. Guan. Gaze Analysis System for Immersive 360° Video for Preservice Teacher Education. *IEEE Virtual Reality 2023*.
13. P. Scharpf, M. Schubotz, H. Cohl, C. Breitinger, and B. Gipp. Discovery and Recognition of Formula Concepts using Machine Learning, *Scientometrics*.
14. H. Zhao, G. W. Bryant, W. Griffin, J. E. Terrill, and J. Chen. Evaluating Glyph Design for Showing Large-Magnitude-Range Quantum Spins. *IEEE Transactions on Visualization and Computer Graphics.*
15. J. Zwolak and J. Taylor. Colloquium: Advances in Automation of Quantum Dot Devices Control. *Reviews of Modern Physics*.

In Review

1. V. Albert, D. Aasen, W. Xu, W. Ji, J. Alicea, and J. Preskill. Spin Chains, Defects, and Quantum Wires for the Quantum-Double Edge.
2. B. Alexander, H. Cohl, and H. Volkmer. Internal and External Harmonics in Bi-cyclide Coordinates.
3. A. Avagyan, E. Knill, and S. Glancy. Multi-Mode Gaussian State Analysis with Total Photon Counting.
4. I. Burenkov, A. Semionova, Hala, T. Gerrits, A. Rahmouni, D. Anand, Y. Li-Baboud, O. Slattery, A. Battou, and S. Polyakov. Fundamental Coexistence Limit of Quantum States with White Rabbit Synchronization in Optical Quantum Networks.
5. I. Burenkov, A. Semionova, Hala, T. Gerrits, A. Rahmouni, D. Anand, Y. Li-Baboud, O. Slattery, A. Battou, and S. Polyakov. Synchronization and Coexistence in Quantum Networks.
6. B. Cloteaux. A Note on the Minimal Hamming Distance to a Graphic Sequence.
7. B. Cloteaux. How Much Regularity Forces a Sequence to be Graphic?
8. B. Cloteaux. Graphic Approximation of Integer Sequences.
9. H. Cohl and R. Costas-Santos. Nonterminating Transformations and Summations Associated with some q-Mellin-Barnes Integrals.
10. H. Cohl and L. Ritter. Two-dimensional Contiguous Relations for Linearization Coefficients of Orthogonal Polynomials in the Askey-scheme.

11. E. Culf, T. Vidick, and V. Albert. Group Coset Monogamy Games and an Application to Device-Independent Continuous-variable QKD.
12. R. Dalka and J. Zwolak. Restoring the Structure: A Modular Analysis of Ego-driven Organizational Networks.
13. R. DeJaco, M. Roberts, E. Romsos, P. Vallone, and A. Kearsley. Reducing Bias and Quantifying Uncertainty in Fluorescence Produced by PCR.
14. P. Faist, M. Woods, V. Albert, J. Renes, J. Eisert, and J. Preskill. Time-energy Uncertainty Relation for Noisy Quantum Metrology.
15. S. Gandhari, V. Albert, T. Gerrits, J. Taylor, and M. J. Gullans. Continuous-Variable Shadow Tomography.
16. M. Henn, T. Bui, and S. Woods. Investigating the Harmonic Dependence of MPI Resolution
17. M. Henn, K. Quelhas, and S. Woods. Investigating the Influence of Sampling Frequency on X-Space MPI Image Reconstructions.
18. J. Iosue, K. Sharma, M. Gullans, and V. Albert. Continuous-variable Quantum State Designs: Theory and Applications.
19. A. Kwiatkowski, E. Shojaee, S. Agrawal, A. Kyle, C. Rau, S. Glancy, and E. Knill. Constraints on Gaussian Error Channels and Measurements for Quantum Communication.
20. A. Kyle, C. Rau, W. Warfield, A. Kwiatkowski, J. Teufel, K. Lehnert, and T. Dennis. Optically Distributing Remote Two-node Microwave Entanglement using Doubly Parametric Quantum Transducers.
21. Z. H. Levine, B. K. Alpert, A, L. Dagel, J. W. Fowler, E. S. Jimenez, N. J. Nakamura, D. S. Swetz, P. Szypryt, K. R. Thompson, and J. N. Ullom. A Tabletop X-Ray Tomography Instrument for Nanometer-Scale Imaging: Reconstructions.
22. R. Luke, A. Kearsley, N. Pisanic, Y. Manabe, D. Thomas, C. Heaney, and P. Patrone. Modeling in Higher Dimensions to Improve Diagnostic Testing Accuracy: Theory and Examples for Multiplex Saliva-based SARS-CoV-2 Assays.
23. R. Luke, A. Kearsley, and P. Patrone. Optimal Classification and Generalized Prevalence Estimates for Diagnostic Settings with More than Two Classes.
24. L. Melara, R. Evans, S. Cho, A. Balijepalli, and A. Kearsley. Optimal Bandwidth Selection in Stochastic Regression of Bio-FET Measurements.
25. H. Mahboubi, K. Sayrafian, and A. G. Aghdam. A Low Complexity Power Maximization Strategy for Coulomb Force Parametric Generators.
26. V. Mai, R. La, T. Zhang, and A. Battou. Distributed Optimization with Global Constraints Using Noisy Measurements.
27. V. Mai, R. La, T. Zhang, Y. Huang, and A. Battou. Federated Learning with Server Learning for Non-IID Data.
28. V. Mai, R. La, and T. Zhang. Accelerated Federated Learning on Non-IID Data via Server Learning.
29. W. McKenzie, Y. Li-Baboud, M. Morris, G. Baumgartner, A. Rahmouni, P. Kuo, O. Slattery, B. Crabill, M. Merzouki, A. Battou, and T. Gerrits. Sub-200 ps Quantum Network Node Synchronization over a 128 km Link White Rabbit Architecture.
30. N. Nakamura, P. Szypryt, A. L. Dagel, B. K. Alpert, D. A. Bennett, W. B. Doriese, M. Durkin, J. W. Fowler, D. T. Fox, J. D. Gard, R. N. Goodner, J. Z. Harris, G. C. Hilton, E. S. Jimenez, B. L. Kernen, K. W. Larson, Z. H. Levine, D. McArthur, K. M. Morgan, G. O'Neil, C. G. Pappas, C. D. Reintsema, D. R. Schmidt, P. A. Schulz, D. S. Swetz, K. R. Thompson, J. N. Ullom, L. R. Vale, C. T. Vaughan, C. Walker, J. C. Weber, and J. W. Wheeler. A Tabletop X-Ray Tomography Instrument for Nanometer-Scale Imaging: Integration of a Scanning Electron Microscope with a Transition-Edge Sensor Spectrometer.
31. J. Nolan, D. Audus, and J. Douglas. Computation of Alpha-capacity of General Sets in R^d using Stable Random Walks.
32. P. Patrone and A. Kearsley. Minimizing Uncertainty in Prevalence Estimates.
33. P. Patrone, M. DiSalvo, A. Kearsley, G. McFadden, and G. Cooksey. Reproducibility in Cytometry: Signals Analysis and its Connection to Uncertainty Quantification.
34. C. Qu, B. Schneider, A. Kearsley, W. Keyrouz, and T. Allison. Prediction of Mass Spectra via Molecular Structure Based Machine Learning.
35. K. Quelhas, M. Henn, R. Farias, W. Tew, and S. Woods. Parallel MPI Image Reconstructions in GPU
36. A. Rahmouni, P. Kuo, Y. Shi, M. Jabir, N. Lal, I. Burenkov, Y. Li-Baboud, M. Merzouki, A. Battou, S. Polyakov, O. Slattery, and T. Gerrits. Experimental Demonstration of Local Area Entanglement Distribution between Two Distant Nodes, Coexisting with Classical Synchronization.

37. M. Särestöniemi, K. Sayrafian, T. Myllylä, J. Iinatti. A Preliminary Study of On/Off-Body Propagation Channels for Brain Telemetry Using a Flexible Wearable Antenna.
38. B. Saunders, S. Brooks, R. Buckmire, R. Vincent-Finley, F. Backeljauw, S. Becuwe, B. Miller, M. McClain, and A. Cuyt. Validated Computation of Special Mathematical Functions.
39. Y. Shi, T. Gerrits, and O. Slattery. Towards Continuous Fiber Birefringence Compensation with Single-Photon-Level Light.
40. M. Vazquez, T. Berry, T. Sauer, and G. Doğan. Texture Segmentation from a Manifold Learning Perspective.
41. O. Yousuf, I. Hossen, M. Daniels, M. Leuker-Boden, A. Dienstfrey, and G. Adam. Device Modeling Bias in ReRAM-based Neural Network Simulations.
42. Y. Xu, Y. Wang, E.-J. Kuo, and V. Albert. Qubit-Oscillator Concatenated Codes: Decoding Formalism and Code Comparison.

Inventions

Invention Disclosures and Patents in Review

1. A. Balijepalli, J. Majikes, A. Kanwal, P. Vallone, K. Kiesler, E. Romsos, and A. Kearsley. US Department of Commerce, assignee. Agile nucleic acid sensor and measuring a biomarker. United States Patent Application US 17/845,682. October 13, 2022.
2. G. Cooksey, A. Kearsley, and P. Patrone. Multiplexed Amplitude Modulation Photometer and Performing Multiplexed Amplitude Modulation Photometry. Provisional Patent Application 20210055201.
3. G. Cooksey, A. Kearsley, and P. Patrone. Serial Flow Cytometer. Provisional Patent Application 20210302300.
4. A. Kearsley, P. Patrone, E. Romsos, and P. Vallone. System and Method for Data Analysis in Quantitative PCR Measurements. Provisional Patent Application 20210395807.
5. K. Sayrafian. Lung Fluid Monitor and Determining Fluid Level in a Lung. Patent Application Serial Number PCT/US22/48217, Oct. 28, 2022
6. S. Seif Tabrizi, M. Hafezi, and Y.-K. Liu. Systems and Methods for Compressed Sensing Measurement of Long-Range Correlated Noise. Provisional Patent Application, NIST Docket 21-020 US1, May 13, 2022.

Presentations

Note: Names of (co-)presenters with an ACMD affiliation during this reporting period are underlined.

Invited Talks

1. V. Albert. "Spin Chains, Defects, and Quantum Wires for the Quantum-Double Edge." Condensed Matter Theory Center Seminar, University of Maryland, College Park, MD, November 1, 2022.
2. V. Albert. "Modern Quantum Tools for Bosonic Systems." 24th Annual Southwest Quantum Information and Technology (SQuInT) Workshop, Berkeley, CA, October 20, 2022.
3. V. Albert. "Overview of Quantum Error Correction." Noisy Intermediate-Scale Quantum Systems: Advances and Applications, Kavli Institute of Theoretical Physics, Santa Barbara, CA, September 13, 2022.
4. V. Albert. "Spin Chains, Defects, and Quantum Wires for the Quantum-Double Edge." Quantum Information Group Meeting, University of Sydney, Australia, July 27, 2022.
5. V. Albert. "Molecular Rotational State Spaces for Quantum Information Processing." 30th Annual International Laser Physics Workshop (LPHYS'22), Online, July 22, 2022.
6. V. Albert. "Spin Chains, Defects, and Quantum Wires for the Quantum-Double Edge." Quantum Science and Condensed Matter (QST/CM) Seminar, Swiss Federal Institute of Technology Lausanne (EPFL), Switzerland, June 16, 2022.
7. V. Albert. "Molecular Rotational State Spaces for Quantum Information Processing." Telluride Research Science Center Workshop: From Fundamentals of Molecular Spin Qubit Design to Molecule-Enabled Quantum Information, Telluride, CO, June 7, 2022.
8. V. Albert. "Molecular Rotational State Spaces for Quantum Information Processing." 53rd Annual Meeting of the American Physical Society Division of Atomic, Molecular and Optical Physics (DAMOP), Orlando, FL, June 1, 2022.
9. V. Albert. "Spin Chains, Defects, and Quantum Wires for the Quantum-Double Edge." CMT Seminar (virtual), Racah Institute of Physics, the Hebrew University of Jerusalem, Israel, January 6, 2022.
10. V. Albert. "Lindbladians with Multiple Steady States." University of Ulm, Germany, Online, December 16, 2021.

11. P. Bedekar, A. Kearsley, and P. Patrone. "Optimal Time-dependent Classification for Diagnostic Testing." Applied and Computational Mathematics Seminar, George Mason University, Fairfax, VA, November 18, 2022.
12. P. Bedekar, A. Kearsley, and P. Patrone. "Optimal Time-dependent Classification for Diagnostic Testing." 2nd European Conference on Mathematical and Theoretical Biology, Heidelberg, Germany, September 19, 2022.
13. R. Boisvert and W. Guthrie. "A Cavalcade of Distinguished Mathematicians and Statisticians at NIST." 75th Anniversary of Mathematics and Statistics at NIST, Online, June 28, 2022.
14. R. Boisvert. "Quantum Information Science in the NIST Information Technology Laboratory." International Federation for Information Processing Working Group 2.5 Annual Meeting, Online, August 24, 2022.
15. D. Brager. "Mathematically Investigating Retinitis Pigmentosa." Laboratory for Systems Medicine, University of Florida, December 16, 2021.
16. R. Buckmire, B. Saunders, R. Vincent-Finley, and S. Brooks. "Saunders ADJOINT Team Update on Validated Numerical Computations Research." MSRI African Diaspora Joint Mathematics (ADJOINT) Reunion Workshop, Online, July 1, 2022.
17. H. Cohl. "Jacobi Functions of the First and Second Kind (part I)." LSU Harmonic Analysis Seminar, Department of Mathematics, Louisiana State University, Baton Rouge, LA, Online, September 28, 2022.
18. H. Cohl. "Jacobi Functions of the First and Second Kind (part II)." LSU Harmonic Analysis Seminar, Department of Mathematics, Louisiana State University, Baton Rouge, LA. Online. October 19, 2022.
19. H. Cohl. "Symmetric and Nonsymmetric Representations for Poisson Kernels of Askey-Wilson Polynomials." Functional Equations and Applications (RIPOEFA) Seminar, Ibero-American Network of Researchers in Orthogonal Polynomials, Online, October 28, 2022.
20. M. Coudron. "Quasi-polynomial Time Approximation of Output Probabilities of Constant-depth, Geometrically-local Quantum Circuits." Simons Institute Seminar, University of California at Berkeley, April 20, 2022.
21. M. Coudron. "Approximating Output Probabilities of Shallow, Geometrically-local Quantum Circuits." QuICS Stakeholder Day, University of Maryland, College Park, MD, March 3, 2021.
22. M. Coudron. "Simulating Shallow Quantum Circuits." Algorithms, and AI for Real Problems Research Experience for Undergraduates (REU), University of Maryland, College Park, MD, June 2021.
23. R. DeJaco, M. Roberts, E. Romsos, P. Vallone, and A. Kearsley. "Reducing Bias and Quantifying Uncertainty in Fluorescence Produced by PCR." Post-Doctoral Applied Mathematics and Statistics Seminar, Johns Hopkins University, Baltimore, MD October 13, 2022.
24. R. DeJaco, J. Majikes, P. Patrone, A. Liddle, and A. Kearsley. "Thermodynamic and Fluorescent Properties of Intercalating Dyes from Temperature-Programmed PCR Measurements with Modeling and Optimization." 2022 American Institute of Chemical Engineers (AIChE) Annual Meeting, Phoenix, AZ, November 15, 2022.
25. R. DeJaco, M. Roberts, E. Romsos, P. Vallone, and A. Kearsley. "Reducing Bias and Quantifying Uncertainty in Fluorescence Produced by PCR." Applied Mathematics Seminar, George Mason University, Fairfax, VA, October 21, 2022.
26. R. DeJaco and A. Kearsley. "Formation of Traveling Waves in Single-Solute Chromatography." Partial Differential Equations (PDE) Seminar Series, Ohio State University, Columbus, OH, November 8, 2022.
27. G. Doğan. "Topology Optimization for Image Analysis." SIAM Conference on Imaging Science, Online, March 21, 2022.
28. G. Doğan. "Efficient Algorithms to Compute Elastic Shape Distances between Closed Curves." The Annual Meeting of International Association of Applied Mathematics and Mechanics, Aachen, Germany, August 15, 2022.
29. R. Evans. "A Mathematical Model for Biological Field Effect Transistors." Minisymposium on Modeling and Estimation in Mathematical Biology, Society of Mathematical Biology Annual Meeting, Heidelberg, Germany, September 19, 2022.
30. R. Evans, S. Cho, A. Balijepalli, and A. Kearsley. "A Mathematical Model for Simulating Bio-FET." Society of Industrial and Applied Mathematics (SIAM) Annual Meeting, Pittsburgh, PA, July 11, 2022.
31. R. Evans, S. Cho, A. Balijepalli, and A. Kearsley. "Mathematical Modeling for Biological Field

Effect Transistors." Applied Mathematics and Mathematical Medicine and Biology Seminar, Department of Mathematical Sciences, University of Delaware, Newark, DE, May 12, 2022.

32. R. Evans, A. Balijepalli, and A. Kearsley. "A Mathematical Model for Biological Field Effect Transistors." Minisymposium on Mathematical Modeling in Biology and Medicine, Part III, American Mathematical Society Spring Eastern Sectional Meeting, Online, March 19, 2022.

33. J. Fong. "A Progress Report on Research to Upgrade Table T-1472.1 of ASME BPVC Section V (NDE) Article 14 (System Qualification)." Working Group on Monitoring and Non-Destructive Evaluation (MANDE) Subcommittee Meeting, ASME Boiler and Pressure Vessel Code (BPVC) Section XI (Inspection) Subgroup on Reliability and Integrity Management, October 31, 2021.

34. J. Fong. "A Dynamic Risk-informed Approach to a Feasibility Study of a Pan-Arctic Emergency Response System with a Do-Nothing Option." International Conference Arctic Frontiers 2022, Tromso, Norway, Online, May 08, 2022.

35. J. Fong. "Analytical, Software-Aided, and Solution-Verified Computational Mechanics." 75th Anniversary of Mathematics and Statistics at NIST, Online, June 29, 2022.

36. J. Fong. "ASME Boiler and Pressure Vessel Code (BPVC) Section V (NDE), Article 14 on Examination System Qualification (2015 Edition): Proposed Revision to Align with Requirements of the New BPVC Section XI (Inspection) Division 2 on Reliability Management." Committee Meeting of the ASME BPVC-XI SG-RIM Working Group on Monitoring and NDE (MANDE), ASME Code Week, Pittsburgh, PA, November 06, 2022.

37. J. Fong. "ASME Boiler and Pressure Vessel Code (BPVC) Section V (NDE), Article 14 on Examination System Qualification (2015 Edition): Proposed Revision to Align with Requirements of the New BPVC Section XI (Inspection) Division 2 on Reliability Management." Committee Meeting of the ASME BPVC-V SG on General Requirements, ASME Code Week, Pittsburgh, PA, November 9, 2022.

38. T. Gerrits and A. Miller. "Single-Photon Measurement Infrastructure for Quantum Applications (SPMIQA): Needs and Priorities." QED-C Plenary Meeting, Online, March 2022.

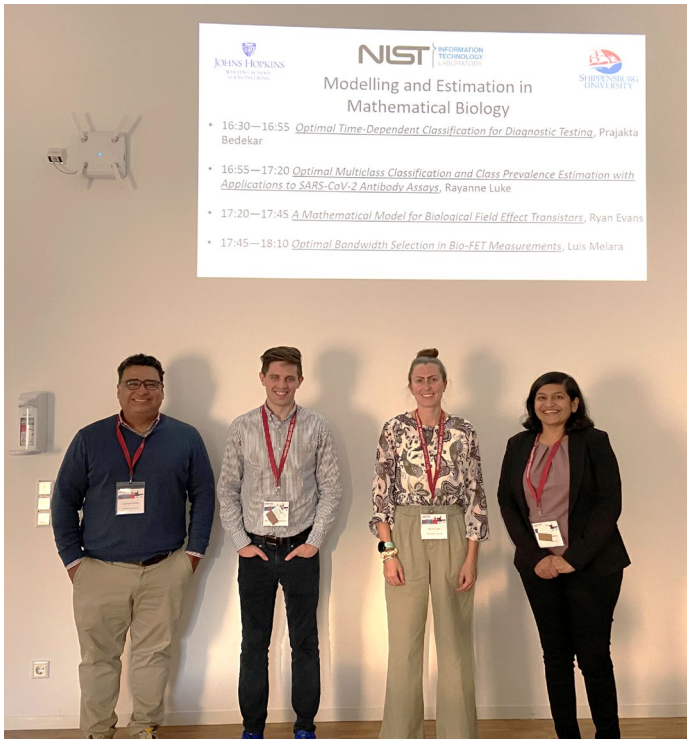

Figure 91. *Anthony Kearsley of ACMD organized a Minisymposium entitled Modelling and Estimation in Mathematical Biology at the European Conference on Mathematical and Theoretical Biology held in Heidelberg Germany on September 22, 2022. Speakers were (from l. to r.) Luis Melara of Shippensburg State University, Ryan Evans of ACMD, and ACMD postdocs Rayanne Luke and Prajakta Bedekar.* (Photo courtesy of A. Kearsley.)

39. T. Gerrits. "Optical Quantum Network Metrology." 11th Advanced Lasers and Photon Sources Conference, Yokohama, Japan, Online, April 18, 2022.

40. T. Gerrits, D. Anand, A. Battou, J. Bienfang, I. Burenkov, Hala, Y. Li-Baboud, S. Polyakov, A. Rahmouni, L. Sinclair, and O. Slattery. "Future Time Synchronization Needs for Quantum Networks." Workshop on Synchronization and Timing Systems, Denver, CO, May 10, 2022.

41. T. Gerrits. "Optical Quantum Network Metrology." Quantum Engineering Workshop, Caltech, Online, May 2022.

42. T. Gerrits. "Photon-number Resolving Transition Edge Sensors for QIP." Applications of Superconducting Electronics and Detectors Workshop, Jefferson Lab, Newport News, Online, December 2022.

43. S. Langer and A. Reid. "Microstructure Modeling with OOF2 and OOF3D." nanoHub, Online, July 27, 2022. URL: https://nanohub.org/resources/36380

44. Y.-K. Liu. "Compressed Sensing Measurement of Long-Range Correlated Noise." Johns Hopkins University Applied Physics Laboratory, Laurel, MD, September 19, 2022.
45. Y.-K. Liu. "Quantum Computing, Cybersecurity, and the Next Big Thing." 75th Anniversary of Mathematics and Statistics at NIST, Online, June 30, 2022.
46. Y.-K. Liu. "Don't Look Now: Quantum Computing and Cybersecurity." Keynote, NSF 2022 Secure and Trustworthy Cyberspace (SaTC) Principal Investigators' Meeting, Arlington, VA, June 1, 2022.
47. Y.-K. Liu. "Compressed Sensing Measurement of Long-Range Correlated Noise." Statistics, Optimization and Machine Learning Seminar, University of Colorado at Boulder, Online, March 29, 2022.
48. Y.-K. Liu. "Pseudorandom States Based on Computational Hardness." Edinburgh Workshop on Quantum t-Designs and Applications in Quantum Computing, Online, March 25, 2022.
49. R. Luke, A. Kearsley, N. Pisanic, Y. Manabe, D. Thomas, C. Heaney, and P. Patrone. "Improving Diagnostic Testing Accuracy by Moving to Higher Dimensional Probability Models with Applications to Saliva-Based SARS-CoV-2 Assays." Mathematics Department Seminar, Shippensburg University, Shippensburg, PA, October 6, 2022.
50. R. Luke, A. Kearsley, N. Pisanic, Y. Manabe, D. Thomas, C. Heaney, and P. Patrone. "Improving Diagnostic Testing Accuracy by Moving to Higher Dimensional Probability Models with Applications to Saliva-Based SARS-CoV-2 Assays." Mathematical Modeling Seminar, Rochester Institute of Technology, Rochester, NY, October 4, 2022.
51. R. Luke, A. Kearsley, and P. Patrone. "Multiclass Classification and Prevalence Estimation with Applications to SARS-CoV-2 Antibody Assays." Society for Mathematical Biology Annual Meeting, Modelling and Estimation in Mathematical Biology Minisymposium, University of Heidelberg, Heidelberg, Germany, September 19, 2022.
52. R. Luke, A. Kearsley, and P. Patrone. "Multiclass Classification and Prevalence Estimation with Applications to SARS-CoV-2 Antibody Assays." Applied and Computational Mathematics Seminar, George Mason University, Fairfax, VA, September 2022.
53. R. Luke, A. Kearsley, N. Pisanic, Y. Manabe, D. Thomas, C. Heaney, and P. Patrone. "Improving Diagnostic Testing Accuracy by Moving to Higher Dimensional Probability Models with Applications to Saliva-Based SARS-CoV-2 Assays." American Mathematical Society Eastern Sectional Meeting, Mathematical Modeling in Biology and Medicine Special Session, Online, March 19-20, 2022.
54. R. Luke, A. Kearsley, N. Pisanic, Y. Manabe, D. Thomas, C. Heaney, and P. Patrone. "Improving Diagnostic Testing Accuracy by Moving to Higher Dimensional Probability Models with Applications to Saliva-Based SARS-CoV-2 Assays." Department of Mathematical Sciences Winter Research Symposium, University of Delaware, Newark, DE, February 25, 2022.
55. L. Ma and L. Ding. "Hybrid Quantum Edge Computing Network." Society of Photo-Optical Instrumentation Engineers (SPIE) Optical Engineering + Applications, 2022, San Diego, CA, October 4, 2022.
56. J. Masterson, D. Anderson, and A. Kearsley. "Mathematical Modeling in Cryobiology." SIAM Annual Meeting, Pittsburgh, PA, July 11, 2022.
57. D. Middlebrooks, P. Patrone, A. Kearsley, G. Cooksey, and G. McFadden. "Separating Flow Cytometry Populations Based on Probabilistic Analysis." Haynes-Granville-Brown Session of Presentations by Recent Doctoral Recipients, Joint Mathematics Meetings, Online, April 6-9, 2022
58. D. Middlebrooks, P. Patrone, A. Kearsley, G. Cooksey, and G. McFadden. "Separating Flow Cytometry Populations Based on Probabilistic Analysis." Applied and Computational Math Seminar, George Mason University, Fairfax, VA, November 11, 2022
59. D. Middlebrooks and J. Zwolak. "Cold-Start Tuning." Niels Bohr Institute Seminar, University of Copenhagen, Copenhagen, Denmark, December 8, 2022.
60. A. Moorthy, A. Kearsley, and W. Wallace. "Identifying Novel Fentanyl Analogs from Mass Spectral Measurements." American Institute of Chemical Engineers (AIChE) Annual Meeting, Phoenix, AZ, November 15, 2022.
61. J. Nolan. "Sample Path Estimates of Non-Newtonian Capacity." Electrostatic Society of America Meeting, Charlotte, NC, Online, June 15, 2022.
62. J. Nolan. "Calculating Alpha-capacity via Stable Random Walks." Institute of Mathematical Statistics Annual Meeting, London, UK, June 30, 2022.
63. J. Nolan. "Simulating Entering and Exiting Balls by an Isotropic Stable Process." International Conference on Statistical Distributions and Applications, Marshall University, Huntington, WV, October 15, 2022.

64. P. Patrone. "Reproducibility in Cytometry: Signals Analysis, Uncertainty Quantification, and Implications for Doublet Deconvolution." Thermofisher Scientific, Online, September 9, 2022.

65. P. Patrone, A. Kearsley, P. Bedekar, and R. Luke. "Minimizing Uncertainty in Serology: Time-Dependent Antibody Kinetics and Vaccine-Induced Seroconversion." Seronet Monthly Meeting, Online, September 22, 2022.

66. A. Rahmouni, L. Ma, X. Tang, T. Gerrits, L. Cai, Q. Li, and O. Slattery. "Towards Entangled Photon Pair Generation from SiC-based Microring Resonator." Society of Photo-Optical Instrumentation Engineers (SPIE) Optical Engineering + Applications, 2022, San Diego, CA, October 4, 2022.

67. M. Roberts, A. Moorthy, E. Sisco, and A. Kearsley. "Probability Distribution-Based DART-MS Compound Discrimination." SIAM Annual Meeting, Pittsburgh, PA, July 11, 2022.

68. B. Saunders, S. Brooks, R. Buckmire, and R. Vincent-Finley. "Rounding Error Analysis for Validated Computation of Special Functions." Special Session on the MSRI African Diaspora Joint Mathematics (ADJOINT) Workshop, Joint Mathematics Meetings, Online, April 6, 2022.

69. B. Saunders, S. Brooks, R. Buckmire, R. Vincent-Finley, F. Backeljauw, S. Becuwe, B. Miller, M. McClain, and A. Cuyt. "Validated Computation of Special Mathematical Functions." Association for Women in Mathematics (AWM) Special Session on Celebrating the Mathematical Contributions of the AWM, Joint Mathematics Meetings, Online, April 7, 2022.

70. B. Saunders. "The Handbook of Mathematical Functions and the DLMF." 75th Anniversary of Mathematics and Statistics at NIST, Online, June 28, 2022.

71. B. Saunders. "Research in Computational and Applied Mathematics at the National Institute of Standards and Technology: NIST's DLMF and More." Applied Mathematics and Scientific Computing Seminar, Temple University, Philadelphia, PA, November 30, 2022.

72. W. Sherman. "Scientific Visualization in VR." Virtual Reality and 3D-User Interaction class (CSCI-5619), University of Minnesota, Minneapolis MN, October 5, 2022.

73. O. Slattery. "An Introduction to Quantum Communication and Quantum Cryptography." Advanced Technology Academic Research Center Seminar Series, Online, December 22, 2021.

74. O. Slattery, L. Ma, A. Rahmouni, X. Tang, T. Gerrits, Q. Li and M. Spencer. "Quantum Communication and Networking Project – Silicon Carbide in Quantum Communication." 7th International Conference on Electronic Materials and Nanotechnology for the Green Environment, Jeju, Korea, November 6, 2022.

75. J. Ziegler and J. Zwolak. "A Data-efficient Quantum Dot Charge Tuning Framework." HRL Laboratories, Malibu, CA, August 1, 2022.

76. J. Ziegler, F. Luthi, M. Ramsey, F. Borjans, G. Zheng, and J. Zwolak. "A Data-efficient Quantum Dot Charge Tuning Framework." Intel, Hillsboro, OR, Online, July 25, 2022.

77. J. Ziegler, F. Luthi, M. Ramsey, T. Watson, and J. Zwolak. "Autonomous Identification of Quantum Dot Device Failure Modes." Optical, Molecular, and Quantum Institute Seminar, University of Oregon, Eugene, OR, February 9, 2022.

78. J. Ziegler, F. Luthi, M. Ramsey, T. Watson, and J. Zwolak. "Autonomous Identification of Quantum Dot Device Failure Modes." Intel, Hillsboro, OR, February 8, 2022.

79. J. Zwolak. "Auto-tuning Quantum Dot Arrays with Rays." Qdev Seminar, Niels Bohr Institute, University of Copenhagen, Denmark, July 26, 2022.

80. J. Zwolak. "Tuning Quantum Dot Arrays with Rays." R. G. Herb Condensed Matter Seminar, University of Wisconsin-Madison, Madison, WI, March 31, 2022.

81. J. Zwolak. "Tuning Quantum Dot Arrays with Rays." American Physical Society March Meeting 2022, Chicago, IL, March 17, 2022.

82. J. Zwolak. "Tuning Quantum Dot Arrays with Rays." Physics Department Colloquium, Kansas State University, Manhattan, KS, February 28, 2022.

Conference Presentations

1. J. Amstutz, J. Stone, J. Guenther, and W. Sherman. "A Tour of the ANARI API." ANARI Webinar, Khronos Group, Online, March 2, 2022.

2. A. Avagyan. "Multi-mode Gaussian State Analysis with Total Photon Counting." Mathematical Results in Quantum Theory (QMATH 15), University of California at Davis, September 13, 2022.

3. P. Bedekar, A. Kearsley, and P. Patrone. "Optimal Time-dependent Classification for Diagnostic

Testing." Society for Industrial and Applied Mathematics Annual Meeting, Pittsburgh, PA, July 11, 2022.

4. P. Bedekar, A. Kearsley, and P. Patrone. "Optimal Time-dependent Classification for Diagnostic Testing." Biology and Medicine through Mathematics Conference, Virginia Commonwealth University, Richmond, VA, May 18, 2022.

5. P. Bedekar, A. Kearsley, and P. Patrone. "Optimal Time-dependent Classification and Prevalence Estimation for Antibody Testing." 2nd Workshop in Mathematical and Computational Biology, Online, June 9, 2022.

6. J. Bienfang, T. Gerrits, P. Kuo, O. Slattery, S. Polyakov, and A. Migdall. "A Dictionary of Single-Photon Terms to Support the Emerging Quantum Industry." Single Photon Workshop, Seoul, Korea, November 1, 2022.

7. S. Bhushan, L. Ma, X. Tang, and O. Slattery. "Electromagnetically Induced Transparency Based Quantum Memory in Vapor Cell." IEEE International Workshop on Quantum Communication and Quantum Cryptography, IEEE Conference on Communications and Network Security (CNS), Online, October 4, 2021.

8. B. Cloteaux. "Graphic Approximation of Integer Sequences." Southeastern International Conference on Combinatorics, Graph Theory & Computing, Boca Raton, FL, March 7, 2022.

9. B. Cloteaux. "On the Performance of Automatic Exposure Determination Using Bluetooth-based Proximity Estimation." IEEE International Conference on Communications (ICC), Seoul, South Korea May 16, 2022.

10. N. Coble and M. Coudron. "Quasi-polynomial Time Approximation of Output Probabilities of Constant-depth, Geometrically-local Quantum Circuits." IEEE 62nd Annual Symposium on Foundations of Computer Science (FOCS), Denver, CO, February 7, 2022.

11. H. Cohl. "Special Values for Continuous *q*-Jacobi Polynomials and Applications." Manawatu-Wellington Applied Maths Conference, Wellington, New Zealand, Online, December 1, 2021.

12. H. Cohl. "Special Values for Continuous *q*-Jacobi Polynomials and Applications." Canadian Mathematical Society 2021 Winter Meeting, Ottawa, Canada, Online, December 4, 2021.

13. H. Cohl. "The Anti-symmetry Relation for Continuous *q*-Jacobi Polynomials." 2022 Baylor Analysis Fest: From Operator Theory to Orthogonal Polynomials, Combinatorics, and Number Theory, Waco, TX, Online, May 24, 2022.

14. H. Cohl. "The Anti-symmetry Relation for Continuous q-Jacobi Polynomials." 16th International Symposium on Orthogonal Polynomials, Special Functions and Applications, Montreal, Quebec, Canada, Online, June 13, 2022.

15. H. Cohl. "Representations and Special Values for Nonsymmetric and Symmetric Poisson Kernels of the Askey-Wilson Polynomials." American Mathematical Society Fall Western Sectional Meeting, University of Utah, Salt Lake City, UT, October 22, 2022.

16. R. DeJaco and A. Kearsley. "Understanding the Break-through Curve Measurement When Adsorption is Fast." American Institute of Chemical Engineers Annual Meeting, Phoenix, AZ, November 15, 2022.

17. M. Donahue. "Energetics of Spin-flop and Spin-flip Transitions in Homogeneous Antiferromagnets." Magnetism and Magnetic Materials Conference (MMM 2022), Minneapolis, MN, Online, October 31, 2022.

18. R. Evans, A. Balijepalli, and A. Kearsley. "A Mathematical Model for Biological Field Effect Transistors." American Mathematical Society Fall Eastern Sectional Meeting 2022, Amherst, MA, October 1, 2022.

19. J. Fong. "Fatigue-life Prediction and Design for Uncracked and Cracked Components: Deterministic, A- and B-basis Probabilistic, and Reliability Target Approaches." ASME Pressure Vessels & Piping Division Conference, Las Vegas, NV, July 21, 2022.

20. J. Fong. "A Doubly-Asymptotic FEM Algorithm for Estimating the Ultimate of a Sequence of Increasingly-Dense-Meshed Finite Element Solutions." 15th World Congress on Computational Mechanics (WCCM2022) Yokohama, Japan, Online, July 23, 2022.

21. S. Geller. "Improving Quantum State Detection with Adaptive Sequential Observations." Southwest Quantum Information and Technology Network Workshop, Berkeley, CA, October 20, 2022.

22. T. Gerrits, I. Burenkov, Y. Li-Baboud, A. Rahmouni, D. Anand, O. Slattery, A. Battou, and S. Polyakov. "White Rabbit-Assisted Quantum Network Node Synchronization with Quantum Channel Coexistence." Conference on Lasers and

Electro-Optics (CLEO), San Jose, CA, May 16, 2022.

23. S. Guo, S. Koh, A. Fritsch, I. Spielman, and J. Zwolak. "Quantifying Reliability of Machine Learning Predictions via Physics-Informed Metrics." SIAM Conference on Uncertainty Quantification (UQ22), Atlanta, GA, April 12, 2022.

24. M. Henn. "Uncertainty Estimation for 2D Magnetic Particle Imaging." International Workshop on Magnetic Particle Imaging, Würzburg, Germany, Online, March 21, 2022

25. S. Koh, S. Guo, A. Fritsch, I. Spielman, and J. Zwolak. "Dark Soliton Tracking and Sorting System: Combining Machine Learning with Physics." American Physical Society March Meeting, Chicago, IL, March 14, 2022.

26. P. Kuo. "Towards Noncritical Phasematching in Thin-Film Lithium Niobate Waveguides." SPIE Photonics West, San Francisco, CA, Online, February 21, 2022.

27. A. Kwiatkowski. "Constraints on Gaussian Error Channels and Measurements for Quantum Communication." IEEE International Workshop on Quantum Communication and Quantum Cryptography, IEEE Conference on Communications and Network Security (CNS 2021), Online, October 6, 2021.

28. A. Kwiatkowski and L. Stephenson. "Resource-efficient Fully Randomized Benchmarking." 53rd Annual Meeting of the APS Division of Atomic, Molecular and Optical Physics, Orlando, Florida, June 1, 2022.

29. R. La. "Story of Two Populations in Epidemics: Is Every Infection Counted?" International Conference on Complex Networks and Their Applications, Madrid, Spain, Online, November 30, 2021.

30. R. La. "Investments in Robustness of Complex Systems: Algorithm Design." 11th International Conference on Complex Networks and Their Application, Palermo, Italy, November 8, 2022.

31. R. Luke, A. Kearsley, and P. Patrone. "Multiclass Classification and Prevalence Estimation with Applications to SARS-CoV-2 Antibody Assays." Southeastern-Atlantic Regional Conference on Differential Equations, North Carolina State University, Raleigh, NC, November 12-13, 2022.

32. R. Luke, A. Kearsley, and P. Patrone. "Multiclass Classification and Prevalence Estimation with Applications to SARS-CoV-2 Antibody Assays." Biology and Medicine through Mathematics, Virginia Commonwealth University, Richmond, VA, May 18, 2022.

33. C. Marante, J. Randazzo, H. Gharibnejad, B. Schneider, J. Olsen, and L. Argenti. "Correlation Effects in Molecular Ionization with ASTRA, a Transition-Density-Matrix Approach to Close Coupling." APS Division of Atomic, Molecular and Optical Physics Annual Meeting, Orlando, FL, May 30, 2022.

34. V. Marbukh. "Towards Robust Fog/Edge Computing Infrastructure with Risk Adjusted Multi-Connectivity." 9th International Conference on Future Internet of Things and Cloud (FiCloud'22), Online, August 22, 2022.

35. V. Marbukh. "Towards Landau Theory of Systemic Risk in Large-Scale Networked Systems: Work in Progress." International School and Conference on Network Science, 7th International Winter Conference (NetSci'22), Online, February 8, 2022.

36. V. Marbukh. "Towards Shapley Value Based Security Risk Attribution in Sensor Networks." The IEEE/ACM Information Processing in Sensor Networks (IPSN'22), Online, May 4, 2022.

37. V. Marbukh. "Towards Reliability/Security Risk Metrics for Large-Scale Networked Infrastructures: Work in Progress." Probabilistic Safety Assessment and Management Conference (PSAM'22), Honolulu, HI, June 26, 2022.

38. V. Marbukh. "Systemic Risk of Undesirable Contagion within System Time Horizon: Work in Progress." European Conference on Safety and Reliability (ESREL'22), Online, August 28, 2022.

39. P. Patrone. "Reproducibility in Cytometry: Signals Analysis, Uncertainty Quantification, and Implications for Doublet Deconvolution." Cyto 2022, Philadelphia PA, June 3-7, 2022.

40. P. Patrone. "Rewriting the Rules for Diagnostics: Implications of Probability and Measure Theory for SARS-CoV-2 Testing." Biology and Medicine through Mathematics (BAMM), Richmond VA, May 17, 2022.

41. D. Porter. "IMMUTABLE Values & Data Structures." SQLite & Tcl Conference (S&T) 2021, Houston, TX, Online, November 17, 2021.

42. A. Rahmouni, T. Gerrits, A. Migdall, O. Slattery, P. Shaw, and J. Rice. "A Self-Validated Detector

for Characterization of Quantum Network Component." IEEE International Workshop on Quantum Communication and Quantum Cryptography, IEEE Communications and Network Security, Online, October 4, 2021.

43. A. Rahmouni, T. Gerrits, A. Migdall, O. Slattery, P. Shaw, and J. Rice. "A Self-Validated Detector for Characterization of Quantum Network Components." Conference on Lasers and Electro-Optics (CLEO), San Jose, CA, May 16, 2022.

44. A. Rahmouni, T. Gerrits, and O. Slattery. "Progress Towards a Portable Polarization-entangled Photon Source and Receiver Toolset for Quantum Network Metrology." Quantum 2.0 Conference and Exhibition, Denver, CO, June 18, 2022.

45. A. Rahmouni, L. Ma, L. Cai, X. Tang, T. Gerrits, Q. Li, and O. Slattery. "Towards Entangled Photon Pair Generation from SiC-based Microring Resonator." Conference of the Society of Photo-Optical Instrumentation Engineers (SPIE): Optics and Photonics, San Diego, CA, August 21, 2022.

46. A. Rahmouni, S. Saha, O. Slattery, and T. Gerrits. "Hyperspectral Photon-Counting Optical Time Domain Reflectometry." Conference of the Society of Photo-Optical Instrumentation Engineers (SPIE): Optics and Photonics, San Diego, CA, August 21, 2022.

47. A. Rahmouni, L. Ma, L. Cai, X. Tang, T. Gerrits, Q. Li, and O. Slattery. "Microring-based Photon Pair Sources in the 4H-SiC-on-Insulator Platform." Single Photon Workshop, Seoul, Korea, November 1, 2022.

48. K. Sayrafian. "Evaluation of the Bluetooth-based Proximity Estimation for Automatic Exposure Determination." IEEE Consumer Communications & Networking Conference, Online, January 8-11, 2022.

49. K. Sayrafian. "Statistical Pathloss Model for UWB Wireless Capsule Endoscopy." IEEE802.15.6ma Standard Task Group Meeting, Montreal, Canada, July 10-15, 2022.

50. K. Sayrafian. "On the Performance of Automatic Exposure Determination Using Bluetooth-based Proximity Estimation." European Cooperation in Science and Technology (COST) Intelligence-Enabling Radio Communications for Seamless Inclusive Interactions (INTERACT, CA20120) Technical Meeting, Valencia, Spain, September 20-22, 2022.

51. O. Slattery, L. Ma, X. Tang, T. Gerrits, A. Rahmouni, N. Lal, S. Saha, Y. Shi, and A. Varshney. "Overview of the NIST Quantum Network Testbed Activities." Quantum Economic and Development Consortium (QED-C) Plenary, Denver, CO, June 22, 2022.

52. B. Schneider, K. Bartschat, K. Hamilton, L. Carr, I. Bray, A. Scrinzi, F. Martin, J. Vasquez, A. Brown, J. Gorfinkiel, S. Pamidighantam, R. Lucchese, N. Douguet, and C. Fischer. "A Science Gateway for Atomic, Molecular and Optical Science (AMOS): Democratizing AMOS Research and Education." APS Division of Atomic, Molecular and Optical Physics Annual Meeting, Orlando, FL, May 30, 2022

53. W. Sherman. "Immersive Visualization with the ParaView Open Source Tool." Free and Open Source Extended Reality (FOSS-XR) Conference 2022, Minneapolis, MN, October 6, 2022.

54. W. Sherman. "Open-source and Standards-based Immersive Visualization." SIGGRAPH '22, Online, July 28, 2022.

55. W. Sherman. "ANARI: A Shortcut to Real-time Raytracing in VR Using an Open API for Advanced Rendering." 4th Annual XR Conference, Sandia Laboratories, Albuquerque, NM, July 14, 2022.

56. W. Sherman and S. Su. "Immersive Visualization with ParaView & VTK." 4th Annual XR Conference, Sandia Laboratories, Albuquerque, NM, July 14, 2022

57. A. Seshadri. "On the Separation of Correlation-Assisted Sum Capacities of Multiple Access Channels." IEEE International Symposium on Information Theory, Espoo, Finland, June 30, 2022.

58. A. Sheshadri. "Versatile Fidelity Estimation with Confidence." Southwest Quantum Information and Technology Workshop, Berkeley, CA, October 20, 2022.

59. S. Su, W. Sherman, I. Lopez Coto, K. Sayrafian, and J. Terrill. "Immersive ParaView: An Immersive Scientific Workflow for the Advancement of Measurement Science." Workshop on Visual Analytics in Immersive Environments (VAinIE), IEEE International Symposium on Mixed and Augmented Reality (ISMAR), Singapore, October 21, 2022.

60. S. Su. "High Performance Computing and Visualization Group at NIST." Pitch Your Lab, IEEE

International Symposium on Mixed and Augmented Reality (ISMAR) Singapore, Oct 20, 2022.

61. S. Su. "Obstacles to Adoption of XR, Particularly in the Federal / DOD Space." Applied Physics Laboratory Extended Reality (XR) Symposium, July 28, 2022.

62. S. Su, W. Sherman, S. Satterfield, T. Griffin, S. Ressler, W. George, S. Feng, and J. Terrill. "Visualization Ecology Applications for Measurement Science: A Visualization Gap Approach." VisGap - The Gap between Visualization Research and Visualization Software, Rome, Italy, June 13, 2022.

63. J. Ziegler, T. McJunkin, E. Joseph, S. Kalantre, B. Harpt, D. Savage, M. Lagally, M. Eriksson, J. Taylor, and J. Zwolak. "Building a Noise-Tolerant Framework for Quantum Dot Auto Tuning Framework." SIAM Conference on Uncertainty Quantification (UQ22), Atlanta, Georgia, April 12, 2022.

64. J. Ziegler, F. Luthi, M. Ramsey, T. Watson, and J. Zwolak. "Autonomous Identification of Quantum Dot Device Failure Modes." American Physical Society March Meeting, Chicago, IL, March 14, 2022).

Poster Presentations

1. A. Abane, D. Anand, A. Amlou, L. Ait Ouchegggou, Y. Li-Baboud, A. Battou, J. Bienfang, I. Burenkov, Hala, P. Kuo, A. Migdall, S. Polyakov, A. Rahmouni, D. Reddy, P. Shaw, O. Slattery, and T. Gerrits. "Optical Quantum Network Metrology." 3rd Workshop on Quantum Repeaters and Networks, Chicago, August 19, 2022.

2. A. Abane, D. Anand, A. Amlou, L. Ait Ouchegggou, Y. Li-Baboud, A. Battou, J. Bienfang, I. Burenkov, Hala, P. Kuo, A. Migdall, S. Polyakov, A. Rahmouni, D. Reddy, P. Shaw, O. Slattery, and T. Gerrits. "Optical Quantum Network Metrology." Single Photon Workshop, Seoul, South Korea, October 31, 2022.

3. M. Alhejji. "On Simulating Quantum Erasure." Southwest Quantum Information and Technology Workshop, Berkeley, CA, October 20, 2022.

4. L. Argenti, C. Marante, J. Randazzo, H. Gharibnejad, B. Schneider, and J. Olsen. "ASTRA, a Transition-Density-Matrix Method for Attosecond Molecular Dynamics." APS Division of Atomic, Molecular and Optical Physics (DAMOP) Annual Meeting, Orlando, FL, May 30, 2022

5. D. Brager, E. Erisman, A. Moorthy, and A. Kearsley. "Numerical Library Scaling for Improved Hitlists." American Society of Mass Spectrometry (ASMS) Annual Meeting, Minneapolis, MN, June 6, 2022.

6. D. Brager, A. Kearsley, and D. Anderson. "A Spatially Dependent Model for Photoreceptors in a Healthy Eye." Biology and Medicine Through Mathematics Conference, Virginia Commonwealth University, Richmond Virginia, May 18, 2022.

7. R. Dalka, D. Sachmpazidi, C. Henderson, and J. Zwolak. "Network Analysis of Likert-style Surveys." American Association of Physics Teachers Summer Meeting, Grand Rapids, MI, July 12, 2022.

8. R. DeJaco, J. Majikes, J. Liddle, and A. Kearsley. "Extracting Thermodynamic and Fluorescent Properties of Intercalating Dyes from Temperature-Programmed PCR Measurements with Modeling, Optimization, and Uncertainty Quantification." SIAM Conference on the Mathematics of Data Science, San Diego, CA, September 28, 2022.

9. R. DeJaco, M. Roberts, E. Romsos, P. Vallone, and A. Kearsley. "Reducing Bias and Quantifying Uncertainty in Fluorescence Produced by PCR." SIAM Washington-Baltimore Section Fall Meeting, Arlington, VA, November 4, 2022.

10. R. DeJaco, J.Majikes, J. Liddle, and A. Kearsley. "Extracting Thermodynamic and Fluorescent Properties of Intercalating Dyes from Temperature-Programmed PCR Measurements with Modeling and Optimization." American Institute of Chemical Engineering (AIChE) Annual Meeting, Phoenix, AZ, November 15, 2022.

11. G. Doğan. "Python Package for Shape Analysis and Image Segmentation." 75th Anniversary of Mathematics and Statistics at NIST, Online, June 29, 2022.

12. G. Doğan. "Scikit-Shape: Python Toolbox for Shape Analysis and Segmentation." SIAM Conference on the Mathematics of Data Science, San Diego, CA, September 26, 2022.

13. G. Doğan. "VEMOS: Visual Explorer for Metrics of Similarity." SIAM Conference on Mathematics of Data Science, San Diego, CA, September 26, 2022.

14. S. Dontha, S. Tan, S. Smith, S. Choi, and M. Coudron. "Approximating Output Probabilities of Shallow Quantum Circuits which are Geometrically-local in any Fixed Dimension." Quantum

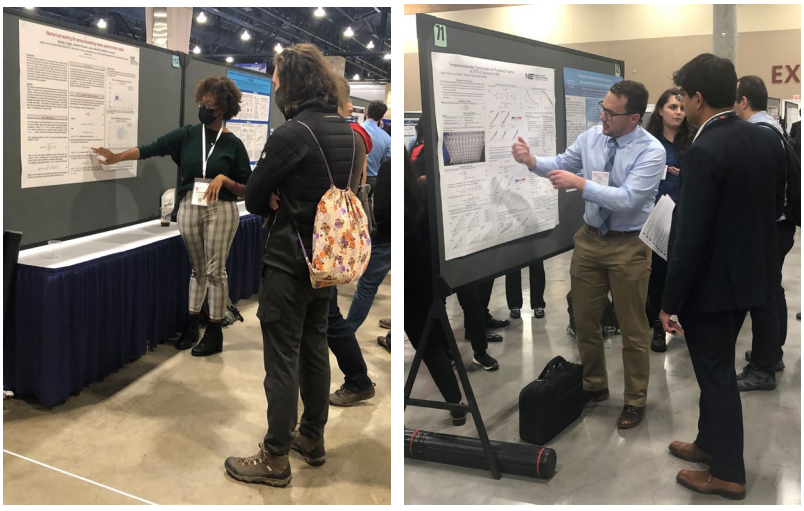

Figure 92. *ACMD postdocs presented their work in a wide variety of venues this year. Left: Danielle Brager at the American Society for Mass Spectroscopy held in Minneapolis in June 2022. Right: Robert DeJaco at the SIAM Conference on the Mathematics of Data Science held in San Diego in September 2022.* (Photos courtesy of A. Kearsley.)

Information Processing (QIP) Conference, Pasadena, CA, March 7, 2022.

15. N. Douguet, N. Saito, S. Han, Y. Wu, A. Chew, N. Ishii, T. Kanai, B. Schneider, J. Olsen, L. Argenti, Z. Chang, and J. Itatani. "Attosecond Electronic Dynamics of Core-Excited States of N_2O in the Soft X-ray Region." APS Division of Atomic, Molecular and Optical Physics (DAMOP) Annual Meeting, Orlando, FL, May 30, 2022

16. S. Glancy. "Multi-mode Gaussian State Analysis with Total Photon Counting." Southwest Quantum Information and Technology Workshop, Berkeley, CA, October 20, 2022.

17. S. Koh, S. Guo, A. Fritsch, I. Spielman, and J. Zwolak. "Integrating Machine Learning and Physics-based Heuristics for Solitonic Excitation Classification in Bose-Einstein Condensates." Conference for Undergraduate Women in Physics, Online, January 24, 2022.

18. P. Kuo. "Towards Noncritical Phasematching in Thin-film Lithium Niobate Frequency Converters." Frontiers in Optics, Online, November 1, 2021.

19. A. Kwiatkowski. "Choosing Sequence Lengths for Single-shot-randomized Clifford Benchmarking." Southwest Quantum Information and Technology Workshop, Berkeley, CA, October 20, 2022.

20. R. Luke, A. Kearsley, and P. Patrone. "Multiclass Classification and Prevalence Estimation with Applications to SARS-CoV-2 Antibody Assays." Society for Industrial and Applied Mathematics Washington, D.C./Baltimore Sectional Meeting, Arlington, VA, November 4, 2022.

21. R. Luke, A. Kearsley, and P. Patrone. "Multiclass Classification and Prevalence Estimation with Applications to SARS-CoV-2 Antibody Assays." 75th Anniversary of Mathematics and Statistics at NIST, Online, June 29, 2022.

22. R. Luke, A. Kearsley, and P. Patrone. "Multiclass Classification and Prevalence Estimation with Applications to SARS-CoV-2 Antibody Assays." Association for Women in Mathematics Research Symposium, Institute for Mathematics and its Applications, Minnesota, MN, June 16-19, 2022.

23. R. Luke, A. Kearsley, N. Pisanic, Y. Manabe, D. Thomas, C. Heaney, and P. Patrone. "Improving Diagnostic Testing Accuracy by Moving to Higher Dimensional Probability Models with Applications to Saliva-Based SARS-CoV-2 Assays." Johns Hopkins Postdoctoral Conference, Online, April 28, 2022.

24. L. Ma. "Quantum Communications and Networks for Edge Computing." Sixth ACM/IEEE Symposium on Edge Computing, San Jose, CA, December 14, 2021.

25. V. Marbukh. "Towards Risk Adjusted Wireless Access Under Jamming: Reliability Through Multi-Connectivity." IEEE Consumer Communications & Networking Conference (CCNC'22), Online, January 8, 2022.

26. D. Middlebrooks, P. Patrone, A. Kearsley, G. Cooksey, and G. McFadden. "Separating Flow Cytometry Populations Based on Probabilistic Analysis." International Society for Advancement of Cytometry CYTO 2022, Philadelphia, PA, June 3, 2022

27. D. Middlebrooks, P. Patrone, A. Kearsley, G. Cooksey, and G. McFadden. "Data Analysis of Flow Cytometry Data: A Probabilistic Approach." SIAM Conference on Mathematics of Data Science, San Diego, CA, September 26, 2022

28. C. Ochoa, J. Zwolak, J. Freericks, and L. Doughty. "Investigating Students' Fluency with Quantum Ideas in the Context of Interaction-free Experiments." Physics Education Research Conference, Grand Rapids, MI, July 14, 2022.

29. P. Patrone and A. Kearsley. "Estimating Prevalence Without Classification." Seronet Investigators Meeting, Online, March 23, 2022.
30. P. Patrone, P. Bedekar, N. Pisanic, D. Thomas, Y. C. Manabe, A. Kearsley, and C. Heaney. "Diagnostics Under Uncertainty: Minimizing Indeterminate Classes and Implications for Populations with Decreased Antibody Response." Seronet Investigator's Meeting, Online, March 23, 2022.
31. A. Rahmouni, T. Gerrits, P. Kuo, R. Dileep, L. Ma, X. Tang, and O. Slattery. "Portable Polarization-entangled Photon Source and Receiver Toolset for Quantum Network Metrology." SPIE Optics and Photonics, San Diego, CA, August 21, 2022.
32. A. Rahmouni, T. Gerrits, A. Migdall, O. Slattery, P. Shaw, and J. Rice. "A Low-cost Optical Trap Detector for Characterization of Quantum Network Components." Single Photon Workshop 2022, Seoul, South Korea, October 31, 2022.
33. M. Roberts, A. Moorthy, E. Sisco, and A. Kearsley. "Probability Distribution-based Peak Matching with DART-MS Spectra for Compound Discrimination." American Society of Mass Spectrometry (ASMS) Annual Meeting, Minneapolis, MN, June 6, 2022.
34. B. Schneider, R. Schneider, and H. Gharibnejad. "A Coupled Volterra Integral Equation Approach to Solving the Time-Dependent Schrödinger Equation." APS Division of Atomic, Molecular and Optical Physics Annual Meeting, Orlando, FL, 2022
35. O. Slattery, L. Ma, T. Gerrits, A. Ranmouni, S. Bhushan, and X. Tang. "The Quantum Communications and Networking Project at the Information Technology Laboratory at NIST." International Workshop on Quantum Communication and Quantum Cryptography, IEEE Conference on Communications and Network Security, Online, October 4, 2021.
36. J. Ziegler and J. Zwolak. "Tuning Arrays with Rays: Data-efficient Quantum Dot Auto-tuning." 75th Anniversary of Mathematics and Statistics at NIST, Online, June 30, 2022.
37. J. Zwolak, S. Guo, S. Koh, A. Fritsch, and I. Spielman. "Integrating Machine Learning and Physics-based Heuristics for Solitonic Excitation Classification in Bose-Einstein Condensates." 75th Anniversary of Mathematics and Statistics at NIST, Online, June 30, 2022.

NIST News Releases

The following news items released by the NIST Public Affairs Office describe work in which ACMD staff members have participated.

1. DC-Area U.S. Government Agencies Announce the Washington Metropolitan Quantum Network Research Consortium, June 27, 2022.
2. NIST Announces First Four Quantum-Resistant Cryptographic Algorithms, July 5, 2022.
3. New Device Design Brings Unparalleled Confidence to Cell Measurements, July 20, 2022.

Web Services

ACMD provides a variety of information and services on its website. Below is a list of major services provided that are currently under active maintenance.

1. *Digital Library of Mathematical Functions*: a repository of information on the special functions of applied mathematics.
2. *Digital Repository of Mathematical Formulae*: a repository of information on special function and orthogonal polynomial formulae.
3. *DLMF Standard Reference Tables on Demand*: an online software testing service providing tables of values for special functions, with guaranteed accuracy to high precision.
4. *Error-correction Zoo*: a repository of information about classical and quantum error-correcting codes.
5. *muMAG*: a collection of micromagnetic reference problems and submitted solutions.

Software Released

ACMD distributes a large number of software packages that have been developed in the course of its work. Listed below are particular packages which have seen new releases during the reporting period.

1. ACTS: Test suite generation (t-way with constraints). Version 3.02. R. Kacker and D. R. Kuhn. URL: https://csrc.nist.gov/Projects/automated-combinatorial-testing-for-software/downloadable-tools
2. CAVE Interaction Plugin and Extended Reality Interface in ParaView. Version 5.11.0. W. Sherman, S. Su, S. Wittenburg, S. Satterfield, T. Griffin, and J. E. Terrill. URL: https://gitlab.kitware.com/paraview/paraview

3. CCM: Combinatorial coverage measurement (Java version with support of constraints). R. Kacker and D. R Kuhn. URL: https://csrc.nist.gov/Projects/automated-combinatorial-testing-for-software/downloadable-tools
4. FMM3D: A set of libraries to compute N-body interactions governed by the Laplace and Helmholtz equations, to a specified precision, in three dimensions, on a multi-core shared-memory machine. Version 1.0.1 (6/29/22). Z. Gimbutas, L. Greengard, L. Lu, M. Rachh, V. Rokhlin. URL: https://github.com/flatironinstitute/FMM3D/
5. FreeVR: Open-source Virtual Reality Integration Library. Version 0.7d (07/01/22). W. Sherman. URL: http://freevr.org
6. Itcl: C++ inspired object oriented commands for Tcl. Versions 4.2.2 (11/5/2021), 4.2.3 (11/22/2022). D. G. Porter. URL: https://sourceforge.net/projects/tcl/files/Tcl/
7. LaTeXML: A LaTeX to XML, HTML, MathML+ Converter. Release 0.8.7 (12/16/2022). B. R. Miller. URLs: https://dlmf.nist.gov/LaTeXML/, https://github.com/brucemiller/LaTeXML/
8. MWrap: A MEX interface generation system in the spirit of SWIG or matwrap. Version 1.1.1 (8/28/22). D. Bindel, Z. Gimbutas, A. Barnett, L. Lu, M. Rachh. URL: https://github.com/zgimbutas/mwrap/
9. OOF2: Object-Oriented Finite element software for modeling materials microstructure. Versions 2.2.2 (2/3/22), 2.2.3 (9/14/22). S. Langer. URL: https://www.ctcms.nist.gov/oof/oof2/
10. OOFCanvas: A gtk compatible graphics canvas for OOF2. Versions 1.0.2 (2/3/22), 1.0.3 (9/14/22). S. Langer. URL: https://www.ctcms.nist.gov/oof/oof2/
11. OOMMF: The Object Oriented MicroMagnetic Framework. Version 2.0b0 (9/30/22), M. J. Donahue and D. G. Porter. URL: https://math.nist.gov/oommf/software-20.html
12. perm_hmm: State inference using Partially Observable Markov Decision Processes. Version 1.0 (10/2/22). S. Geller, S. Glancy, and E. Knill. URL: https://github.com/usnistgov/perm_hmm
13. Scikit-shape: Python Package for Shape and Image Analysis. Version 0.3 (9/21/22), G. Doğan. URL: http://scikit-shape.org
14. Software for Solving Large-Scale Generalized Eigenvalue Problems on Distributed Computers. Version 1 (11/16/21). J. Sims. DOI: 10.18434/mds2-2293
15. Soldet: An object-oriented package for solitonic feature detection in absorption images of Bose-Einstein condensate. Version 1 (5/27/2022). J. Zwolak. DOI: 10.18434/mds2-2641
16. Tcl/Tk: Extensible scripting language and GUI toolkit. Versions 8.6.12 (11/5/2021), 8.6.13 (11/22/2022). D. G. Porter. URL: https://sourceforge.net/projects/tcl/files/Tcl/
17. TDBC: Database connection commands for Tcl. Versions 1.1.3 (11/5/2021), 1.1.5 (11/22/2022). D. G. Porter. URL: https://sourceforge.net/projects/tcl/files/Tcl/
18. Thread: Thread management commands for Tcl. Versions 2.8.7 (11/5/2021), 2.8.8 (11/22/2022). D. G. Porter. URL: https://sourceforge.net/projects/tcl/files/Tcl/

Data Released

1. Dark Solitons in BECs Dataset. Version 2 (8/24/22). J. Zwolak. DOI: 10.18434/mds2-2363
2. Optical Spectra Data for Backward-Wave Spontaneous-Parametric Downconversion. Version 1 (12/2/22). P. Kuo. DOI: 10.18434/mds2-2776
3. QFlow 2.0: Quantum dot data for machine learning. Version 1 (5/10/22). J. Zwolak. DOI: 10.18434/T4/1423788

Conferences, Minisymposia, Lecture Series, Courses

ACMD Seminar Series

Stephen Langer served as Chair of the ACMD Seminar Series. There were 19 talks presented during this period; talks are listed chronologically.

1. Maryam Yashtini (Georgetown University). Counting Objects by Diffused Index: Geometry-free and Training-free Approach. December 13, 2022.
2. Lap-Fai (Craig) Yu (George Mason University). Creating the Extended Reality of the Future with Artificial Intelligence and Computational Design. November 30, 2022.
3. Ioannis Sakiotis (Old Dominion University). PAGANI and m-Cubes: Parallel Adaptive GPU Algorithms for Numerical Integration. November 15, 2022.
4. Eleni Adam (Old Dominion University). NPGREAT: Assembling the Human Telomeres and Subtelomeres with the Use of Ultralong Nanopore and Linked-Read Datasets. November 1, 2022.
5. Tim Kelley (North Carolina State University). Anderson Acceleration: Convergence Theory and Numerical Experience. October 18, 2022.

6. Gabriel D. Chaves-O'Flynn (Polish Academy of Sciences). Thermally Activated Transitions Between Micromagnetic States. October 14, 2022.
7. Melinda Kleczynski (University of Delaware). Using Topological Data Analysis to Reveal the Structure of Ecological Systems. October 4, 2022.
8. John Holmes (Ohio State University). Analysis of the Modified Burgers Equation on the Half Line. September 20, 2022.
9. Kaitlyn Hood (Purdue University). Modeling Pairwise Particle Interactions in an Inertial Microfluidic Channel. August 9, 2022.
10. Mallory Gaspard (Cornell University). Optimal Driving Under Traffic Signal Uncertainty. June 7, 2022.
11. Ryan Schneider (University of California San Diego). A Volterra Integral Equation Approach to the Time Dependent Schrödinger Equation. May 24, 2022.
12. Barbara Lee Keyfitz (Ohio State University). Conservation Laws, Lagrangian Dynamics, Diffeomorphisms and Weak Solutions. May 10, 2022.
13. Illya Hicks (Rice University). Discrete Optimization Techniques for Network and Data Analysis. April 26, 2022.
14. Helen Moore (University of Florida). Standards for Model Evaluation Applied to Systems Pharmacology Models: Focus on Sensitivity Analysis. March 29, 2022.
15. Matthew Roberts (NIST ACMD). Probability Distributions in Peak Matching for DART-MS. March 8, 2022.
16. Andrew Glaws (National Renewable Energy Laboratory). Invertible Neural Networks for Wind Turbine Airfoil and Blade Design. November 30, 2021.
17. Paul Patrone (NIST ACMD). Optimal Decision Theory for SARS-CoV-2 Antibody Testing. November 16, 2021.
18. Harbir Antil. (George Mason University). Optimization Based Deep Neural Networks with Applications. November 9, 2021.
19. Pulkit Grover. (Carnegie-Mellon University). Information-theoretic Techniques for Examining and Affecting Biological and Artificial Computing Systems for Human-Centered Goals. October 5, 2021.

Courses and Shortcourses

1. V. Albert and M. Gullans. "Advanced Topics in Theory of Computing: Quantum Error Correction and Fault-Tolerance." University of Maryland, College Park, MD, Fall 2021.
2. V. Albert and A. Barg. "Advanced Topics in Theory of Computing: Classical and Quantum Codes." University of Maryland, College Park, MD, Spring 2022.
3. V. Albert. "Bosonic Coding: Introduction and Use Cases." Course 209 - Quantum Fluids of Light and Matter, International School of Physics "Enrico Fermi," Italian Physical Society, Varenna, Italy, July 2-7, 2022.
4. V. Albert. "Primer on Quantum Error Correction." Quantum Computing Hard- and Software (QCHS) Summer School, Swiss Federal Institute of Technology Lausanne (EPFL), Lausanne, Switzerland, June 14, 2022.

Conference Organization

Leadership

1. R. Boisvert. Co-organizer, 75th Anniversary of Mathematics and Statistics at NIST, Online, June 28-30, 2022.
2. T. Burns. Co-organizer, 75th Anniversary of Mathematics and Statistics at NIST, Online, June 28-30, 2022.
3. M. Donahue. Co-Organizer and Chair, New Approaches in Computational Magnetism, Magnetism and Magnetic Materials Conference (MMM 2022), Hybrid (Minneapolis, MN), October 31 – November 4, 2022.
4. P. Kuo. Subcommittee Chair. 2022 Conference on Lasers and Electro-optics FS 3: Quantum Photonics, San Jose CA, May 15-20, 2022.
5. P. Kuo. Subcommittee Chair. 2023 Conference on Lasers and Electro-optics FS 3: Quantum Photonics, San Jose CA, May 7-12, 2023.
6. L. Ma, Lead Organizer, IEEE International Workshop on Quantum Communication and Quantum Cryptography, IEEE Conference on Communications and Network Security 2021, Online, October 6, 2021.
7. O. Slattery, Co-Organizer, QCRYPT 2023, College Park, MD. August 2023.

Committee Membership

1. V. Albert. Member, Program Committee, Quantum Information Processing Conference, Ghent, Belgium, February 4-10, 2023.
2. H. Cohl. Member, Organizing Committee, 16th International Symposium on Orthogonal Polynomials, Special Functions and Applications, Montreal, Quebec, Canada, June 13-17, 2022.
3. S. Glancy. Member, Program Committee, Southwest Quantum Information Technology Workshop, Berkeley, CA, October 20-22, 2022.
4. R. Kacker. Member, Program Committee, International Workshop on Combinatorial Testing (IWCT), 2022 IEEE International Conference on Software Testing, Verification and Validation (ICST). Valencia, Spain, April 4-13, 2022.
5. P. Kuo. Member, Program Committee. 2022 SPIE Photonics West: Quantum Computing, Communication, and Simulation II, San Francisco, CA February 21-27, 2022.
6. R. La. Member, Technical Program Committee, IEEE International Conference on Computer Communications (INFOCOM 22), Online, May 2-5, 2022.
7. R. La. Member, Technical Program Committee, IEEE International Conference on Computer Communications (INFOCOM 22), Hybrid, Stevens Institute of Technology, Hoboken, NJ, May 17-20, 2023.
8. R. La. Member, Technical Program Committee, International Conference on Complex Networks and Their Applications (Complex Networks 22), Palermo, Italy, November 8-10, 2022.
9. N. Lal. Member, Organizing Committee, QCRYPT 2023, College Park, MD. August 2023.
10. L. Ma. Member, Organizing Committee, QCRYPT 2023, College Park, MD. August 2023.
11. W. Sherman. Ex-officio Member, Executive Committee, Community Alliance for Advanced Visualization (CAAV).
12. W. Sherman. Member, Program Committee, IEEE Conference on Virtual Reality and 3D User Interfaces (IEEE VR), Hybrid, Shanghai, China, March 25-29, 2023.
13. W. Sherman. Co-Organizer, Birds of a Feather: Immersive Visualization, SIGGRAPH '22, July 28, 2022.
14. S. Su. Member. Program Committee, ACM Symposium on Virtual Reality Software and Technology (VRST), Hybrid, Tsukuba, Japan, November 29 – December 1, 2022.
15. S. Su. Member. Program Committee, IEEE Conference on Virtual Reality and 3D User Interfaces (IEEE VR), Hybrid, Shanghai, China, March 25-29, 2023.
16. S. Su. Member. Program Board, 15th International Conference on Virtual, Augmented and Mixed Reality, HCI International, Copenhagen, Denmark, July 23-28, 2023.

Session Organization

1. H. Cohl. Co-Organizer, Minisymposium: All Things Hypergeometric (Classical, Basic, and Elliptic) and q-series, 16th International Symposium on Orthogonal Polynomials, Special Functions and Applications, Montreal, Quebec, Canada, June 13-17, 2022.
2. H. Cohl. Co-Organizer, Special Session: Hypergeometric Functions and q-series, 2022 AMS Fall Western Sectional Meeting, Salt Lake City, Utah, October 22-23, 2022.
3. H. Cohl. Co-Organizer, Special Session: Hypergeometric Functions, q-series and Generalizations, Spring AMS Eastern Virtual Sectional Meeting, April 1-2, 2023.
4. G. Doğan. Co-Organizer, Minisymposia 85, 95, 106: Advances in Shape Analysis. SIAM Conference on Imaging Science, Online, March 21-25, 2022.
5. A. Kearsley. Organizer, Minisymposium: Mathematical Modelling and Simulation of Biological Field Effect Transistors. SIAM Annual Meeting, Pittsburgh, PA, July 14, 2022.
6. A. Kearsley. Organizer, Minisymposium: Modelling and Estimation in Mathematical Biology. European Conference on Mathematical and Theoretical Biology, Heidelberg Germany, September 22, 2022.
7. J. Zwolak. Co-Organizer, Minisymposium: Uncertainty and Reliability of Machine Learning Methods. SIAM Conference on Uncertainty Quantification, Atlanta, GA, April 12-15, 2022.

Other Professional Activities

Internal

1. R. Boisvert. Coordinator, ITL Quantum Information Program.

2. R. Boisvert. Member, NIST Research Computing Advisory Committee
3. T. Burns. Co-Director, ITL Summer Undergraduate Research Fellowship (SURF) Program.
4. B. Cloteaux. Member, NIST Editorial Review Board.
5. M. Coudron. Co-Organizer, QuICS Weekly Research Seminar.
6. T. Gerrits. Organizer, Quantum Optics Meeting Series.
7. Z. Gimbutas. Member, ITL Awards Committee.
8. S. Glancy. Member, Boulder Summer Undergraduate Research Fellowship (SURF) Committee.
9. S. Glancy. Member, ITL Diversity Committee.
10. A. Kearsley. ITL Representative, NIST Engineering Biology Working Group
11. P. Kuo. Member, NIST Diversity, Equity, Inclusion and Accessibility (DEIA) Implementation Team
12. P. Kuo. Member, ITL Space Task Force.
13. P. Kuo. Member, NIST Quantum Networking Grand Challenge Small Team (advisory board).
14. L. Ma. Organizer, Quantum Repeater Journal Club.
15. D. G. Porter. Editorial Board. Journal of Research of NIST.
16. D. G. Porter. Member, ITL Awards Committee
17. O. Slattery. Laser Safety Representative, ITL Safety Committee.
18. O. Slattery. Member, ITL Space Task Force.
19. O. Slattery. ITL Representative, NIST Laser Safety Committee.
20. J. Zwolak. Member-At-Large, NIST AI Community of Interest Steering Committee.

External

Editorial

1. R. Boisvert. Associate Editor, *ACM Transactions on Mathematical Software*.
2. H. Cohl. Member, Editorial Board, *The Ramanujan Journal*.
3. H. Cohl. Co-Editor, OP-SF NET Newsletter, SIAM Activity Group on Orthogonal Polynomials and Special Functions.
4. H. Cohl. Co-Editor, Richard A. Askey Memorial Volume, *The Ramanujan Journal*.
5. H. Cohl. Co-Editor, Liber Amicorum, a Friendship Book for Dick Askey.
6. T. Gerrits. Associate Editor, *Optics Express*.
7. Z. Gimbutas. Member, Editorial Board, *Advances in Computational Mathematics.*
8. S. Glancy. Associate Editor, *Quantum Information Processing*.
9. R. La. Associate Editor, *IEEE/ACM Transactions on Networking.*
10. B. Saunders. Associate Editor, MAA *Mathematics Magazine*.
11. B. Saunders. Webmaster/SIAM Engage Moderator, SIAM Activity Group on Orthogonal Polynomials and Special Functions (SIAG/OPSF).
12. K. Sayrafian. Associate Editor, *International Journal of Wireless Information Networks*.
13. B. Schneider. Associate Editor in Chief, *Computing in Science and Engineering*.
14. B. Schneider. Specialist Editor, *Computer Physics Communications*.

Boards and Committees

1. R. Boisvert. Member, International Federation of Information Processing Working Group 2.5 (Numerical Software).
2. R. Boisvert. Member, Reproducibility Badging and Definitions Working Group, National Information Standards Organization (NISO).
3. B. Cloteaux. Member, Advisory Board, Department of Computer Science, New Mexico State University.
4. A. Dienstfrey. Vice-Chair, International Federation of Information Processing Working Group 2.5 (Numerical Software).
5. J. Fong. Member, American Society of Mechanical Engineers (ASME) Boiler and Pressure Vessel Code Committee.
6. S. Glancy. Member, IEEE Working Group on Metrics and Benchmarks for Quantum Computing Devices and Systems.
7. S. Glancy. Member, Standards Technical Advisory Committee, Quantum Economic Development Consortium.
8. P. Kuo. DC-QNet Interfaces specifications working group
9. Y.-K. Liu. Research Challenge Lead, NSF Quantum Leap Challenge Institute for Robust Quantum Simulation, University of Maryland, College Park.

10. B. Miller. Member, Ph.D. Thesis Committee, Deyan Ginev, Computer Science, University of Erlangen, Germany.
11. D. Porter. Member, Tcl Core Team.
12. S. Ressler. Member, Immersive Web Working Group, World Wide Web Consortium (W3C).
13. S. Ressler. NIST Representative, Advisory Committee, World Wide Web Consortium (W3C).
14. S. Ressler. NIST Representative, Khronos Group.
15. S. Ressler. Member, 3D Formats Working Group, Khronos Group.
16. B. Saunders. Member, Board of Trustees, Society for Industrial and Applied Mathematics (SIAM).
17. B. Saunders. Member, SIAM Systems Oversight Committee.
18. B. Saunders. Member, SIAM Human Resources Committee.
19. B. Saunders. MD-DC-VA Section Representative, Mathematical Association of America (MAA) Congress.
20. B. Saunders. Member, Nominating Committee, SIAM Activity Group on Geometric Design.
21. B. Saunders. Chair, AWM-MAA Falconer Lecture Nominating Committee
22. B. Saunders. Member, Awards Review Panel, Washington Academy of Sciences.
23. B. Saunders. Member, Advisory Board, DoD Center of Excellence on Advanced Electro-Photonics with Two-Dimensional Materials, Morgan State University, Baltimore, MD.
24. K. Sayrafian. Co-Chair, Vertical Track 1: Health and Well-Being), COST CA20120: Intelligence-Enabling Radio Communications for Seamless Inclusive Interactions.
25. W. Sherman. Member, OpenXR Working Group, Khronos Group.
26. W. Sherman. Member, ANARI Working Group, Khronos Group.
27. S. Su. Member, 3D Formats Working Group, Khronos Group.
28. S. Su. Member, OpenXR Working Group, Khronos Group.
29. S. Su. Member, ANARI Working Group, Khronos Group.

Adjunct Academic Appointments

1. V. Albert. Adjunct Assistant Professor, Department of Physics, University of Maryland, College Park, MD.
2. V. Albert. Member, Applied Mathematics & Statistics, and Scientific Computation (AMSC) Program, University of Maryland, College Park, MD.
3. M. Coudron. Adjunct Assistant Professor, Department of Computer Science, University of Maryland, College Park, MD.
4. S. Glancy. Lecturer, Department of Physics, Colorado University, Boulder, CO.
5. A. Kearsley. Lecturer, Department of Applied Mathematics and Statistics, Johns Hopkins University, Baltimore MD.
6. E. Knill. Lecturer, Department of Physics, Colorado University, Boulder, CO.
7. E. Knill. Fellow, Center for Theory of Quantum Matter, Department of Physics, Colorado University, Boulder, CO.
8. P. Kuo. Adjunct Associate Professor, Department of Physics, University of Maryland, College Park, MD.
9. Y. Liu. Co-Director, Joint Center for Quantum Information and Computer Science (QuICS), and Adjunct Associate Professor, Department of Computer Science, University of Maryland, College Park, MD.
10. K. Sayrafian. Affiliate Associate Professor, Electrical and Computer Engineering Department, Concordia University, Montreal Canada.
11. W. Sherman. W. Sherman, Adjunct Lecturer, Luddy School of Informatics and Computing, Indiana University, Bloomington.
12. S. Su. Adjunct I, Department of Media Arts & Technologies, Montgomery College, Rockville, MD.
13. J. Zwolak. Adjunct Assistant Professor, Department of Physics, University of Maryland, College Park, MD.

Thesis Direction

1. V. Albert. Member, Member, Ph.D. Thesis Committee, University of Maryland: Z.-P. Cian.
2. V. Albert. Member, Member, Ph.D. Thesis Committee, University of Maryland: Y. Wang.
3. V. Albert. Ph.D. Thesis Advisor, University of Maryland: S. Jain.

Figure 93. *ACMD staff undertake a variety of outreach efforts each year. Here Danielle Middlebrooks of ACMD (on screen at left) serves on a career panel for a series of professional development workshops run by the University of Texas Rio Grande Valley Pathways to Math program, which is a Research Experience for Undergraduates (REU) program. funded by the Sloan foundation.* (Photo courtesy of Josef Sifuentes of UTRGV.)

4. V. Albert. Ph.D. Thesis Advisor, University of Maryland: E. Kubischta.
5. V. Albert. Ph.D. Thesis Co-Advisor, University of Maryland: J. Kunjummen.
6. V. Albert. Ph.D. Thesis Co-Advisor, University of Maryland: J. Iosue.
7. M. Donahue. Member, Ph.D. Thesis Committee, University of Colorado, Boulder: Mingyu Hu.
8. Z. Gimbutas. Member, Ph.D. Thesis Committee, Department of Mathematics, Southern Methodist University: A. Slobodkins.
9. S. Su. Member, M.S. Thesis Committee, Multimedia University: J. Wee.
10. Y.-K. Liu. Member, Ph.D. Thesis Committee, University of Maryland, College Park: Z.-P. Cian.
11. Y.-K. Liu. Co-Advisor, University of Maryland, College Park: K. Huang
12. K. Sayrafian. Co-Advisor, University of Zagreb, Zagreb, Croatia: K. Krhac.
13. J. Zwolak. Ph.D. Thesis Co-Advisor, University of Maryland: S. Guo.

Community Outreach

1. V. Albert. Undergraduate Advisor, University of Maryland.
2. R. Boisvert. Panelist, Keene State College (NH) Mathematics Career Night, March 25, 2022.
3. M. Coudron. Project Leader, Summer 2021 Combinatorics, Algorithms, and AI for Real Problems Research Experience for Undergraduates (REU), University of Maryland.
4. G. Doğan. Organizer. Odyssey of the Mind Program, Cabin John Middle School, Potomac, MD, October 2021 – March 2022.
5. A. Kearsley, Panelist, Industry Leadership and Network Workshop, Institute for Innovation and Entrepreneurship at the University of California at Davis, Tapia Celebration of Diversity in Computing, Washington DC, September 7th, 2022.
6. D. Middlebrooks. Panelist, The Math Alliance: Fifteen Years of Building a New American Community in the Mathematical and Statistical Sciences, Joint Mathematics Meeting, Seattle, WA, Online, April 8, 2022.
7. D. Middlebrooks. Panelist, Professional Development Session, The University of Texas Rio Grande Valley Research Experience for Undergraduates (REU) Program on Applied Mathematics and Computational and Data Science, UT Rio Grande Valley, Edinburg, TX, Online, July 8, 2022.
8. D. Middlebrooks. Panelist, Professional Development Session, Girls Talk Math Summer Camp, University of Maryland, College Park, MD, July 15, 2022
9. D. Middlebrooks. "Research in a Physical Science Laboratory: Opportunities and Ongoing Work of a Spelman Graduate." Math Senior Seminar, Spelman College, Atlanta, GA, October 24, 2022.
10. B. Saunders. SIAM Visiting Lecturer.
11. B. Saunders. Interviewed for Documentary: The Journey of Some African American Mathematicians. MSRI (Mathematical Sciences Research Institute) and National Association of Mathematicians (NAM). See http://www.zalafilms.com/jbm/
12. S. Su. Interaction with Magnet Program. Poolesville High School, September 8, 2022.
13. J. Zwolak. Preparing students for competition in for Math Olympiads for Elementary & Middle Schools. Mary of Nazareth Catholic School, since October 2022.

14. J. Zwolak. "Mathematical and Computational Science Research at NIST." Drexel University, Philadelphia, PA, November 7, 2022.

Awards and Recognition

External

1. P. Bedekar, A. J. Kearsley, and P. N. Patrone. 2nd Place Best Contributed Talk Award ("Optimal time-dependent classification and prevalence estimation for antibody testing"), 2nd Workshop in Mathematical and Computational Biology, Online, June 9-10, 2022.
2. R. Kacker. Fellow, Washington Academy of Sciences.
3. P. Patrone. Excellence in Research in Applied Mathematics, Washington Academy of Science.
4. P. Patrone, Fellow, Washington Academy of Science.
5. K. Sayrafian. Fellow, Washington Academy of Sciences.

Internal

1. R. Boisvert. 2022 ITL Outstanding Mentor.
2. R. Evans and A. Kearsley. 2021 DOC Silver Medal (Group Award) .
3. T. Gerrits. 2021 DOC Silver Medal (Group Award).
4. S. Glancy and E. Knill. 2022 DOC Gold Medal (Group Award).
5. Katjana Khrac and Kamran Sayrafian. 2022 ITL Outstanding Conference Paper.
6. Y.-K. Liu. 2022 ITL Outstanding Contribution Award, 2022.
7. R. Luke. Most Outstanding Poster Award (Engineering, Manufacturing, Mathematical & Computer Sciences category), NIST Early Career Poster Presentation, March 30, 2022.
8. G. McFadden. 2022 NIST Portrait Gallery of Distinguished Scientists, Engineers, and Administrators.
9. P. Patrone and A. Kearsley. 2022 ITL Outstanding Journal Paper.
10. Chris Schanzle. 2022 ITL Outstanding Technical Support.
11. Vivian Xiao. 2022 ITL Outstanding Student.

Funding Received

During FY 2022 ACMD's yearly allocation of base funding from the NIST Information Technology Laboratory was supplemented with funding from a variety of internal and external competitions. Such funding represented 23% of the Division's FY 2022 budget.

Note: For multi-year awards and joint awards, only projects with new funding received by ACMD during FY 2022 are listed. Names of ACMD participants are underlined.

External

1. M. Donahue. NIST Support for DARPA Magnetic Miniaturized and Monolithically Integrated Component (M3IC) Program, DARPA. (Joint with PML)
2. B. Schneider. XSEDE Computing Allocation for AMP Gateway: A Gateway for Atomic and Molecular Physics.

Internal

1. V. Albert. Facilitating Quantum Technology Through Machine Learning. 2022 ITL Building the Future Program.
2. M. Coudron. Verification of Protein Structure Prediction Algorithms. 2022 ITL Building the Future Program.
3. C. Dennis, T. Moffat, A. Biacchi, A. Hight Walker, S. Woods, W. Tew, and M. Donahue. Thermal MagIC: An SI-Traceable Method for 3D Thermal Magnetic Imaging and Control. NIST Innovations in Measurement Science.
4. A. Dienstfrey. Advanced Hardware for AI Advantage. ITL AI Initiative. (Joint with PML)
5. G. Doğan. Better Deep Learning by Incorporating Expectations. 2022 ITL Building the Future Program.
6. R. Evans, C. Schanzle, S. Cho, A. Balijepalli, and A. Kearsley. Modeling for Medical Diagnostic Technology. 2022 ITL Building the Future Program.
7. R. Fitzgerald, D. Bergeron, S. Nour, D. Schmidt, D. Swetz, G. Shaw, B. Alpert, and M. Verkouteren. True Becquerel: A New Paradigm for 21st Century Radioactivity Measurements. NIST Innovations in Measurement Science.
8. S. Glancy and E. Knill. Establishing the Science and Technology of Networks for Superconducting

Quantum Computers. NIST Innovations in Measurement Science. (Joint with PML)

9. K. Lehnert, K. Silverman, D. Moody, J. Teufel, R. Mirin, S.-W. Nam, E. Knill, P. Hale, and T. Dennis. Establishing the Science of Networks for Superconducting Quantum Computers. NIST Innovations in Measurement Science Program.
10. D. Leibfried, A. Wilson, E. Knill, and S. Glancy. A Practical Quantum Repeater Unit. NIST Quantum Networking Grand Challenge.
11. L. Ma and O. Slattery. Integrated Entangled Photon Source Based on Silicon Carbide Devices. 2022 ITL Building the Future Program.
12. P. Patrone, A. Kearsley, R. DeJaco, E. Romsos, and P. Vallone. Advanced Analysis and Uncertainty Quantification for Diagnostic Testing. 2022 ITL Building the Future Program.
13. P. Patrone, A. Kearsley, G. McFadden, G. Cooksey, S. Sarkar, and L. Wang. NIST-in-a-drop: Revolutionizing Measurements of Single-cell Kinetics. NIST Innovations in Measurement Science.
14. M. Roberts, A. Kearsley, A. Moorthy, E. Sisco, and C. Schanzle. Compound Identification Algorithms for the DART-MS Library. 2022 ITL Building the Future Program.
15. K. Sayrafian. A Wireless Wearable Technology to Determine Accumulation of Fluid in the Lungs – Part II. 2022 ITL Building the Future Program.
16. O. Slattery, A. Battou, and N. Zimmerman. Quantum Network Testbeds on NIST Campus and on DC-QNet. NIST Quantum Networking Grand Challenge.
17. O. Slattery. Novel Bell State Analyzer for WDM-compatible Entanglement Swapping and Teleportation. Quantum Network Initiative.
18. J. Ziegler, J Zwolak, Z. Grey, and C. Greenberg. Assessing Uncertainty in Machine Learning for Quantum Physical Systems. 2022 ITL Building the Future Program.

Grants Funded

ACMD awards a small amount of funding through the NIST Grants Program for projects that make direct contributions to its research programs. During FY 2022 the following cooperative agreements were active.

1. George Washington University: *Algorithmic Development for AI Coprocessors.* PI: Gina Adam. • Supports NIST Neuromorphic Computing program.
2. Prometheus Computing LLC: *Security, Resiliency and Dynamics of Interdependent Self-Organizing Networks*. PI: Assane Gueye. • Supports ACMD Foundations of Measurement Science for Information Systems program.
3. Purdue University: *Effective Range of Fluid-Mediated Particle-Particle Interactions in an Optofluidic Flow Meter.* PI: Kaitlyn Hood. • Supports NIST-in-a-Drop Innovations in Measurement Science program.
4. Theiss Research: *Exploiting Alternate Computing Technologies*. PI: Alan Mink. • Supports ITL Quantum Information Science and NIST Neuromorphic Computing programs.
5. University of Edinburgh: *Rigorous and Presentable Asymptotics for Special Functions and Orthogonal Polynomials*. PI: Adri Olde-Daalhuis. • Supports NIST Digital Library of Mathematical Functions project.
6. University of Maryland: *Joint Center for Quantum Information and Computer Science (QuICS)*. PI: Andrew Childs• Supports ITL Quantum Information Science program.
7. University of Minnesota: *NIST-IMA Postdoctoral Fellowship in Analysis of Machine Learning*. PI: Daniel Spirn. • Supports ITL Artificial Intelligence program.
8. University of Texas at Arlington: *SENTINEL: Security Interaction Testing for IoT Systems and Blockchains*. PI: Yu Lei. • Supports ITL Combinatorial Testing project.

External Contacts

ACMD staff members interact with a wide variety of organizations in the course of their work. Examples of these follow.

Industrial Labs

Amazon AWS
Boeing Company
Chakra Consulting
ColibrITD (France)
Computational Physics, Inc.
Corning
Deltares (Netherlands)
Fraunhoffer IGD (Germany)
GE Global Research Center
Google
Honeywell
HRL Laboratories
IBM
Intel
Intertek
Kitware

Microsoft Research
MPACT Corp.
NTT Corporation (Japan)
Photon Spot Inc.
Prorenata Labs
PsiQuantum
Quantum Opus
Qunnect
Roche, Regeneron, Abbott Labs
Rolls-Royce Corporation
Sivinathan Labs
SRI
Xanadu Quantum Technologies, Inc.

Government/Non-profit Organizations

American Society of Mechanical Engineers
Argonne National Laboratory
Army Research Laboratory
arXiv.org
Association for Computing Machinery
Centers for Disease Control
CENAM (Mexico)
Flatiron Institute
Food and Drug Administration
IEEE Computer Society
Johns Hopkins University Applied Physics Laboratory
Khronos Group
Korean Institute of Science and Technology (S. Korea)
Laboratory for Telecommunication Sciences
Lawrence Berkeley National Laboratory
Mathematical Sciences Research Institute
NASA Goddard Space Flight Center
NASA Ames Research Center
National Institute of Biomedical Imaging and Bioengineering
National Institutes of Health
National Physical Laboratory (UK)
National Reconnaissance Office
National Research Council (Canada)
National Security Agency
National Renewable Energy Laboratory (NREL)
Naval Research Laboratory
Oak Ridge National Laboratory
QIMR Berghofer Medical Research Inst (Australia)
OpenMath Society
Pacific Northwest National Laboratory
Physikalisch-Technische Bundesanstalt (Germany)
Quantum Economic Development Consortium
Sandia National Laboratories
SBA Research (Austria)
Stanford Research International (SRI)
Theiss Research
US Department of Energy
US Geological Survey
US Holocaust Memorial Museum
US Naval Observatory
US Office of Naval Research (USNO)
Washington Metro Quantum Network Research Consortium
World Wide Web Consortium

Universities

Aarhus University (Denmark)
Alfréd Rényi Institute of Mathematics (Hungary)
American University
Amherst College
Beijing Institute of Technology (China)
Brown University
California Institute of Technology
Carnegie Mellon University
China University of Petroleum (China)
Clarkson University
Clemson University
Colorado School of Mines
Columbia University
Concordia University (Canada)
Consejo Nacional de Investigaciones Científicas y Técnicas (Argentina)
Coppin State University
Cornell University
Courant Institute of Mathematical Sciences
Curtin University (Australia)
Dalian University of Science and Tech (China)
Delft University of Technology (The Netherlands)
Drake University
Drexel University
East China U. of Science and Tech (China)
Federal University of Ceará (Brazil)
Florida State University
Freie Universität Berlin (Germany)
George Mason University
George Washington University
Harvard University
Humboldt University (Germany)
Imperial College London (UK)
Indiana University
Indian Institute of Technology (India)
Jacobs University Bremen (Germany)
Johannes Kepler University Linz (Austria)
Johns Hopkins University
Kennesaw State University
Khallikoke College (India)
Korteweg-de Vries Institute for Mathematics (The Netherlands)
Louisiana State University
Ludwig-Maximilians University (Germany)
Massachusetts Institute of Technology (MIT)
Morgan State University
Multimedia University (Malaysia)
National University of Singapore (Singapore)
Norfolk State University
Northeastern University

Occidental College
Ohio State University
Old Dominion University
Open University (UK)
Purdue University
Rice University
Royal Institute of Technology (Sweden)
ShanghaiTech University (China)
Shandong University (China)
Southern Methodist University
Southern University and A&M College
Stanford University
Technical University of Denmark (Denmark)
Temple University
Texas A&M University
Texas Tech University
Tokyo University of Science (Japan)
Tsinghua University (China)
Tufts University
Universidad Autonoma de Madrid (Spain)
Universidad Loyola Andalucia (Spain)
University of Amsterdam (The Netherlands)
University of Antwerp (Belgium)
University of Belfast (UK)
University of British Colombia (Canada)
University of California, Berkeley
University of California, Davis
University of California, Los Angeles
University of California, San Diego
University of Central Florida
University of Chicago
University of Colorado, Colorado Springs
University of Colorado, Boulder
University of Copenhagen
University of Delaware
University of Edinburgh (UK)
University of Erlangen (Germany)
University of Konstanz (Germany)
University of Illinois, Urbana-Champaign
University of Limerick (Ireland)
University of Manchester (UK)
University of Maryland, Baltimore County
University of Maryland, College Park
University of Massachusetts
University of New Mexico
University of Oregon
University of Ottawa (Canada)
University of Rochester
University of San Paolo (Brazil)
University of Saskatchewan (Canada)
University of Sheffield (UK)
University of Southern California
University of South Carolina
University of Strathclyde (UK)
University of Sydney (Australia)
University of Texas at Arlington
University of Texas at Austin
University of Texas at Dallas
University of Texas at Rio Grande Valley
University of Washington
University of Wisconsin, Madison
University of Wisconsin, Milwaukee
University of Wuppertal (Germany)
Virginia Commonwealth University
Virginia Polytechnic Institute
Weizmann Institute of Science (Israel)
Western Michigan University
Yale University

Part V

Appendix

Staff

ACMD consists of full-time permanent Federal staff located at NIST laboratories in Gaithersburg, MD and Boulder, CO. This full-time staff is supplemented with a variety of special appointments. The following list reflects all non-student appointments held during any portion of the reporting period (October 2021 – December 2022). Students and interns are listed in Table 3 page 129.

* Denotes staff at NIST Boulder.
† Denotes part-time Federal staff.

Division Staff

Ronald Boisvert, *Chief*, Ph.D. (Computer Science), Purdue University, 1979
Catherine Graham, *Administrative Assistant*
*Elsie (Meliza) Lane, *Administrative Assistant*
Lochi Orr, *Administrative Assistant*, A.A. (Criminal Justice), Grantham University, 2009
†Alfred Carasso, Ph.D. (Mathematics), University of Wisconsin, 1968
Roldan Pozo, Ph.D. (Computer Science), University of Colorado at Boulder, 1991
Kamran Sayrafian, Ph.D. (Electrical and Computer Engineering), University of Maryland, 1999
Christopher Schanzle, B.S. (Computer Science), University of Maryland Baltimore County, 1989

Mathematical Analysis and Modeling Group

Timothy Burns, *Leader*, Ph.D. (Mathematics), University of New Mexico, 1977
*Daniel Flynn, *Administrative Assistant*, B.S. (Political Science), Iowa State University, 2016
*Bradley Alpert, Ph.D. (Computer Science), Yale University, 1990
*Andrew Dienstfrey, Ph.D. (Mathematics), New York University, 1998
Ryan Evans, Ph.D. (Applied Mathematics), University of Delaware, 2016
†Jeffrey Fong, Ph. D. (Applied Mechanics and Mathematics), Stanford University, 1966
*Zydrunas Gimbutas, Ph.D. (Applied Mathematics), Yale University, 1999
*Zachary Grey, Ph.D. (Computational and Applied Mathematics), Colorado School of Mines, 2019
Raghu Kacker, Ph.D. (Statistics), Iowa State University, 1979
Anthony Kearsley, Ph.D. (Computational and Applied Mathematics), Rice University, 1996
Danielle Middlebrooks, Ph.D. (Applied Mathematics, Statistics and Scientific Computing), University of Maryland, 2020
Paul Patrone, Ph.D. (Physics), University of Maryland, 2013

NRC Postdoctoral Associates
Danielle Brager, Ph.D. (Mathematical Biology), Arizona State University, 2020
Robert DeJaco, Ph.D. (Chemical Engineering), University of Minnesota, 2020
Deborah McGlynn, Ph.D. (Civil and Environmental Engineering), Virginia Tech, 2022
Matthew Roberts, Ph.D. (Mathematical Sciences), Michigan Technological University, 2019

Faculty Appointee (Name, Degree / Home Institution)
Daniel Anderson, Ph.D. / George Mason University
Michael Mascagni, Ph.D. / Florida State University
John Nolan, Ph.D. / American University
Florian Potra, Ph.D. / University of Maryland Baltimore County

Guest Researchers (Name, Degree / Home Institution)
Prajakta Bedekar, Ph.D. / Johns Hopkins University
Natesh Ganesh, Ph.D. / University of Colorado
Kaitlyn Hood, Ph.D. / Purdue University
Fern Hunt, Ph.D. / *NIST Scientist Emeritus*

Yu (Jeff) Lei, Ph.D. / University of Texas at Arlington
Rayanne Luke, Ph.D. / Johns Hopkins University
Geoffrey McFadden, Ph.D / *NIST Scientist Emeritus*
Dimitrios Simos, Ph.D. / SBA Research, Austria

Mathematical Software Group

Bonita Saunders, *Leader,* Ph.D. (Mathematics), Old Dominion University, 1985
Javier Bernal, Ph.D. (Mathematics), Catholic University, 1980
Howard Cohl, Ph.D. (Mathematics), University of Auckland, 2010
Günay Doğan, Ph.D. (Applied Mathematics and Scientific Computing), University of Maryland, 2006
Michael Donahue, Ph.D. (Mathematics), Ohio State University, 1991
Stephen Langer, Ph.D. (Physics), Cornell University, 1989
Bruce Miller, Ph.D. (Physics), University of Texas at Austin, 1983
Donald Porter, D.Sc. (Electrical Engineering), Washington University, 1996
Barry Schneider, Ph.D. (Physics), University of Chicago, 1969

NRC Postdoctoral Associates
William Earwood, Ph.D. (Chemistry), University of Mississippi, 2022
Camilo Montoya, Ph.D. (Mathematics), Florida International University, 2022
Lisa Ritter, Ph.D. (Mathematics), University of Hawai'i at Mānoa, 2021
Stephen Sorokanich, Ph.D. (Mathematics), University of Maryland, College Park, 2022

Faculty Appointees (Name, Degree / Home Institution)
Abdou Youssef, Ph.D. / George Washington University

Guest Researchers (Name, Degree / Home Institution)
Joel Bowman, Ph.D. / Emory University
Nicolas Douguet, Ph.D. / Kennesaw State University
Heman Gharibnejad, Ph.D. / Computational Physics Inc.
Mark Alexander Henn, Ph.D. / University of Maryland
Justin Kauffman, Ph.D. / Virginia Polytechnic Institute and State University
Daniel Lozier, Ph.D. / NIST, Retired
Adri Olde Daalhuis, Ph.D. / University of Edinburgh
Jeppe Olsen, Ph.D. / Aarhus University, Denmark
Chen Qu, Ph.D. / GBS Dakota IT, LLC
Moritz Schubotz, Ph.D. / University of Karlsruhe, Germany

Computing and Communications Theory Group

Ronald Boisvert, *Acting Leader*, Ph.D. (Computer Science), Purdue University, 1979
Victor Albert, Ph.D. (Physics), Yale University, 2017
Lucas Brady, Ph.D. (Physics), University of California at Santa Barbara, 2018
Brian Cloteaux, Ph.D. (Computer Science), New Mexico State University, 2007
Matthew Coudron, Ph.D. (Computer Science), Massachusetts Institute of Technology, 2017
Thomas Gerrits, Ph.D. (Physics), Radboud University Nijmegen, 2004
*Scott Glancy, Ph.D. (Physics), University of Notre Dame, 2003
*Emanuel Knill, *NIST Fellow,* Ph.D. (Mathematics), University of Colorado at Boulder, 1991
Paulina Kuo, Ph.D. (Physics), Stanford University, 2008
Yi-Kai Liu, Ph.D. (Computer Science), University of California, San Diego, 2007
Lijun Ma, Ph.D. (Precision Instruments and Machinery), Tsinghua University, 2001
Vladimir Marbukh, Ph.D. (Mathematics) Leningrad Polytechnic University, 1986
Oliver Slattery, *Project Leader*, Ph.D. (Physics), University of Limerick, 2015

Faculty Appointees (Name, Degree / Home Institution)
James Lawrence, Ph.D. / George Mason University
Richard La, Ph.D. / University of Maryland
Debasis Mitra, Ph.D. / Columbia University

Guest Researchers (Name, Degree / Home Institution)
Isabel Beichl, Ph.D. / NIST, Retired
Sumit Bhushan, Ph.D. / Indian Institute of Technology
Sesha Challa / Pusan National University (India)
Nijil Lal Cheriya Koyyottummal, Ph.D. / University of Napoli Federico II
Hristina Georgieva, Ph.D. / Physikalisch-Technische Bundesanstalt (PTB)
Assane Gueye, Ph.D. / Prometheus Computing
Navin Lingaraju, Ph.D. / University of Maryland, College Park
*Karl Mayer, Ph.D. / Honeywell
Alan Mink, Ph.D. / Theiss Research
Anouar Rahmouni, Ph.D. / Moroccan Foundation for Advanced Sci., Innovation and Research
Samprity Saha, Ph.D. / Virginia Commonwealth University
Yicheng Shi, Ph.D. / National University of Singapore
*Ezad Shojaee, Ph.D. / University of Colorado
Francis Sullivan, Ph.D. / IDA Center for Computing Sciences
Xiao Tang, Ph.D. / NIST Retired
*James Van Meter, Ph.D. / HRL Laboratories
Yinxiao Xiang, Ph.D. / Izum, Inc.

High Performance Computing and Visualization Group

Judith Terrill, *Leader*, Ph.D. (Information Technology), George Mason University, 1998
William George, Ph.D. (Computer/Computational Science), Clemson University, 1995
Terence Griffin, B.S. (Mathematics), St. Mary's College of Maryland, 1987
Sandy Ressler, M.F.A. (Visual Arts), Rutgers University, 1980
William Sherman, M.S. (Computer Science), University of Illinois, 1989
Simon Su, Ph.D. (Computer Science), University of Houston, 2001
Justyna Zwolak, Ph.D. (Physics), Nicolaus Copernicus University, Poland, 2011

NRC Postdoctoral Associates
Joshua Ziegler, Ph.D. (Physics), University of Oregon, 2020

Guest Researchers (Name, Degree / Home Institution)
John Hagedorn, M.S. / Chakra Consulting
Steven Satterfield, M.S. / NIST Retired
James Sims, Ph.D. / NIST (retired)

Glossary of Acronyms

1D	one-dimensional
2D	two-dimensional
3D	three-dimensional
ACCESS	NSF Advanced Cyberinfrastructure Coordination Ecosystem
ACI	American Concrete Institute
ACM	Association for Computing Machinery
ACMD	NIST/ITL Applied and Computational Mathematics Division
ACTS	Advanced Combinatorial Testing System (software)
ADC	apparent diffusion coefficient
ADJOINT	African Diaspora Joint Mathematics Workshop
ADS	autonomous driving system
AI	artificial intelligence
AL	Analytic Methods (DLMF chapter)
AMOS	atomic molecular and optical science
AMOSG	Atomic Molecular and Optical Science Gateway
AMS	American Mathematical Society
ANARI	Analytic Rendering Interface for Data Visualization
ANN	artificial neural network
API	application programming interface
APS	American Physical Society
AR	augmented reality
arXiv	preprint archive at https://arxiv.org/
ARL	Army Research Laboratory
ASES	Aspects of Student Experience Survey
ASME	American Society of Mechanical Engineers
ASTM	American Society for Testing and Materials
AWM	Association for Women and Computing
arXiv	preprint archive housed at Cornell University (http://arxiv.org/)
Be	beryllium
BEC	Bose-Einstein Condensate
Bio-FET	biological field effect transistor
BMP	Bateman Manuscript Project
BPVC	Boiler and Pressure Vessel Code
Bq	becquerel: absolute activity of radionuclide mixtures
BS	base station
BVOC	biogenic volatile organic compounds
BW	backward wave
CA	California
CAD	computer aided design
Caltech	California Institute of Technology
CAS	computer algebra system
CAVE	CAVE Automatic Virtual Environment
CCM	Combinatorial Coverage Measurement (software)
CDC	Centers for Disease Control and Prevention
CENAM	Center for Metrology of Mexico
CI	configuration interaction
CICM	Conference on Intelligent Computer Mathematics
CFD	combination frequency differencing
CFPG	Coulomb force parametric generator
CFSF	Continued Fractions for Special Functions
CLEO	Conference on Lasers and Electro-Optics
CMA	Computational Mathematics Research Group at the University of Antwerp
CMOS	complementary metal-oxide semiconductor

CNN	convolutional neural network
CO	Colorado
CONICET	National Scientific and Technical Research Council of Argentina
COVID	coronavirus disease
CPU	central processing unit
CR	convex relaxation
CRADA	cooperative R&D agreement
CS	coordinating server
CSF	configuration state function
CT	computed tomography
CT	combinatorial testing
CTL	NIST Communications Technology Laboratory
CV	continuous (quantum) variables
CY	calendar year
DARPA	Defense Advanced Research Projects Agency
DART-MS	Direct Analysis in Real Time Mass Spectrometry
DC-QNet	DC area Quantum Network testbed
DD	double (quantum) dot
DGR	NIST Domestic Guest Researcher
DL	deep learning
DLMF	Digital Library of Mathematical Functions
DNA	deoxyribonucleic acid
DNN	deep neural network
DOC	Department of Commerce
DOI	digital object identifier
DQC	data quality control
DRMF	Digital Repository of Mathematical Formulae
DS	double stranded
DV	discrete (quantum) variable
EBSD	electron backscatter diffraction
eCF	Wolfram Computational Knowledge of Continued Fractions Project
eDNA	environmental DNA
EH	energy harvesting
E-Health	electronic health care
E-Hy-CI	exponentially correlated Hy-CI
EL	NIST Engineering Laboratory
EPA	Environmental Protection Agency
ERaR	entropic rate at risk
ESBD	electron back-scatter diffraction
FEDVR	finite element discrete variable
FEM	finite element method
FFT	fast Fourier transform
FGR	NIST Foreign Guest Researcher Program
FIPO	fast IPO
FL	federated learning
FY	fiscal year
GDS	Graphic Design System (file format for electronic design automation)
GHG	greenhouse gas
glTF	standard file format for three-dimensional scenes and models
GMSE	NIST Graduate Measurement Science and Engineering internship program
GNN	graph neural network
GPU	graphical processing unit
GUI	graphical user interface
HA-PTP	classical time synchronization protocol
HEC	High End Computing
HEV	high end visualization
HIM	helium ion microscope

HMD	head-mounted display
HPC	high performance computing
HPCVG	ACMD High Performance Computing and Visualization Group
HTML	hypertext markup language
Hy	Hylleraas
Hy-CI	Hylleraas-Configuration Interaction technique
IARPA	Intelligence Advanced Research Projects Agency
IC	integrated circuit
ICP	inductively coupled plasma
ICST	International Conference of Software Testing
IDE	integrodifferential equation
IEEE	Institute of Electronics and Electrical Engineers
IFIP	International Federation for Information Processing
IMS	NIST Innovations in Measurement Science program
IoT	Internet of things
IPO	in parameter order
IR	infrared
IU	Indiana University
IT	information technology
ITL	NIST Information Technology Laboratory
ITVOLT	iterative Volterra integral equation solver
IU	Indiana University
IVE	immersive visualization environment
IWCT	International Workshop on Combinatorial Testing
KLS	Koekoek, Lesky and Swarttouw
LaCASt	Java tool to convert math expressions from LaTeX to computer algebra systems
LaTeX	a math-oriented text processing system
LaTeXML	a LaTeX to Math ML converter
LBNL	Lawrence Berkeley National Laboratory
LIDAR	light detection and ranging
LTS	Laboratory for Telecommunication Sciences
M3IC	DARPA Magnetic, Miniaturized, and Monolithically Integrated Components program
MAA	Mathematical Association of America
MathML	Mathematical Markup Language (W3C standard)
MD	Maryland
MEH	micro energy harvester
MGB	Mathematically Gifted and Black
MGI	Materials Genome Initiative
MIT	Massachusetts Institute of Technology
ML	machine learning
MLP	mathematical language processing
MML	NIST Material Measurement Laboratory
MOL	method of lines
MOS	Magnus, Oberhettinger, and Soni
MOT	magneto-optical trap
MR	mixed reality
MRAM	magneto-resistive random-access memory
MRI	magnetic resonance imaging
MS	mass spectrometry
MSGI	NSF Mathematical Sciences Graduate Internship program
MSRI	Mathematical Sciences Research Institute (Berkeley)
muMAG	Micromagnetic Activity Group
NALS	network analysis for Likert-style surveys
nanoHUB	Web portal for nanotechnology research at https://nanohub.org/
NASA	National Aeronautics and Space Administration
NBS	National Bureau of Standards (former name of NIST)
NCCOE	NIST National Cybersecurity Center of Excellence

NG-QNET	NIST Gaithersburg Quantum Network
NIBIB	National Institute of Biomedical Imaging and Biotechnology
NIH	National Institutes of Health
NISQ	noisy intermediate-scale quantum
NIST	National Institute of Standards and Technology
NISTIR	NIST Internal Report
NITRD	Networking and Information Technology Research and Development
nm	nanometer
NN	neural network
NRC	National Research Council
NREL	National Renewable Energy Laboratory
NRL	Naval Research Laboratory
NSF	National Science Foundation
OD	object detector
ODE	ordinary differential equation
ONA	organizational network analysis
OOF	Object-Oriented Finite Elements (software)
OOF3D	3D version of OOF
OOMMF	Object-Oriented Micromagnetic Modeling Framework (software)
OP	orthogonal polynomials
OpenXR	Open Extended Reality
OPSF	orthogonal polynomials and special functions
OS	photoreceptor outer segments
OTDR	optical time-domain reflectometry
OU	organizational unit
PAML	physics-assisted machine learning
PCA	principal component analysis
PCB	printed circuit board
PCR	polymerase chain reaction
PDE	partial differential equation
PDF	probability density function
PER	physics education research
PET	positron emission tomography
PI	principal investigator
PIE	physics-informed excitation
PIT	physics-informed tuning
PLOS	Public Library of Science
PML	NIST Physical Measurement Laboratory
PQNI	Platform for Quantum Networking Innovation
PPKTP	periodically poled $KTiOPO_4$
PQC	post-quantum cryptography
PREP	NIST Professional Research Education Program
PT	Painlevé transcendents (DLMF chapter)
PTB	Physikalisch-Technische Bundesanstalt (German metrology institute)
PUF	physically unclonable function
QAOA	quantum approximate optimization algorithm
QEC-C	Quantum Economic Development Consortium
QD	quantum dot
QDPD	Quaternion-based Dissipative Particle Dynamics simulation code
QIP	quantum information processing (conference)
QN	quantum network
ONA	organizational network analysis
QNGC	Quantum Networking Grand Challenge
QoS	quality of service
qPCR	quantitative polymerase chain reaction
QuAIL	NASA Ames Quantum Artificial Intelligence Laboratory
QuICS	UMD-NIST Joint Center for Quantum Information and Computer Science

R&D	research and development
RAVEN	IARPA Rapid Analysis of Various Emerging Nanoelectronics program
RBC	ray-based classification
RBF	radial basis function
REU	Research Experience for Undergraduates
RF	radio frequency
RGM	reduced gradient method
RIE	reactive ion etching
RIM	reliability and integrity management
ROI	region of interest
RPE	retinal pigment epithelium
RSA	Rivest-Shamir-Adelman public key cryptographic algorithm
SARS	severe acute respiratory syndrome
SARS-CoV-2	the virus that causes the respiratory disease COVID-19
SEM	scanning electron microscope
SFWM	spontaneous four wave mixing
SHIP	Summer High School Internship Program
SIAM	Society for Industrial and Applied Mathematics
SiC	silicon carbide
SIGGRAPH	ACM Special Interest Group on Graphics
SNSPD	superconducting nanowire single-photon detectors
SPD	single-photon detectors
SPDC	spontaneous parametric down conversion
SPO	NIST Special Programs Office
SPIE	International Society for Optical Engineering
SRM	standard reference material
SS	single stranded
SURF	NIST Student Undergraduate Research Fellowship program
SVM	support vector machine
SVOP	several variable orthogonal polynomials (DLMF chapter)
SVP	NIST Student Volunteer Program
TDSE	time domain Schrodinger equation
TEM	transmission electron microscope
TES	transition edge sensor
TFLN	thin-film lithium niobate
TLS	transport layer security
UC	University of California
UCSD	University of California at San Diego
UMD	University of Maryland
UMIACS	University of Maryland Institute for Advanced Computer Studies
UQ	uncertainty quantification
URL	universal resource locator
USGS	US Geological Survey
USHMM	United States Holocaust Memorial Museum
USNO	US Naval Observatory
VA	Virginia
VEMOS	Visual Explorer for Metric of Similarity (software)
ν-OTDR	photon-counting OTDR
VR	virtual reality
VTK	visualization software library
W3C	World Wide Web Consortium
WAS	Washington Academy of Sciences
WHO	World Health Organization
WRS	White Rabbit Switch (time synchronization protocol)
XR	extended reality
XSEDE	NSF eXtreme Science and Engineering Discovery Environment
ZE	Zeta and related functions (DLMF chapter)